

Rationalisation and Design of Hydrogen Bonding Patterns in Co-crystals and Polymorphs.

Iain D.H. Oswald



**A Thesis submitted in fulfilment of the requirements for the
degree of Doctor of Philosophy to the School of Chemistry,
University of Edinburgh.**

September 2004



Declaration

I declare that this thesis was written by myself and that the work detailed in this is my own, or I have contributed substantially to such work, except where specific reference is made to the work of another. This work has not been submitted for any other degree or professional qualification.

Iain Oswald

Abstract

This thesis describes the determination and analysis of the crystal structures of a series of hydrogen-bonded, organic compounds. The subjects chosen for study were targeted with the aim of forming closely-related structural motifs in the solid state.

The crystal structures of five hemiadducts of paracetamol with 1,4-dioxane, N-methylmorpholine, morpholine, N,N-dimethylpiperazine and piperazine, and a related 1:1 adduct of paracetamol with 4,4'-bipyridine are described. All structures are characterised by the formation of chains of paracetamol molecules, linked either via OH...O=C interactions [C(9) chains in graph set notation] or NH..O=C interactions [C(4) chains], depending on the presence or absence of substituent groups on the guest molecule. In all cases except for the morpholine and bipyridine adduct these chains are connected by H-bond interactions with the guest molecules residing on crystallographic inversion centres. In the bipyridine adduct this linkage also involves a π -stacking interaction; in the morpholine adduct it is formed between the OH groups of two opposed paracetamol molecules. Most adducts (that with 4,4'-bipyridine is an exception) decompose on heating to give monoclinic paracetamol. This is the first systematic study of a series of co-crystals containing paracetamol.

The crystal structures of eight new co-crystals of quinol with pyrazine, piperazine, morpholine, pyridine, piperidine, 4,4'-bipyridine, N-methylmorpholine and N,N'-dimethylpiperazine are also reported. Quinol forms 1:1 co-crystals with pyrazine, piperazine and N,N'-dimethylpiperazine, but 1:2 co-crystals with morpholine, 4,4'-bipyridine, N-methylmorpholine, pyridine and piperidine. This difference can be rationalised in most cases by the presence of respectively two or one strong H-bond acceptor(s) in the guest molecule. The exception to this generalisation is 4,4'-bipyridine, which forms a 1:2 co-crystal, possibly to optimise crystal packing. All structures are dominated by hydrogen bonding between quinol and the guest molecules. A doubly-bridging motif, which connects pairs of quinol and guest molecules via NH...O or CH...O interactions, is present in all but the sterically-hindered N,N'-dimethylpiperazine and N-methylmorpholine co-crystals.

Co-crystals of *isonicotinamide* have been prepared with formic and acetic acids. In both structures a similar $R_2^2(8)$ amide-dimer motif is formed by the *isonicotinamide*, with the guest molecules forming contacts between the amide or acid groups and the pyridine moiety of the host. The *isonicotinamide*:formic acid adduct shows proton migration with a change in temperature.

Existing methodologies for crystal structure prediction work tolerably well for small, rigid molecules, prediction tests often appear to fail to predict known polymorphs, even though many hundreds of energetically similar structures may be predicted instead. Many algorithms attempt to maximise density, it is possible that 'failed' prediction attempts have in fact yielded polymorphs which are stable at high pressure, but which have not yet been identified experimentally. Crystal structures of all isomers of monofluorophenol and monochlorophenol have been determined both at low temperature and high pressure. All except the 3-substituted isomers show some degree of polymorphism with applied pressure. 2-chlorophenol, for example, forms H-bonded chains in the solid state; these are disposed about crystallographic 3_2 screw axes at low temperature, but 2_1 axes at high pressure (0.12 GPa). Previous work on the packing characteristics of alcohols suggests that the chlorophenyl group in this case is behaving as a large group at low temperature, but a small group at high pressure.

Acknowledgements

I would like to thank Dr Simon Parsons for all his help and guidance over the past three years with crystallography and English and making my PhD an enjoyable experience despite the jokes!!! Dr Sam Motherwell at the Cambridge Crystallographic Data Centre for useful discussions on projects. Dr Colin Pulham for starting me off in this area of research back in my undergraduate days.

Dr David Allan for his advice on high-pressure experimental techniques. Dr Graeme Day from the Pfizer Institute for all his work on crystal structure prediction and his help with my many questions. Dr Andy Parkin for his help throughout my PhD. Dr Alice Dawson for all her help, chats and space group facts!! Everyone from the Chemical Crystallography group past and present for making Edinburgh crystallography group an enjoyable place to work; Pam, James, Fran, Patty, Stephen. Thanks to Stephen Moggach for putting up with my tantrums whilst I was writing this thesis. Thanks to my two flatmates over the past two years, Chris and Elaine, who have made Roseneath Terrace the place to be. To all my friends for taking me away from this work, for a few hours at least.

Jane Liggat for helping me to escape work and listening to my many rants; sorry if I've been a grouch. My family for all their support and advice during my perpetual student life.

Lecture courses and meetings attended*Courses*

Nov. 2001	Introduction to HTML	Edinburgh
Dec. 2001	More HTML	Edinburgh
Dec. 2001	Unix 1	Edinburgh
Apr. 2002	BCA Rietveld refinement workshop	Nottingham
Dec. 2002	Unix 2	Edinburgh
Apr. 2003	BCA Intensive Crystallography course	Durham
Jun. 2003	Fortran 90	Edinburgh
Jun. 2004	Thesis workshop	Edinburgh

Conferences attended

Apr. 2002	BCA Spring Meeting	Nottingham	<i>Poster</i>
May. 2002	CCDC Student day	Cambridge	<i>Talk</i>
Aug. 2002	IUCr XIX	Geneva	<i>Poster</i>
Sep. 2002	USIC 2002	Edinburgh	<i>Talk</i>
Nov. 2002	BCA CCG Autumn Meeting	London	
Dec. 2002	BCA PCG Winter Meeting	Edinburgh	
Apr. 2003	BCA Spring Meeting	York	<i>Talk</i>
Apr. 2003	CCDC Student day	Cambridge	<i>Talk</i>
Sep. 2003	USIC 2003	Strathclyde	<i>Poster</i>
Nov. 2003	BCA IG Autumn Meeting	London	
Apr. 2004	Young Crystallographers Satellite Meeting	Manchester	<i>Talk</i>
Apr. 2004	BCA Spring Meeting	Manchester	<i>Poster</i>
May. 2003	CCDC Student day	Cambridge	<i>Talk</i>
Aug. 2004	ECM 22	Budapest	<i>Talk</i>

Publications

“A 3D interlocked structure from a 2D template: Structural requirements for the assembly of a square-planar metal-coordinated [2]rotaxane.”, Fuller, A-M., Leigh, D. A., Lusby, P. J., Oswald, I. D. H., Parsons, S. & Walker, D. B. (2004). *Angew. Chem. Int. Ed.* **43**, 3914-3918.

“Structure and Dynamics of Dinuclear Zirconium(IV) Complexes.”, Zhong, W., Parkinson, J. A., Parsons, S., Oswald, I. D. H., Coxall, R. A. & Sadler, P. J. (2004). *Inorg. Chem.* **43**, 3561-3572.

“Rationalisation of co-crystal formation through knowledge-mining.”, Oswald, I. D. H., Motherwell, W. D. S., Parsons, S., Pidcock, E. & Pulham, C. R. (2004). *Cryst. Rev.*, **10**, 57-66.

“Structures of piperazine, piperidine and morpholine.”, Parkin, A., Oswald, I. D. H. & Parsons, S. (2004). *Acta Cryst. B* **60**, 219-227.

“Pressure-induced formation of a solvate of paracetamol.”, Fabbiani, F. P. A., Allan, D. R., Dawson, A., David, W. I. F., McGregor, P. A., Oswald, I. D. H., Parsons, S. & Pulham, C. R. (2004) *Chem. Commun.* **24**, 3004-3005.

“Kinetics of aquation and anation of ruthenium(II) arene anticancer complexes, acidity and X-ray structures of aqua adducts.”, Wang, F., Chen, H., Parsons, S., Oswald, I. D. H., Davidson, J. E. & Sadler, P. J. (2003) *Chem. Eur. J.* **9**, 5810-5820.

“Triboluminescent materials and devices.”, Sage, I. C., Bourhill, G. H., Oswald, I. (2003) *PCT Int. Appl.* pp45.

“The formation of paracetamol (acetaminophen) adducts with hydrogen-bond acceptors.”, Oswald, I. D. H., Allan, D. R., McGregor, P. A., Motherwell, W. D. S., Parsons, S. & Pulham, C. R. (2002). *Acta Cryst, B* **58**, 1057-1066.

“A paracetamol-morpholine adduct.”, Oswald, I. D. H., Allan, D. R., McGregor, P. A., Motherwell, W. D. S., Parsons, S. & Pulham, C. R. (2002). *Acta Cryst, E* **58**, o1290-o1292.

“Do triboluminescence spectra really show a spectral shift relative to photoluminescence spectra?”, Duignan, J. P., Oswald, I. D. H., Sage, I. C., Sweeting, L. M., Tanaka, K., Ishihara, T., Hirao, K. & Bourhill, G. (2002). *J. Lumin.* **97**, 115-126.

“The solid-state photoluminescent quantum yield of triboluminescent materials.”, Bourhill, G., Palsson, L. O., Samuel, I. D. W., Sage, I. C., Oswald, I. D. H. & Duignan, J. P. (2001). *Chem. Phys. Lett.* **336**, 234-241.

“Getting light through black composites: embedded triboluminescent structural damage sensors.”, Sage I., Humberstone L., Oswald I., Lloyd P., Bourhill G. (2001) *Smart Mater. Struct.* **10**: 332-337.

“Embedded triboluminescent structural damage sensors.”, Sage I., Humberstone L., Oswald I., Lloyd P., Bourhill G. (2000) *Proceedings of SPIE-The International Society for Optical Engineering*, 4104 (Organic Photorefractives, Photoreceptors, and Nanocomposites), 1-8.

“Two isostructural triboluminescent lanthanide complexes.”, Clegg, W., Sage, I., Oswald, I., Brough, P. & Bourhill, G. (2000) *Acta Cryst C* **56**, 1323-1325.

Contents

Declaration	i
Abstract	ii
Acknowledgements	iv
Lecture courses and meetings attended	v
Publications	vi
Chapter 1 Introduction	1
1.1 Nature of the Chemical bond	2
1.1.1 Definition	2
1.1.2 Classification of hydrogen bonds	4
1.1.3 Theory of hydrogen bonds	7
1.2 The Hydrogen bond in the solid state	8
1.2.1 σ -bond co-operativity	8
1.2.2 Resonance-assisted hydrogen bonding	8
1.3 Prediction of hydrogen bond formation	9
1.3.1 Cambridge Structural Database and knowledge-mining	10
1.3.2 Graph Set Analysis	13
1.3.3 Topology	18
1.4 Crystal Engineering	21
1.5 References	23
Chapter 2 The Formation of Paracetamol (Acetaminophen) Adducts with Hydrogen-Bond Acceptors	26
2.1 Introduction	27
2.2 Experimental	27
2.2.1 Synthesis	27
2.2.2 Differential Scanning Calorimetry	28
2.2.3 Crystallography	28
2.3 Results	33
2.3.1 Paracetamol	33
2.3.2 The paracetamol:1,4-dioxane adduct	34

2.3.3	The paracetamol:4,4'-bipyridine adduct	36
2.3.4	The paracetamol:N-methylmorpholine/N,N'-dimethylpiperazine adduct	37
2.3.5	The paracetamol:morpholine adduct	38
2.3.6	The paracetamol:piperazine adduct	40
2.3.7	Differential Scanning Calorimetry	41
2.4	Discussion and conclusions	42
2.5	References	46
Chapter 3 The Formation of Quinol Co-crystals with Hydrogen-		
Bond Acceptors		47
3.1	Introduction	48
3.2	Experimental	49
3.2.1	Synthesis	49
3.2.2	Crystallography	50
3.3	Results	57
3.3.1	Quinol:1,4-Dioxane	57
3.3.2	Quinol:Pyrazine	59
3.3.3	Quinol:Piperazine	60
3.3.4	Quinol:2Morpholine	61
3.3.5	Quinol:2Pyridine	63
3.3.6	Quinol:2Piperidine	65
3.3.7	Quinol:2(4,4'-bipyridine)	66
3.3.8	Quinol:2N-methylmorpholine	68
3.3.9	Quinol:N,N'-dimethylpiperazine	69
3.4	Discussion and conclusions	70
3.5	References	74
Chapter 4 Co-Crystals of Formic and Acetic Acids with Isonicotinamide:		
Proton Migration in Formic Acid:Isonicotinamide		76
4.1	Introduction	77
4.2	Experimental	79
4.2.1	Synthesis	79

4.2.2	Crystallography	79
4.2.3	Variable Temperature study of <i>isonicotinamide:formic acid</i>	79
4.3	Results	83
4.3.1	<i>Isonicotinamide:formic acid</i>	83
4.3.2	<i>Isonicotinamide:acetic acid</i>	86
4.3.3	Comparison of <i>isonicotinamide</i> adducts	88
4.3.4	Variable temperature study	89
4.4	References	95
 Chapter 5 <i>The Low-Temperature and High-Pressure Crystal Structures of 2-chlorophenol and 4-fluorophenol</i>		 98
5.1	Introduction	99
5.2	Experimental	101
5.2.1	General Procedures	101
5.2.2	Crystal Growth at Ambient Pressure	101
5.2.3	Crystal Structure Determination of Ambient Pressure Phases	101
5.2.4	Crystal Growth at High Pressure	102
5.2.5	Structure Determinations of 2-Chlorophenol and 4-Fluorophenol at High-pressure	102
5.2.6	Inter-conversion of 4-fluorophenol-I and II	105
5.2.7	Software and other general crystallographic procedures	107
5.2.8	Computational Details (<i>Dr Graeme Day</i>)	107
5.3	Results	111
5.3.1	2-Chlorophenol at 100 K	112
5.3.2	2-Chlorophenol at 0.12 GPa	113
5.3.3	4-Fluorophenol at 150 K	115
5.3.4	4-Fluorophenol at 0.28 GPa	117
5.3.5	Crystal Structure Prediction: 2-Chlorophenol	118
5.3.6	Crystal Structure Prediction: 4-Fluorophenol	124
5.4	Discussion	130
5.4.1	Crystal Packing at low-temperature and high-pressure	130
5.4.2	Crystal Structure Predictions	135
5.5	Conclusions	135
5.6	References	136

Chapter 6	<i>The Crystal Structures of the Monofluoro- and Monochloro-Phenols at Low Temperature and High-Pressure</i>	141
6.1	Introduction	142
6.2	Experimental	144
6.2.1	Low temperature crystal growth	144
6.2.2	Crystal structure determination at low temperature	144
6.2.3	High-pressure: General Procedures	144
6.2.4	High-pressure crystal growth	145
6.2.5	Crystal structure determination at high-pressure	145
6.2.6	2-Fluorophenol	146
6.2.7	Recovery of 4-chlorophenol grown at high-pressure	147
6.2.8	Software and other general procedures	147
6.3	Results	152
6.3.1	3-Fluorophenol	152
6.3.2	3-Chlorophenol	153
6.3.3	4-Chlorophenol phase-I at 150 K	155
6.3.4	4-Chlorophenol phase-II at 150 K and at 0.02 GPa	157
6.3.5	2-Fluorophenol-I at 150 K	159
6.3.6	2-Fluorophenol-II at 0.36 GPa and 403 K	161
6.4	Discussion	163
6.5	Conclusions	165
6.6	References	165
Chapter 7	<i>Conclusions</i>	168
Appendices		171

Chapter 1

Introduction

1.1 Nature of the hydrogen bond

1.1.1 Definition

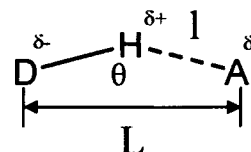
In the early part of the 20th Century many groups reported weak intermolecular interactions, that now can be attributed to hydrogen bonding, but no single definition was given, at that time, for these interactions. It was only in the 1920s that a formal definition of these weak interactions began to emerge. Latimer & Rodebush (1920) and Huggins (1922) provided definitions to classify intermolecular interactions, but it was Pauling who first defined the hydrogen bond. He wrote in his book *Nature of the Chemical bond* (1939): *Under certain conditions an atom of hydrogen is attracted by rather strong forces to two atoms instead of only one, so that it may be considered to be acting as a bond between them. This is called a hydrogen bond.*

This definition satisfied the scientific community for two decades before Pimental and McClellan (1960) realised that the definition did not take into account the scope of the large range of hydrogen bonds and that it needed to be reformulated. Their definition required that there is a specific donor and acceptor atom present within the hydrogen bond. *A hydrogen bond exists between the functional group, A-H, and an atom or a group of atoms, B, in the same or different molecules when (a) there is evidence of a bond formation (association or chelation), (b) there is evidence that this new bond linking A-H and B specifically involves a hydrogen atom already bonded to A.*

In his review of hydrogen bonding Steiner (2002) highlighted a few problems with this definition. He realised that, as it stands, it could include other interactions such as van der Waals contacts. The chemical nature of each of the participating groups was not specified; including the overall polarities and charges. He proposed an amendment to the definition of Pimental and McClellan. *An X-H...A interaction is called a "hydrogen bond", if 1. It constitutes a local bond, and 2. X-H acts as a donor to A.* The second point of Steiner's definition excludes van der Waals contacts as it implies donation of a proton from the X group to the A group. This definition of a hydrogen bond is specific to a range of interactions where the hydrogen acts as a proton, with the X and A groups being electronegative groups, though this does not exclude donor atoms such as carbon.

The notation described by Steiner (X-H...A) is used widely in the literature to signify hydrogen bonding interactions. In this Thesis, however, this notation is modified to D-H...A

where D is the donor atom and A is the acceptor atom. This simple description of a hydrogen bond can be defined using three geometrical parameters; two distances and one angle (Scheme 1.1). The two distances are defined as l and L and the angle defined as θ (Scheme 1.1).



Scheme 1.1: A simple model of a hydrogen bond showing the geometrical parameters: l = H...A distance, L = D...A distance and θ = D-H...A angle.

The determination of these parameters has become routine with the advancement in X-ray crystallographic techniques. Although X-ray crystallography is the method of choice for structure determination in the solid state, it has some disadvantages with regard to hydrogen bonding because it relies on scattering by electrons. Hydrogen has only one electron, which is involved in the D-H bond, and this causes an apparent shortening of the covalent bond (if the electron density is seen at all). Hydrogen atoms can usually be located nowadays for small organic systems, though this is still problematic for crystals with heavy scatterers. These problems have led to the use of the D...A distances as a guide to whether hydrogen bonding exists between two groups. An advantage of this is that the D...A distances are more precisely determined in comparison to H...A distances. The disadvantage to this method is that some intermolecular interactions are labelled as hydrogen bonds when they should only be considered as van der Waals interactions. An example of this was in the first determination of α -glycine (Albrecht & Corey, 1939). The structure of α -glycine has four hydrogen bonding contacts per molecule when considering only the N...O contacts implying the presence of a bifurcated hydrogen bond (the first reported incidence of this type of H-bond). Recent studies of α -glycine by neutron diffraction shows one of the H...O contacts is outside that expected for a hydrogen bond (2.362(2) Å) and that this interaction should be considered as a van der Waals contact (Figure 1.1, Langan *et al.*, 2002). The above example shows that in ambiguous cases accurate hydrogen atom determination is crucial to the correct assignment of interactions in the solid state.

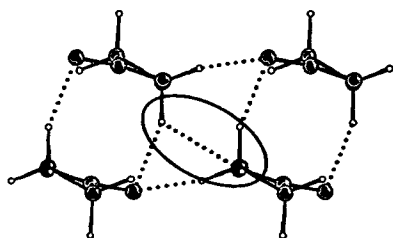


Figure 1.1: Intermolecular interactions observed in α -glycine. Classification of H-bonds with regard to N...O distances led to the incorrect assignment of a vdW contact as a hydrogen bond (circled). N...O distance 2.9504(10) Å; H...O 2.362(2) Å; NH...O 114.92(17)°.

The best method for the determination of hydrogen atom positions is neutron diffraction, the method by which the above problem was solved. Indeed, hydrogen atoms determined by X-ray diffraction are usually normalised so that D-H distances are set to those determined by neutron diffraction (Jeffrey, 1997). This allows the direct comparison of hydrogen bonds with those in the literature. Table 1.1 gives an example where the normalised hydrogen bond distances from the X-ray experiment are comparable with neutron diffraction studies.

Carbohydrate	O-H (Å)		H...O (Å)		
	X-ray	Neutron	X-ray	Normalised	Neutron
Methyl α -D-altropyranoside	0.81	0.971	1.90	1.74	1.736
	0.88	0.961	2.00	1.91	1.922
Methyl α -D-glucopyranoside	0.87	0.985	1.84	1.74	1.738
	0.97	0.969	1.76	1.76	1.770
Methyl α -D-mannopyranoside	0.80	0.976	1.98	1.81	1.810
	0.67	0.957	2.22	1.96	1.998
	0.96	0.959	2.07	2.05	2.052

Table 1.1: Hydrogen bonding distances of some carbohydrates using both X-ray and Neutron diffraction. The H-bond distances determined using X-rays have been normalised (O-H 0.97; N-H 0.99; C-H 1.01) for comparison with Neutron values.

1.1.2 Classification of hydrogen bonds

The parameters described in the previous section enabled Jeffrey to classify hydrogen bonds further into strong, moderate and weak hydrogen bonds (Table 1.2, Jeffrey, 1997).

	Strong	Moderate	Weak
Interaction type	mostly covalent	mostly electrostatic	electrostatic
Bond lengths			
H.....B (Å)	~1.2-1.5	~1.5-2.2	~2.2-3.2
A.....B (Å)	2.2-2.5	2.5-3.2	3.2-4.0
Bond angles(°)	175-180	130-180	90-150
Bond energy (kJ mol ⁻¹)	58-167	17-63	<17

Table 1.2: Properties of strong, moderate and weak hydrogen as defined by Jeffrey (1997).

The strong interactions are exemplified by hydrogen bifluoride (D...A, 2.293(3) Å, Silva *et al.*, 2001). These hydrogen bonds have a large energy associated with them (148-160 kJ/mol) and are predominantly covalent in nature. The donor and acceptor atoms in this system are undefined as the hydrogen is centred within the bond. Moderate hydrogen bonds are wide spread and are classed as 'normal' by Steiner. Terms like 'conventional' are also applied. These interactions are typified by alcohol...carbonyl contacts such as those in paracetamol (Chapter 2). The O(H)...O(C) H-bond length in paracetamol has been determined as 2.724(5) Å (Haisa *et al.*, 1974), and this is typical of this type of interaction. Unlike the strong H-bonds the hydrogen atom resides on the alcohol rather than in the centre of the bond. There are some systems that have a borderline strong interaction (2.42 – 2.61 Å) between the donor and acceptor atoms yielding unusual proton behaviour. This is exemplified by *isonicotinamide:formic acid* (Chapter 4) (O...N 2.5468(16) Å) where the proton is disordered over two sites. Other examples of this behaviour are seen in benzoic acid (Wilson *et al.*, 1996); migration of the proton from one atom to the other has also been observed in co-crystals of pentachlorophenol with methylpyridines (Steiner *et al.*, 2000, Steiner *et al.*, 2001) and in the co-crystal of urea and phosphoric acid (Wilson, 2001; Parkin *et al.*, 2004a). Weak interactions, such as CH...O, have been an area of heated debate in the past but are now widely accepted as 'weak hydrogen bonds' (Desiraju & Steiner, 1999).

Diffraction methods, and H-bonding distances derived from them, are not the only method for the characterisation of the H-bond. Infrared spectroscopy (IR) has been used to follow the formation of a hydrogen bond through the decrease in the D-H stretching frequency (Jeffrey, 1997). The analysis of bond stretching frequencies makes IR spectroscopy a very sensitive method for the study of H-bonds, weak H-bonds were first detected

spectroscopically (Jeffrey, 1997). A schematic of the potential energy (P.E.) curve for a free and hydrogen bonded D-H is shown in Figure 1.2.

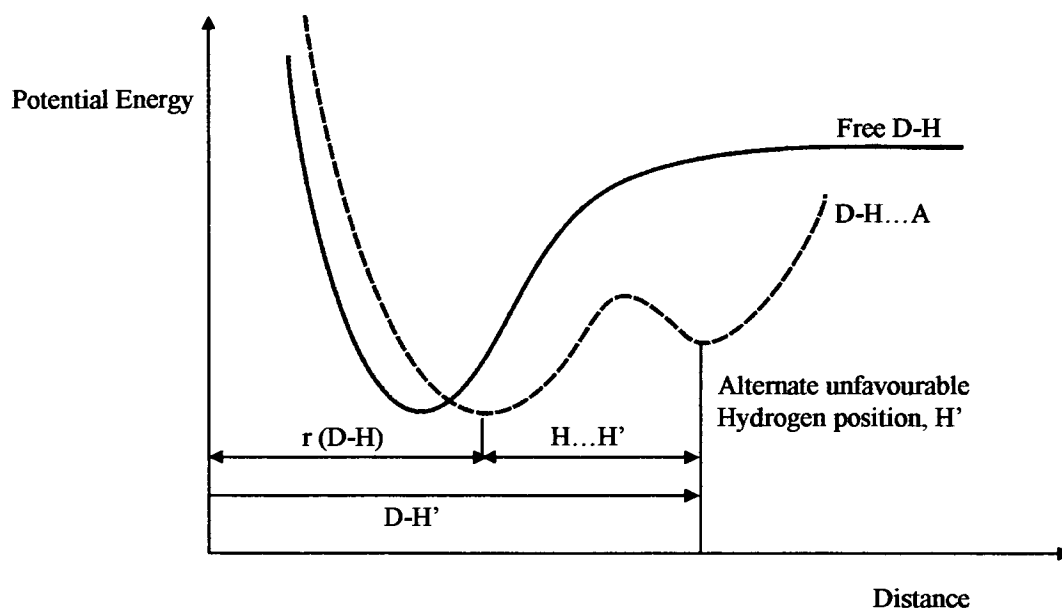


Figure 1.2: Schematic of a potential energy curve for a free and hydrogen bonded D-H group. (Jeffrey, 1997)

The potential energy well for the free D-H group shows one deep minimum in which the hydrogen atom resides. On formation of a hydrogen bond the D-H distance elongates slightly and a second minimum is formed corresponding to the interaction of hydrogen with the acceptor atom. An example of the elongation of the D-H bond with increase in hydrogen bonding is observed in ammonia where the N-H bond was calculated to be 1.008(4) Å in the gas phase and 1.061(5) Å in the solid state where the N-H group is involved in H-bonding (Morrison & Siddick, 2003). The unsymmetrical P.E. curve shown in Figure 1.2 is typical of a moderate hydrogen bond. Stronger hydrogen bonds tend to form symmetrical P.E. wells where the minima are energetically equal (Figure 1.3). The potential energy barrier between the two minima is much lower than with moderate H-bonds and can allow hydrogen migration with a change in environment such as temperature (see Chapter 4). With even stronger interactions the potential energy barrier can disappear altogether leaving a single minimum (a centred H-bond).

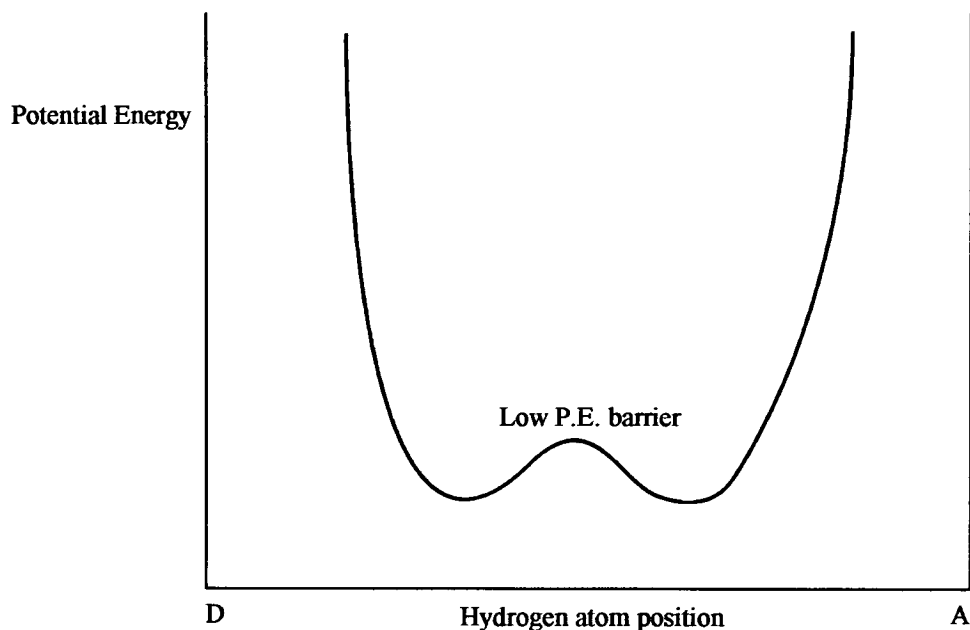


Figure 1.3: Schematic of the potential energy diagram for a strong hydrogen bond. Note the low potential energy barrier. The low barrier can allow proton migration to occur with small changes in environment.

The potential energy curves shown in Figure 1.2 and 1.3 show the total energy in the hydrogen bond. Much like the overall crystal structure lattice energy, hydrogen bond energies are a complex addition of many different energy terms.

1.1.3 Theory of hydrogen bonds

Theoretical calculations of the hydrogen bond energies have been investigated since the 1970s where Morokuma (1977) first partitioned the hydrogen bond into five different energy contributions. These come in the form of electrostatics (E_{el}), polarisation (E_{pol}), charge transfer (E_{ct}), dispersion (E_{disp}) and exchange repulsion (E_{ex}). Although different theories have evolved since then, the separation of the hydrogen bond energies still follows the same general divisions as those used by Morokuma. Each energy term contributes differently to the overall hydrogen bonding energy depending on the strength of hydrogen bond. Calculations have shown that the main energy contribution to a moderate hydrogen bond is the electrostatic term (Morokuma, 1977). Stronger hydrogen bonds are not modelled well using simple electrostatic terms as the hydrogen bond is pseudocovalent in nature (Steiner, 2002).

1.2 *The Hydrogen bond in the solid state*

The potential energy curves described in the previous section represent the interaction between an isolated donor and acceptor group. When incorporated into the crystal lattice these simple potential energy curves change as there are many different forces that combine to determine the most thermodynamically stable structure. Characteristic motifs are frequently associated with hydrogen bonds formed between specific functional groups, for example, certain motifs, like the OH...OH... chains in alcohols and dimers in carboxylic acids are more common than other motifs. One reason behind the formation of these types of motif can be attributed to the effects known as σ -bond co-operativity and resonance-assisted hydrogen bonding.

1.2.1 σ -bond co-operativity

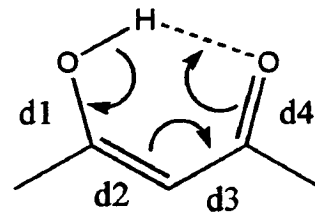
The effect known as σ -bond co-operativity can occur when two hydrogen bonded groups closely interact to form a stronger hydrogen bond. An example of this behaviour is observed in OH...OH...chains. On formation of a hydrogen bond to A, the donating group, D-H, becomes more polar. If this second group, A-H, hydrogen bonds to another group it too will become more polar increasing the strength of the D-H...A interaction. This helps to explain the clustering of hydroxyl groups into chain and ring motifs.

1.2.2 *Resonance-assisted hydrogen bonding (RAHB)*

Resonance-assisted hydrogen bonding (RAHB) occurs in systems where there is conjugated π -bonding. Examples of such systems are the β -diketone enolates, amide groups and carboxylic acid groups. In a hydrogen-bonded amide chain the ability of the amide group to form resonant forms means that there is a flow of electron density towards the acceptor group (Figure 1.4a). The increase of electron density on the acceptor together with the decrease of electron density around the donor H results in the H-bond being much more polar and hence stronger. Etter (1982) observed that amide carbonyls were better acceptors than lone carbonyl groups which could be, in part, attributed to resonance-assisted hydrogen bonding. Gilli *et al.* (1989) observed RAHB in intramolecular hydrogen bonds in β -diketone enolates (Scheme 1.2), comparisons were made of the bond lengths around the diketone moiety and a delocalisation parameter was defined: $[Q = (d1-d4)+(d3-d2)]$ (see Scheme 1.2).

The value of Q is an indication of the delocalisation around the ring; a Q value of zero indicates that the system is completely delocalised. (Figure 1.4b).

RAHB is of great interest in the context of DNA base pairing where the purine adenine always pairs with the pyrimidine thymine. The ability of both groups to form resonant forms enhances the hydrogen bonds between the two bases (Figure 1.4c).



Scheme 1.2: Resonance-assisted hydrogen bonding in β -diketone enolates; d1 to d4 are bond lengths in Å.

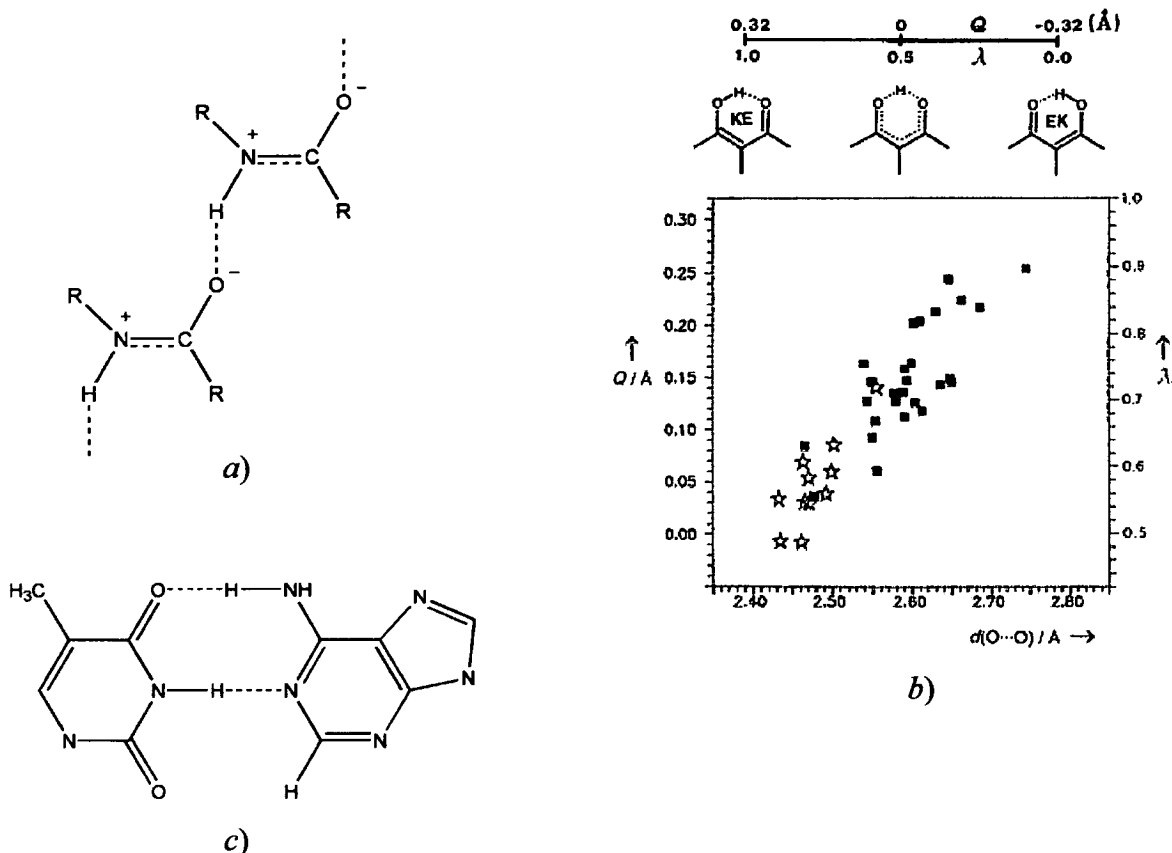


Figure 1.4: a) Resonant form of an amide chain. b) The graph shows the parameter Q (measure of π -delocalisation) against the O...O distance (Å) in a set of enolones (taken from Steiner, 2002); the amount of π -delocalisation decreases with O...O separation. The value λ is the state of the fragment; a λ value of 1, 0.5 & 0 means that the fragment is in the ketoenol, fully delocalised or enolketo states, respectively. c) Resonance-assisted hydrogen bonding in DNA, the purine from adenine pairing with the pyrimidine of thymine.

1.3 Prediction of hydrogen bond formation

The two effects described above enhance H-bonding between groups that are predisposed to them. An investigation into the hierarchy of hydrogen bonds was first

attempted by Etter in 1990. She formulated rules of hydrogen bonding that could be applied to predict which bonds would be formed in a crystal structure.

There are three general rules that can be applied to all types of molecules as well as rules that can be applied to specific molecules such as nitroanilines and diarylureas: 1) All good donors and acceptors are used in hydrogen bonding; 2) Six-membered-ring intramolecular hydrogen bonds form in preference to intermolecular bonds; and 3) The best proton donors and acceptors remaining after intramolecular hydrogen-bond formation form intermolecular hydrogen bonds to one another. These rules are still applied today although other statistical methods are being developed to quantify the likelihood of formation of different types of bonds.

1.3.1 Cambridge Structural Database and knowledge mining

The Cambridge Structural Database (CSD) (Allen, 2002; Allen & Motherwell, 2002), contains over 300,000 crystal structures of organic and organometallic compounds, and it provides statistical evidence to test hypotheses proposed by experimentalists. For example, Taylor and Kennard (1982) used the Database to show that CH...O interactions can be classified as hydrogen bonds. With the advancement of X-ray crystallography and the speed with which crystal structures are determined the database has grown rapidly over recent years. The increase in size of the CSD implies that searches conducted on the database are becoming more statistically meaningful every year (though many searches still yield surprisingly few hits). Allen *et al.* (1999) have used the database to study the probability of formation of 75 different biomolecular ring systems. The probability of formation parameter (P_m) was calculated by counting the number of times a specific motif was formed (N_{obs}) and dividing that result by the number of times it could have been formed (N_{poss}). They concluded that the likelihood of formation of a certain motif increases with the number of points of recognition in that motif; a motif with three hydrogen bonds present is much more likely to form than those with only two bonds. One surprising result was that the carboxylic acid dimer, which is assumed to be a very robust motif, had a P_m of 33%. This is much lower than might have been expected for this motif. The reason given for this low value was competition for the carboxyl group from other acceptors such as water. If this parameter was calculated again on C, H and O structures with no other donors or acceptors the P_m increased to 95% indicating that this is the likely cause for the low probability in this study.

Steiner (2001) studied the hydrogen bonding in carboxyl groups further by looking at the competition between acceptors for carboxyl donors using the CSD. He found that only 29% of donor contacts from carboxyl are to other carboxyl groups and of these 85% formed the acid dimer with the other 15% forming acyclic motifs. 71% of all interactions from the carboxyl moiety are to a variety of different acceptors. He devised a measure of success that can be calculated for different acceptor groups so that they can be directly compared with one another. The relative success is defined as:

$$succ(A) = n(OH...A) / [n(OH...A) + n(OH...O_{\text{carboxyl}})].$$

The success rate was high for such groups as the carboxylate (97%) and N(pyridine) (91%) but low for groups such as ether (13%). Both studies have great implications for crystal engineering and structural prediction where results of hydrogen bond competition could prove very useful.

Oswald *et al.* (2004) took a different approach to using the CSD in which the database was used to rationalise the formation of a set of paracetamol co-crystals. By this method, the various functional groups present within the molecules studied were identified and a matrix of donors and acceptor molecules was created (Table 1.3 shows a sample). The CSD was used to search for the various combinations of donor and acceptor molecules and the average hydrogen bond distance (DH...A) was calculated. The length of interaction was taken to correspond to the strength of a hydrogen bond (a reasonable assumption as the H-bond is primarily an electrostatic interaction), and with reference to this matrix, the structures of six co-crystals with paracetamol were rationalised from the structure of pure paracetamol.

Both polymorphs of paracetamol use the same two hydrogen bonds, a stronger OH...OC and a weaker NH...O(H). On co-crystallisation with a guest molecule the weaker of the two interactions (NH...O(H)) is broken first with the stronger interaction only being broken when increased steric factors and extra H-bonding moieties are introduced to the system by the guest molecule. A similar method was also applied to the analysis of co-crystals of quinol (Chapter 3).

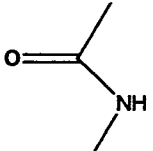
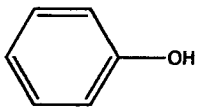
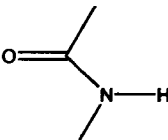
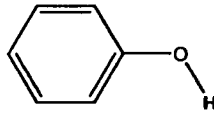
	Acceptor (O or N in each case)		
Donor (NH or OH)			
	Sample size Max NH..A /Å Min NH..A /Å Mean NH..A /Å	1250 2.20 1.73 1.92	14 2.14 1.79 2.01
	Sample size Max OH..A /Å Min OH..A /Å Mean OH..A /Å	49 2.19 1.60 1.78	256 2.20 1.67 1.87

Table 1.3: The matrix created to help rationalise the formation of a series of paracetamol adducts. On the left of the table are the donor moieties in paracetamol and on the top are the acceptor moieties. The values are the sample size, maximum, minimum and mean distances for the interactions taken from the CSD (2002).

Recent publications by Infantes and Motherwell (2004*a, b*) described a new relational database that contains information about interactions around a number of different functional groups. *CSDcontact* provides information on many different functional groups such as the number of donor and acceptor contacts to the group. This information can be correlated with the accessible surface area on a group or ratio of donors to acceptors to produce graphs that may reveal underlying trends. Figure 1.5 shows a graph for a ketone oxygen acceptor. The number of occurrences, for zero, one or two contacts, has been plotted against the average accessible surface area for the Keto-O. It can be seen from this graph that no contacts occur when there is low accessibility to the oxygen surface. As the accessible surface area increases the number of observed contacts increases also. Use of this type of database can help to give a better understanding of the hydrogen bonding that may occur in a molecule with certain functional groups so that given a molecular formula the directions of likely H-bonds may be calculated.

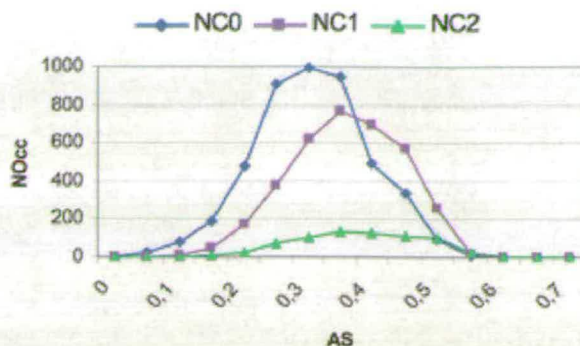


Figure 1.5: Diagram for a keto-O group showing the number of occurrences, Nocc, against average accessible surface, AS. The separate graphs are for different number of contacts. (Motherwell and Infantes, 2004a)

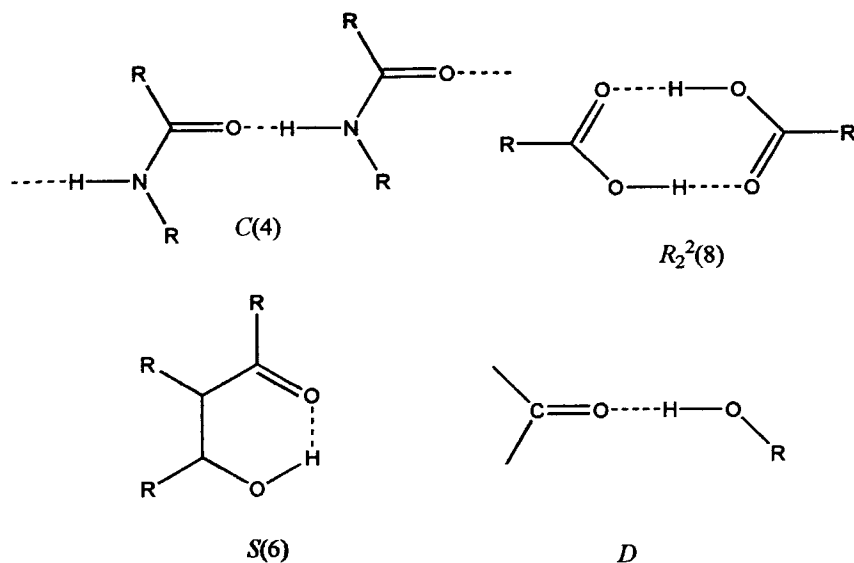
1.3.2 Graph Set Analysis

Analysis and description of H-bonding patterns in crystal structures can become daunting in cases where the molecules form complicated 3-dimensional networks. The work of Etter *et al.* (1990) simplifies the problem of crystal structure description to topological analysis of the structure using Graph Set Analysis. Previous attempts had been made by Wells (1962) and Hamilton & Ibers (1968) to simplify crystal structures to points and lines for molecules and hydrogen bonds, respectively. Kuleshova & Zorky (1980) developed these early attempts with use of graph theory to organic systems. Etter *et al.* furthered the idea to looking at molecules rather than points. Since its development Graph Set Analysis has become an integral part of crystal structure description and is used widely in structural papers. Although widely used in the literature there were still some common misinterpretations with regard to the assignment of Graph Sets, which Bernstein *et al.* (1995) addressed in their paper. The main advantage of this analysis is that it can be used to break complex hydrogen bonded structures down into small repeated motifs.

The notation used by Etter *et al.* is defined as:

$$G_d^a(n),$$

where G represents the pattern descriptor, d denotes the number of donor atoms, a designates the number of acceptor atoms and n represents the number of atoms used in the pattern or *degree*. There are four different pattern descriptors that can be used; C , R , S , D . C denotes an infinite hydrogen bonded chain, R denotes a ring pattern, S denotes an intramolecular bond and D represents a discrete hydrogen bond. Examples of these types of patterns are shown in Scheme 1.3.



Scheme 1.3: Possible patterns and their graph set. From top left: Amide chain motif comprising of four atoms, $C(4)$; carboxylic dimer formed over an inversion centre resulting in a $R_2^2(8)$ motif; An intramolecular hydrogen bond between an alcohol and a carbonyl group $S(6)$; A discrete hydrogen bond that does not take part in any other pattern, D .

The parameter n is the degree of the pattern. Chains motifs count the number of atoms in the repeating unit as the degree, a catemeric amide chain has a $C(4)$ graph set (Scheme 1.3). Intramolecular patterns (S) and intermolecular ring (R) patterns count the number of atoms in the ring. The example of an intermolecular ring motif shown in Scheme 1.3 is a characteristic motif for monofunctional carboxylic acids, and amides. Patterns designated D are discrete pattern and usually only involve one donor and one acceptor that are not part of any other patterns.

The number of motifs present in the crystal structure is dependent on the number of crystallographically different hydrogen bonds in the system; by definition, each motif consists of only one crystallographically distinct hydrogen bond. The graph sets for each motif can be combined to describe the crystal structure in terms of a *unitary* level graph set where all the descriptors for each motif are listed (see the following example). It may be more informative to describe a system using two crystallographically different hydrogen bonds. These graph sets are described as *binary* graph sets but for consistency, the unitary graph set is preferred at the start of an analysis. It is possible to describe the structure in terms of *ternary* or higher level graph sets should this be the most informative descriptor.

The list of graph sets produced from this analysis should give the pathways through the structure that have the lowest degree (number of atoms). These graph sets are commonly

termed the *basic* graph sets. Other pathways through the structures may involve the same hydrogen bonds but have a higher degree; these are termed *complex* graph sets.

The structure of paracetamol can be used to illustrate the technique of graph set analysis. Figure 1.6 shows the structure of form II of paracetamol, viewed down the *b*-axis. It is a layered structure with only two crystallographically distinct hydrogen bonds; there are only two unitary motifs designated for this structure. The first hydrogen bond is the OH...O=C interaction; when followed through the structure the set of these interactions form chains (*C*). The formation of the chain utilises only one donor atom and one acceptor atom therefore *a* and *d*, in the above definition, have a value of 1; convention states that if these values are 1 they are often omitted from the designator. There are nine atoms contained in the repeating unit resulting in a $C_1^1(9)$ or $C(9)$ graph set. If the same procedure is followed for the NH...O(H) hydrogen bond a second unitary descriptor, $C(7)$, is formed; the complete unitary graph set is then $C(9)C(7)$. The unitary graph set may not include 'obvious' features in the structure such as other chain motifs and rings, because they involve more than one crystallographically independent H-bond. Another description of this structure uses the $C(9)$ descriptor as above and also a binary chain graph set, $C_2^2(6)$, running perpendicular to it (Figure 1.6). In addition to these two chain motifs the structure can be described as consisting of rings containing four donor and acceptor atoms and having a degree of 22 described by a complex binary graph set, $R_4^4(22)$. Analysis of a 3-dimensional hydrogen bonded network, however, is a very complicated procedure and for this the CCDC has developed a routine in RPLUTO to help with this procedure (Motherwell *et al.*, 1999).

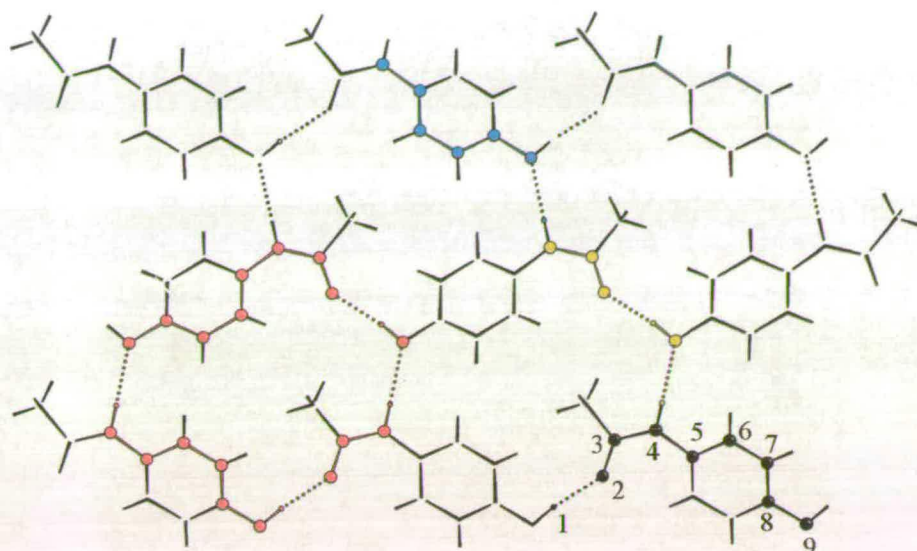


Figure 1.6: Orthorhombic paracetamol viewed down the b -axis with its graph sets highlighted. $C(9)$, black (with numbering); $C(7)$, blue; $C_2^2(6)$, yellow and $R_4^4(22)$, red.

The advantage of graph set analysis is that it assists in making comparisons between two structures. This is exemplified by α - and γ -glycine. The similarities of these two structures are difficult to discern until graph set notation is applied. Despite crystallising in very different space groups with apparently very different motifs (spiral chains and layers) the same $C(5)$ graph set motif is retained in both structures (Figure 1.7).

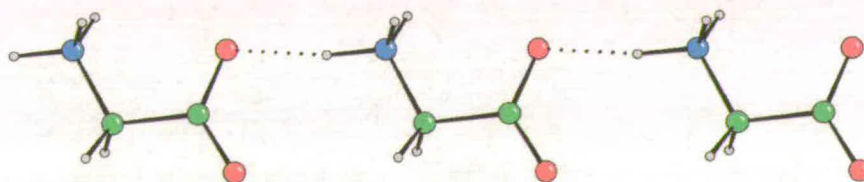


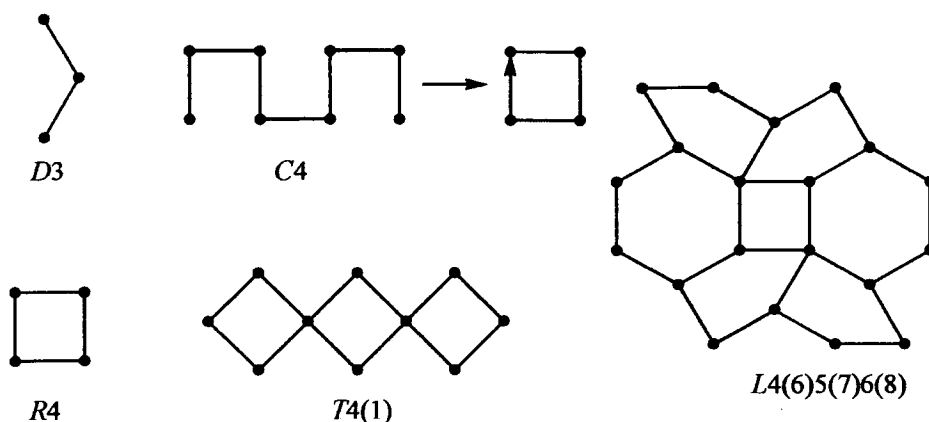
Figure 1.7: The $C(5)$ chain observed in both alpha and gamma polymorphs of glycine. It is the interaction of these chains that differ in each polymorph.

Describing the structures in this way may provide a better understanding of the crystallisation process of glycine. This example does, however, highlight a problem with graph set notation. In some circumstances it can help visualise the similarities within structures, but it can also give identical graph sets to two completely different polymorphs. This is an inherent problem of reducing structures to strings of descriptors. Another example

is in MOGUL where ‘wrong’ structures are sometimes compared (Bruno *et al.*, 2004). By referring to a structure by its graph set one may neglect important information about the crystal structure. Paracetamol is another example, where both polymorphs have identical graph sets. The simple description of the crystal structure that graph set notation affords fails to describe the non-polar layers in Form II as opposed to the polar nature of the layers in Form I (Chapter 2). Graph set analysis has proved to be a useful tool in structural chemistry but the oversimplification of structures means that visual comparison of structures in three-dimensions using a visualisation program like MERCURY (Bruno *et al.*, 2002) will always be necessary.

Other groups have followed Etter *et al.* by applying graph set techniques to specific classes of structures. A recent publication by Infantes and Motherwell (2002) has shown that water molecules, incorporated in structures as water of crystallisation, form regular motifs. This study was extended to include contacts to the organic hosts (Infantes *et al.*, 2003a). They established nomenclature for different water motifs observed in the CSD. Patterns include discrete chains (*D*) and rings (*R*), infinite chains (*C*), tapes (*T*) and layers (*L*); examples of these are shown in Scheme 1.4. The first four of these descriptors are augmented by the number of atoms in the pattern, *n*. The tape motif is composed of rings that either share a common water molecule (edge sharing) or are linked together through a hydrogen bond. This designator is given a second number in brackets that indicates how many atoms are shared by neighbouring rings to form the tape motif. If no atoms are shared, then a further descriptor, *A_k*, is used which indicates the number of atoms linking the rings together. The layer motif has a much larger descriptor, *L_{m(r)n(s)p(t)}*, where rings of size *m, n and p* are surrounded by *r, s, t* adjacent rings.

Infantes and Motherwell found that discrete chains of water molecules were by far the most common motif found for water molecules. The common observation of water ‘pockets’ can be attributed to these patterns. Other popular motifs were rings with four to six atoms. They found that the organic molecules helped to extend these discrete entities into extended motifs. The promotion of hydrate formation by different functional groups was also investigated, and it was shown that the likelihood increased with the polarity of the functional groups (e.g. COO⁻). The number of polar groups per formula unit also enhanced the possibility of hydration.



Scheme 1.4: Possible water motifs with their descriptors. *D3*, discrete chain of 3 water molecules; *C4*, extended chain with a repeating unit of four water molecules in a helix; *R4* ring of four water molecules; *T4(1)* rings of four molecules joined via a one shared water; *L4(6)5(7)6(8)*, layer of waters with rings of sizes 4, 5 and 6. Each ring is surrounded by 6, 7 and 8 other rings, respectively.

1.3.3 Topology

Graph set and other analyses of hydrogen bonding patterns have focussed on the arrangements of the hydrogen bonding functionalities with respect to one another. The overall packing arrangement is a secondary factor in these analyses. Alcohols, such as those described in Chapters 5 and 6 by graph set analysis, usually form chain motifs, but this fails to describe the packing arrangement of the R-groups, which are just as important.

A well-known investigation of molecular packing patterns was performed by Kitaigorodskii (1973), who showed that many molecular crystal structures can be viewed as arrays of close-packed spheres with distortions imposed by the deviations of the molecules themselves from spherical symmetry. This idea has been further developed by Blatov. This type of analysis is based on the packing of hard spheres. There are three different arrangements that can be adopted; hexagonal closed packing (HCP), cubic closed packed (CCP) and body centred cubic (BCC). The first two types of packing represent the most efficient packing arrangement with each sphere being surrounded by 12 others and differ only in the arrangement of layers with respect to each other. Hexagonal close packed has two different layers, which pack to give an ABABAB layered structure. Cubic closed packed has three different layers that combine to give ABCABC layering. Body centred cubic has less efficient packing where the co-ordination number is 14. In this arrangement eight close

contacts form the corners of the cube with the other six molecules taking positions at the heart of adjacent cubes. These packing arrangements account for the majority of elemental metallic crystal structures.

The packing of spheres can be analysed using Voronoi-Dirichlet polyhedra (VDP). Voronoi-Dirichlet analysis is a method for partitioning space. Figure 1.8*a* shows a two-dimensional example of a Voronoi-Dirichlet plot. The space is partitioned into smaller areas by drawing a line bisecting every pair of points on the map. The end result is a map divided into many different polygons. Very close points form the longest edges of the polygon and longer interactions forming the shortest edges. These plots can be extended to three dimensions to give polyhedra where the largest faces of the polyhedra correspond to the strongest interactions. The number of sides of the polyhedra is the co-ordination number associated with that point. The resulting VDPs for HCP, CCP and BCC solids are shown in Figure 1.8*b*.

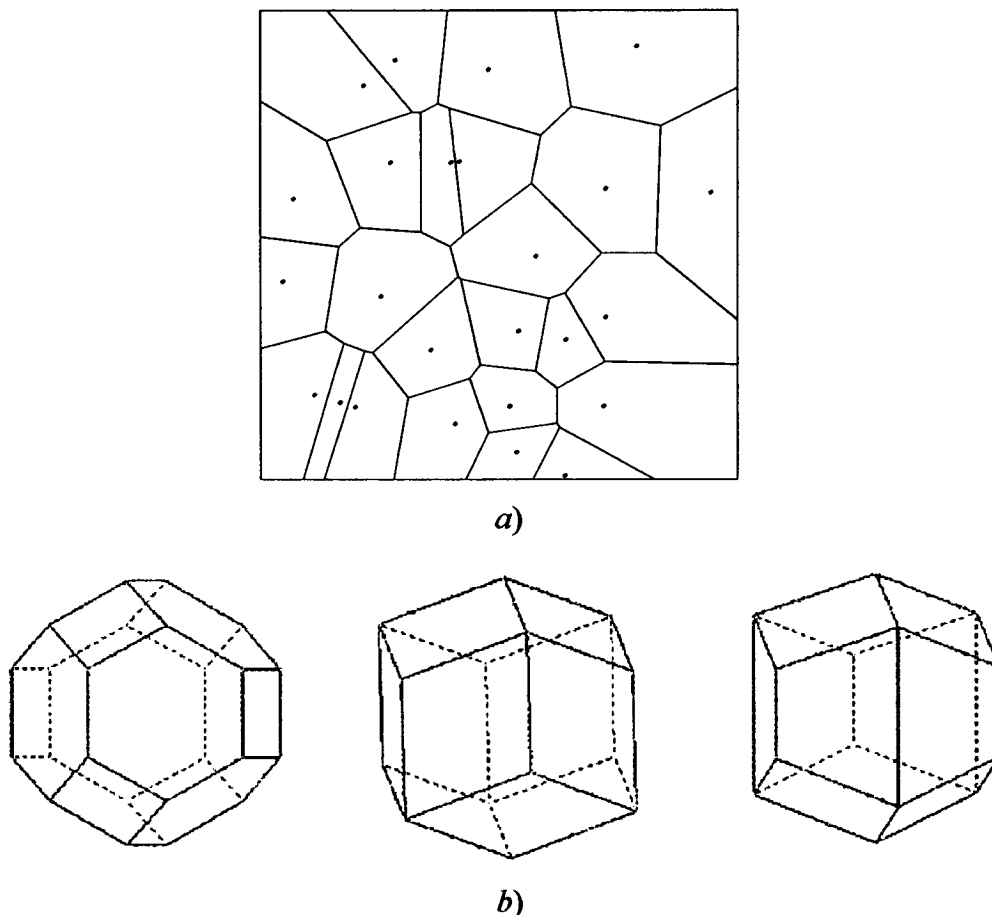


Figure 1.8: *a*) The partitioning of two-dimensional space into Voronoi-Dirichlet polygons (Byers, 1992)(<http://www.wcrl.ars.usda.gov/cec/java2/dirichle.htm>). *b*) The VDPs for perfect body centred cubic, cubic closed packed and hexagonal closed packed.

Blatov & Peresypkina (2000) have developed the VDP analysis further to consider molecular solids. The crystal structure is simplified to an array of molecular centroids. An example of the use of VDPs is given by Parkin *et al.* (2004b), where VDPs are used to analyse the packing behaviour in the series of cyclohexane, piperidine, piperazine and morpholine, which have differing H-bonding capabilities; piperidine has one NH group substituted into the ring, piperazine has a further substitution of a NH group in the 4 position and morpholine replaces one of the NH groups with an oxygen. Cyclohexane crystallises in a layered structure with the molecules lying parallel to these layers. The crystal structures of all three derivatives show the same layered structure but with hydrogen bonding between the layers. As a result of the H-bonding the molecules are orientated perpendicular to the layers.

Calculation of the VDP for cyclohexane shows the co-ordination number to be 14. Closer inspection of the VDP reveals that two faces of the polyhedra are very small indicating very little interaction with those points, and the cyclohexane is better described as 12 co-ordinate. The VDP for cyclohexane is very similar to that of a CCP structure. The other molecules studied all behave similarly, where two interactions could be deemed as insignificant compared with the others, giving a final co-ordination number of 12. The derivatives pack in two different arrangements. Piperazine adopts a CCP arrangement of centroids, whereas piperidine and morpholine adopt HCP geometry. This is attributed to the location of the molecules with respect to inversion centres present in the space group (piperidine, $P2_1/c$) or 'effective' space group (considering only the centroids in the case of morpholine). Distortion from ideal arrangement was correlated with H-bond formation.

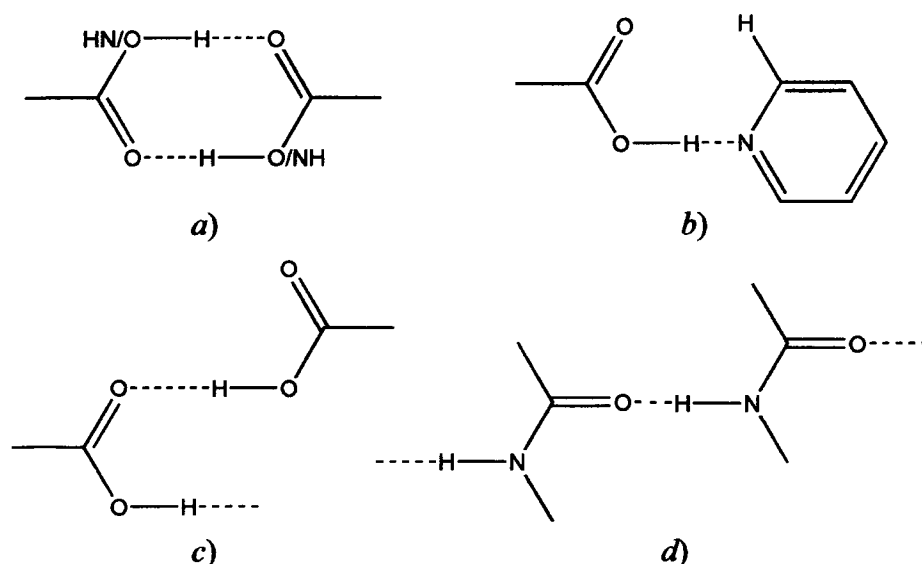
All the methods outlined in this section from analysis of hydrogen bonding patterns to analysis of molecular packing are of great importance to two growing areas of research, crystal structure prediction and crystal engineering. Crystal structure prediction is very much in its infancy although present research shows that is becoming more accurate (Chapter 5). Results from analysis of crystal structures whether it be H-bonding patterns or packing studies can be used to help inform the prediction procedure. Successful modelling of crystal structures by computer has great implications for many areas of research not least in drug design. The modelling of active sites in biological molecules and drug interaction with them is of great interest to the pharmaceutical industry. Studying intermolecular interactions via crystal engineering can provide information that can be incorporated into simulations to provide better drug designs.

1.4 Crystal engineering

Crystal engineering (co-crystallisation) is described as *the understanding of intermolecular interactions in the context of crystal packing and in the utilisation of such understanding in the design of new solids with desired physical and chemical properties* (Desiraju, 1995). Many parallels have been drawn between crystal engineering and organic synthesis where molecules are compared to atoms and intermolecular interactions are compared to covalent bonds. One can trace this idea back to the early articles on graph theory where the molecules were represented by nodes or 'atoms' and the intermolecular interactions as 'bonds' to define H-bonded patterns. So wide-spread is this analogy that green chemists refer to crystal engineering as 'non-covalent derivatisation' (Anastas & Warner, 2002). A demonstration of the power of co-crystals to mimic covalently bonded structures was presented by Infantes *et al.* (2003b). In this paper they compared the crystal structures of seven covalently bonded molecules with the crystal structures of their supermolecular analogues. In this study molecules with a tetrazine group were replaced by the carboxylic dimer analogues which are geometrically similar. They found that three out of the seven engineered structures matched the structures of the covalent compounds, two had similarities in the packing of the molecules but two compounds showed no similarities. No attempt was made to screen for different polymorphs, an attempt to do so may have yielded structures matching the covalent counterparts.

Green chemists look to non-covalent derivatisation as a way of obtaining compounds with modified physical properties whilst reducing the side effects of organic synthesis such as the production of harmful side products and copious use of environmentally harmful solvents in the manufacturing process. Infantes' paper shows that supermolecular analogues can structurally mimic covalently bonded molecules in the solid state, whether these derivatives can also provide the chemical requirements remains to be seen.

The engineering of crystal structures relies on *synthons* being formed to combine molecules together into larger supermolecules (Scheme 1.5). The goal of crystal engineering has been to try and find a hierarchy of synthon synthesis i.e. to find which synthons will be formed first. This is very closely related to Etter's goal with regard to single intermolecular interactions. Supramolecular synthons usually consist of more than one intermolecular interaction, but from the crystal engineering point of view are regarded as one entity. A few exceptions to this rule were highlighted by Desiraju (1995) in his review such as interhalogen contacts e.g. Cl...Cl.



Scheme 1.5: Typical synthons used in crystal engineering. *a)* the carboxylic acid/amide dimer; *b)* carboxylic acid:pyridine *c)* carboxylic acid catemer *d)* *trans*-amide catemer.

Many of the synthons used in crystal engineering are familiar from the work in graph set analysis; carboxylic acid dimers, $R_2^2(8)$ and *trans*-amide chains, $C(4)$. These synthons involving 'normal' hydrogen bonds make regular appearances in crystal engineering studies because they can be relied upon to form given a specific system. Other synthons that are receiving more attention in the literature are those that involve both strong and weak interactions like the carboxylic acid:pyridine synthon. This synthon involves a 'normal' H-bond between an oxygen and nitrogen but it is stabilised by a secondary CH...OC interaction. In his recent paper, Bond (2003) has studied the crystal structures of a range of carboxylic acids with pyrazine where this synthon was used.

The ultimate though, as yet, unattainable goal for crystal engineering is that supramolecular synthons can be added, removed or replaced from any system to create a new co-crystal; *This would be ideal, indeed a Utopian situation* (Desiraju, 1995). Unfortunately, for the moment, this is an unachievable goal. There are many factors that influence the crystallisation process, factors that are not fully understood. There are many occasions where co-crystals are predicted to form but for some reason they do not. It may be that during pre-crystallisation, in the liquid state, that polymorphs and adducts are formed. Studies of the liquid structures of formamide and α -glycine have shown that whilst in the liquid state the molecules form H-bonded dimers, which may explain the predominance of dimers in the solid

state structures of formamide and α -glycine (Pullman *et al.*, 1978 & Miyake *et al.*, 1985; Gidalevitz *et al.*, 1997).

1.5 References

Aakeröy, C. B., Beatty, A. M., Helfrich, B. A. & Nieuwenhuyzen, M. (2003). *Cryst. Growth & Design* **3**, 159-165.

Albrecht, G. & Corey, R. B. (1939). *J. Am. Chem. Soc.* **61**, 1087-1103.

Allen, F. H., Motherwell, W. D. S., Raithby, P. R., Shields, G. P. & Taylor, R. (1999). *New J. Chem.* **23**, 25-34.

Allen, F. H. (2002). *Acta Cryst.* **B58**, 380-388.

Allen, F. H. & Motherwell, W. D. S. (2002). *Acta Cryst.* **B58**, 407-422.

Anastas, P. T. & Warner, J. C. (2002). *Green Chemistry*. Oxford University Press, Oxford, UK.

Bernstein, J., Davis, R. E., Shimoni, L. & Chang, N-L. (1995). *Angew. Chem. Int. Ed. Engl.* **34**, 1555-1573.

Blatov, V. A. & Peresykina, E. V. (2000). *Acta Cryst.* **B56**, 510-511.

Bond, A. D. (2003). *Chem. Comm.* **2**, 250-251.

Bruno, I. J., Cole, J. C., Edgington, P. R., Kessler, M., Macrae, C. F., McCabe, P., Pearson, J. & Taylor, R. (2002). *Acta Cryst.* **B58**, 389-397.

Bruno, I. J., Cole, J. C., Kessler, M., Luo, J., Motherwell, W. D. S., Purkis, L., Smith, B. R., Taylor, R., Cooper, R. I., Harris, S. E. & Orpen, A. G. (2004). *Submitted for publication*.

Bunting, J. W., Toth, A., Heo, C. K. M. & Moors, R. G. (1990). *J. Am. Chem. Soc.* **112**, 8878-8885.

Byers, J. A. (1992). *J. Anim. Ecol.* **61**, 759-768.

Dasgupta, P. K. & Nara, O. (1990). *Anal. Chem.* **62**, 1117-1122.

Desiraju, G. R. (1995). *Angew. Chem. Int. Ed. Engl.* **34**, 2311-2327.

Desiraju, G. R. & Steiner, T. (1999). *The Weak Hydrogen Bond in Structural Chemistry and Biology*, Oxford University Press, Oxford, UK.

Etter, M. C. (1982). *J. Am. Chem. Soc.* **104**, 1095-1096.

- Etter, M. C. (1990). *Acc. Chem. Res.* **23**, 120-126.
- Etter, M. C., MacDonald, J. C. & Bernstein, J. (1990). *Acta Cryst.* **B46**, 256-262.
- Gidalevitz, D., Feidenhans'l, R., Matlis, S., Smilgies, D.-M., Christensen, M. & Leiserowitz, L. (1997). *Angew. Chem. Int. Ed. Engl.* **36**, 955-959.
- Gilli, G., Bellucci, F., Ferretti, V. & Bertolasi, V. (1989). *J. Am. Chem. Soc.* **111**, 1023-1028.
- Haisa, M., Kashino, S. & Maeda, H. (1974). *Acta Cryst.* **B30**, 2510-2512.
- Hamilton, W. C. & Ibers, J. A. (1968). *Hydrogen Bonding in Solids*, Benjamin, New York.
- Huggins, M. L. (1922). *J. Phys. Chem.* **26**, 601-625.
- Infantes, L. & Motherwell, S. (2002). *CrystEngComm*, **4**, 454-461.
- Infantes, L., Chisholm, J. & Motherwell, S. (2003a). *CrystEngComm*, **5**, 480-486.
- Infantes, L., Mahon, M. F., Male, L., Raithby, P. R., Teat, S. J., Sauer, J., Jagerovic, N., Elguero, J., & Motherwell, S. (2003b). *Helvetica Chimica Acta.* **86**, 1205-1221.
- Infantes, L. & Motherwell, W. D. S. (2004a). *Chem. Comm.* **10**, 1166-1167.
- Infantes, L. & Motherwell, W. D. S. (2004b). *Struc. Chem.* **15**, 173-184.
- Jeffrey, G. A. (1997). *An Introduction to Hydrogen Bonding*, Oxford University Press, Oxford, UK.
- Kitaigorodskii, A. I. (1973). *Molecular Crystals and Molecules*. Academic Press, New York.
- Kuleshova, L. N. & Zorky, P. M. (1980). *Acta Cryst.* **B36**, 2113-2115.
- Langan, P., Mason, S. A., Myles, D. & Schoenborn, B. P. (2002). *Acta Cryst.* **B58**, 728-733.
- Latimer, W. M. & Rodebush, W. H. (1920). *J. Am. Chem. Soc.* **42**, 1419-1433.
- Miyake, M., Kaju, O., Nakagawa, N. & Suzuki, T. (1985). *J. Chem. Soc. Faraday Trans. 2*, **81**, 277-281.
- Morokuma, K. (1977). *Acc. Chem. Res.* **10**, 294-300.
- Morrison, C. A. & Siddick, M. M. (2003). *Chem. Eur. J.* **9**, 628-634.
- Motherwell, W. D. S., Allen, F. H. & Shields, G. P. (1999). *Acta Cryst.* **B55**, 1044-1056.
- Oswald, I. D. H., Motherwell, W. D. S., Parsons, S., Pidcock, E. & Pulham, C. R. (2004). *Cryst. Rev.*, **10**, 57-66.
- Parkin, A., Harte, S. M., Goeta, A. E. & Wilson, C. C. (2004a). *New J. Chem.* **28**, 718-721.

Parkin, A., Oswald, I. D. H. & Parsons, S. (2004b). *Acta Cryst. B* **60**, 219-227.

Pauling, L., (1939) *The Nature of the Chemical Bond*, Cornell University Press, Ithaca, N.Y.

Pimental, G. C. & McClellan, A. L. (1960). *The Hydrogen Bond*, Freeman, San Francisco.

Pullman, A., Berthod, H., Giessner-Prettre, C., Hinton, J. F. & Harpool, D. (1978). *J. Am. Chem. Soc.* **100**, 3991-3994.

Silva, M. R., Paixao, J. A., Beja, A. M. & Da Veiga, L. A., (2001). *J. Fluor. Chem.* **107**, 117-120.

Steiner, T., Majerz, I. & Wilson, C. C. (2000). *Chem. Commun.*, **14**, 1231-1232.

Steiner, T., Majerz, I. & Wilson, C. C. (2001). *Angew. Chem. Int. Ed.* **40**, 2651-2654.

Steiner, T. (2001). *Acta Cryst. B* **57**, 103-106.

Steiner, T. (2002). *Angew. Chem. Int. Ed.* **41**, 48-76.

Taylor, R. & Kennard, O. (1982). *J. Am. Chem. Soc.* **104**, 5063-5070.

Wells, A. F. (1962). *Structural Inorganic Chemistry*. Oxford: Clarendon Press.

Wilson, C. C., Shankland, N. & Florence, A. J., (1996). *Chem. Phys. Lett.* **253**, 103-107.

Wilson, C.C. (2001). *Acta Cryst. B* **57**, 435-439.

Chapter 2

The Formation of Paracetamol (Acetaminophen) Adducts with Hydrogen-Bond Acceptors.[†]

[†] Oswald, I. D. H., Allan, D. R., McGregor, P. A., Motherwell, W. D. S., Parsons, S., Pulham, C. R. (2002) *Acta Cryst.*, **B58**, 1057-1066.

2.1 Introduction

There have been a number of detailed studies on the polymorphic behaviour of Paracetamol (acetaminophen, *p*-hydroxylacetanilide or Tylenol). Form I, which is monoclinic, was first characterised by Haisa *et al.* (1976), and has since been shown to be the thermodynamically more stable form. Form II is orthorhombic, and was described by the same group in 1974. The orthorhombic form can be grown by using a single orthorhombic crystal as a seed from a super-saturated aqueous solution of paracetamol. This method however can result in the crystals changing to the monoclinic form if left in contact with the solution for any length of time (Nichols & Frampton, 1998). The same authors showed that the only method that gives the orthorhombic polymorph reproducibly is growth from the melt. They also showed that this form is stable if dried and stored in a stoppered vial, and that neither grinding nor compression induces a transition to the monoclinic form. In a very careful study Boldyreva (2000) has shown that application of hydrostatic pressures up to 4.2 GPa does not induce a transition from the monoclinic to the orthorhombic form. The behaviour of the orthorhombic form is of interest for its ability to undergo plastic deformation when compressed, thereby facilitating the production of tablets of paracetamol.

With the exception of a recent report of paracetamol trihydrate from this laboratory (McGregor *et al.*, 2002), little structural work appears to have been carried out on solvates or other co-crystals of paracetamol, although a thermochemical study showed the existence of a hemisolvate of paracetamol with 1,4-dioxane (Fachaux *et al.*, 1995). In this chapter the preparation and characterisation of six new adducts of paracetamol with 1,4-dioxane, 4,4'-bipyridine, N-methylmorpholine, N,N'-dimethylpiperazine, morpholine and piperazine is described (these are referred to as *guest molecules* below; see Schemes 2.1 and 2.2). All these molecules, except for morpholine, can be considered to be at least pseudo-centrosymmetric with respect to their hydrogen bonding properties.

2.2 Experimental

2.2.1 Synthesis

All starting materials were obtained from Sigma-Aldrich except for 1,4-dioxane (May and Baker) and were used as received.

Paracetamol:0.5 1,4-Dioxane (1): A saturated solution of paracetamol (1.51 g, 10 mmol) in 1,4-dioxane (2 cm³, 23 mmol) was refluxed and allowed to cool. Colourless crystals were formed overnight at 293 K according to the published procedure (Fachaux *et al.*, 1995).

Paracetamol:4,4'-Bipyridine (2): Paracetamol (0.51 g, 3.40 mmol) was refluxed with an equimolar amount of 4,4'-bipyridine (0.52 g, 3.33 mmol) in ethanol (1 cm³). Pale yellow needle-like crystals were formed on standing overnight at room-temperature

Paracetamol:0.5N-methylmorpholine (3): Paracetamol (0.43 g, 2.85 mmol) and N-methylmorpholine (1 cm³, 9.11 mmol) were refluxed and allowed to cool. The flask was maintained at 277 K leading to the formation of colourless rod-shaped crystals.

Paracetamol:0.5N,N'-dimethylpiperazine (4): Paracetamol (0.55 g, 3.64 mmol) and N,N'-dimethylpiperazine (3 cm³, 22.2 mmol) were refluxed together and allowed to cool. A large excess of N,N'-dimethylpiperazine was required to dissolve the paracetamol completely. The flask was maintained at 277 K leading to the formation of colourless rod-shaped crystals.

Paracetamol:0.5Morpholine (5): Paracetamol (0.57 g, 3.8 mmol) was refluxed with morpholine (0.37 g, 4.3 mmol). Colourless crystals formed directly from the reaction mixture after a week at 277 K.

Paracetamol:0.5Piperazine (6): Paracetamol (0.62 g, 4.1 mmol) was refluxed together with piperazine (0.35 g, 4.1 mmol) in ethanol (1 cm³). Colourless crystals formed on cooling to 293 K.

Ethanol was required in the reactions of paracetamol with piperazine and 4,4'-bipyridine because these compounds are both solids at room temperature.

2.2.2 Differential Scanning Calorimetry (DSC)

DSC traces were recorded using a Perkin Elmer Pyris DSC 1. Samples were contained in open aluminium pans and purged with helium during the temperature scans to facilitate the removal of any volatile products of thermal decomposition. Samples were heated from 298 K to 453 K at a rate of 10 K/min.

2.2.3 Crystallography

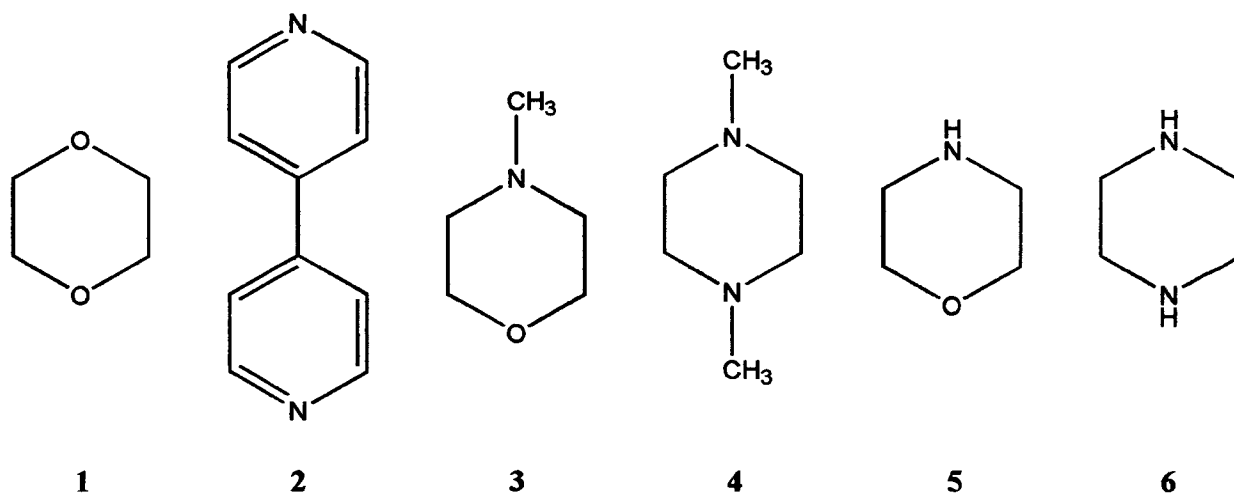
X-ray diffraction intensities were collected either on a Stoe Stadi-4 diffractometer with Cu-K α radiation or a Bruker SMART APEX CCD diffractometer with Mo-K α radiation.

Both instruments were equipped with Oxford Cryosystems low-temperature devices (Cosier & Glazer, 1986). An absorption correction for the four-circle data was applied using ψ -scans (SHELXTL, 1997a, based on the procedure described by North, *et al.*, 1968); the multiscan procedure SADABS (Sheldrick, 1997b, based on the procedure described by Blessing, 1995) was applied to the CCD data sets. All structures are in space group $P2_1/c$, except the morpholine adduct which formed in $P2_12_12_1$, and were solved by direct methods and refined by full-matrix least squares against F^2 using all data (SHELXTL). H-atoms were placed in calculated positions and allowed to ride on their parent atoms; methyl groups were treated with the Sheldrick (1997a) rotating rigid group model. Hydrogen atoms involved in H-bonding were located in difference maps and refined freely. All non-H atoms were modelled with anisotropic displacement parameters.

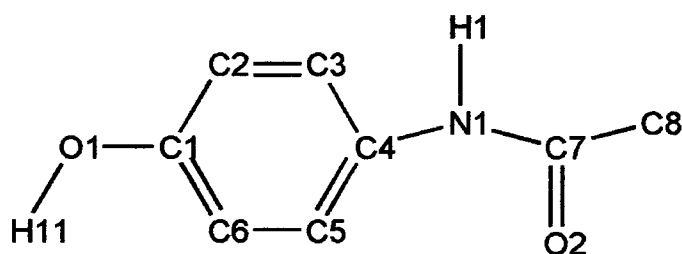
One of the two crystallographically independent dioxane molecules in the 1,4-dioxane adduct was disordered over two orientations about a crystallographic inversion centre. The occupancies of the two components were fixed at 0.75 and 0.25 after competitive refinement. Similarity restraints were applied to the geometries and displacement parameters of the two components. The program ROTAX (Cooper *et al.*, 2002) suggested that the crystal may have been twinned by a two-fold rotation about the [1 0 0] direct lattice direction. Incorporation of this into the model reduced $R1$ slightly from 7.02% to 6.86%, with a twin scale factor of 2.6(3)%. This is barely significant, and the twinning is omitted in the model presented here.

In the N-methylmorpholine adduct, the N-methylmorpholine is disordered over a crystallographic inversion centre with the nitrogen and oxygen atoms sharing an equivalent site. A composite scattering factor $[0.5f(\text{N}) + 0.5f(\text{O})]$ was used for this site; the occupancy of the methyl group was fixed at 0.5.

A consistent numbering scheme was used for the paracetamol molecules in all structures and this is shown in Scheme 2.2. Where there is more than one paracetamol molecule in the asymmetric unit the labels in Scheme 2.2 are augmented with the letters A and B. Labels for atoms forming part of the guest molecules carry the letters S, T etc. A full listing of crystal, data collection and refinement parameters is listed in Table 2.1, a set of H-bonding parameters are given in Table 2.2. The figures were produced using CAMERON (Watkin *et al.*, 1993). Other analysis utilised the p.c. version of the program PLATON (Spek, 2002; Farrugia, 1999). Crystallographic information files for all structures reported here are available on the CD at the back of this Thesis.



Scheme 2.1: Guest molecules used to form adducts with paracetamol. From left to right the structures show 1,4-dioxane, 4,4'-bipyridine, N-methylmorpholine, N,N'-dimethylpiperazine, morpholine and piperazine. The structure numbers, 1 – 6 refer to the adducts that these molecules form with paracetamol.



Scheme 2.2: Paracetamol, with atomic numbering scheme.

Adduct	(1)	(2)	(3)	(4)	(5)	(6)
Formula	C ₂₀ H ₂₆ N ₂ O ₆	C ₁₈ H ₁₇ N ₃ O ₂	C ₂₁ H ₂₉ N ₃ O ₅	C ₂₂ H ₃₂ N ₄ O ₄	C ₂₀ H ₂₇ N ₃ O ₅	C ₂₀ H ₂₈ N ₄ O ₄
Weight	390.43	307.35	403.47	416.52	389.45	388.46
Radiation	Cu-K α	Mo-K α	Mo-K α	Mo-K α	Mo-K α	Mo-K α
Crystal System	Monoclinic	Monoclinic	Monoclinic	Monoclinic	Orthorhombic	Monoclinic
Space group	<i>P</i> 2 ₁ / <i>c</i>	<i>P</i> 2 ₁ / <i>c</i>	<i>P</i> 2 ₁ / <i>c</i>	<i>P</i> 2 ₁ / <i>c</i>	<i>P</i> 2 ₁ 2 ₁ 2 ₁	<i>P</i> 2 ₁ / <i>c</i>
<i>a</i> /Å	12.421(5)	11.2906(10)	10.5749(8)	10.6970(9)	7.2791(9)	15.893(5)
<i>b</i> /Å	12.056(4)	24.103(2)	11.0220(8)	11.0240(9)	14.6277(18)	5.1664(17)
<i>c</i> /Å	13.396(3)	11.5526(10)	9.3894(7)	9.4896(8)	18.303(2)	12.993(4)
β /°	91.51(3)	96.1484(16)	101.145(2)	100.684(2)	90	113.633(5)
Volume /Å ³	2005.4(11)	3125.8(5)	1073.77(14)	1099.65(16)	1948.9(4)	977.4(6)
No. reflections for cell	80	5375	2729	3488	3801	1227
2 θ _{max} (°)	51.26	58.36	54.98	58.16	57.94	57.10
<i>Z</i>	8	8	2	2	4	2
<i>D</i> _c (Mg/m ³)	1.293	1.306	1.248	1.258	1.327	1.320
μ mm ⁻¹	0.795	0.087	0.090	0.088	0.096	0.093
Reflections collected	4865	20270	6517	7034	12312	5628
Unique [<i>R</i> _{int}]	3499 [0.0532]	7766 [0.0220]	2444 [0.0221]	2724[0.0164]	4733 [0.0308]	2309 [0.048]
No. <i>I</i> > 2 σ	2508	6044	1890	2512	4265	1778
<i>T</i> _{min} / <i>T</i> _{max}	0.602/0.826	0.830/1	0.792/ 0.962	0.833/1	0.868/1	0.690/1
Parameters	285	433	147	146	276	140
<i>R</i> ₁ [<i>F</i> > 4 σ (<i>F</i>)]	0.0702	0.0471	0.0408	0.0525	0.0462	0.0779
w <i>R</i> ₂ (<i>F</i> ² , all data)	0.2243	0.1280	0.1082	0.1339	0.1028	0.1652
<i>S</i>	1.078	1.038	0.973	1.059	1.066	1.179
ρ _{max} / eÅ ⁻³	0.50	0.36	0.22	0.40	0.26	0.34
ρ _{min} / eÅ ⁻³	-0.26	-0.25	-0.22	-0.19	-0.27	-0.47

Table 2.1: Crystallographic data for the adducts of paracetamol with 1,4-dioxane (1), 4,4'-bipyridine (2), N-methylmorpholine (3), N,N'-dimethylpiperazine (4), morpholine (5) and piperazine (6). All data were collected at 150 K.

Adduct	Donor	Acceptor	Obs. H...A distances		Typical normalised Distance /Å
			/normalised distance / Å		
(1)	N1A-H1A	O1S	2.03	1.90	2.03
	O1A-H11A	O2B	1.82	1.67	1.78
	O1B-H11B	O2A ⁱ	1.86	1.71	1.78
	N1B-H1B	O1U	1.92	1.77	2.03
	N1B-H1B	O1T	2.13	2.00	2.03
(2)	O1A-H11A	O2B	1.755(19)	1.68	1.78
	N1A-H1A	N10S	2.047(18)	1.92	1.96
	O1B-H11B	O2A ⁱⁱ	1.81 (2)	1.71	1.78
	N1B-H1B	N1T ⁱⁱⁱ	2.100 (18)	2.01	1.96
(3)	O1-H11	O1S/N1S ^{iv}	1.88 (2)	1.81	1.90/1.82
	N1-H1	O2 ^v	1.925(16)	1.80	1.92
(4)	N1-H1	O2 ^{vi}	1.98 (2)	1.84	1.92
	O1-H11	N1S ^{vii}	1.81 (2)	1.82	1.82
(5)	O1A-H11A	O1B ^{viii}	1.97 (2)	1.76	1.87
	N1A-H1A	O2B ^{ix}	2.033 (18)	1.87	1.92
	O1B-H11B	N4S ^x	1.79 (3)	1.69	1.82
	N1B-H1B	O2A ^{xi}	2.061 (19)	1.86	1.92
(6)	O1-H11	N1S	1.79(3)	1.74	1.82
	N1-H1	O2 ^{xii}	2.14 (3)	2.06	1.92
	N1S-H1S	O1 ^{xii}	2.30 (3)	2.21	2.03

Symmetry operators:

I	x, y, z+1	iv	-x+1, -y+2, -z	vii	-x+1, -y, -z	x	-x+1, y+1/2, -z+1/2
ii	x-1, y, z-1	v	x, -y+3/2, z-1/2	viii	x+1/2, -y+3/2, -z	xi	-x+1, y-1/2, -z+1/2
iii	-x, y-1/2, -z+1/2	vi	x, -y+1/2, z-1/2	ix	x+1/2, -y+1/2, -z	xii	x, y+1, z

Table 2.2: Table of H-bonding parameters. Standard uncertainties are omitted in the case of the 1,4-dioxane adduct because the H-positions were calculated and not refined. N-H and O-H distances were normalised to 1.009 and 0.983 Å to aid comparison with Cambridge Database search results (Table 2.3).

2.3 Results

2.3.1 Paracetamol

Crystal structures of the monoclinic and orthorhombic polymorphs of paracetamol have been reported several times, but here we have used the structures reported by Nichols and Frampton (1998) [Cambridge Structural Database (CSD: Allen *et al.*, 1983) reference codes HXACAN07 and HXACAN08]. Our motive for discussing them here is to highlight certain features of their graph sets that enable structural relationships to be drawn between them and the adducts that form the subject of the rest of this chapter.

Packing in both polymorphs is dominated by the formation of NH...OH and OH...O=C hydrogen bonds (Figure 2.1) giving rise to layered two-dimensional networks. Both polymorphs of paracetamol have identical graph sets (Bernstein *et al.*, 1995), in which the OH...O=C and NH...OH H-bonds respectively form $C(9)$ and $C(7)$ motifs at the unitary level. In both polymorphs these are disposed about crystallographic glide planes. In the monoclinic form the hydrogen-bonded layers are arranged parallel to the (0 1 0) planes, which means that the layers are polar: in Figure 2.1a all the molecules have the methyl group on the left. This polarity is reversed in neighbouring layers by crystallographic inversion centres. In the orthorhombic form glide planes run perpendicular to the layers, so that the layers are non-polar: in Figure 2.1b the methyl groups lie on the left and right hand sides of the molecules in alternate $C(9)$ chains.

The angles between mean planes of the amide and phenyl groups in orthorhombic and monoclinic paracetamol are 17.7 and 20.5°, respectively. Analogous angles observed in this work are given in the figure captions and range from 3.03° to 41.72°. $P\pi$ - $p\pi$ bonding between the phenyl ring and the amide group favours a dihedral angle of zero, and some correlation between this angle and the N-C(phenyl) bond length might have been expected, though none is evident at the precision of these structure determinations. This angle is evidently a rather easily deformed structural parameter, and is presumably at the mercy of crystal packing forces. As we now show in the following sections hydrogen bonding is the dominant feature in these structures, and the torsion observed is presumably a consequence of the optimisation of these interactions.

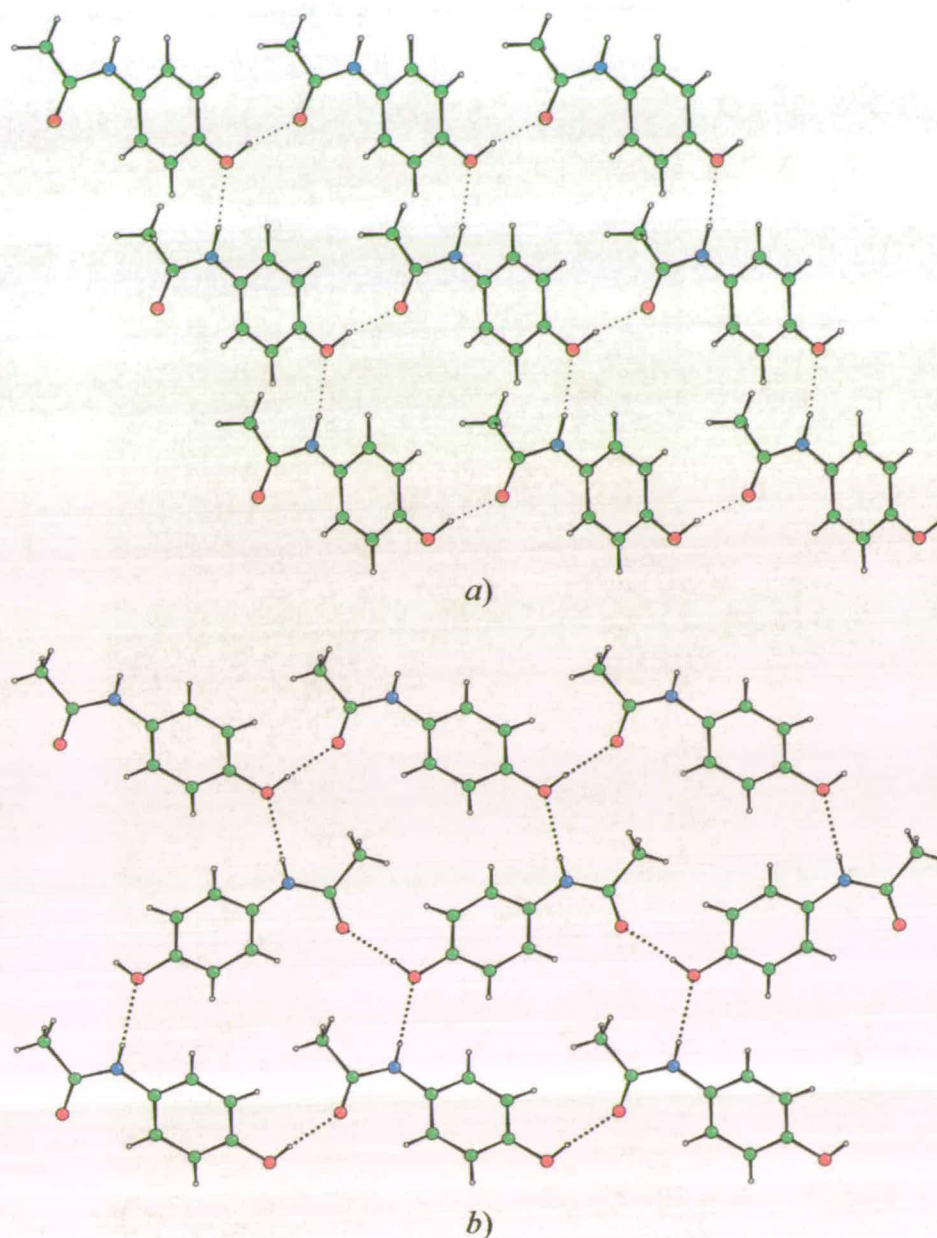


Figure 2.1 top (a): Monoclinic paracetamol (Form I) viewed along the b -axis; the c -axis runs diagonally from top left to bottom right, so that the $C(9)$ chains are established by the n -glide.

Bottom (b): Orthorhombic paracetamol (Form II) viewed along the c -axis; the a -axis runs horizontally, the b -axis runs from top to bottom. The $C(9)$ chains referred to in the text run from left to right, and the $C(7)$ chains run approximately vertically. Colour scheme C green, H grey, O red and N blue; the same colour scheme is used for all diagrams.

2.3.2 The paracetamol:1,4-dioxane adduct (1)

The asymmetric unit in the crystal structure of the 1,4-dioxane adduct of paracetamol consists of two paracetamol molecules and two half molecules of 1,4-dioxane. The latter both reside on crystallographic inversion centres. One of the 1,4-dioxane molecules (labelled T/U in the tables and supplemental data) is disordered, although both components participate in hydrogen bonding. The occupancy ratio is 0.75:0.25 and in the discussion that follows we

have ignored the minor component (U). There is some evidence from electron density difference maps that the other 1,4-dioxane molecule (labelled S) is disordered as well, although, if present, the distinction between the components is on the limit of the resolution of our data set. An ordered model for this part of the structure is therefore presented here. The structure is depicted in Figure 2.2.

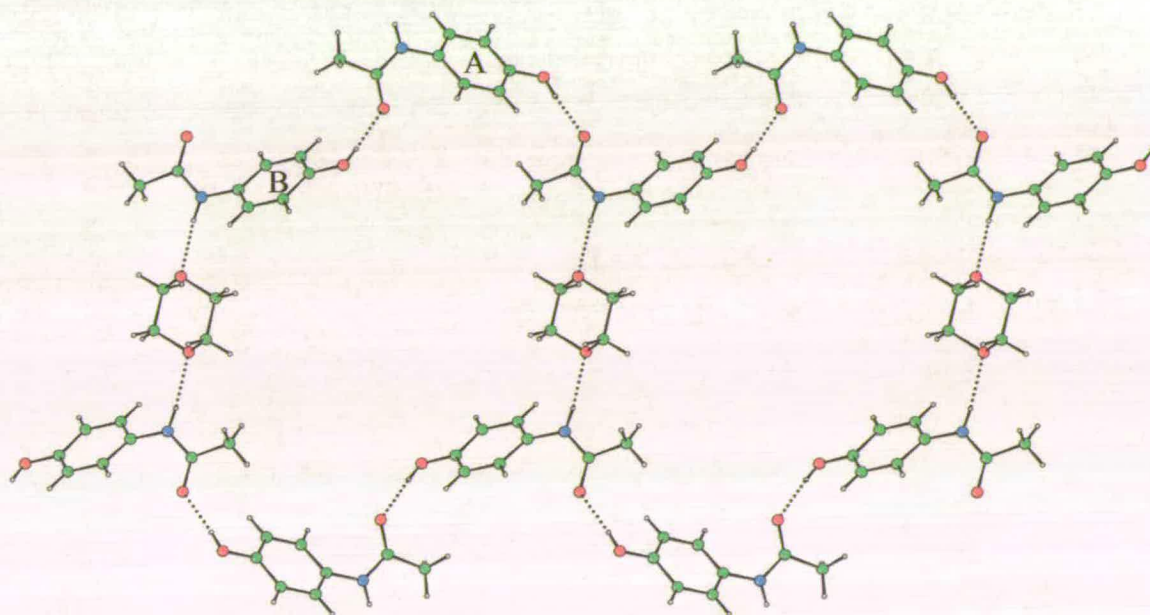


Figure 2.2: Paracetamol:1,4-dioxane adduct viewed perpendicular to (2 1 0), the *c*-axis runs horizontally. The C(9) chains referred to in the text run from left to right and are linked together by 1,4-dioxane molecules. The dihedral angles between the amide and phenyl mean planes in the two independent paracetamol molecules are 41.72(15) and 39.37(14)° for molecules A and B, respectively.

The C(9) chains formed by H-bonding between OH...O=C moieties of neighbouring molecules described above with regard to the crystal structures of paracetamol are also observed in the structure of the 1,4-dioxane adduct. In order to accommodate the 1,4-dioxane molecules these chains are sinusoidal, with the two crystallographically independent paracetamol molecules alternating along the chain. The NH groups point towards the oxygen atoms of 1,4-dioxane molecules forming NH...O hydrogen bonds. Since both 1,4-dioxane molecules reside on inversion centres the space group symmetry builds up two-dimensional sheets in which chains of paracetamol are linked by 1,4-dioxane bridges (Figure 2.2). In graph set notation the bridges can be described as $D^2_2(6)$. The two-dimensional sheets are

parallel to the (2 1 0) lattice planes, and the rather open structure depicted in Figure 2.2 is 'filled in' by symmetry equivalent sheets parallel to (2 $\bar{1}$ 0).

2.3.3 The paracetamol:4,4'-bipyridine adduct (2)

The oxygen atoms in 1,4-dioxane formally have two lone pairs of electrons, each of which could potentially act as an H-bond acceptor. In practice, however, motifs in which ethers act as double H-bond acceptors only occur rarely, and so for practical crystal-packing purposes it can be considered to be a centrosymmetric molecule containing two H-bond acceptors. 4,4'-bipyridine is similar, although a torsion about the central C-C bond breaks the inversion symmetry. Recrystallisation of paracetamol from a solution of 4,4'-bipyridine in ethanol yields a 1:1 co-crystal, rather than the hemi-solvate obtained with 1,4-dioxane, a possible effect of the greater basicity of 4,4'-bipyridine.

The crystal structure of paracetamol:4,4'-bipyridine contains two independent molecules each of paracetamol and 4,4'-bipyridine. As in the 1,4-dioxane adduct the paracetamol molecules form $C(9)$ chains through OH...O=C hydrogen bonds (Figure 2.3). The two crystallographically independent paracetamol molecules alternate along the chain. The disposition of the molecules within the chains is rather similar to that in orthorhombic paracetamol, except that alternate molecules are rotated through 180° about the chain axis in order to accommodate the 4,4'-bipyridine molecules.

The NH bonds of paracetamol act as H-bond donors to the aromatic nitrogen atoms of the 4,4'-bipyridine molecules, forming a discrete (D) graph set. However, since this crystal is a 1:1 adduct there are insufficient H-bond donors for the number of acceptors present, and only one of the two N-atoms in each 4,4'-bipyridine acts as an acceptor. The result is that there are no H-bonded pathways connecting the $C(9)$ paracetamol chains. The structure thus consists of a paracetamol backbone with attached 4,4'-bipyridine molecules. These motifs are interconnected by π -stacking between the 4,4'-bipyridine molecules, building up sheets that run parallel to the (1 0 $\bar{1}$) planes.

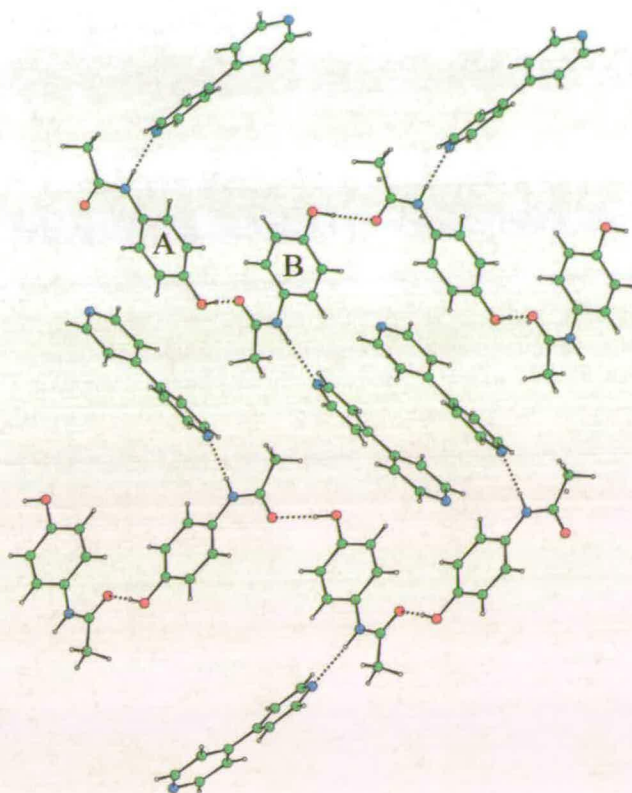


Figure 2.3: Paracetamol: 4,4'-bipyridine viewed perpendicular to (1 0 $\bar{1}$), the b -axis runs from top to bottom. The $C(9)$ chains referred to in the text run from left to right and are linked together by a pair of π -stacked 4,4'-bipyridine molecules. The dihedral angles between the amide and phenyl mean planes in the two independent paracetamol molecules are 14.68(8) and 13.27(9) $^\circ$ for molecules A and B, respectively.

2.3.4 The paracetamol: *N*-methylmorpholine/*N,N'*-dimethylpiperazine adducts, (3) & (4)

N-methylmorpholine and *N,N'*-dimethylpiperazine are closely related to 1,4-dioxane by the substitution of one or both oxygen atoms by *N*-Me, and paracetamol forms 2:1 adducts with both compounds, as it does with 1,4-dioxane. The *N,N'*-dimethylpiperazine adduct consists of one crystallographically independent paracetamol molecule with the *N,N'*-dimethylpiperazine residing on a crystallographic inversion centre. The *N*-methylmorpholine adduct is isostructural with this, with the guest molecule disordered about the inversion centre.

The crystal structures are similar to those of the 1,4-dioxane and 4,4'-bipyridine adducts in that the packing can be described with reference to chains of paracetamol molecules. However, rather than $C(9)$ motifs formed through $\text{OH}\cdots\text{O}=\text{C}$ H-bonds, the paracetamol molecules define a $C(4)$ graph set through $\text{NH}\cdots\text{O}=\text{C}$ bonds (Figure 2.4). The NH moiety of the paracetamol now fulfils the role of the OH groups in the 1,4-dioxane structure, and *N,N'*-dimethylpiperazine and *N*-methylmorpholine are similar to 1,4-dioxane

with regard to their H-bonding properties. Therefore, although the nature of the paracetamol chain differs from the 1,4-dioxane adduct, the roles of the morpholine and piperazine molecules are similar, and both act to link paracetamol chains via $D_2^2(6)$ graph set. Overall, this structure consists of a two-dimensional network, although the sheets formed have a corrugated or zig-zag appearance in cross-section. Alternate regions of the network are approximately parallel to the $(3\ 1\ 0)$ and $(3\ \bar{1}\ 0)$ planes. Just as in the 1,4-dioxane adduct, the open structure of Figure 2.4 is filled in by symmetry equivalent networks.

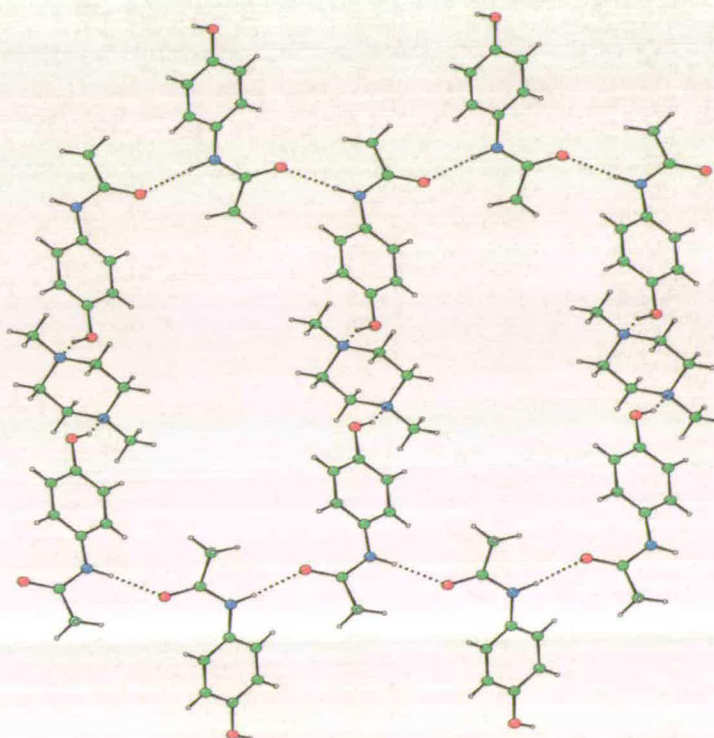


Figure 2.4: Paracetamol: N,N' -dimethylpiperazine adduct (isostructural to N -methylmorpholine adduct) viewed along the a -axis, the c -axis runs from left to right and the b -axis from top to bottom. The $C(4)$ chains referred to in the text run from left to right and are linked together by N,N' -dimethylpiperazine molecules. The dihedral angles between the amide and phenyl mean planes in the paracetamol molecules are $33.75(7)$ and $34.11(6)^\circ$ in the N,N' -dimethylpiperazine and N -methylmorpholine adducts, respectively.

2.3.5 The paracetamol:morpholine adduct (5)

Morpholine is related to N -methylmorpholine by the substitution of the methyl group by hydrogen, and it is unique in this series because the H-bonding characteristics of the two hetero-centres are not the same: the NH group is a donor and acceptor, the ether O-atom potentially a double, but more usually a single, acceptor. The asymmetric unit of the morpholine hemi-adduct consists of two crystallographically independent paracetamol molecules (labelled A and B) and one molecule of morpholine (labelled S in the tables).

The crystallographically independent paracetamol molecules alternate in the pattern ...ABABAB... along a chain formed by ...HNCO...NHCO... linkages between neighbouring amide groups. Because these molecules are crystallographically independent these H-bonds formally constitute discrete graphs at the unitary level, although it is clear from Figure 2.5 that they are closely related to the $C(4)$ graphs observed in the crystal structures of the N-methylmorpholine and N,N'-dimethylpiperazine adducts described above. For consistency we continue to use this designation, although it is not formally correct [the binary graph $C_2^2(8)$ takes proper account of symmetry].

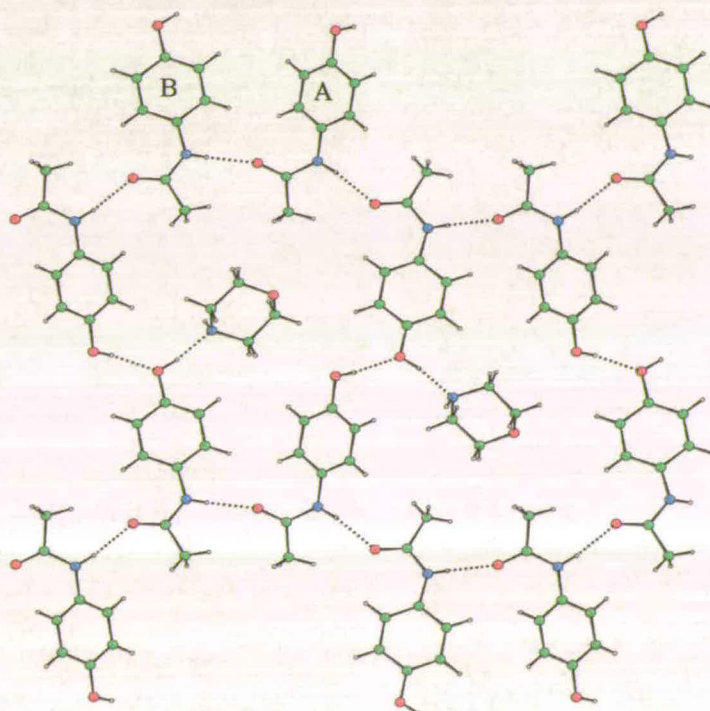


Figure 2.5: Paracetamol:morpholine adduct viewed along the a -axis. The c -direction runs from left to right, the b -direction up and down. The labels A and B refer to the crystallographically independent paracetamol molecules referred to in the text. The $C(4)$ chains referred to in the text run from left to right and are linked together by hydrogen bonds between opposed OH groups. This forms a grid-like array with the morpholine molecules residing in the grid cavities. The dihedral angles between the amide and phenyl mean planes in the two independent paracetamol molecules are $36.03(6)$ and $3.04(3)^\circ$ for molecules A and B, respectively.

The chains are formed by 2_1 operations parallel to c , leading to a pair-wise alternation of the centres of the paracetamol molecules above and below the chain. This pattern is reminiscent of the structures of the N-methylmorpholine and N,N'-dimethylpiperazine adducts, except that in these cases the alternation applies to single molecules. The potential for this arrangement to lead to some steric hindrance between the phenyl groups of

neighbouring molecules is avoided by adjacent molecules veering slightly away from each other and an increase in the torsional angle between the phenyl group and amide group from $3.04(3)^\circ$ in molecule B to $36.03(6)^\circ$ in molecule A.

Lattice translation along the *b*-direction generates further *C*(4) chains, and these are linked together by discrete [*D*] H-bonds in which an OH group from an 'A' molecule in one chain acts as a donor to an OH group of a 'B' molecule in a neighbouring chain. This is the only structure in the series in which pairs of paracetamol molecules interact via their hydroxyl moieties.

The two sets of H-bonds described above - the *C*(4) chains and the *D* links between chains - form a grid like network parallel to the (1 0 0) planes. The morpholine molecules fit into the cavities of the grid. As in the *N*-methylmorpholine adduct, the amine nitrogen atom acts as an acceptor to the OH group of one of the paracetamol molecules (B), but this is the only H-bonding interaction formed by the morpholine. The NH group of the morpholine is in an axial position to accommodate this interaction.

This scheme satisfies all the H-bonding potential of the two paracetamol molecules, with the exception of the hydroxyl acceptor of molecule A. The weakest acceptor in the system (the ether function of the morpholine) does not participate in H-bonding at all. A rather surprising feature of this structure given the excess of acceptors present, is that the NH donor functionality of the morpholine amine moiety is also unsatisfied. However, this is consistent with the relatively long NH...OH hydrogen bonds observed in the piperazine adduct (which is described in the next section) and the generally poor H-bond donor ability of secondary amines (see below).

2.3.6 *The paracetamol:piperazine adduct (6)*

Piperazine is related to *N,N'*-dimethylpiperazine by substitution of the two methyl groups by hydrogen. The asymmetric unit of the piperazine adduct, in common with the *N,N'*-dimethylpiperazine adduct, consists of one paracetamol molecule and a molecule of piperazine on a crystallographic inversion centre.

There are *C*(4) chains, consisting of NH...O=C H-bonds, linked via $D_2^2(6)$ motifs consisting of OH...N bonds (Figure 2.6). Piperazine is a weak H-bond donor as well as being an acceptor, and the extra NH donor moiety is satisfied by rotating alternate paracetamol molecules about the *C*(4) chain axis, leading to *D*-type NH...OH hydrogen bonds. This

rotation produces ribbons, which run parallel to the b -axis, rather than the infinite 2-dimensional networks.

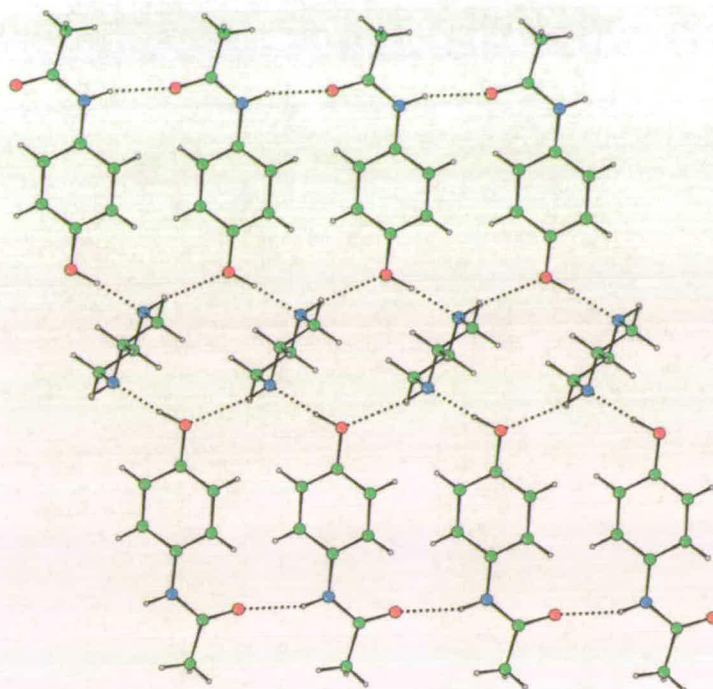


Figure 2.6: Paracetamol:piperazine adduct viewed perpendicular to $(3\ 0\ 2)$, the b -axis runs from left to right. The $C(4)$ chains referred to in the text run from left to right and are linked together by piperazine molecules. The latter also act as weak hydrogen bond donors. The dihedral angles between the amide and phenyl mean planes in the paracetamol molecule is $33.21(14)^\circ$.

2.3.7 Differential scanning calorimetry

Decomposition of a co-crystal of paracetamol is a potential strategy for the production of the orthorhombic polymorph. In all cases except for the 4,4'-bipyridine adduct, DSC traces exhibited thermal events attributable to loss of the guest molecule followed by a strong endotherm, corresponding to melting, at 438-444 K. The melting point of monoclinic paracetamol is 442 K, respectively (Nichols & Frampton, 1998). The same authors showed that DSC traces for orthorhombic paracetamol either show melting at 430 K or a phase transition to the monoclinic form at the same temperature, depending on the method of preparation. The DSC traces observed in this study can therefore be interpreted in terms of decomposition leading to formation of the monoclinic polymorph.

Thermal decomposition temperatures follow the trend that might be predicted on the basis of the boiling points of 1,4-dioxane (374 K), N-methylmorpholine (388 K), morpholine (401 K), N,N'-dimethylpiperazine (404 K) and piperazine (419 K). Two exotherms were

observed for the 1,4-dioxane solvate at 299 K and 338 K, in agreement with the previous study (Fachaux *et al.*, 1995). This is plausibly interpreted as sequential loss of the two crystallographically independent 1,4-dioxane molecules. 1,4-Dioxane is readily lost at room temperature from a crystalline sample of this adduct, and the DSC trace of a sample which had been allowed to stand for ten minutes showed only one exotherm with an onset temperature of 330 K. Decomposition of the morpholine, N-methylmorpholine and N,N'-dimethylpiperazine adducts occur as broad exotherms with onsets at approximately 327 K, 335 K and 373 K, respectively. The DSC trace of the piperazine adduct showed one endotherm at 413 K.

4,4'-Bipyridine sublimates at 578 K under ambient pressure, and it is the least volatile compound to have been studied in this work. The DSC trace of the co-crystal exhibits a weak endotherm at 399 K followed by a strong endotherm at 402K; no thermal event attributable to the melting of pure paracetamol was observed. The strong endotherm occurs at a similar temperature to the decomposition events observed for the other adducts, and it is likely to correspond to a melting process forming paracetamol solvated by liquid 4,4'-bipyridine (*mpt.* 374-377 K). Unlike the other solvents studied here 4,4'-bipyridine is not lost to leave pure paracetamol because its boiling point is well beyond the temperature of adduct decomposition. It is likely that the small peak corresponds to a phase transition.

2.4 Discussion and conclusions

This Chapter has described the formation of five new paracetamol hemi-adducts with 1,4-dioxane, N-methylmorpholine, N,N'-dimethylpiperazine, morpholine and piperazine and a 1:1 adduct with 4,4'-bipyridine. This is the first such systematic study of paracetamol co-crystals to have been undertaken. As is to be expected the crystal structures of all adducts are dominated by hydrogen bond formation, and comparisons between them were much facilitated by the use of graph set analysis in the form described in the illuminating review by Bernstein *et al.* (1995).

Although ether oxygen can potentially act as a double acceptor, it rarely does so, and so with the exception of morpholine all the guest molecules studied are at least pseudocentrosymmetric with respect to their H-bonding properties. The 1,4-dioxane, N-methylmorpholine, N,N'-dimethylpiperazine and piperazine adducts all consist of H-bonded chains of paracetamol molecules linked together by the guest molecules, which all reside on crystallographic inversion centres. In the 4,4'-bipyridine adduct the chains are

linked via a pair of π -stacked pyridine rings, though the structure as a whole is still centrosymmetric. The morpholine adduct does not conform to this pattern, although chains of paracetamol are still present. The arrangements of paracetamol chains described in this Chapter tend to lend themselves to the formation of centrosymmetric crystal structures, and this seems to favour adduct formation in the centrosymmetric guest molecules. It is perhaps significant that we have been unable to prepare an adduct with 1,3,5-trioxane, a molecule closely related to 1,4-dioxane, but which lacks inversion symmetry.

The donor groups which appear in this series are amidic NH, phenol OH and secondary amine NH; the acceptors are amidic O, phenolic O, secondary or tertiary amine N, ether O and pyridine N. The results of searches of the CSD for typical H-bond geometries involving these functionalities are listed in Table 2.3, searching criteria are given in the legend to that table. The pattern of adduct formation observed in this study is quite consistent with the data in Table 2.3 if the reasonable assumption is made that the H-bond strength is related to the average donor hydrogen-acceptor distance. The donor group O- or N-H to acceptor distances observed in this study were normalised to typical neutron values (O-H 0.983 Å and N-H 1.009 Å) to aid ready comparison with typical H-to-acceptor distances derived from our CSD search, and this comparison is made in Table 2.2. Our hydrogen bond distances agree tolerably well with typical values; they are often on the short side, as might be expected with low temperature data.

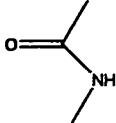
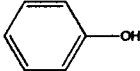
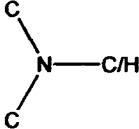
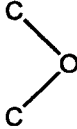

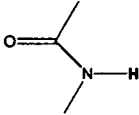
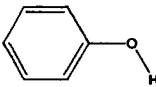
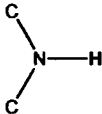
Donor (NH or OH)	Acceptor (O or N in each case)					
						
	Sample size Max NH...A / Å Min NH...A / Å Mean NH...A / Å	1250 (2.2) 1.73 1.92	14 2.14 1.79 2.01	11 2.17 1.80 1.96	31 2.19 1.83 2.03	40 2.19 1.81 1.96
	Sample size Max OH...A / Å Min OH...A / Å Mean OH...A / Å	49 2.19 1.60 1.78	256 2.20 1.67 1.87	49 2.19 1.66 1.82	53 2.20 1.62 1.90	76 2.18 1.53 1.81
	Sample size Max NH...A / Å Min NH...A / Å Mean NH...A / Å	5 2.17 2.08 2.13	1 (NOLZOD) - - 2.03	12 2.20 2.00 2.14	4 2.18 2.11 2.13	Not applicable

Table 2.3: Summary of the results of searches of the CSD (Version 5.23, April 2002) for typical distances in hydrogen-bonded systems containing identical functional groups to the paracetamol adducts studied. The distances to hydrogen atoms were normalised to typical neutron distances (C-H 1.083, N-H 1.009 and O-H 0.983 Å). Only 'organic' structures where the *R*-factor is less than 0.05, with no errors or disorder were included, and ionic or polymeric structures were excluded. The C-atoms attached to the amine moieties were specified to be sp³ hybridised. The donor-H to acceptor distance was specified to be 1.50-2.20 Å.

The strongest H-bonds in Table 2.3 are formed between phenolic OH (as donor) and amide O (as acceptor). These are observed in the *C*(9) chains formed in structures of both polymorphs of paracetamol. In pure paracetamol hydrogen bonds are formed between the remaining NH donor and OH acceptor to form *C*(7) chains, but on adduct formation with 1,4-dioxane and 4,4'-bipyridine it is these, weaker, interactions that break to accommodate the guest molecules, preserving the strongly bound *C*(9) chains, and forming hydrogen bonds between the amide NH of paracetamol and either the ether oxygen or pyridyl nitrogen atoms of the guest molecule. These observations are consistent with the results obtained in the variable pressure study of monoclinic paracetamol by Boldyreva *et al.* (2000), where the NH...O contacts were found to be more compressible than the OH...O contacts.

Neither 1,4-dioxane nor 4,4'-bipyridine has any group attached to the donor oxygen or nitrogen atoms. All of the other molecules studied carry either hydrogen or methyl groups in these positions, and reference to Figures 2.2 or 2.3 shows that a structure based on *C*(9) paracetamol chains would suffer some steric crowding between these groups and either the phenyl or methyl group attached to the amide moiety. In order to avoid steric overcrowding in the morpholine, piperazine, *N,N'*-dimethylpiperazine and *N*-methyldmorpholine adducts the paracetamol utilises its NH group as a donor. Table 2.3 shows that the most effective acceptor for this group is amide CO, and this explains the formation of *C*(4) paracetamol chains in all four of these structures.

In the structures of *N*-methyldmorpholine and *N,N'*-dimethylpiperazine hydrogen bonds are formed between the OH group of paracetamol and the N or O of the guest molecule. In morpholine and piperazine both the OH group of paracetamol and the NH group(s) of the guest could act as either donors or acceptors. Table 2.3 shows that secondary aliphatic amines are particularly poor hydrogen bond donors, and so the hydroxyl group acts as the donor in both cases. In fact so poor a donor is secondary amine NH that it is left unsatisfied in the morpholine adduct, even in the presence of excess acceptor functions. The weakness of these NH...N hydrogen bonds relative to OH...O or NH...O systems may be a consequence of the size of nitrogen relative to oxygen, a feature recently emphasised by Brown (2002). However in piperazine the NH groups do act as weak donors, and this induces a change in conformation of these *C*(4) chains relative to the *N,N'*-dimethylpiperazine adduct which condenses the sheets into ribbons.

In the case of morpholine the *C*(4) chains are linked by the OH group of a paracetamol molecule in one chain acting as an H-bond donor to a similar group in a neighbouring chain. On the basis of the structures of the other adducts the role might have been expected to be fulfilled by the ether moiety of the morpholine. Table 2.3 shows that these interactions are of rather similar strength, and this might explain the apparently anomalous behaviour observed in this adduct.

In the 1,4-dioxane adduct alternate *C*(9) paracetamol chains have reversed polarity. In the adducts based on *C*(4) chains, the resemblance to orthorhombic paracetamol is less obvious, although inspection of Figure 2.1*b* shows that removal of alternate molecules along the *C*(7) graph followed by a small displacement would yield NH...O=C *C*(4) chains. Viewed in this light desolvation might have been predicted to yield the orthorhombic polymorph of paracetamol, although in practice it was shown by DSC that in all cases except

for paracetamol:4,4'-bipyridine (for which we did not observe desolvation at all) the thermodynamically more stable monoclinic polymorph was formed.

2.5 References

- Allen, F. H., Kennard, O. & Taylor, R. (1983). *Acc. Chem. Res.* **16**, 146-153.
- Bernstein, J., Davis, R. E., Shimoni, L. & Chang, N-L. (1995). *Angew. Chem. Int. Ed. Engl.* **34**, 1555- 1573.
- Blessing, R. H. (1995). *Acta Cryst.* **A51**, 33-38.
- Boldyreva, E. V., Shakhtshneider, T. P., Vasilchenko, M. A., Ahsbahs, H. & Uchtmann, H. (2000). *Acta Cryst.* **B56**, 299-309.
- Brown, I.D. (2002). *The Chemical Bond in Inorganic Chemistry*. IUCr Monographs on Crystallography, Oxford University Press, Oxford, UK. Chapter 7.
- Cooper, R. I., Gould, R. O., Parsons, S. & Watkin, D. J. (2002). *J. Appl. Cryst.* **35**, 168-174.
- Cosier, J., & Glazer, A. M. (1986). *J. Appl. Cryst.* **19**, 105-107.
- Farrugia, L. J. (1999). *J. Appl. Cryst.*, **32**, 837-838.
- Fachaux, J.-M., Guyot-Hermann, A.-M., Guyot, J.-C., Conflant, P., Drache, M., Veessler, S. & Boistelle, R. (1995). *Powder Technology*, **82**, 123-128.
- Haisa, M., Kashino, S., Kawaii, R. & Maeda, H. (1976). *Acta Cryst.* **B32**, 1283-1285.
- Haisa, M., Kashino, S. & Maeda, H. (1974). *Acta Cryst.* **B30**, 2510-2512.
- Nichols, G. & Frampton, C. S. (1998). *J. Pharm. Sci.* **87**, 684-693.
- North, A. C. T., Phillips, D. C. & Mathews, F. S. (1968). *Acta. Cryst.* **A24**, 351-359.
- McGregor, P. A., Allan, D. R., Parsons, S. & Pulham, C. R. (2002). *J. Pharm. Sci.* **91**, 1308-1311.
- Sheldrick, G. M. (1997a). *SHELXTL*. Bruker-AXS, Madison, Wisconsin, USA.
- Sheldrick, G. M. (1997b). *SADABS*. Bruker-AXS, Madison, Wisconsin, USA.
- Spek, A. L. (2002). *PLATON- A Multipurpose Crystallographic Tool*, Utrecht University, Utrecht, The Netherlands.
- Watkin, D. J., Pearce, L. & Prout, C. K. (1993). *CAMERON - A Molecular Graphics Package*. Chemical Crystallography Laboratory, University of Oxford, England.

Chapter 3

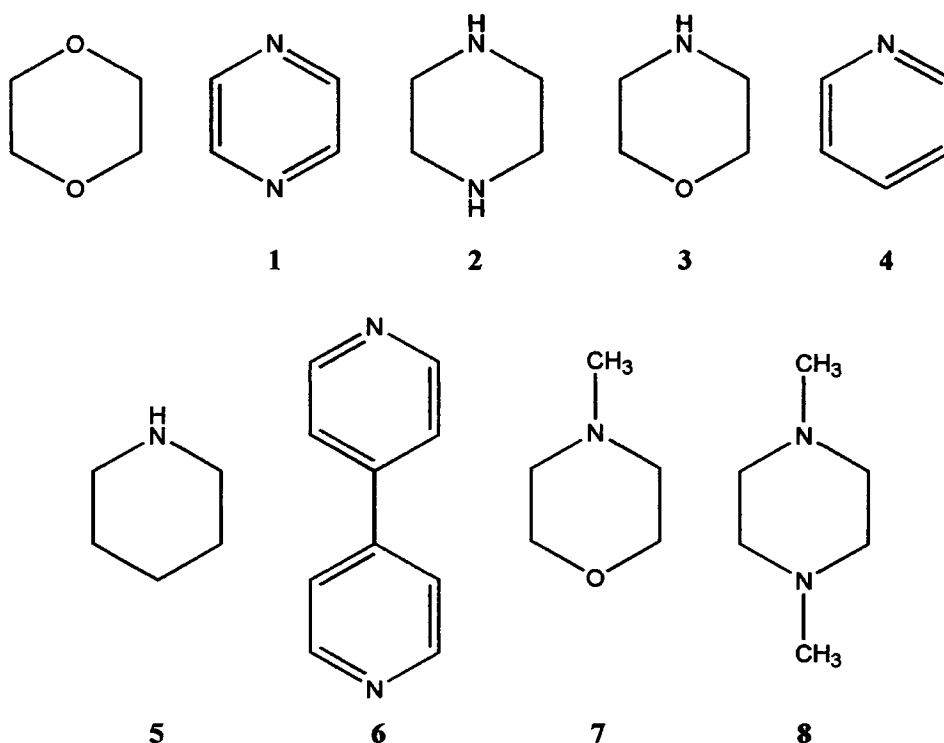
**The Formation of Quinol Co-crystals with
Hydrogen-Bond Acceptors.[‡]**

[‡] Oswald, I. D. H., Motherwell, W. D. S. & Parsons, S. (2004). *Submitted for publication*

3.1 Introduction

Quinol, or hydroquinone, is widely used to stabilise compounds that are susceptible to polymerisation. It has been shown to crystallise in three polymorphic forms. The structure of the α -polymorph ($R\bar{3}$) was determined by Bolte and Lerner (2001); the β -polymorph was determined by Lindeman *et al.* (1981) and found to belong to the same space group, but with a smaller cell ($Z' = \frac{1}{2}$ rather than $Z' = 3$). These two polymorphs were previously identified by Caspari (1926 & 1927) but there was some ambiguity in the determination of the space group. The γ -polymorph was found to crystallise in space group $P2_1/c$ (Maartmann-Moe, 1966).

Quinol shows a great propensity for co-crystallising with a variety of different compounds. A search of the Cambridge Structural Database version 5.25 (CSD: Allen, 2002; Allen & Motherwell, 2002) shows that there are ninety-two co-crystals of quinol with a range of organic compounds. Of all the structures in the database over half were co-crystals of quinol with hydrogen bond acceptors, including 1,4-dioxane (Barnes *et al.*, 1990). A previous paper from this laboratory (Oswald *et al.*, 2002) described how molecules analogous to 1,4-dioxane yielded a series of crystal structures with closely related packing motifs, and in this Chapter, the crystal structures of co-crystals of quinol with pyrazine, piperazine, morpholine, pyridine, piperidine, 4,4'-bipyridine (hereafter referred to as guest molecules) are reported. These all crystallise in a manner related to that of the 1,4-dioxane co-crystal. The structures of the N-methylmorpholine and N,N'-dimethylpiperazine co-crystals, which were also determined, highlight the effect of steric hindrance on the common structural motifs present for the unsubstituted guest molecules. Scheme 3.1 shows all the guest molecules used in the series.



Scheme 3.1: Guest molecules used to form co-crystals with quinol. From left to right the structures show, top: 1,4-dioxane, pyrazine, piperazine, morpholine, pyridine; bottom: piperidine, 4,4'-bipyridine, N-methylmorpholine and N,N'-dimethylpiperazine. The structure numbers, 1 – 8 refer to the adducts that these molecules form with quinol.

3.2 Experimental

3.2.1 Synthesis

All starting materials were obtained from Sigma-Aldrich and used as received.

Quinol:Pyrazine (1): Quinol (0.70 g, 6.36 mmol) was refluxed with pyrazine (0.51 g, 6.38 mmol) in ethanol (3 cm³) until the solid dissolved. The solution was allowed to cool to room temperature to produce crystals as colourless blocks.

Quinol:Piperazine (2): Quinol (0.60 g, 5.45 mmol) was refluxed with piperazine (0.50 g, 5.81 mmol) in ethanol (3 cm³) until the solid dissolved. The solution was allowed to cool to room temperature to produce crystals in the form of colourless blocks.

Quinol:2Morpholine (3): Quinol (0.65 g, 5.90 mmol) was refluxed with morpholine (0.53 g, 5.95 mmol) with a little ethanol until the solid dissolved. Colourless, crystalline blocks were obtained on cooling to 277 K.

Quinol:2Pyridine (4): Quinol (0.49 g, 4.45 mmol) was dissolved in an excess of pyridine and drawn into a glass capillary (o.d. 0.32 mm). A polycrystalline sample was obtained on freezing the sample at 253 K and a crystal grown using the laser-assisted zone-refinement procedure of Boese and Nussbaumer (1994).

Quinol:2Piperidine (5): Quinol (0.49 g, 4.45 mmol) was refluxed in a minimum volume of piperidine to dissolve the solid. The solution was allowed to cool to room temperature to produce crystals as colourless blocks.

Quinol:2bipyridine (6): Quinol (0.59 g, 5.84 mmol) was refluxed with 4,4'-bipyridine (0.87 g, 5.58 mmol) in 3 cm³ of ethanol until the solid dissolved. The solution was allowed to cool to room temperature to produce colourless laths.

Quinol:2N-methylmorpholine (7): Quinol (0.55 g, 5.00 mmol) was dissolved in N-methylmorpholine (1.00 g, 10.30 mmol) and drawn into a glass capillary (o.d. 0.38 mm). A crystal was grown at 240 K from a polycrystalline sample of the frozen liquid by Boese's method (see above).

Quinol:N,N'-dimethylpiperazine (8): Quinol (0.65 g, 5.90 mmol) was refluxed with N,N'-dimethylpiperazine (3 cm³, 20.10 mmol) in a little ethanol until the solid dissolved. The solution was held at 277 K to produce colourless crystalline blocks.

3.2.2 Crystallography

X-ray diffraction intensities were collected with Mo-K α radiation on a Bruker SMART APEX CCD diffractometer equipped with an Oxford Cryosystems low-temperature device (Cosier & Glazer, 1986). Absorption corrections were carried out using the multiscan procedure SADABS (Sheldrick, 1997a, based on the procedure described by Blessing, 1995). All structures were solved by direct methods and refined by full-matrix least squares against F^2 using all data (SHELXTL, Sheldrick, 1997b). H-atoms were placed on C-atoms in calculated positions and allowed to ride on their parent atoms; methyl groups were treated with the Sheldrick (1997b) rotating rigid group model except one methyl group in the N,N'-dimethylpiperazine co-crystal which exhibited high thermal motion or some disorder (not modelled), where the positions were calculated purely on stereochemical grounds. Hydrogen atoms involved in H-bonding were located in difference maps and refined freely. All non-H atoms were modelled with anisotropic displacement parameters.

The diffraction pattern of the piperazine co-crystal indexed readily on the cell $a = 7.1977(18) \text{ \AA}$, $b = 8.859(2) \text{ \AA}$, $c = 13.247(4) \text{ \AA}$, $\alpha = 80.420(6)^\circ$, $\beta = 74.400(4)^\circ$, $\gamma = 66.153(4)^\circ$. This can be transformed to a pseudo-monoclinic C -centred cell, although the Laue symmetry was clearly $\bar{1}$ and not $2/m$. While the structure solved and refined without difficulty, it appeared to be twinned by a two-fold rotation about $[1\ 0\ 0]$ - the pseudo-monoclinic b -axis. The R -factor was 6%, and bond distances and angles were normal. Symmetry checking (PLATON, Spek, 2004) implied that the structure could be described using a smaller unit cell, and closer inspection of the intensities revealed that data with $k + l = 3n$ had an average $I/\sigma(I)$ some eight times larger than the rest of the data. [This could also be readily recognised in the Patterson function, which had a peak with a height of about two-thirds that of the origin peak at approximately $(0, 1/3, 1/3)$.] The data set was transformed using the matrix

$$\begin{pmatrix} 0 & \frac{1}{3} & \frac{1}{3} \\ 0 & -\frac{2}{3} & \frac{1}{3} \\ 1 & -\frac{1}{3} & -\frac{1}{3} \end{pmatrix},$$

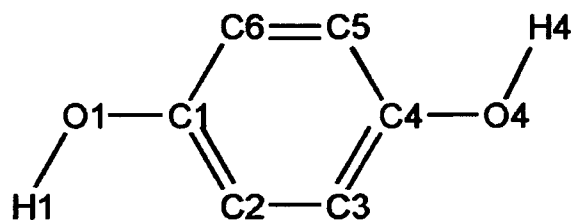
and refined using a two fold rotation about $[1\ 0\ 1]$, which corresponds to the matrix:

$$\begin{pmatrix} -\frac{1}{3} & 0 & \frac{2}{3} \\ -\frac{1}{3} & -1 & -\frac{1}{3} \\ \frac{4}{3} & 0 & \frac{1}{3} \end{pmatrix}.$$

Reflections where $h+l = 3n$ contain contributions from both twin domains; the twin scale factor was 0.1185(16).

A consistent numbering scheme was used for the quinol molecules in all structures and this is shown in Scheme 3.2. Where there is more than one quinol molecule in the asymmetric unit the labels in Scheme 3.2 are augmented with the letters A and B. Labels for atoms forming part of the guest molecules carry the letters S, T etc. A full listing of crystal, data collection and refinement parameters is given in Table 3.1, a set of H-bonding parameters is given in Table 3.2. Structures were visualised using SHELXTL or MERCURY (Taylor & Macrae, 2001; Bruno *et al.*, 2002); the figures were produced using CAMERON (Watkin *et al.*, 1993). Other analysis utilised the p.c. version of the program PLATON (Spek, 2002; Farrugia, 1999). Searches of the Cambridge Crystallographic Database (Allen & Motherwell,

2002) were carried out with the program CONQUEST, utilising version 5.25 of the database. Crystallographic information files for all structures reported here are available on the CD at the back of this Thesis.



Scheme 3.2: Quinol, with atomic numbering scheme.

Co-crystals	(1)	(2)	(3)	(4)
Formula	C ₁₀ H ₁₀ N ₂ O ₂	C ₁₀ H ₁₆ N ₂ O ₂	C ₁₄ H ₂₈ N ₂ O ₄	C ₁₆ H ₁₆ N ₂ O ₂
Weight	190.20	196.25	284.36	268.31
Radiation	Mo-K α	Mo-K α	Mo-K α	Mo-K α
Crystal system	Monoclinic	Triclinic	Monoclinic	Monoclinic
Space Group	<i>P</i> ₂ ₁ / <i>c</i>	<i>P</i> $\bar{1}$	<i>P</i> ₂ ₁ / <i>n</i>	<i>P</i> ₂ ₁ / <i>c</i>
<i>a</i> /Å	8.901(3)	5.7060(15)	6.6652(13)	6.4990(9)
<i>b</i> /Å	7.666(2)	6.7599(19)	5.5881(11)	16.459(2)
<i>c</i> /Å	6.984(2)	7.0771(18)	20.034(4)	7.1794(10)
α /°	90	100.269(4)	90	90
β /°	90.091(6)	112.446(3)	94.942(4)	112.986(3)
γ /°	90	90.163(3)	90	90
Volume/Å ³	476.6(3)	247.50(11)	743.4(3)	707.00(17)
No. reflections for cell	834	2430	1472	1519
2 θ _{max} (°)	57.50	57.56	56.96	57.74
<i>Z</i>	2	1	2	2
<i>D</i> _c (Mg/m ³)	1.325	1.317	1.270	1.260
μ (mm ⁻¹)	0.095	0.093	0.093	0.084
Reflections collected	2873	3814	4226	5091
No. Unique [<i>R</i> _{int}]	1141 [0.0230]	1194 [0.0294]	1730 [0.0381]	1700 [0.0309]
No. <i>I</i> > 2 σ	926	1194	1427	1345
<i>T</i> _{min} / <i>T</i> _{max}	0.787, 1.000	0.874, 1.000	0.675, 1.000	0.593, 1.000
Parameters	68	73	99	95

Table 3.1: Crystallographic data for the co-crystals of quinol with pyrazine (1), piperazine (2), morpholine (3), pyridine (4). All data were collected at 150 K. The table is continued on the next page.

Co-crystals	(1)	(2)	(3)	(4)
$R_1 [F > 4\sigma(F)]$	0.0471	0.0512	0.0845	0.0834
$wR_2 (F^2, \text{all data})$	0.1150	0.1180	0.2105	0.1716
S	1.067	1.091	1.175	1.330
$\Delta\rho_{\text{max}} / \text{e}\text{\AA}^{-3}$	0.261	0.318	0.439	0.282
$\Delta\rho_{\text{min}} / \text{e}\text{\AA}^{-3}$	-0.296	-0.331	-0.305	-0.386

Co-crystals	(5)	(6)	(7)	(8)
Formula	$\text{C}_{16}\text{H}_{28}\text{N}_2\text{O}_2$	$\text{C}_{26}\text{H}_{22}\text{N}_4\text{O}_2$	$\text{C}_{16}\text{H}_{28}\text{N}_2\text{O}_4$	$\text{C}_{12}\text{H}_{20}\text{N}_2\text{O}_2$
Weight	280.40	422.49	312.41	224.30
Radiation	Mo-K α	Mo-K α	Mo-K α	Mo-K α
Crystal system	Monoclinic	Triclinic	Triclinic	Triclinic
Space Group	$P2_1/c$	$P\bar{1}$	$P\bar{1}$	$P\bar{1}$
$a/\text{\AA}$	10.4230(15)	7.820(4)	6.9612(10)	8.9620(8)
$b/\text{\AA}$	5.2619(7)	8.619(4)	7.3146(11)	9.4944(8)
$c/\text{\AA}$	15.221(2)	9.201(4)	9.659(2)	14.7119(13)
$\alpha/^\circ$	90	111.897(7)	106.182(3)	90.501(2)
$\beta/^\circ$	109.920(3)	109.851(7)	104.481(3)	92.919(2)
$\gamma/^\circ$	90	94.657(8)	106.201(2)	99.664(2)
Volume/ \AA^3	784.84(19)	525.7(4)	423.94(12)	1232.26(19)
No. reflections for cell	774	2247	2797	1812
$2\theta_{\text{max}}(^\circ)$	58.04	57.40	57.50	57.86
Z	2	1	1	4
$D_c (\text{Mg}/\text{m}^3)$	1.187	1.335	1.224	1.209
$\mu (\text{mm}^{-1})$	0.078	0.087	0.087	0.083

Table 3.1: Crystallographic data for the co-crystals of quinol with piperidine (5), 4,4'-bipyridine (6), N-methylmorpholine (7) and N,N'-dimethylpiperazine (8). All data were collected at 150 K. (cont'd).

Co-crystals	(5)	(6)	(7)	(8)
Reflections collected	4754	4641	3788	11345
No. Unique [R_{int}]	1896 [0.0284]	2428 [0.0308]	1972 [0.0199]	5844 [0.0392]
No. $I > 2\sigma$	1327	2067	1794	3873
$T_{\text{min}} / T_{\text{max}}$	0.661, 1.000	0.763, 1.000	0.774, 1.000	0.898, 1.000
Parameters	99	150	106	308
$R_1 [F > 4\sigma(F)]$	0.0561	0.0541	0.0452	0.0743
$WR_2 (F^2, \text{all data})$	0.1358	0.1436	0.1199	0.1615
S	1.042	1.044	1.070	1.030
$\Delta\rho_{\text{max}} / \text{e}\text{\AA}^{-3}$	0.241	0.312	0.239	0.498
$\Delta\rho_{\text{min}} / \text{e}\text{\AA}^{-3}$	-0.194	-0.260	-0.265	-0.430

Table 3.1: Crystallographic data for the co-crystals of quinol (cont'd).

Co-crystal	Donor	Acceptor	D...A distance (Å)	Obs. H...A Distance/normalised distance (Å)	Distance/normalised distance (Å)	Typical normalised distance (Å)	Angle DHA (°)
(1)	O1A-H1A	N1S	2.7585(17)	1.85(2)	1.78	1.81	177(2)
	C3S-H3S	O1A ^{vi}	3.347(2)	2.40	2.27	2.52	177
(2)	N1S-H1S	O1A ⁱ	3.0498(19)	2.35(2)	2.25	1.94	138.1(17)
	O1A-H1A	N1S	2.6708(18)	1.80(3)	1.71	1.82	167(2)
(3)	N1S-H1S	O1A	3.032(3)	2.36 (3)	2.24	1.94	137(3)
	O1A-H1A	N1S ⁱⁱ	2.686(3)	1.85 (4)	1.73	1.82	164(3)
	C2S-H2S2	O4S ^{xii}	3.693(3)	2.75	2.66	2.60	160
	C3S-H3S1	O4S ^{xiii}	3.672(4)	2.81	2.73	2.60	147
(4)	O1A-H1A	N1S	2.728(3)	1.88 (3)	1.75	1.82	174(3)
	C2S-H2S	O1A ^{xi}	3.385(3)	2.49	2.37	2.52	156
(5)	N1S-H1S	O1A ⁱⁱⁱ	3.2782(19)	2.43(2)	2.28	1.94	168.8(18)
	O1A-H1A	N1S ⁱⁱⁱ	2.747(2)	1.82 (2)	1.77	1.82	173(2)
(6)	O1A-H1A	N1S	2.740(2)	1.84 (2)	1.76	1.81	176(2)
	C5S-H5S	O1A ^{vii}	3.456(2)	2.59	2.47	2.52	152
	C9S-H9S	O1A ^{viii}	3.394(2)	2.46	2.33	2.52	169
(7)	O1A-H1A	N1S	2.7367(12)	1.87 (2)	1.77	1.82	167(2)
	C1S-H1S3	O4S ^x	3.4115(15)	2.61	2.54	2.60	139
	C6S-H6S1	O4S ^x	3.5646(14)	2.60	2.52	2.60	163

Symmetry operators:

i	-x+1, -y+1, -z+2	vi	x, y-1, z	xi	-x, -y+1, -z+1
ii	-x+2, -y+2, -z	vii	x-1, y, z	xii	-x+3/2, y+1/2, -z+1/2
iii	-x+2, y+1/2, -z+1/2	viii	-x, -y+1, -z+2	xiii	-x+3/2, y-1/2, -z+1/2
iv	x-1, y-1, z	ix	x, y+1, z	xiv	x+1, y, z
v	-x+1, -y, -z+1	x	-x, -y, -z+2	xv	-x+1, -y+1, -z

Table 3.2: Table of H-bonding parameters. C-H, N-H and O-H distances were normalised to 1.083, 1.009 and 0.983 Å, respectively, to aid comparison with Cambridge Database search results (Table 3.3).

Co-crystal	Donor	Acceptor	D...A distance (Å)	H...A Distance/		Typical normalised distance (Å)	Angle DHA (°)
				Obs. normalised distance (Å)	Distance (Å)		
(8)	O1A-H1A	NIT	2.733(3)	1.86 (3)	1.77	1.82	167(3)
	O4A-H4A	N1U ^{iv}	2.744(3)	1.79 (3)	1.78	1.82	166(3)
	O1B-H1B	N1V	2.765(3)	1.83 (3)	1.79	1.82	169(3)
	O4B-H4B	N1S ^v	2.739(3)	1.84 (3)	1.79	1.82	163(3)
	C2A-H2A	O1B	3.446(3)	2.67	2.57	2.60	139
	C2B-H2B	O1A ^{vi}	3.328(3)	2.60	2.51	2.60	133
	C5B-H5B	O4B ^v	3.442(3)	2.65	2.54	2.60	142
	C1S-H1S1	O4A ^{xiv}	3.560(3)	2.63	2.53	2.60	159
	C3T-H3T2	O1B ^{xv}	3.405(3)	2.71	2.65	2.60	128

Symmetry operators:

i	-x+1, -y+1, -z+2	vi	x, y-1, z	xi	-x, -y+1, -z+1
ii	-x+2, -y+2, -z	vii	x-1, y, z	xii	-x+3/2, y+1/2, -z+1/2
iii	-x+2, y+1/2, -z+1/2	viii	-x, -y+1, -z+2	xiii	-x+3/2, y-1/2, -z+1/2
iv	x-1, y-1, z	ix	x, y+1, z	xiv	x+1, y, z
v	-x+1, -y, -z+1	x	-x, -y, -z+2	xv	-x+1, -y+1, -z

Table 3.2: Table of H-bonding parameters. C-H, N-H and O-H distances were normalised to 1.083, 1.009 and 0.983 Å, respectively, to aid comparison with Cambridge Database search results (Table 3.3) (cont'd).

3.3 Results

3.3.1 Quinol:1,4-Dioxane

The structure of the quinol:1,4-dioxane co-crystal has been determined by Barnes *et al.* (1990) [CSD Refcode SENJOK]. In this Chapter co-crystals of quinol with several compounds which are related to 1,4-dioxane by their hydrogen bonding properties are discussed; the structure of the quinol:1,4-dioxane co-crystal is described here in order to be able to make comparisons with the co-crystals that form the subject of the rest of this Chapter.

The asymmetric unit of quinol:1,4-dioxane (space group $P2_1/a$) consists of half-molecules of each component. The primary H-bonding motif in the structure is a $C_2^2(12)$ (Bernstein *et al.*, 1995) chain formed by O-H...O(ether) hydrogen bonds which connect alternating quinol and 1,4-dioxane molecules; these chains run from the top left to lower right in Figure 3.1. The chains are staggered, which allows the acceptor functionality of the hydroxyl to be filled by a close contact with a C-H moiety of a 1,4-dioxane molecule in a neighbouring chain [CH...O 2.60 Å, the sum of van der Waals radii of H and O is 2.72 Å]. Interactions of this type link the chains together into a layer. CH...O interactions of similar dimensions are observed in both phases of 1,4-dioxane (Buschmann *et al.*, 1986) and in morpholine (Parkin *et al.*, 2004).

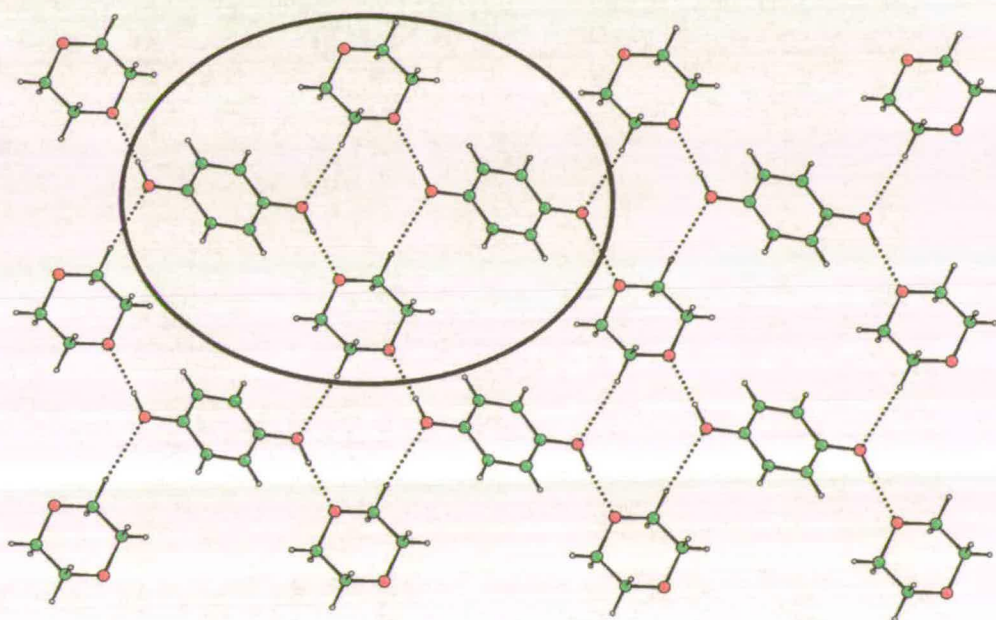


Figure 3.1: Quinol:1,4-dioxane (CSD refcode: SENJOK) viewed perpendicular to the (1 0 0) planes. Colour scheme: C green, H grey and O red. The staggered arrangement of the chains allows a bridging motif through the OH...O interaction and a close contact between a CH and the O of the hydroxyl group giving a $R_4^4(10)$ graph set (circled). The layers occupy the (2 0 0) planes in the structure, and alternate layers have chains running along the [0 1 1] and $[0 \bar{1} 1]$ directions.

A doubly-bridging subunit composed of two quinol molecules and two 1,4-dioxane molecules is circled in Figure 3.1. Each quinol is H-bonded to one of the 1,4-dioxane molecules, but it also accepts a CH...O interaction from the second. At this level of graph set analysis there are four donors consisting of pairs of OH and CH moieties, and four acceptors formed by pairs of ether and phenol oxygen atoms. It is useful for the purposes of drawing

comparisons with the other structures in this series to highlight this secondary level, $R_4^4(10)$ ring motif in which two quinol molecules are doubly-bridged by two 1,4-dioxane molecules.

3.3.2 Quinol:Pyrazine (1)

Although pyrazine is chemically rather different to 1,4-dioxane, the two molecules are similar in that they both consist of six-membered rings with centrosymmetrically-related hydrogen bond acceptors in the 1 and 4 positions. In addition, although the ether oxygen can potentially act as a double acceptor, it rarely does so, and so the N-atoms in pyrazine and the O-atoms in 1,4-dioxane can both be considered to be monofunctional H-bond acceptors.

The asymmetric unit of quinol:pyrazine contains half-molecules of quinol and pyrazine, both occupying inversion centres in space group $P2_1/c$. The structure is very similar to the 1,4-dioxane co-crystal, and the primary graph set consists of a $C_2^2(12)$ chain formed by alternating quinol and pyrazine molecules, which are hydrogen-bonded via OH...N interactions (H...N 1.85(2) Å, see Table 3.2); the chains run from top left to lower right in Figure 3.2. The orientation of pyrazine enables a close contact to be formed between a C-H and the O of the hydroxyl group (2.40 Å), which serves to link chains to form a layer. Thus a $R_4^4(10)$ subunit (circled in Figure 3.2) composed of two quinol molecules doubly-bridged by two guest molecules, which characterised the 1,4-dioxane co-crystal, is also observed here.

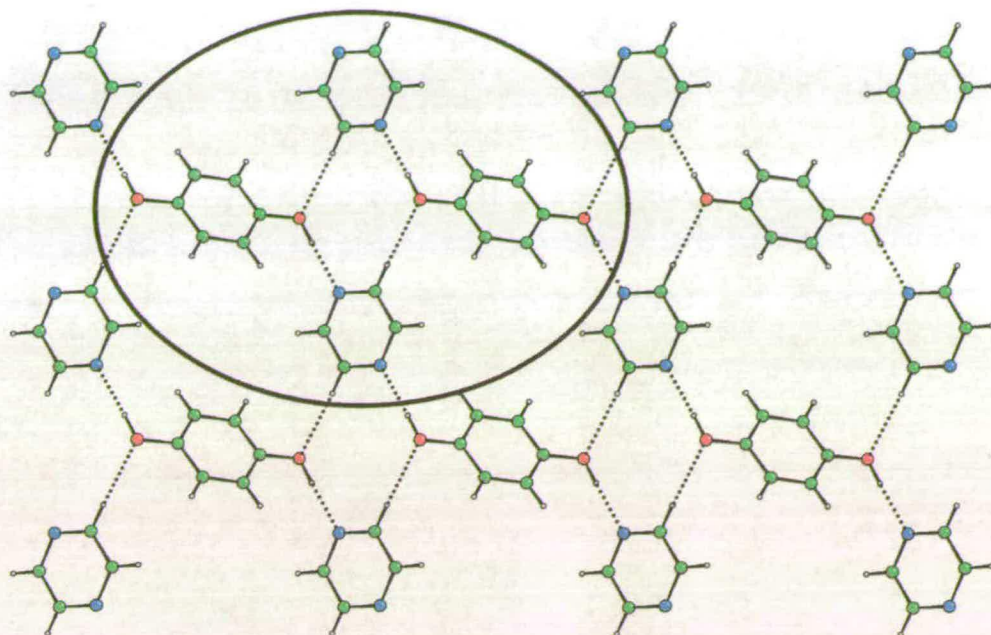


Figure 3.2: Quinol:pyrazine (1) viewed perpendicular to the (0 0 1) planes. A similar doubly-bridging motif to the 1,4-dioxane structure is observed, here involving an aromatic CH as a donor to the phenolic oxygen, producing an $R_4^4(10)$ graph set (circled). The layers occupy the (0 0 2) planes, and alternate layers contain chains passing along the $[1\ 1\ 0]$ and $[1\ \bar{1}\ 0]$ directions (note that the source of the differences in Miller indices between the 1,4-dioxane and this pyrazine co-crystals is that the former has published coordinates referred to $P2_1/a$, while the latter is in $P2_1/c$). Colour scheme: C green, H grey, O red and N blue; this colour scheme is adopted in all Figures.

3.3.3 Quinol:Piperazine (2)

In quinol:piperazine both components are located on inversion centres. The amine hydrogen atom (the position of which was derived from a difference Fourier map) favours the axial position in the piperazine molecule. The structure is depicted in Figure 3.3.

Piperazine is related to 1,4-dioxane by substitution of two NH groups for the ether oxygen atoms. As in 1,4-dioxane and pyrazine the N atoms act as monofunctional H-bond acceptors, but they can, in addition, act as H-bond donors. $C_2^2(12)$ chains are formed via OH...N H-bonds, and run from top left to lower right in Figure 3.3. NH...O hydrogen bonds are formed between the quinol and piperazine molecules in neighbouring chains, forming layers. The doubly-bridging subunit (circled in Figure 3.3), which was observed in the 1,4-dioxane and pyrazine co-crystals, is also observed here, although it forms an $R_4^4(8)$ graph, rather than $R_4^4(10)$, because the donor capacity of piperazine is 'built into' the amine group.

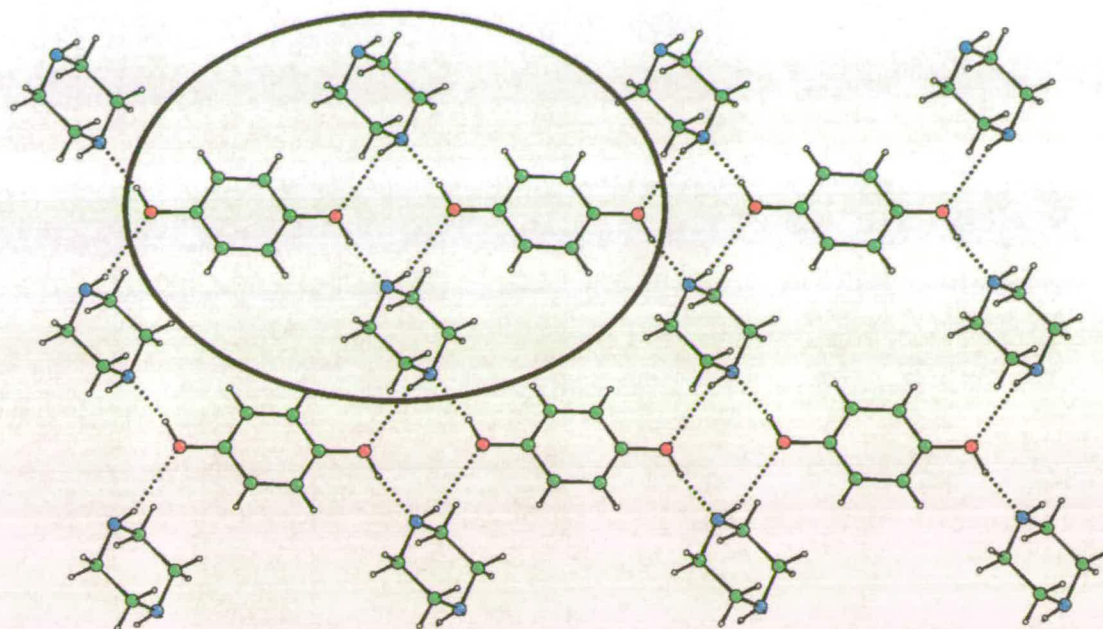


Figure 3.3: Quinol:piperazine (2) viewed perpendicular to the (1 1 0) planes. The donor-acceptor function of the amine moiety allows the co-crystal to form an $R_4^4(8)$ H-bonded doubly-bridging motif (circled).

3.3.4 Quinol:2Morpholine (3)

Morpholine is related to 1,4-dioxane through the substitution of one of the oxygen atoms with protonated nitrogen. This co-crystal crystallises with one molecule of morpholine and half a molecule of quinol in the asymmetric unit, and in this respect it differs from the 1,4-dioxane, pyrazine and piperazine co-crystals which all have 1:1 stoichiometry. The quinol resides on a crystallographic inversion centre. The hydrogen atom (H1S) attached to the nitrogen in the morpholine molecule was located in a difference Fourier map, and found to occupy the less favourable axial position.

The hydrogen bonding functionality of the quinol molecules, which form OH...N H-bonds to the morpholine molecules, resembles that in the piperazine co-crystal. However, the ether oxygen atoms do not participate in hydrogen bonding, and the $C_2^2(12)$ chain motif observed in the piperazine co-crystal corresponds to a discrete $D_2^2(10)$ motif consisting of one quinol and two morpholine molecules in this co-crystal (see Figure 3.4a running diagonally from top left to lower right): the ether oxygen atoms act like chain-stoppers. Neighbouring quinol:2morpholine units are linked by NH...O H-bonding interactions. A doubly-bridging subunit (ringed in Figure 3.4a) analogous to those observed in the structures described above

therefore also appears in this co-crystal. As in the piperazine co-crystal its secondary level graph set descriptor is $R_4^4(8)$.

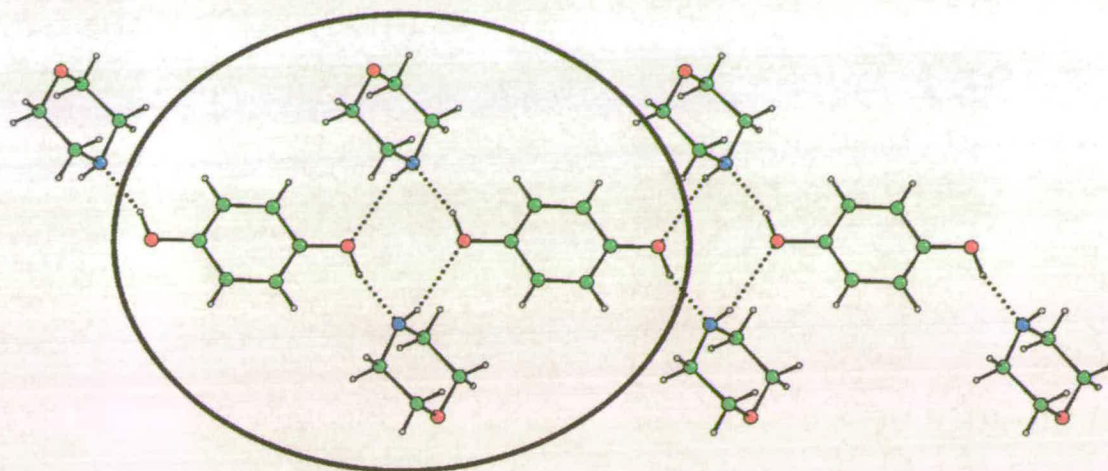


Figure 3.4a: Quinol:2morpholine (**3**) ribbon viewed perpendicular to the (1 1 2) planes. The morpholine co-crystal forms the same H-bonded bridging structure as piperazine ($R_4^4(8)$, circled), however, this does not extend into a layer due to the relatively weak acceptor ability of the ether oxygen, which does not take part in H-bonding.

The ether oxygen atom does not participate in any interactions which would be considered significant using a criterion based on sums of van der Waals radii, with the result that the structure is based on ribbons, and not layers. The structure partitions into one set of regions at $c = 0, 1 \dots etc.$ where the ribbons run parallel to $[1\ 1\ 0]$, and a second set through the middle of the unit cell ($c = 0.5$) where the ribbons run parallel to $[\bar{1}\ 1\ 0]$ (Figure 3.4b). The overall effect is to interleave morpholine molecules. The angle between the mean planes of morpholine molecules in neighbouring ribbons passing along $[1\ 1\ 0]$ and $[\bar{1}\ 1\ 0]$ is $78.4(4)^\circ$ and the closest contacts made by O4S are to H-atoms attached to C2S and C3S (2.75 and 2.81 Å, respectively)

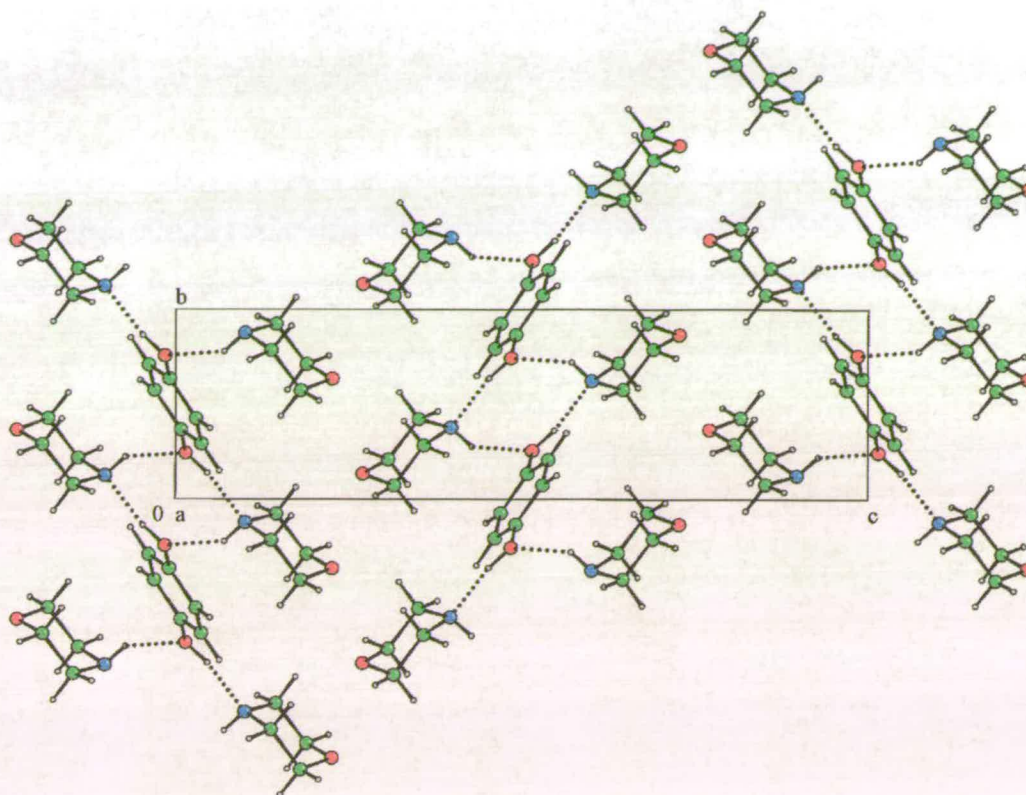


Figure 3.4b: The structure of quinol:2morpholine (**3**) viewed down the a -axis showing the interleaved morpholine molecules. The ribbons at $c = 0, 1, \dots$ etc. run parallel to $[1\ 1\ 0]$ and the second set of ribbons at $c = 0.5$ run parallel to $[\bar{1}\ 1\ 0]$.

3.3.5 Quinol:2Pyridine (**4**)

Pyridine is related to pyrazine through the substitution of one of the nitrogen atoms by CH. This co-crystal crystallises with one molecule of pyridine and a half molecule of quinol in the asymmetric unit. The quinol molecule resides on a crystallographic inversion centre.

The H-bonding activity in the quinol molecules is identical to that observed in the pyrazine co-crystal (see above and Figure 3.2). The quinol donates to two symmetrically equivalent pyridine molecules through a OH...N interactions (Figure 3.5a) to form a discrete $D_2^2(10)$ motif consisting of one quinol and two pyridine molecules. This is analogous to the structure of the morpholine co-crystal, with the CH group in the 4-position of the pyridine acting as a chain-stopper, and, as a result, this structure consists of ribbons. The CH adjacent to the nitrogen atom of a pyridine in a neighbouring quinol:2pyridine unit acts as the donor group to the phenolic oxygen, yielding the same doubly-bridging $R_4^4(10)$ motif as observed in the pyrazine co-crystal (ringed in Figure 3.5a). Neighbouring ribbons interact with each other

through π -stacking of the pyridine molecules in which the stacking distance is 3.45 Å and the angle between the mean planes of stacked pyridine molecules 5.32(6)° (Figure 3.5b).

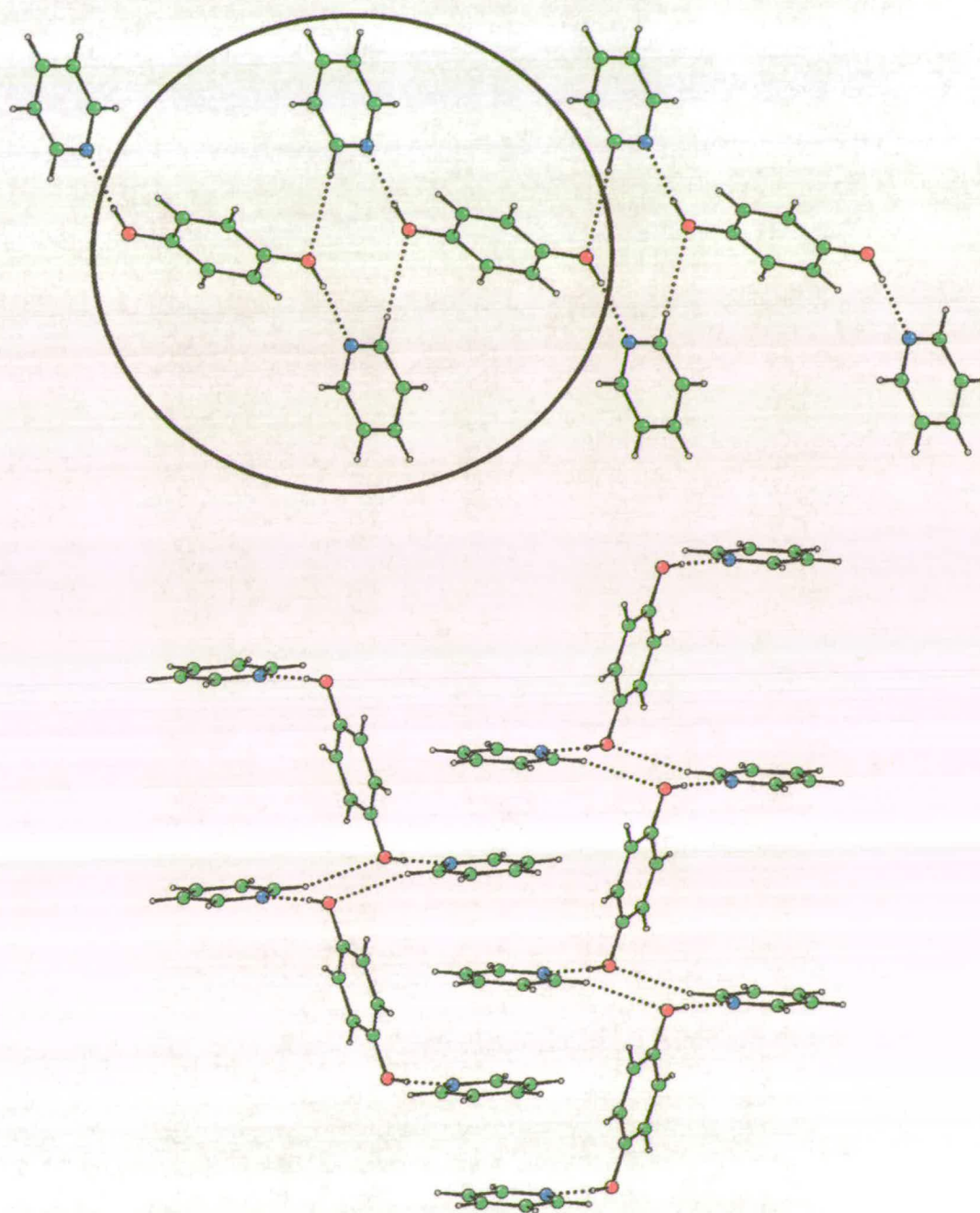


Figure 3.5 top (a): Quinol:2pyridine (4) co-crystal viewed perpendicular to the $(2\ 1\ \bar{2})$ planes. The doubly-bridging motif is present OH...N and CH...O interactions giving a $R_4^4(10)$ graph set (*cf.* pyrazine, circled).

Figure 3.5 bottom (b): Quinol:2pyridine (4) viewed down the a -axis. Colour scheme: C green, H grey, O red and N blue. The π -stacking of pyridine molecules from neighbouring ribbons can clearly be seen.

3.3.6 *Quinol:2Piperidine (5)*

Piperidine is related to morpholine through the substitution of the oxygen atom with a methylene group. This co-crystal crystallises with one molecule of piperidine and half a molecule of quinol in the asymmetric unit (*cf.* the morpholine and pyridine co-crystals). The quinol resides on a crystallographic inversion centre. The hydrogen atom (H1S) attached to the nitrogen in the piperidine molecule was located in a difference Fourier map, and occupies the axial position.

This co-crystal forms a similar structure to morpholine and pyridine in that it consists of discrete $D_2^2(10)$ units, consisting of one quinol and two piperidine molecules, which are linked into a ribbon via NH...O hydrogen bonds. Rather than forming an $R_2^2(8)$ motif the doubly-bridging subunit forms an $R_4^4(18)$ graph set (this is circled in Figure 3.6).

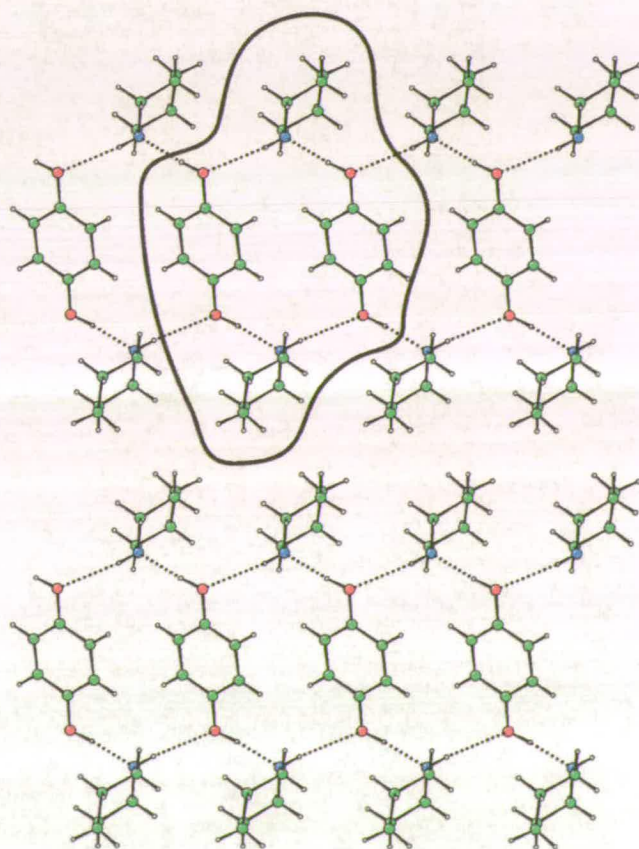


Figure 3.6a: Quinol:2piperidine (5) viewed perpendicular to the $(\bar{1} 0 1)$ planes. Piperidine structure possesses a doubly-bridging structure observed in the other co-crystals, however, the ring graph set formed is much larger, $R_4^4(18)$ (circled), due to the relative orientation of the quinol molecules. Ribbons are formed rather than an extended layer motif, this follows from the absence of strong H-bonding functions in the 4-position in piperidine.

There are a larger number of atoms in this graph set descriptor than in the structures discussed previously because of the difference in the relative orientations of the quinol and

piperidine molecules: compare, for example, Figures 3.3, 3.5a and 3.6a. A view of the packing along the direction of the ribbons ($[0\ 1\ 0]$) is shown in Figure 3.6b.

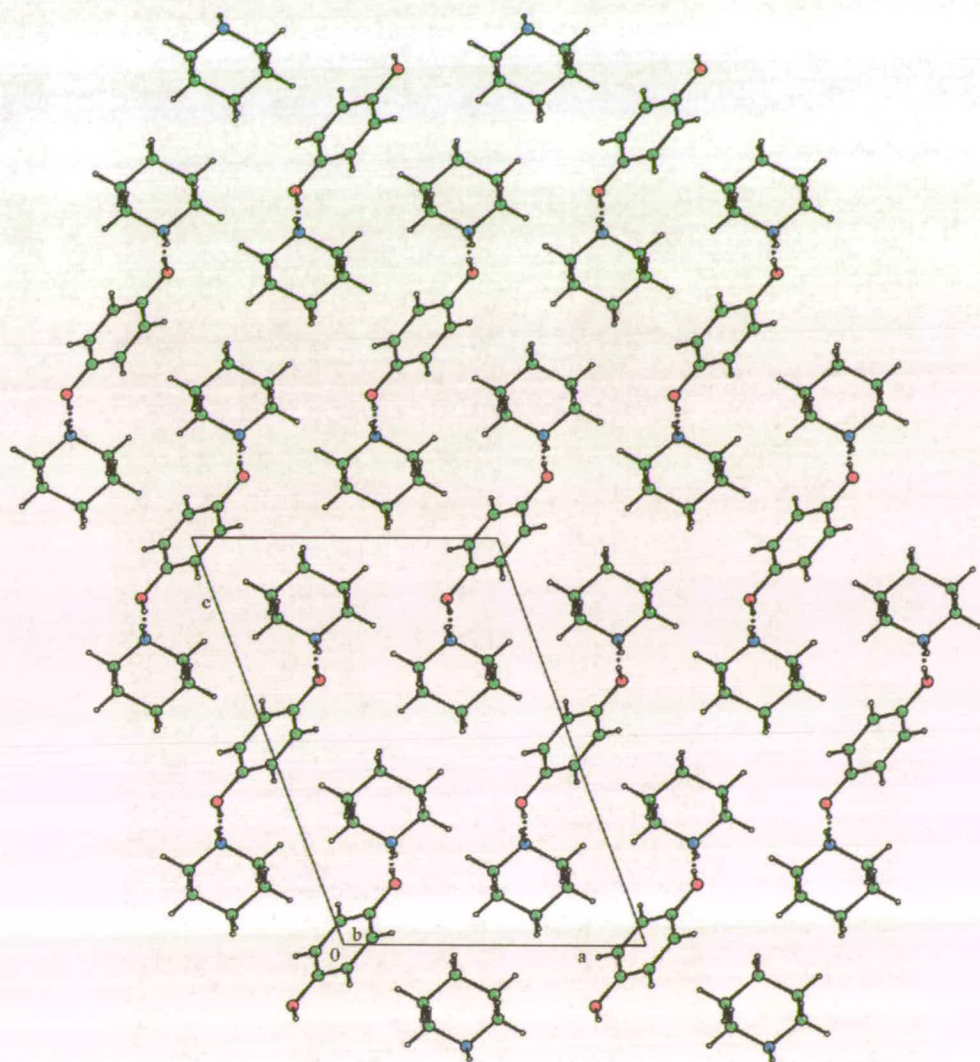


Figure 3.6b: Quinol:2piperidine (5) viewed down the b -axis. The structure is based on ribbons which form along the $[0\ 1\ 0]$ direction and are arranged in the $(\bar{2}\ 0\ 2)$ planes. Piperidine molecules in neighbouring chains occupying the same $(\bar{2}\ 0\ 2)$ plane are interleaved.

3.3.7 Quinol:2(4,4'-bipyridine) (6)

Co-crystals of quinol with 4,4'-bipyridine, N-methylmorpholine and N,N'-dimethylpiperazine were studied in order to investigate the effect of steric hindrance on the doubly-bridging motif that has been observed in all the structures so far described. Like morpholine, 4,4'-bipyridine forms a 1:2 co-crystal with quinol, and the asymmetric unit contains half a molecule of quinol and one molecule of 4,4'-bipyridine. The angle between the C_5N planes in the 4,4'-bipyridine molecules is $28.59(6)^\circ$.

Predictably, the quinol interacts with the 4,4'-bipyridine molecule through a H-bond between O1A...N1B. In terms of the symmetry of its H-bond acceptor functions bipyridine resembles 1,4-dioxane, pyrazine and piperazine. It is, however, much larger, and a structure built on a network resembling those described above would presumably have a prohibitively low density; this may explain the stoichiometry of this co-crystal. As in the other 1:2 co-crystals in this series, the structure contains $D_2^2(10)$ unit consisting of one quinol and two bipyridine molecules. These are then linked into ribbons via a subunit (ringed in Figure 3.7a) in which two quinol molecules are doubly-bridged by CH...O interactions with two bipyridine molecules. The C-H groups adjacent to the N-atoms in bipyridine sometimes act as donors. This is not at all uncommon, and it has even been used in crystal structure design, but it is not observed here. Instead the quinol oxygen atom acts as an acceptor for the hydrogen atom adjacent to the central C-C bond of the bipyridine (C9S-H9S...O1A, 2.46 Å, 169°).

A second CH...O bond exists between C5S-H5S and O1A (2.59 Å, 152°) that connects the ribbons together to form layers. When viewed along the *b*-axis the structure consists of regions of quinol molecules occupying different layers at $c = 0, 1...etc.$ and regions of bipyridine molecules at $c = \frac{1}{2}$ in which bipyridine molecules in different layers interleave (Figure 3.7b). The layers are connected by weak N...H interactions measuring 2.9 to 3.0 Å involving N7S in one layer and H-atoms in another (these contacts are not shown in Figure 3.7b for the sake of clarity).

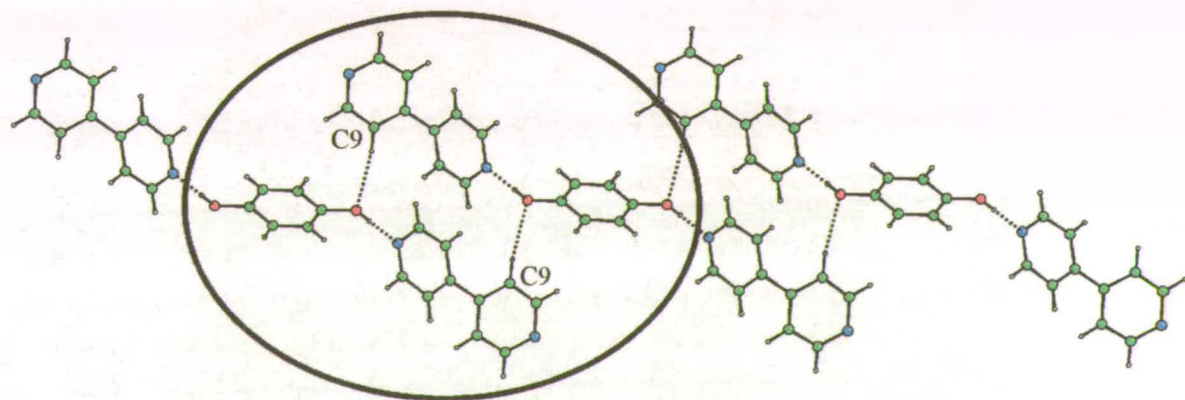


Figure 3.7a: Quinol:2(4,4'-bipyridine) (6) viewed perpendicular to the $(1\ 1\ \bar{2})$ planes. The 'built-in' donor ability is not present in bipyridine therefore the guest uses an aromatic CH...O interaction to build up the bridging motif. The graph set for this motif is the same as the piperidine structure, $R_4^4(18)$ (circled).

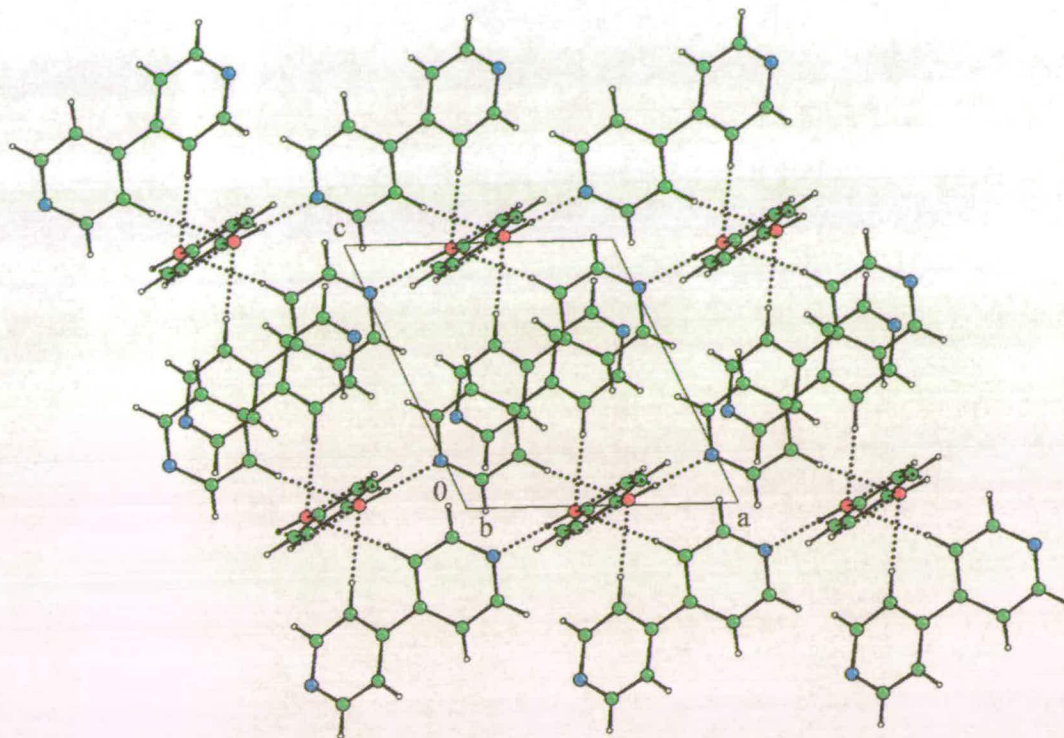


Figure 3.7b: Quinol:2(4,4'-bipyridine) (6) viewed perpendicular b -axis. The different regions of quinol molecules at $c = 0, 1, \dots$ etc. and bipyridine molecules at $c = \frac{1}{2}$. The bipyridine molecules in different layers interleave.

3.3.8 Quinol:2*N*-methylmorpholine (7)

Crystals of *N*-methylmorpholine were grown by Boese's laser-assisted zone refinement method from a 1:2 mixture of quinol and *N*-methylmorpholine held in a capillary mounted on the diffractometer. Crystal growth experiments by more conventional procedures failed to yield anything but crystals of quinol.

The crystal structure contains half a molecule of quinol and a whole molecule of *N*-methylmorpholine in the asymmetric unit. The methyl group of the *N*-methylmorpholine molecule adopts the expected equatorial position. As in the other 1:2 co-crystals there is a $D_2^2(10)$ motif consisting of one quinol and two *N*-methylmorpholine molecules connected by centrosymmetrically-related OH...N hydrogen bonds (Figure 3.8). In the morpholine co-crystal (see above) the $D_2^2(10)$ units were linked together via a doubly-bridging subunit involving NH...O interactions, but substitution of the NH group by N(CH₃) means that this can not occur in the *N*-methylmorpholine co-crystal. The steric bulk of the methyl group also forces a change in the relative orientation of the quinol and guest molecules preventing the alternative O...CH(ring) interaction seen elsewhere in this series. The steric effect of the *N*-methyl group has therefore been to disrupt formation of the doubly-bridging unit

highlighted in Figures 3.1-3.7. $D_2^2(10)$ units are instead linked via $\text{CH}_3\cdots\text{O}$ interactions between N-methylmorpholine molecules, forming ribbons. The ribbons are then linked into a layer by further $\text{CH}\cdots\text{O}$ interactions between N-methylmorpholine molecules.

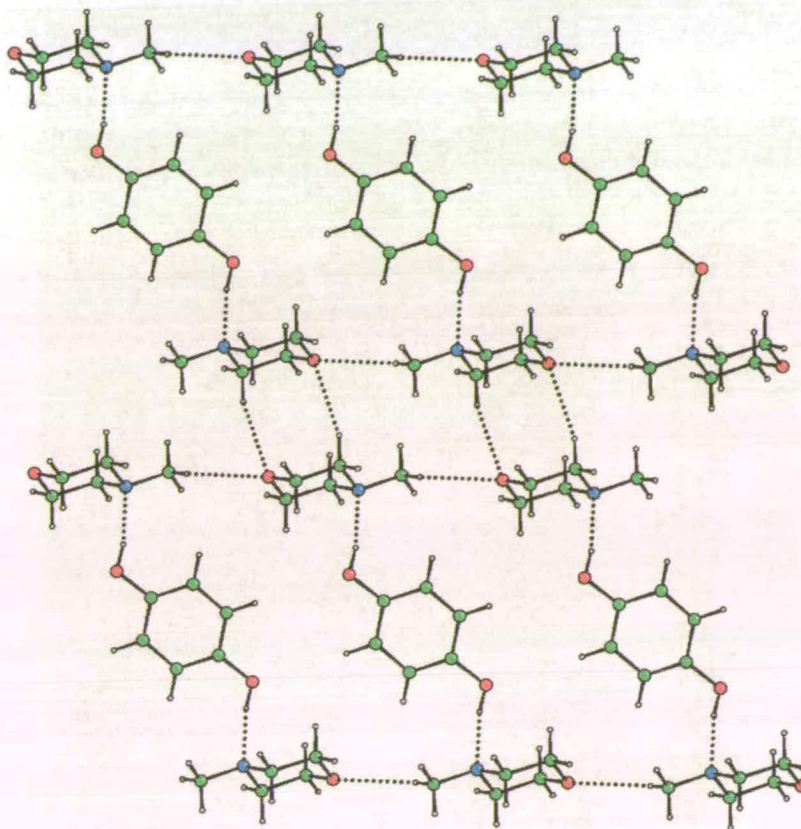


Figure 3.8: Quinol:2N-methylmorpholine (7) viewed perpendicular to the (1 0 1) planes. The methyl group on the nitrogen has prevented formation of a bridging motif.

3.3.9 Quinol:*N,N'*-dimethylpiperazine (8)

In the asymmetric unit of the *N,N'*-dimethylpiperazine co-crystal there are two molecules of quinol and four half-molecules of *N,N'*-dimethylpiperazine, so that the co-crystal has overall 1:1 stoichiometry. In all cases the methyl groups of the *N,N'*-dimethylpiperazine are in the expected equatorial positions.

The strongest intermolecular interactions are $\text{OH}\cdots\text{N}$ hydrogen bonds which build up $C_2^2(12)$ chains (Figure 3.9), similar to those observed in quinol:piperazine co-crystal. There are two symmetrically inequivalent chains present in the structure, both involving one quinol molecule and two independent guest molecules. The quinol is present in a non-centrosymmetric conformer, which results in the chains becoming more sinusoidal than in the piperazine co-crystal. As in the N-methylmorpholine co-crystal described above, the N-methyl groups prevent formation of bridging interactions between chains, which are,

instead, linked by CH...O interactions with other chains that pass through the rather open structure depicted in Figure 3.9.

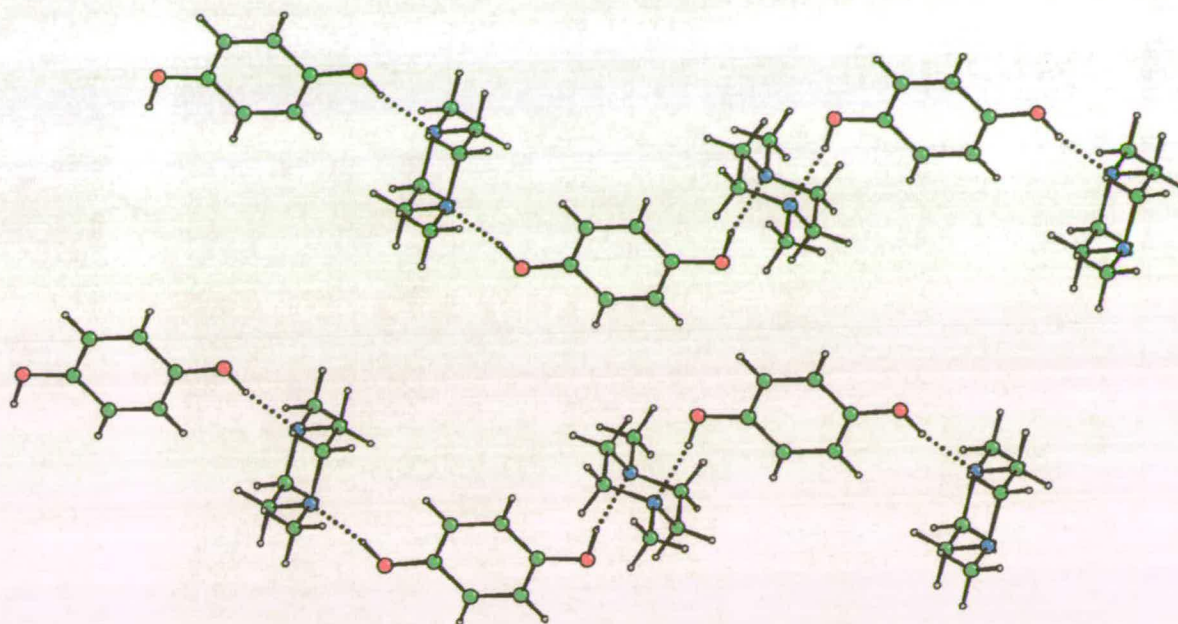


Figure 3.9: Quinol:*N,N'*-dimethylpiperazine (**8**). The methyl groups on the nitrogen cause major structural rearrangement away from the bridging structure observed in other co-crystals in this series. The inequivalent chains run perpendicular to these chains filling the space between the two chains.

3.4 Discussion and conclusions

The previous Chapter on paracetamol co-crystals utilised the Cambridge Structural Database (CSD) in rationalising the formation of a series of co-crystals from pure paracetamol (Oswald *et al.*, 2002, Oswald *et al.*, 2004), and a similar procedure can be used for this series of compounds. There are only two classical H-bond donor-groups in this series, the phenol OH and a secondary amine NH. The aromatic or aliphatic CH groups, adjacent to the heteroatom, with the phenolic oxygen, can also act as donors. The acceptor groups in the series are a phenolic O, secondary or tertiary amine N, ether O and pyridine N. The results of searches of the CSD for typical H-bond geometries involving these functionalities are listed in Table 3.3, searching criteria are given in the legend to that table.

In interpreting the data in Table 3.3, the assumption is made that the strength of hydrogen bonds is related to the donor-hydrogen – acceptor distance with the D-H bond normalised to typical neutron distances (O-H 0.983 Å, N-H 1.009 Å and C-H 1.083 Å).

Amine nitrogen atoms are more strongly basic than phenolic or ether oxygen atoms, and the strongest bonds in Table 3.3 are those from a phenol donor to a secondary or tertiary amine or a pyridine N. In co-crystals of this type H-bonds are formed to the guest in preference to the weaker OH...O(H) found in pure quinol, and where nitrogen atoms are present in the 1 and 4 positions of the guest (i.e. in pyrazine, piperazine and N,N'-dimethylpiperazine) 1:1 co-crystals are formed. H-bonds in which the phenolic and ether oxygen atoms act as acceptors to weak CH donors are similar in strength. This observation helps to rationalise the formation of the 1,4-dioxane co-crystal. It was formed from a solution of quinol in 1,4-dioxane that was allowed to evaporate at room temperature. Under these conditions there is excess 1,4-dioxane present in the system, which would favour the OH...O(ether) interaction, leading to a 1:1 co-crystal of quinol and 1,4-dioxane.

In the co-crystals of quinol with molecules with N, NH or NMe and O, CH or CH₂ respectively in the 1 and 4 positions, the quinol H-bonds exclusively to the nitrogen moiety. In the case of morpholine and N-methylmorpholine the ether O-atom is a much less effective acceptor than the amine nitrogen (Table 3.3); in piperidine and pyridine the CH₂ and CH groups in the 4-positions can, of course, not act as acceptors at all. Quinol selectively binds to the nitrogen group, and, in order to satisfy the H-bonding capacity of quinol, all four of these co-crystals crystallise in a 1:2 quinol-to-guest ratio.

Considerations of H-bonding strength based on the data in Table 3.3 enable the stoichiometries of the majority of co-crystals studied here to be rationalised. The exception is the co-crystal of quinol with 4,4'-bipyridine, which would be predicted to form a 1:1 co-crystal, whereas the observed stoichiometry is 1:2, with only one of the two N-atoms in each bipyridine molecule used in H-bonding; this may be a size effect.

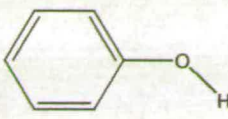
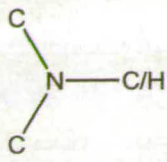


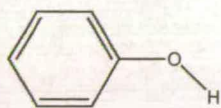
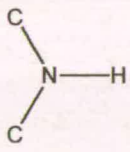
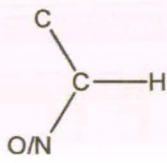
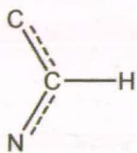
Donor (NH or OH)	Acceptor (O or N in each case)				
					
	Sample size	334	54	57	95
	Max OH..A /Å	2.20	2.19	2.20	2.18
	Min OH..A /Å	1.67	1.66	1.62	1.53
	Mean OH..A /Å	1.87	1.82	1.90	1.81
	Sample size	3	15	5	Not Applicable
	Max NH..A /Å	2.03	2.20	2.18	
	Min NH..A /Å	1.87	2.00	2.11	
	Mean NH..A /Å	1.94	2.14	2.13	
	Sample size	217	109	4273	Not Applicable
	Max CH..A /Å	2.75	2.75	2.75	
	Min CH..A /Å	2.13	2.40	1.87	
	Mean CH..A /Å	2.60	2.64	2.58	
	Sample size	67	Not Applicable	Not Applicable	328
	Max CH..A /Å	2.75			2.75
	Min CH..A /Å	2.18			2.26
	Mean CH..A /Å	2.52			2.59

Table 3.3: Summary of the results of searches of the CSD (Version 5.25, November 2003) for typical distances in hydrogen bonded systems containing identical functional groups to the quinol co-crystals studied. The distances to hydrogen atoms were normalised to typical neutron distances (C-H 1.083, N-H 1.009 and O-H 0.983 Å). Only 'organic' structures where the *R*-factor is less than 0.05, with no errors or disorder were included, and ionic or polymeric structures were excluded. The C-atoms attached to the amine moieties were specified to be sp² or sp³ hybridised. The donor-H to acceptor distance was specified to be 1.50-2.20 Å or 1.50-2.75 Å in the case of the CH donor atoms.

All the 1:1 co-crystals are based on $C_2^2(12)$ chains of alternating quinol and guest molecules. All the 1:2 co-crystals are based on discrete $D_2^2(10)$ motifs containing one quinol and two guest molecules. In all but the two sterically-hindered cases (N-methylmorpholine and N,N'-dimethylpiperazine) the $C_2^2(12)$ chains or $D_2^2(10)$ -based motifs are linked about an inversion centre by NH...O or CH...O interactions in which quinol molecules are doubly-bridged by pairs of guest molecules. This linking of chains builds layers in the 1:1 co-crystals; linking of the discrete units in the 1:2 co-crystals builds ribbons.

These observations also apply to the crystal structure of quinol itself. Three polymorphs of quinol are known, but the simplest is the monoclinic γ -polymorph, and the co-crystals discussed in this Chapter are related to this structure. In the asymmetric unit there are two half molecules of quinol residing on inversion centres. The primary graph set is $C_2^2(14)$ formed by OH...O(H) H-bonds; this corresponds to the $C_2^2(12)$ chains of the 1:1 co-crystals described above. These chains are parallel to one another and H-bond together to form a doubly-bridging $R_4^4(18)$ graph set at the secondary level (Figure 3.10).

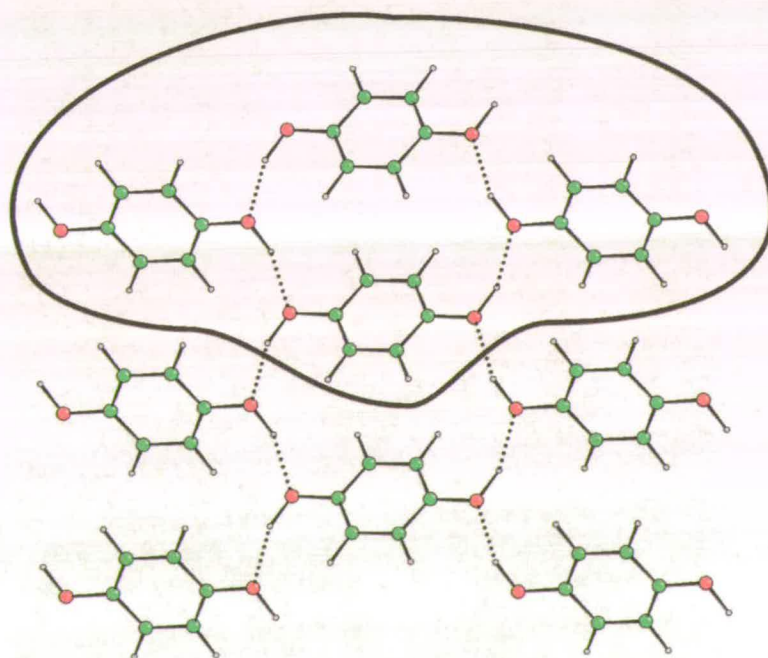


Figure 3.10: γ -quinol viewed down the a -axis. Colour scheme: C green, H grey and O red. γ -quinol is a layered structure where the primary graph set is $C_2^2(14)$; these chains are parallel to one another and H-bond together to form an $R_4^4(18)$ graph set.

3.5 References

- Allen, F. H. & Motherwell, W. D. S. (2002). *Acta Cryst. B58*, 407-422.
- Barnes J. C., Paton, J. D. & Blyth, C. S. (1990). *Acta Cryst. C46*, 1183-1184.
- Bernstein, J., Davis, R. E., Shimoni, L. & Chang, N-L. (1995). *Angew. Chem. Int. Ed. Engl.* **34**, 1555-1573.
- Blessing, R. H. (1995). *Acta Cryst. A51*, 33-38.
- Boese, R. & Nussbaumer, M. (1994). In *Correlations, Transformations, and Interactions in Organic Crystal Chemistry*, D. W. Jones & A. Katrusiak (Editors). (International Union of Crystallography, Crystallographic Symposia, 7), pages 20-37.
- Bolte, M. & Lerner, H-W. (2001). *Private Communication to CSD*, CCDC 161816.
- Bruno, I. J., Cole, J. C., Edgington, P. R., Kessler, M., Macrae, C. F., McCabe, P., Pearson, J. & Taylor, R. (2002). *Acta Cryst. B58*, 389-397.
- Buschmann, J., Müller, E. & Luger, P. (1986). *Acta Cryst. C42*, 873-876.
- Caspari, W. A. (1926). *J. Chem. Soc.* 2944-2948.
- Caspari, W. A. (1927). *J. Chem. Soc.* 1093-1095.
- Cosier, J., & Glazer, A. M. (1986). *J. Appl. Cryst.* **19**, 105-107.
- Farrugia, L. J. (1999). *J. Appl. Cryst.* **32**, 837-838.
- Lindeman, S. V., Shklover, V. E. & Struchkov, Y. T. (1981). *Cryst. Struct. Commun.*, **10**, 1173-1179.
- Maartmann-Moe, K. (1966). *Acta Cryst.* **21**, 979-982.
- Oswald, I. D. H., Allan, D. R., McGregor, P. A., Motherwell, W. D. S., Parsons, S. & Pulham, C. R. (2002). *Acta Cryst. B58*, 1057-1066.
- Oswald, I. D. H., Motherwell, W. D. S., Parsons, S., Pidcock, E. & Pulham, C. R. (2004). *Cryst. Rev.*, **10**, 57-66.
- Parkin, A., Oswald, I. D. H. & Parsons, S. (2004). *Acta Cryst. B60*, 219-227.
- Sheldrick, G. M. (1997a). *SADABS*. Bruker-AXS, Madison, Wisconsin, USA.
- Sheldrick, G. M. (1997b). *SHELXTL*. Bruker-AXS, Madison, Wisconsin, USA.

Spek, A. L. (2002). *PLATON- A Multipurpose Crystallographic Tool*, Utrecht University, Utrecht, The Netherlands.

Taylor, R. & Macrae, C. F. (2001). *Acta Cryst. B57*, 815-827.

Watkin, D. J., Pearce, L. & Prout, C. K. (1993). *CAMERON - A Molecular Graphics Package*. Chemical Crystallography Laboratory, University of Oxford, England.

Chapter 4

Co-Crystals of Formic and Acetic Acids with *Isonicotinamide*: Proton Migration in Formic Acid:*Isonicotinamide*.

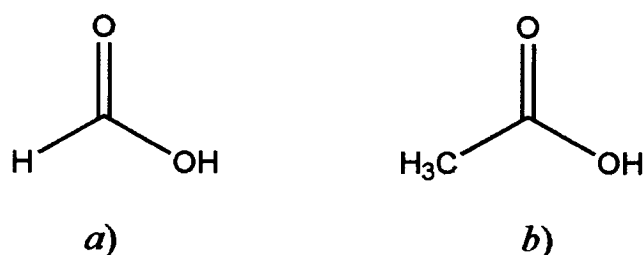
4.1 Introduction

The design of molecular assemblies has received much interest in recent years with its application to drug processing and green chemistry. The assemblies made from the co-crystallisation of two components can be utilised to alter the macroscopic properties of the host compound such as the solubility and hardness. Traditional methods to change the physical properties include the direct derivatisation of the host compound i.e. modifying the covalently attached functional groups. The synthetic methods to achieve the desired derivatisation rely heavily on the use of solvents and toxic reagents; such procedures are becoming less applicable as a result of the tightening of environmental legislation. Co-crystallisation of a host compound with a guest molecule avoids the use of solvents and the production of toxic side products but yields a change in the overall physical properties (Anastas & Warner, 2002). For the use of 'non-covalent derivatisation' to become wide spread in manufacturing industries it is important that a series of reliable supramolecular reactions be found so that they may be utilised in manufacturing processes.

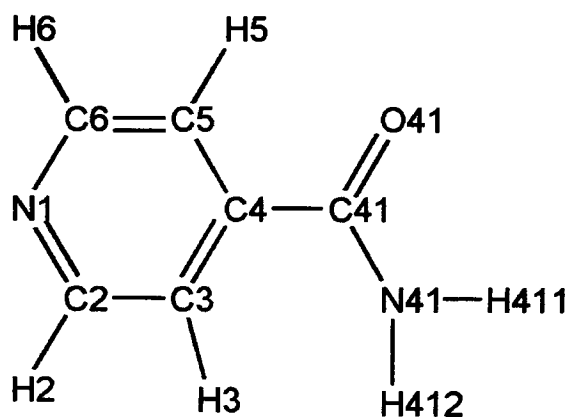
The systematic investigation of co-crystals gives an insight into the variety of hydrogen bonding patterns that can be formed given certain functional groups. Recent studies by Aakeröy *et al.* (2003) and by Vishweshwar *et al.* (2003) have investigated the hydrogen bonding patterns in a series of co-crystals of isonicotinamide (4-amidopyridine) with a view to finding reliable supramolecular reactions. Isonicotinamide has two functional groups that can participate in H-bonding; a pyridine moiety and an amide moiety. It was originally highlighted as a possible co-crystallising agent by Aakeröy *et al.* (2003) because of the structural flexibility which is implied by its existence in two polymorphic forms. Form I crystallises in space group $P2_1/c$ with one molecule in the asymmetric unit whereas form II also crystallises in $P2_1/c$ but with two molecules in the asymmetric unit. All possible types of interactions using amide and pyridine moieties are utilised in the polymorphs of isonicotinamide. Form I shows preference for a homomeric dimer between amide groups (a head-to-head arrangement) whereas form II prefers to form a H-bond between the amide group and the pyridine moiety (a head-to-tail arrangement).

In addition to these two polymorphs, isonicotinamide crystallises in thirty different binary and ternary co-crystals (Aakeröy *et al.*, 2002; Aakeröy *et al.*, 2003; Vishweshwar *et al.*, 2003). This clearly shows the flexibility of isonicotinamide as a host molecule for various carboxylic acids and alcohols. The only systematic study of isonicotinamide with a series of guest molecules was by Vishweshwar *et al.* (2003). In their paper, a series of homologous

alkanedicarboxylic acids with *isonicotinamide* was investigated to reveal the hydrogen bonding patterns formed with varying alkyl chain length. In all other studies of *isonicotinamide* the R-group attached to the carboxylic acid was changed dramatically. In this study we look at co-crystals of the simple carboxylic acids, formic acid and acetic acid, with *isonicotinamide* to understand the rearrangement that occurs on addition of a methyl group. The proton involved in the hydrogen bond between formic acid and *isonicotinamide* shows some disorder, which has been studied with respect to temperature. This behaviour is not seen in acetic acid. Scheme 4.1 shows the guest molecules used in the study. Scheme 4.2 shows the host molecule with numbering scheme.



Scheme 4.1: Guest molecules used to form co-crystals with *isonicotinamide*; *a)* formic acid; *b)* acetic acid.



Scheme 4.2: *Isonicotinamide*, with atomic numbering scheme.

4.2 Experimental

4.2.1 Synthesis

All chemicals were bought from Sigma Aldrich and used as received.

Isonicotinamide:formic acid (1): Isonicotinamide (0.51 g, 4.18 mmol) was dissolved in an excess of formic acid (1.50 g, 32.61 mmol) and warmed until all the solid dissolved. On cooling to room temperature colourless rods were produced.

Isonicotinamide:acetic acid (2): Isonicotinamide (0.49 g, 4.02 mmol) was dissolved in an excess of acetic acid (1.95 g, 32.50 mmol) and warmed until all the solid dissolved. The solution was then cooled to room temperature producing colourless blocks.

4.2.2 Crystallography

X-ray diffraction intensities were collected with Mo-K α radiation on a Bruker SMART APEX CCD diffractometer equipped with an Oxford Cryosystems low-temperature device (Cosier & Glazer, 1986). Absorption corrections were carried out using the multi-scan procedure SADABS (Sheldrick, 2004, based on the procedure described by Blessing, 1995). All structures were solved by direct methods and refined by full-matrix least squares against F^2 using all data (SHELXTL, Sheldrick, 2001). H-atoms were placed on C-atoms in calculated positions and allowed to ride on their parent atoms. Hydrogen atoms involved in H-bonding were located in difference maps and refined freely. All non-H atoms were modelled with anisotropic displacement parameters.

4.2.3 Variable Temperature study of isonicotinamide:formic acid

X-ray diffraction patterns were collected and treated as above at temperatures of 100 K, 115 K, 130 K, 175 K and 240 K. The dataset taken at 240 K suffered from a split in the crystal, which complicated integration of the full dataset. Successful integration was performed on each run separately and the data merged in SORTAV (Blessing, 1997); the absorption corrections were performed before merging.

The co-ordinates obtained from the original structural refinement were input into CRYSTALS (Betteridge *et al.*, 2003) and refined against F^2 . All the hydrogen atoms except for H1, H411 and H412 were geometrically placed and allowed to refine. Hydrogen atoms H411 and H412 were located from the difference map and allowed to refine. The hydrogen

involved in proton disorder was clearly seen in the difference Fourier map produced in MAPVIEW (WINGX, Farrugia, 1999) using only strong data ($I/\sigma(I) > 3.00$). The automatic peak selection in CRYSTALS highlighted only one peak situated between O1 and N1 at 100 K although two peaks could clearly be observed in the difference map. The positional parameters of the disordered hydrogen atom sites were taken from the 115 K model and used as a starting point for the refinement of the 100 K model. The occupancies of each site (H1 attached to N1 & H21 attached to O1) were refined competitively against one another and the positions of the hydrogen refined with a distance restraint of 0.90(1) Å applied to H1-N1; this value is consistent with that observed in the difference maps and with typical distances for such systems. A single isotropic displacement parameter was refined for all the hydrogen atoms. The refinement at all temperatures was stable, converging to $\Delta/\sigma < 0.001$.

A full listing of crystal, data collection and refinement parameters is given in Table 4.1, a set of H-bonding parameters is given in Table 4.2. Structures were visualised using SHELXTL or MERCURY (Taylor & Macrae, 2001; Bruno *et al.*, 2002); the figures were produced using CAMERON (Watkin *et al.*, 1993). Other analysis utilised the p.c. version of the program PLATON (Spek, 2002; Farrugia, 1999). Searches of the Cambridge Crystallographic Database (Allen, 2002; Allen & Motherwell, 2002) were carried out with the program CONQUEST, utilising version 5.25 of the database. Crystallographic information files for all structures reported here are available on the CD at the back of this Thesis.

Adduct	(1)	(2)
Formula	C ₇ H ₈ N ₂ O ₃	C ₈ H ₁₀ N ₂ O ₃
<i>M</i>	168.15	182.18
Radiation	Mo-K α	Mo-K α
Temperature/ K	150	150
Crystal System	Monoclinic	Triclinic
Space group	<i>P</i> 2 ₁ / <i>c</i>	<i>P</i> $\bar{1}$
<i>a</i> /Å	3.7287(5)	3.8267(6)
<i>b</i> /Å	27.331(3)	10.6429(16)
<i>c</i> /Å	7.4848(9)	10.7328(16)
α /°	90	85.258(2)
β /°	96.386(2)	85.479(2)
γ /°	90	84.739(2)
Volume /Å ³	758.05(16)	432.67(11)
No. reflections for cell	4513	2210
2 θ _{max} (°)	57.88	57.14
<i>Z</i>	4	2
<i>D</i> _c (Mg/m ³)	1.473	1.398
μ mm ⁻¹	0.117	0.109
Reflections collected	6691	3813
Unique [<i>R</i> _{int}]	1843[0.0207]	1982[0.0271]
No. <i>I</i> > 2 σ (<i>I</i>)	1792	1809
<i>T</i> _{min} / <i>T</i> _{max}	0.731/1.000	0.701/1.000
Parameters	123	132
<i>R</i> ₁ [<i>F</i> > 4 σ (<i>F</i>)]	0.0514	0.0510
<i>wR</i> ₂ (<i>F</i> ² , all data)	0.1279	0.1377
<i>S</i>	1.192	1.067
ρ _{max} / eÅ ⁻³	0.299	0.291
ρ _{min} / eÅ ⁻³	-0.309	-0.350

Table 4.1: Crystallographic data for the co-crystals of isonicotinamide with formic acid (1), acetic acid (2) (data collected at 150 K).

Adduct	VT100	VT115	VT130	VT175	VT240
Formula	C ₇ H ₈ N ₂ O ₃	C ₇ H ₈ N ₂ O ₃	C ₇ H ₈ N ₂ O ₃	C ₇ H ₈ N ₂ O ₃	C ₇ H ₈ N ₂ O ₃
<i>M</i>	168.15	168.15	168.15	168.15	168.15
Radiation	Mo-K α	Mo-K α	Mo-K α	Mo-K α	Mo-K α
Temperature/ K	100	115	130	175	240
Crystal System	Monoclinic	Monoclinic	Monoclinic	Monoclinic	Monoclinic
Space group	<i>P</i> 2 ₁ / <i>c</i>	<i>P</i> 2 ₁ / <i>c</i>	<i>P</i> 2 ₁ / <i>c</i>	<i>P</i> 2 ₁ / <i>c</i>	<i>P</i> 2 ₁ / <i>c</i>
<i>a</i> /Å	3.7055(3)	3.7131(3)	3.7182(3)	3.7388(4)	3.762(2)
<i>b</i> /Å	27.337(3)	27.342(3)	27.346(3)	27.365(3)	27.296(14)
<i>c</i> /Å	7.4760(8)	7.4843(6)	7.4833(7)	7.4995(7)	7.499(4)
α /°	90	90	90	90	90
β /°	96.675(7)	96.582(6)	96.521(7)	96.238(7)	95.717(13)
γ /°	90	90	90	90	90
Volume /Å ³	752.16(13)	754.83(11)	755.95(12)	762.73(13)	766.2(7)
No. reflections for cell	1467	2882	1487	1234	816
2 θ _{max} (°)	61.02	61.13	61.11	61.00	61.75
<i>Z</i>	4	4	4	4	4
<i>D</i> _c (Mg/m ³)	1.485	1.480	1.477	1.464	1.458
μ mm ⁻¹	0.118	0.118	0.118	0.117	0.116
Reflections collected	7943	11649	7999	8059	14776
Unique [<i>R</i> _{int}]	2212[0.040]	2229[0.083]	2229[0.036]	2244[0.042]	2286[0.0869]
No. <i>I</i> > 2 σ (<i>I</i>)	1408	1342	1339	1275	1772
<i>T</i> _{min} / <i>T</i> _{max}	0.63/0.98	0.68/0.98	0.64/0.98	0.65/0.98	0.50/0.98
Parameters	138	138	138	138	138
<i>R</i> ₁ [<i>F</i> > 4 σ (<i>F</i>)]	0.0473	0.0451	0.0506	0.0511	0.1093
w <i>R</i> ₂ (<i>F</i> ² , all data)	0.1099	0.1010	0.1093	0.1200	0.2436
<i>S</i>	0.7845	0.7402	0.8637	0.8283	1.0552
ρ _{max} / eÅ ⁻³	0.70	0.56	0.54	0.48	0.55
ρ _{min} / eÅ ⁻³	-0.51	-0.52	-0.49	-0.53	-0.54
Occupancy (H1); normal weights	0.60(3)	0.55(3)	0.53(4)	0.50(3)	0.49(8)
Occupancy (H1); Modified Weights	0.571(18)	0.534(19)	0.474(19)	0.38(3)	0.43(2)

Table 4.1(cont'd): Crystallographic data for the co-crystals of isonicotinamide with formic acid at various temperatures (100 K, 115 K, 130 K, 175 K & 240 K).

Adduct	Donor	Acceptor	Obs. H...A Distance/ normalised distance / Å		Typical normalised distance / Å	Angle DHA (°)
(1)	N1-H1	O1	1.36(3)	1.57	1.69	174(3)
	N41-H411	O41 ⁱ	2.00(2)	1.90	1.93	174(2)
	N41-H412	O2 ⁱⁱ	1.96(2)	1.85	1.93	165(2)
	C2-H2	O2	2.72	2.66	2.54	119
	C6-H6	O1 ⁱⁱⁱ	2.41	2.28	2.54	165
	C1-H11	O1 ^{iv}	2.71	2.60	2.54	141
(2)	O1-H1	N1	1.769(10)	1.69	1.66	176(3)
	N41-H411	O41 ^v	2.05(2)	1.89	1.93	177.6(18)
	N41-H412	O2 ^{vi}	2.01(2)	1.93	1.93	169.4(17)
	C2-H2	O1 ^{vii}	2.70	2.62	2.54	125

Symmetry Operators:

i	-x, -y+1, -z+2	v	-x-1, -y+1, -z+1
ii	x-1, y, z+1	vi	-x+1, -y+1, -z
iii	x, 1/2-y, 1/2+z	vii	-x, 2-y, -z
iv	x, 1/2-y, -1/2+z		

Table 4.2: Table of H-bonding parameters. C-H, N-H and O-H distances were normalised to 1.083, 1.009 and 0.983 Å, respectively.

4.3 Results and Discussion

4.3.1 Isonicotinamide:formic acid (1)

Isonicotinamide crystallises in a 1:1 ratio with formic acid in the monoclinic space group $P2_1/c$. The acid and isonicotinamide molecules hydrogen bond together via an interaction between the carboxylic acid group of formic acid and the pyridine nitrogen atom of isonicotinamide. The hydrogen bond is very short (O...N, 2.5468(16) Å) in comparison with other such interactions in the Cambridge Structural Database (average COOH...ArN is

2.63(6) Å). At 100 K electron density difference maps show that the H-atom is predominantly bound to the pyridine, so that the crystal is more correctly described as a salt of formula $[\text{isonicotinamideH}]^+[\text{HCOO}]^-$. This situation changes as the temperature is increased, and this temperature dependence is discussed in more detail below. The C=O bond of the formic acid is on the same side of the molecule as the C=O bond of the amide group in a *cis*-conformation. A secondary CH...O interaction is formed between the acid and the hydrogen atom in the 2-position of the pyridine ring (2.72 Å), which supports the OH...N H-bond. This motif is observed extensively in crystal engineering studies (for example, Bond, 2003).

The amide function of the *isonicotinamide* forms a centrosymmetric $R_2^2(8)$ dimer via NH...O hydrogen bonds (H411...O41, 2.00(2) Å) with the amide group of a symmetry equivalent molecule to form a 'supermolecule'. The supermolecule, which contains two molecules of both the amide and acid components, is a commonly observed motif in many co-crystals of *isonicotinamide* (Figure 4.1a). The supermolecules hydrogen bond together through an interaction between H412...O2 of the amide and acid to form large ring motifs, of with a graph-set descriptor $R_6^6(26)$ (H412...O2, 1.96(2) Å) (Figure 4.1b).

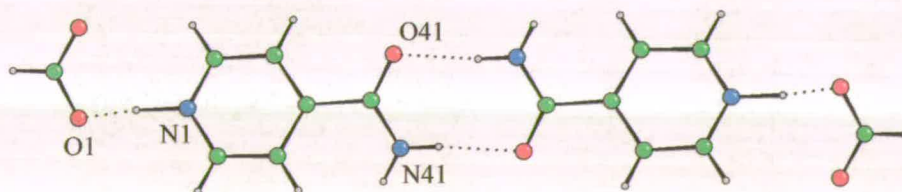


Figure 4.1a: The supermolecule of *isonicotinamide* with formic acid. This supermolecule is formed over an inversion centre creating a $R_2^2(8)$ amide dimer. The C=O bond of the formic acid is on the same side of the molecule as the C=O bond of the amide group in a *cis*-conformation.

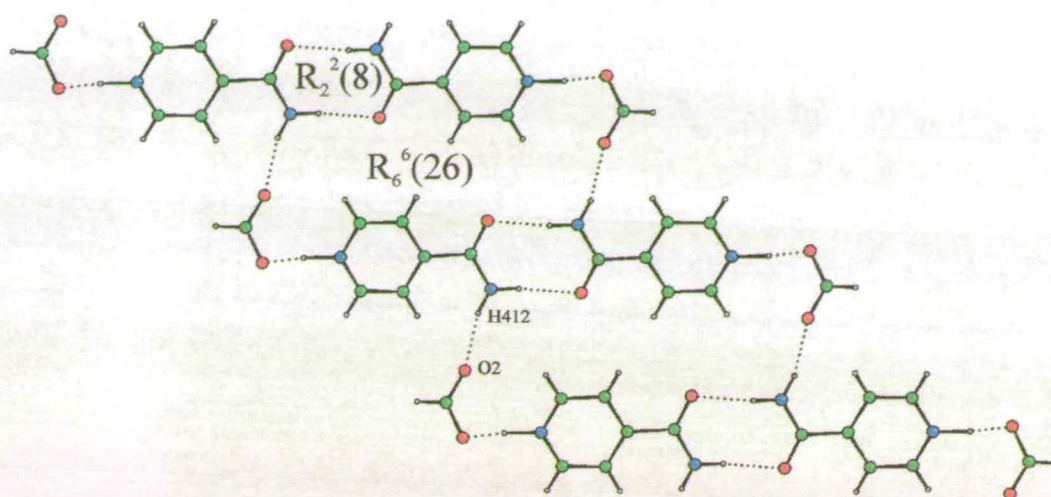


Figure 4.1b: The supermolecules H-bond together through interactions between H411 and O2 forming a ribbons along the [1 0 1]. Large $R_6^6(26)$ rings are formed which are characteristic of *cis-trans-cis* supermolecules. Colour scheme: C green, H white, N blue, O red; the same scheme is used in all figures.

These hydrogen bonding interactions produce ribbons that are orientated along the [1 0 1] direction. The ribbons are stacked along the a -direction with the ribbons at $y = \frac{1}{2}$ interleaving the ribbons at $y = 0, 1, \text{etc.}$ so that when viewed along [1 0 1] each ribbon is seen to be surrounded by six others in a close-packed arrangement (Figure 4.2a). Neighbouring ribbons interact with one another through two CH...O hydrogen bonds between H6...O1 (2.41 Å) and H11...O1 (2.71 Å) (Figure 4.2b).

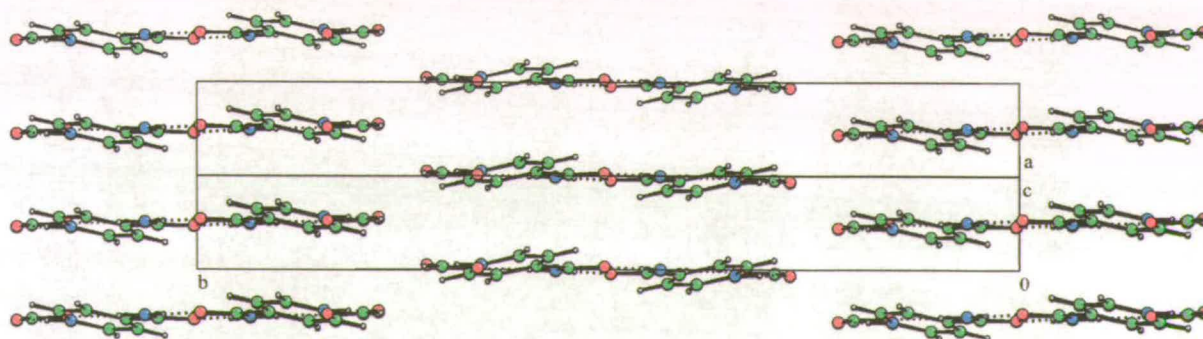


Figure 4.2a: The ribbons are stacked along the a -direction with neighbouring ribbons interleaving one another.

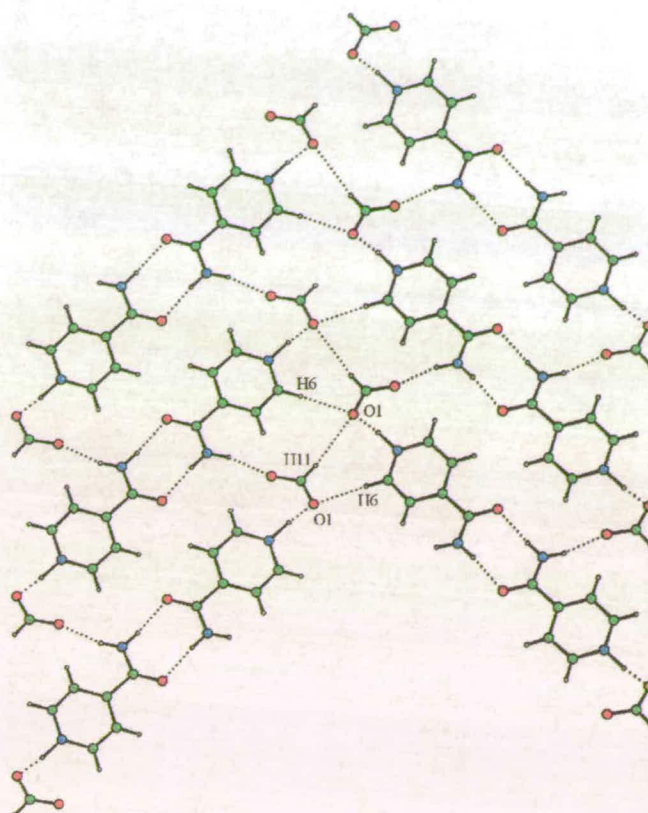


Figure 4.2b: Neighbouring ribbons interact through CH...O contacts between H6...O1 (2.41 Å) and H11...O1 (2.71 Å).

4.3.2 Isonicotinamide:acetic acid (2)

The acetic acid adduct forms a structure which is in many ways similar to the formic acid co-crystal. Centrosymmetric supermolecules are formed, consisting of two *isonicotinamide* units connected through their amide groups, and two carboxylic acid molecules hydrogen bonding to the pyridine groups. By contrast to the formic acid co-crystal, the C=O bond of the acid is on the opposite side of the molecule from the C=O bond of the amide group in a *trans*-conformation (Figure 4.3a). The supermolecules interact through the same H-bonding interaction as the formic acid adduct (H412...O2 2.01(2) Å), but here the large ring motifs have the descriptor $R_4^4(22)$ (Figure 4.3b). These interactions produce a ribbon which runs along the $[2\ 0\ \bar{1}]$ direction

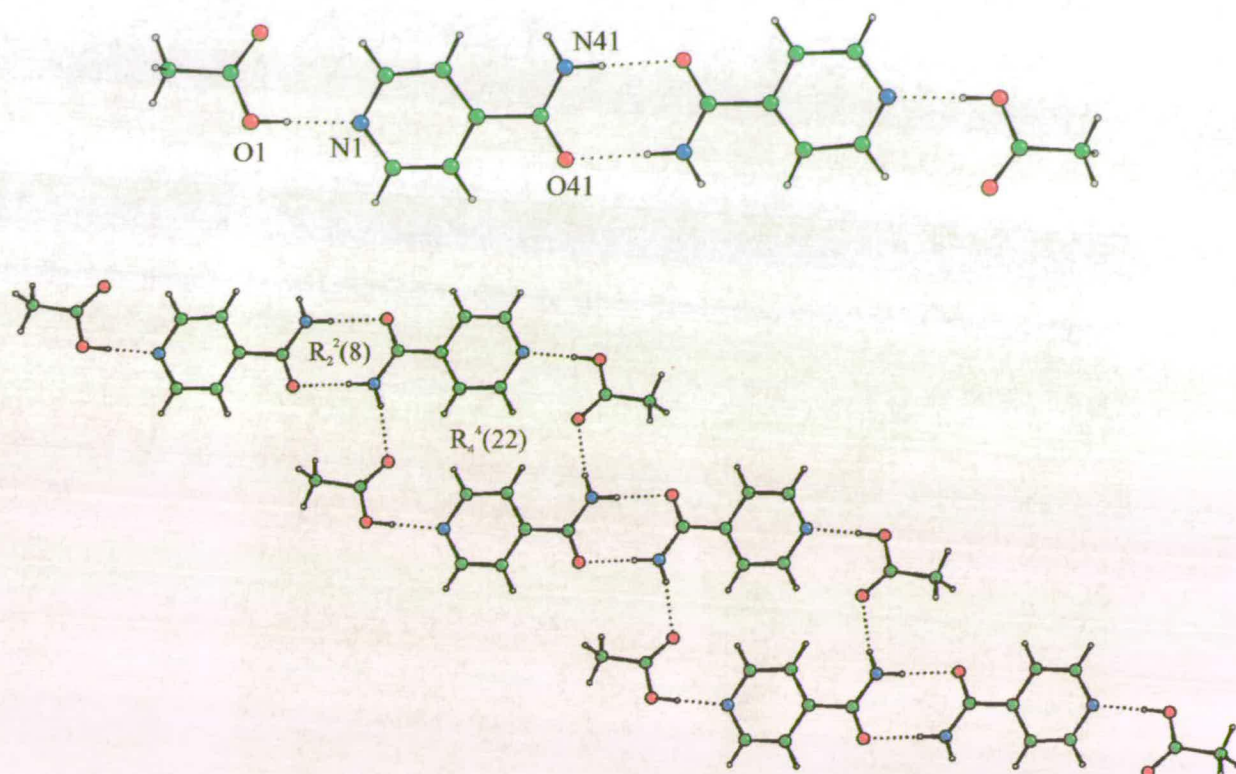


Figure 4.3 top *a*: The supermolecule of *isonicotinamide* with acetic acid again formed over an inversion centre [$R_2^2(8)$]. In contrast to the formic acid adduct the C=O bond of the acetic acid is on a different side of the molecule to the C=O bond of the amide group in a *trans*-conformation. The different orientations of the carbonyl groups with respect to each other affect the way the supermolecules interact with one another.

Bottom *b*: The supermolecules have a much greater horizontal displacement than those in the formic acid adduct as a result of the bulkier R-group attached to the acid. This increase in displacement creates smaller ring motifs in the ribbons. The ribbons run along $[2\ 0\ \bar{1}]$.

The length of the H-bond formed from the acid to the pyridine N (2.6331(15) Å), which was short in the formic acid co-crystal (2.5468(16) Å), is more comparable with those observed in the CSD in the acetic acid co-crystal. Moreover, difference maps show that the hydrogen atom is attached to the acid, so that the designation [*isonicotinamide*][MeCOOH] is most appropriate for this co-crystal. This observation can be ascribed to the lower acidity of acetic acid compared to formic acid (pK_a values: formic acid 3.76 acetic acid 4.75, [*isonicotinamideH*]⁺ 3.58). There is no evidence of proton migration in this moiety at increased temperatures.

In contrast to **1**, neighbouring ribbons are directly adjacent to one another forming a layer of ribbons parallel to (1 1 2) with close contacts formed between a hydrogen atom in the 2-position of the pyridine ring and the OH group of a neighbouring acid (H2...O1, 2.70 Å) (Figure 4.4). There are no contacts between the layers in this structure, however, the pyridine

rings do lie parallel with each other at a distance of 3.45 Å between the planes with the molecules horizontally displaced from one another (ring centroid displacement, 1.65 Å).

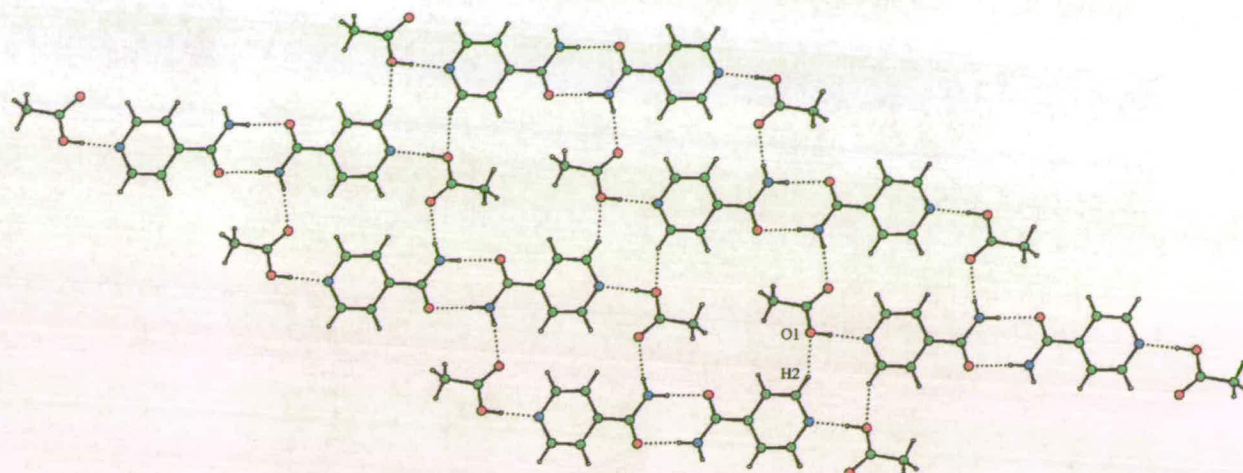


Figure 4.4: Neighbouring ribbons in *isonicotinamide:acetic acid* are directly adjacent to one another forming a layer of ribbons parallel to (1 1 2). The ribbons interact through close contacts between H2 of the pyridine ring and O1 of a neighbouring acid (H2...O1 (2.70 Å)).

4.3.3 Comparison of *isonicotinamide adducts*

Co-crystals of *isonicotinamide* and carboxylic acids have been studied extensively by Aakeröy *et al.* (2002, 2003) and Vishweshwar *et al.* (2003). The adducts isolated crystallise as supermolecules consisting of two *isonicotinamide* and two acid molecules. These structures exhibit ‘supermolecular isomerism’, which arises by rotation around the acid...pyridine H-bond. The two possible conformations are exemplified by the formic acid and acetic acid co-crystals, and are referred to *cis-trans-cis* and *trans-trans-trans*, respectively. The first and third positions in this nomenclature refer to the relative orientation of the carbonyl groups of the acid and amide; the second position refers to the conformation in the $R_2^2(8)$ amide dimer. In a centrosymmetric supermolecule the first and third positions will be the same, and the second *trans*.

The hydrogen bonding patterns that are present in the adducts are dictated by the conformations of the supermolecules. In both the formic and acetic acid derivatives the supermolecules are connected into ribbons by NH...O hydrogen bonds formed between amide and acid moieties of neighbouring supermolecules. Figures 4.1 and 4.3 show that if *cis-trans-cis* supermolecules are formed the orientation of the amide groups are such that they

build $R_6^6(26)$ rings, whereas *trans-trans-trans* molecules build $R_6^6(22)$ rings. The former involve four amide and two acid molecules, while the latter are built from just two of each.

Figure 4.1*b* shows that if the C-H group of the formic acid were to be replaced by a C-Me group, the *cis-trans-cis* arrangement would incur steric repulsion between the methyl group and a phenyl ring. The formation of the *trans-trans-trans* conformer with its larger displacement between supermolecules alleviates this steric hindrance, and presumably explains why this conformer is observed in the acetic acid co-crystal.

There are ten examples of *isonicotinamide* co-crystals with various carboxylic acids that crystallise in the same pattern as those observed in this study. These co-crystals use much bulkier guest molecules than acetic acid. From the behaviour observed in this study one might presume that the *trans-trans-trans* conformer would be preferred by these larger molecules, however this is not the case. The majority of them crystallise as *cis-trans-cis* conformers, but, in general, there is an increase of up to 17° in the amide-phenyl torsion angle (N41-C41-C4-C3) which lessens the steric hindrance between molecules. As a result the stabilising CH...O interaction is lost in all but two of the *cis-trans-cis* structures; a third structure possesses four *isonicotinamide* molecules in the asymmetric unit where two have lost the CH...O interaction. In the formic and acetic acid complexes the torsional angle are 169.01° and 170.57° , respectively. An example of a *cis* conformer showing an increase in torsional angle is the co-crystal with fumaric acid monoethyl ester (CSD entry LUNNEN, Aakeröy *et al.*, 2002). This compound crystallises with a torsional angle of 153.04° along the amide-phenyl bond in the *cis* conformation. Steric effects also work in favour of the *cis*-conformer as in this example. The ethyl moiety of this R-group would possibly incur steric repulsion from a pyridine group of an adjacent supermolecule.

4.3.4 Variable temperature study

The conventional refinement of the crystal structure of the *isonicotinamide*:formic acid adduct showed that the hydrogen involved in the acid...pyridine H-bond was situated closer to the nitrogen atom; this model is the one used in the discussion of the structures given above. However, proton transfer behaviour has been seen in numerous crystal structures, although in most of the compounds studied so far, the donor and acceptor sites are both oxygen atoms. Steiner *et al.* (2001) have studied a co-crystal of pentachlorophenol and 4-methylpyridine by variable temperature neutron diffraction in which the migration of a

hydrogen atom in a N...O H-bond occurred; this was the first study of proton migration in a heteronuclear H-bond.

Parkin *et al.* (2004) have recently shown, in a study of urea:phosphoric acid (which contained an O...H...O hydrogen bond), that although neutron diffraction is the method of choice for location of hydrogen atom positions, examination of Fourier images from X-ray data can show the bonding activity of the hydrogen atom, i.e. to which atom the hydrogen is bonded during the migration process. The two techniques are therefore complementary, and Parkin *et al.* actually conclude that *the Fourier images give a clearer and more realistic picture of the hydrogen behaviour in non-standard hydrogen bonds in the X-ray case than a refinement of the atomic position*. A variable temperature study was therefore conducted on the isonicotinamide:formic acid adduct to observe whether the proton migrated across the N1...O1 hydrogen bond with increasing temperature.

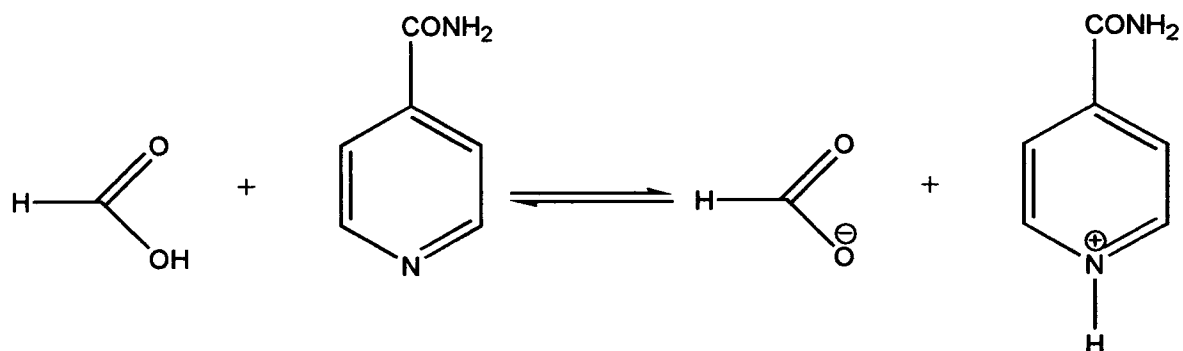
The difference Fourier maps from the variable temperature study are presented in Figure 4.5 (p93-95). In each of the maps the electron density corresponding to the hydrogen atom can be clearly seen. At 100 K the map shows one main peak and a smaller secondary peak in the region between the N1 and O1; the main peak situated closer to the nitrogen, the smaller peak near the midpoint between the two. This suggests that the proton is disordered over two sites at 100 K. As the temperature increases (Figures 4.5*b – e*) the heights of the two peaks become more equal, suggesting that the weighting of the two sites changes with temperature.

There are two possible ways to assess the extent of the hydrogen-atom disorder. A qualitative measure can be derived by simply comparing observed peak heights (in $\text{e}\text{\AA}^{-3}$) from the Fourier difference maps (Parkin *et al.*, 2004). A more quantitative comparison is obtained by refinement of the occupancies of different hydrogen atom sites. The latter was also necessary to ascertain whether the minor-weight H-atom position (H21) occupies a central position between N1 and O1 (i.e. O1...H21...N1, such as occurred in Steiner's study), or whether it becomes attached to O1 (i.e. O1-H21...N1). In order to make this distinction a distance restraint of 0.90(1) \AA was applied to N1-H1 (hydrogen nearest the nitrogen) and the positional parameters for H21 were allowed to refine freely; further details of the refinement strategy are given in the *Experimental* section.

The Fourier map calculated using the data collected at 100 K showed that the peak nearer the nitrogen is 0.19 $\text{e}\text{\AA}^{-3}$ higher than the secondary peak, suggesting that the hydrogen is situated mainly on the nitrogen (Figure 4.5*a*). This is supported by the refinement of the occupancies of each hydrogen atom site. The occupancy of H1 was refined to be 0.60(3) at

100 K. The standard uncertainty of the occupancy of H1 is rather high; a refinement weighted towards the data most sensitive to this parameter (Prince, 1994; Parsons, 2004) yielded a value of 0.571(18). [Although this procedure is still under development, it has been shown to yield improved estimates of the Flack parameter; this is the first occasion that it has been applied to occupancies].

The hydrogen positions were refined to reasonable distances (N1-H1 0.902(10) Å; O1-H21 0.90(6) Å); this shows that the hydrogen atom migrates from N1 to O1, rather than to the mid-point between these two atoms. The equilibrium being observed in this study is therefore:



As the temperature is raised to 115 K, the difference in the heights of the two peaks falls to $0.09 \text{ e}\text{\AA}^{-3}$ (Figure 4.5*b*). The reduction in the difference in peak heights implies that the occupancies for each site equalise, and this is reflected in the refined occupancies where the occupancy of H1 has dropped to 0.534(19).

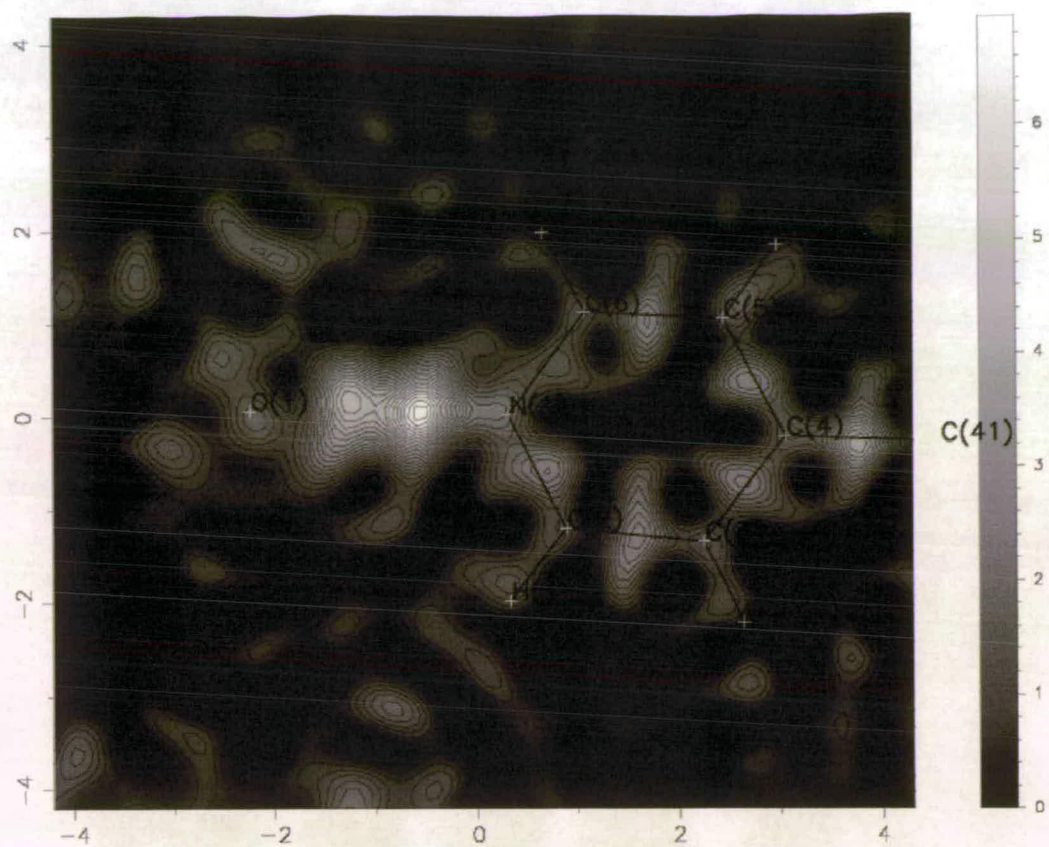
The two Fourier peaks have very similar heights at 130, 175 K, though at 240 K the peak closer to the oxygen (H21) is $0.04 \text{ e}\text{\AA}^{-3}$ bigger than the peak nearer the nitrogen (H1) (Figures 4.5*c-e*). This suggests that as the temperature increases the site attached to O1 becomes slightly favoured. This view is supported by the refined occupancies; at 175 and 240 K the occupancies are essentially the same at *ca* 0.4.

In aqueous solution the equilibrium constant for the reaction above can be estimated to be 0.66 [$= K_a(\text{HCOOH})/K_a(\text{isonicotinamideH}^+)$], which suggests that the occupancy of H1 should be near 0.45. This is not significantly different from the limiting value obtained crystallographically.

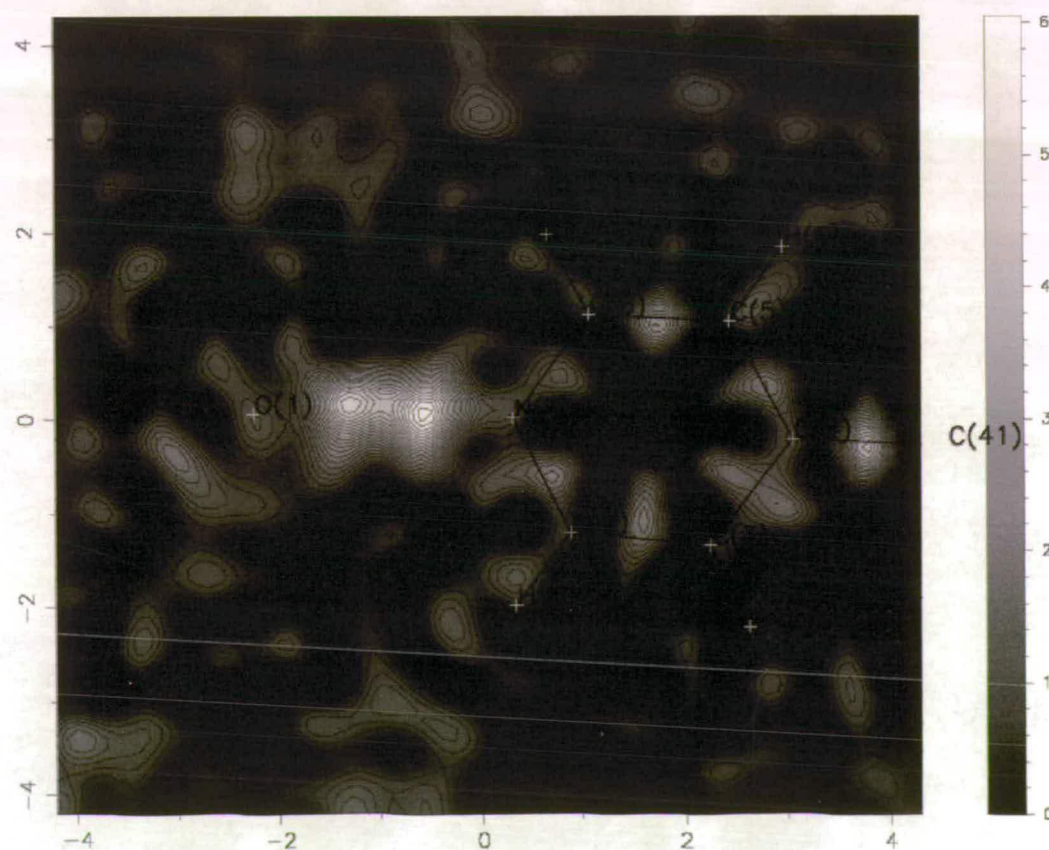
This is only the second example of a system where hydrogen-atom migration occurs between two heteroatoms; the first example occurred in pentachlorophenol:4-methylpyridine (Steiner *et al.*, 2001). In that study only one Fourier peak corresponding to the H-atom position was observed under all conditions; the hydrogen bond could be classified as ‘strong’, with the H-atom residing at approximately the mid-point between the N and O atoms. At low

temperature the centre of gravity of the H-atom position was displaced slightly from the middle of the N...O vector toward the nitrogen; at higher temperature the position was displaced towards the oxygen. Similar behaviour was observed in urea:phosphoric acid using X-ray and neutron methods by Parkin *et al.* (2004). The hydrogen bond in *isonicotinamide:formic acid* is unsymmetrical, and this feature is more characteristic of medium-strength H-bonds. Accordingly, in our study at all temperatures two distinct peaks are present in the difference Fourier maps giving a clear sign of migration from one position, primarily bonded to nitrogen, to an alternative, primarily bonded to oxygen. These two positions are energetically similar, and at no stage was a fully ordered structure obtained. However, this is the first time that migration has been observed in an unsymmetrical heteroatomic H-bonded system.

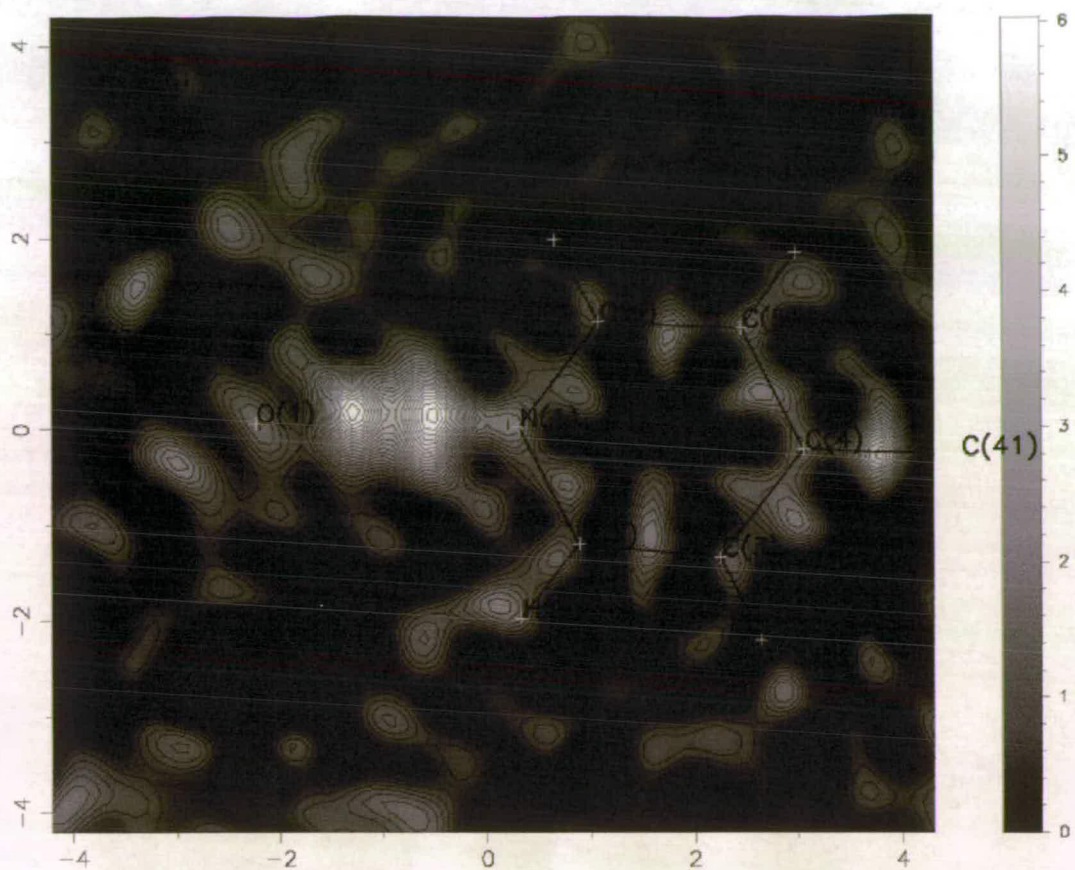
Although we have been able to refine the occupancies of the hydrogen atom sites it has yet to be seen whether these correspond to those obtained by a more accurate method such as neutron diffraction. Neutron diffraction is necessary here in order to characterise this process more precisely, and beam-time on station SXD at ISIS has recently been granted for this study. The same experiment will enable the behaviour at temperatures far below those accessible in this work to be investigated.



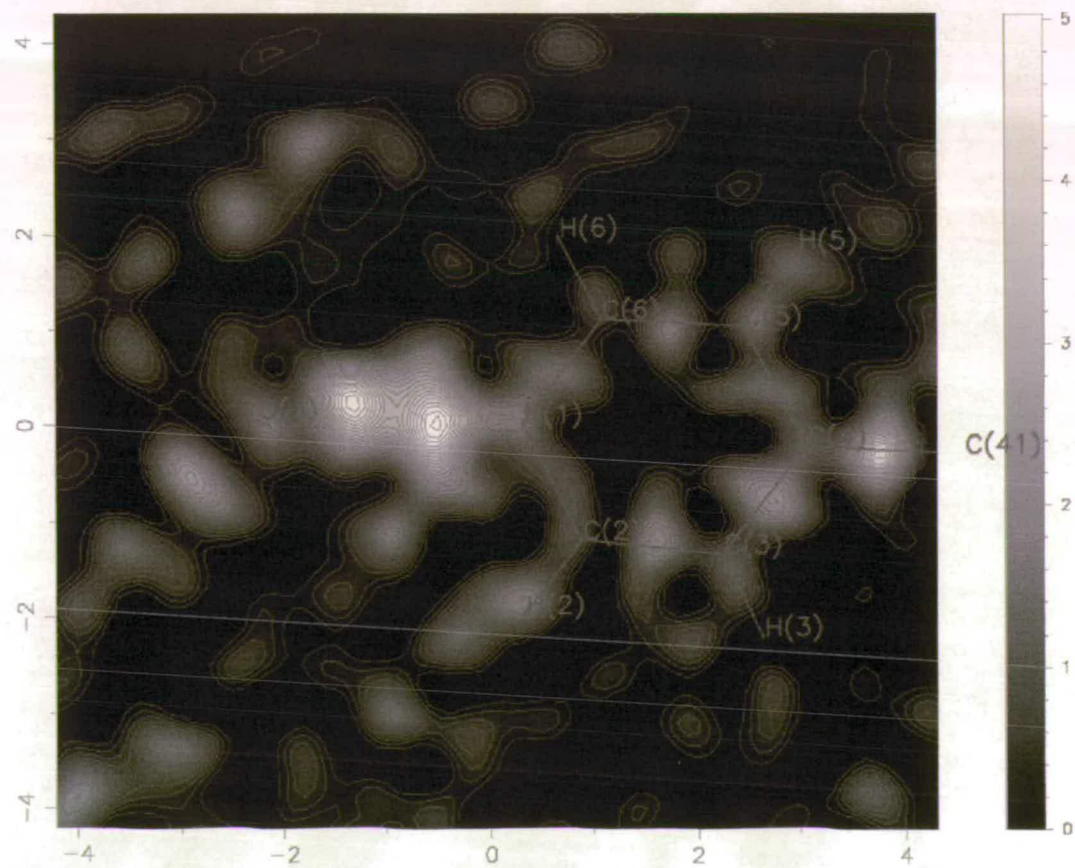
a)



b)



c)



d)

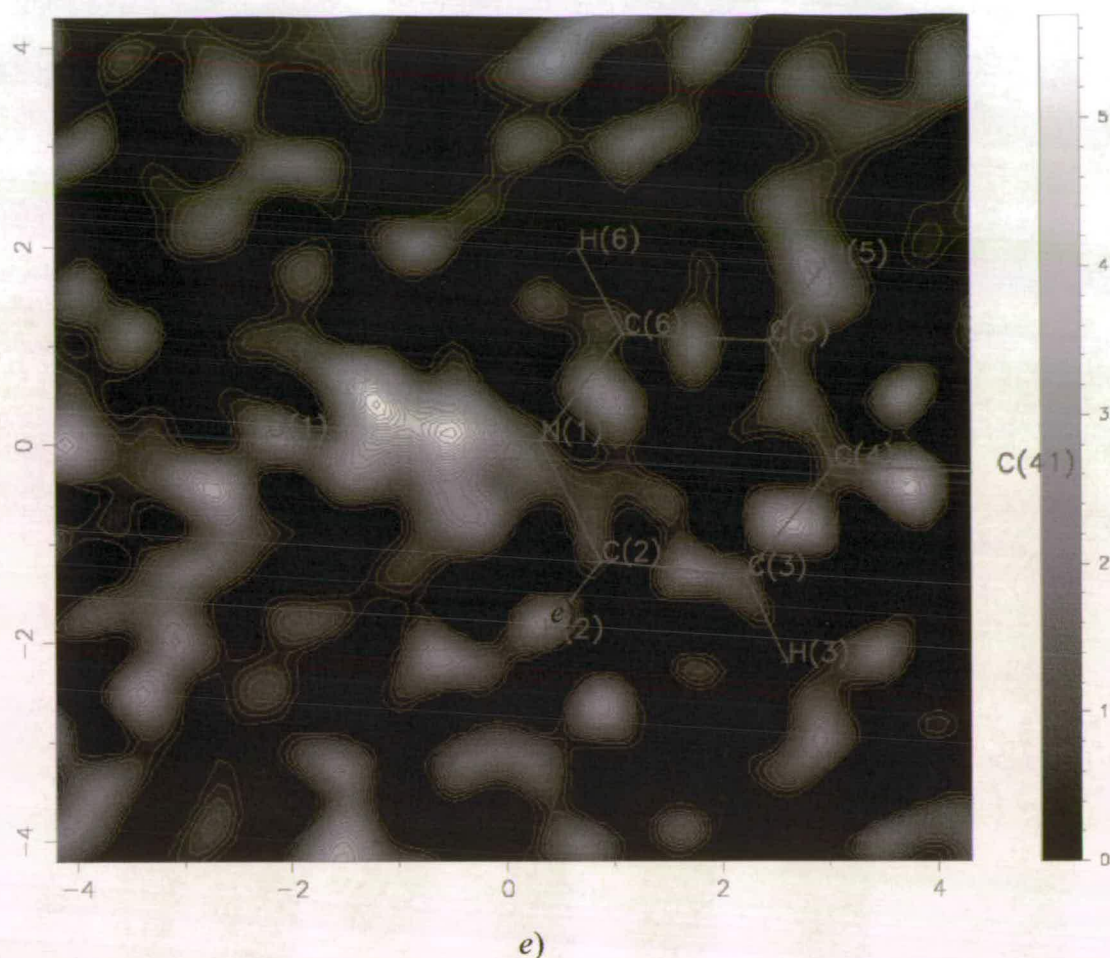


Figure 4.5: Difference Fourier maps (coefficients $F_o - F_c$) of isonicotinamide:formic acid adduct obtained at temperatures of (from top) *a*) 100 K, *b*) 115 K, *c*) 130 K, *d*) 175 K, *e*) 240 K. The maps are calculated on a plane through atoms C2, C6, N1 and O1. The contour levels for each temperature are; 100 K & 240 K, $0.28 \text{ e}\text{\AA}^{-3}$; 115 K & 130 K, $0.24 \text{ e}\text{\AA}^{-3}$; 175 K, $0.20 \text{ e}\text{\AA}^{-3}$.

4.4 References

- Aakeröy, C. B., Beatty, A. M. & Helfrich, B. A. (2002). *J. Am. Chem. Soc.* **124**, 14425-14432.
- Aakeröy, C. B., Beatty, A. M., Helfrich, B. A. & Nieuwenhuyzen M. (2003). *Cryst. Growth & Des.* **3**, 159-165.
- Allen, F. H. (2002). *Acta Cryst.* **B58**, 380-388.
- Allen, F. H. & Motherwell, W. D. S. (2002). *Acta Cryst.* **B58**, 407-422.
- Anastas, P. T. & Warner, J. C. (2002). *Green Chemistry*. Oxford University Press, Oxford, UK.
- Betteridge, P. W., Carruthers, J. R., Cooper, R. I., Prout, K. & Watkin, D. J. (2003). *J. Appl. Cryst.* **36**, 1487.

- Bernstein, J., Davis, R. E., Shimoni, L. & Chang, N-L. (1995). *Angew. Chem. Int. Ed. Engl.* **34**, 1555-1573.
- Blessing, R. H. (1995). *Acta Cryst. A51*, 33-38.
- Blessing, R. H. (1997). *J. Appl. Cryst.* **30**, 421-426.
- Boese, R. & Nussbaumer, M. (1994). In *Correlations, Transformations, and Interactions in Organic Crystal Chemistry*, D.W. Jones & A. Katrusiak (Editors). (International Union of Crystallography, Crystallographic Symposia, 7), pages 20-37.
- Bond, A. D. (2003). *Chem. Comm.* **2**, 250-251.
- Bruker-Nonius (2003). *SAINT* version 7. Bruker-Nonius Inc., Madison, Wisconsin, USA.
- Bruno, I. J., Cole, J. C., Edgington, P. R., Kessler, M., Macrae, C. F., McCabe, P., Pearson, J. & Taylor, R. (2002). *Acta Cryst. B58*, 389-397.
- Cosier, J. & Glazer, A. M. (1986). *J. Appl. Cryst.* **19**, 105-107.
- Farrugia, L. J. (1999). *J. Appl. Cryst.* **32**, 837-838.
- Parkin, A., Harte, S. M., Goeta, A. E. & Wilson, C. C. (2004). *New J. Chem.* **28**, 718-721.
- Parsons, S. (2004). *HATTIE*. A program for the analysis of leverages. The University of Edinburgh.
- Prince, E. (1994). *Mathematical Techniques in Crystallography and Materials Science*. Springer-Verlag, Berlin. Pages 120-123.
- Sheldrick, G. M. (2001). *SHELXTL* version 6.01. University of Göttingen, Germany and Bruker-Nonius Inc., Madison, Wisconsin, U.S.A.
- Sheldrick, G. M. (2004). *SADABS*, Version 2004-1. University of Göttingen, Germany and Bruker-AXS, Madison, Wisconsin, USA.
- Spek, A. L. (2002). *PLATON- A Multipurpose Crystallographic Tool*, Utrecht University, Utrecht, The Netherlands.
- Steiner, T., Majerz, I. & Wilson, C. C. (2001). *Angew. Chem. Int. Ed.* **40**, 2651-2654.
- Taylor, R. & Macrae, C. F. (2001). *Acta Cryst. B57*, 815-827.
- Vishweshwar, P., Nangia, A. & Lynch, V. M. (2003). *Cryst. Growth & Des.* **3**, 783-790.
- Watkin, D. J., Pearce, L. & Prout, C. K. (1993). *CAMERON - A Molecular Graphics Package*. Chemical Crystallography Laboratory, University of Oxford, England.

Wilson, C. C., Shankland, N. & Florence, A. J. (1996). *Chem. Phys. Lett.* **253**, 103-107.

Chapter 5

The Low-Temperature and High-Pressure Crystal Structures of 2-Chlorophenol and 4-Fluorophenol.*

* Oswald, I. D. H., Allan, D. R., Day G. M, Motherwell, W. D. S. & Parsons, S. (2004). *Manuscript in preparation.*

5.1 Introduction

In 1999 and 2001, the Cambridge Crystallographic Data Centre held two blind tests of crystal structure prediction (CSP1999, Lommerse *et al.*, 2000 & CSP2001, Motherwell *et al.* 2002). The aim of these projects was to test how well currently available methods of crystal structure prediction perform when given only the atomic connectivity for an organic compound. Several groups active in the field of crystal structure prediction attempted to predict the crystal structures of compounds of varying size and flexibility. The crystal structures were all previously unpublished, contained less than 40 atoms and crystallised in a common space group with $Z' = 1$. All predictions were carried out assuming ambient pressure conditions. The results of the tests showed that rigid molecules are most amenable to crystal structure prediction, the authors concluding that, '*Crystal structure prediction, although beset by fundamental and technical difficulties, is no longer scandalously hopeless.*'

Most of the subjects used for the crystal structure prediction blind tests had only been characterised in one polymorphic form, though it is well-known that many organic systems may crystallise as different polymorphs under different conditions. The observed structures were thus not guaranteed to be the most thermodynamically stable. This must have relevance with regard to the predictability of their crystal structures, as most prediction methodologies aim to locate the global minimum in lattice energy as the most probable crystal structure. A frequent observation in crystal structure prediction studies is that there are many possible crystal structures within a small energy range of the global minimum in lattice energy (CSP1999 & CSP2001). While the calculations usually locate many more potential polymorphs than are likely to ever be observed, it seems likely that some of the previously unobserved structures from these studies should be accessible through changes in the crystallisation conditions.

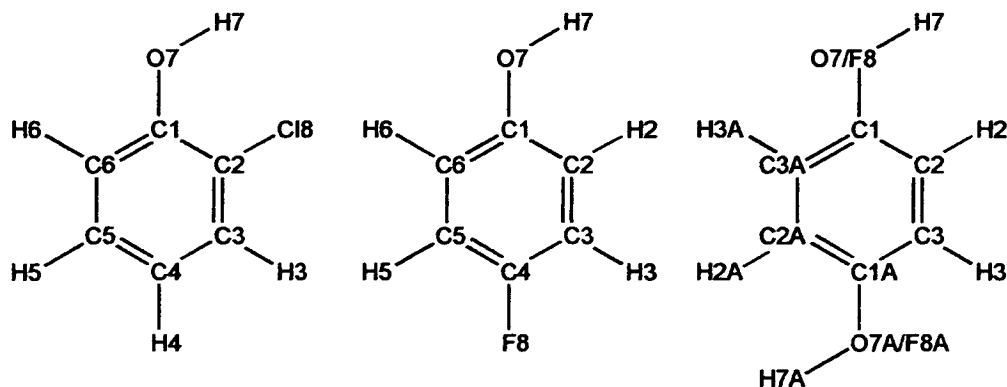
Previous results from this laboratory have shown that high-pressure (0.1 – 10 GPa) is a powerful means for investigating polymorphism in organic systems, for example, new high-pressure phases in alcohols (Allan *et al.*, 1998, Allan & Clark, 1999, Allan *et al.*, 2001, Allan *et al.*, 2002), carboxylic acids (Allan & Clark, 1999, Allan *et al.*, 2000), acetone (Allan *et al.*, 1999), and, very recently, glycine (Dawson *et al.*, 2004*b*) and serine (Moggach *et al.*, 2004) have all been characterised. The area is still relatively underdeveloped, however, and systematic trends are still emerging.

Computational studies of isolated molecules have had an enormous influence on the development of structural chemistry, and it is thus of great interest to test the effectiveness of

computational approaches to the prediction of high-pressure crystal structures. It is not immediately obvious, for example, that potentials developed for ambient pressure predictions should be of any use at high-pressure. High-pressure phases have higher densities than their ambient-pressure counterparts, and, since there is often a reasonable variation of densities amongst the lowest energy predicted structures for a given molecule (Beyer *et al.*, 2001; Anghel *et al.*, 2002), the application of pressure could reorder their thermodynamic stability. Thus, it seems possible that, the highest density predicted crystal structures could in fact be accessible at high-pressure.

The compounds selected for our first investigation to test this idea were the mono-halophenols. Crystal structures in this series have only been lightly investigated: 4-Chlorophenol was studied by Perrin & Michel (1973*a, b*) and shown to exist in two polymorphic forms. However, these systems are ideal for structure prediction tests because the molecules are small and rigid. The compounds are mostly liquids under ambient pressure, and so *in situ* crystal growth by application of pressure can yield new polymorphs directly, avoiding the complications, which can arise by applying pressure to a solid sample. They are also a good test of the two major aspects of prediction methodologies: the location of all possible crystal structures and the calculation of their relative energies. Results of the latest crystal structure prediction blind test (Day *et al.*, 2004*a*) highlighted the prediction of structures with $Z' > 1$ as a major challenge for the search methodologies. Monoalcohols have a tendency to crystallise with more than one molecule in the asymmetric unit, so a complete search for structures must include $Z' > 1$. Furthermore, the strong orientational dependence of close contacts with halogen atoms presents problems for atomistic calculations and their presence tests the quality of inter-atomic potentials that have recently been developed for these atoms.

In this Chapter we describe the crystal structures of two halophenols, 2-chlorophenol and 4-fluorophenol, that exhibit pressure induced polymorphism and also describe the results of crystal structure prediction calculations on the two systems. The intra-molecular structures of 2-chlorophenol and 4-fluorophenol as derived at low-temperature are illustrated in Scheme 5.1, which also shows the atomic numbering scheme used.



Scheme 5.1: Conventional structure diagram and numbering scheme for 2-chlorophenol (Left), 4-fluorophenol at low temperature (Centre) and 4-fluorophenol at high-pressure (Right). The high-pressure crystal structure is disordered over an inversion centre hence those atoms augmented by an A are generated by inversion symmetry.

5.2 Experimental

5.2.1 General Procedures

2-Chlorophenol and 4-fluorophenol were obtained from Sigma-Aldrich and used as received.

X-ray diffraction intensities were collected with Mo-K α radiation on a Bruker SMART APEX CCD diffractometer equipped with an Oxford Cryosystems low-temperature device (Cosier & Glazer, 1986) and an OHCD laser-assisted crystal growth device.

5.2.2 Crystal Growth at Ambient Pressure

2-Chlorophenol (*m.pt.* 280 K) was drawn into a glass capillary (o.d. 0.52 mm) and flame-sealed. The sample was mounted on the diffractometer, and a polycrystalline mass obtained by freezing the sample at 273 K. A crystal was grown using the laser-assisted zone-refinement procedure of Boese and Nussbaumer (1992).

Colourless crystals were grown from a saturated solution of 4-fluorophenol (*m.pt.* 321 K) in ethanol at 277 K.

5.2.3 Crystal Structure Determination of Ambient Pressure Phases

Diffraction data were collected for 2-chlorophenol at 100 K and for 4-fluorophenol at 150 K. Data collection and integration were carried out using the programs SMART (Bruker-

Nonius, 2001) and SAINT (Bruker-Nonius, 2003). The diffraction data were corrected for absorption and other systematic errors using the multiscan procedure SADABS (Sheldrick, 2004, based on the procedure described by Blessing, 1995). The structure was solved by direct methods (SIR92, Altomare *et al.*, 1993) and refined by full-matrix least squares against F^2 using all data (CRYSTALS, Betteridge *et al.*, 2003). H-atoms were placed on C-atoms in calculated positions and allowed to ride on their parent atoms. Hydroxyl hydrogen atoms were located in difference maps and refined with a distance restraint of 0.85 Å to the parent oxygen. All non-H atoms were modelled with anisotropic displacement parameters. In the case of 2-chlorophenol the value of the Flack parameter [0.00(3); Flack, 1983] verified the correct assignment of the absolute structure. Data collection and refinement statistics are collected in Table 5.1. We refer to the low-temperature phases as 2-chlorophenol-I and 4-fluorophenol-I.

5.2.4 *Crystal Growth at High-pressure*

Pressure was applied to the samples using a Merrill-Bassett diamond anvil cell (DAC) equipped with 600 µm culets, a tungsten gasket with a 300 µm hole, beryllium backing disks and a chip of ruby for pressure measurement (Merrill & Bassett, 1974). Pressures were measured by the ruby-fluorescence method by excitation with a 632.817 nm line from a He-Ne laser using a Jobin-Yvon LabRam 300 Raman spectrometer.

2-Chlorophenol and 4-fluorophenol were loaded into the Merrill-Bassett cell as liquids. In the case of 4-fluorophenol, both the sample and the cell were heated with a hot-air gun before loading to prevent crystallisation at ambient temperature. In each case, the cell was closed, and pressure was applied until a polycrystalline mass was produced; the temperature of the cell was increased using a hot-air gun until a single crystallite remained. Slow cooling to ambient temperature yielded a single crystal that filled the entire gasket hole. Crystallisation was monitored visually using a polarising microscope. The crystallisation pressures were 0.12 GPa for 2-chlorophenol and 0.28 GPa for 4-fluorophenol.

5.2.5 *Structure Determinations of 2-Chlorophenol and 4-Fluorophenol at High-pressure*

Data were collected with the cell mounted in two different orientations for 2-chlorophenol but only one for 4-fluorophenol; the diffraction pattern was indexed with the program GEMINI (Sparks, 2000). Data integration (to $2\theta = 45^\circ$) was performed using

SAINT with dynamic masking to account for the shading from the DAC steel body (ECLIPSE, Parsons, 2004a). The program SHADE (Parsons, 2004b) was used to take account of absorption effects of the pressure cell; further systematic errors were treated using SADABS before merging in SORTAV (Blessing, 1997). More detailed data collection and processing procedures used in our laboratory have been described by Dawson *et al.* (2004a).

Indexing the diffraction patterns showed that the phases obtained at high-pressure were different from those obtained on cooling. We refer to the high-pressure phases as 2-chlorophenol-II and 4-fluorophenol-II.

High-pressure data sets obtained by applying DAC techniques to crystals in low-symmetry crystal systems have a low completeness because of shading by the cell-body. This is exacerbated if a crystal happens to grow in an unfavourable orientation inside the cell, and there is very little that can be done to control this. In the case of 2-chlorophenol the completeness obtained was just 37%, and this meant that structure solution by direct methods failed to yield a recognisable solution, while Patterson methods were frustrated by the elongation of the peaks in the direction most affected by pressure-cell shading. This is a common problem with high-pressure data, but fortunately the problem may be overcome by using global optimisation methods originally devised for structure solution from powder diffraction data (Shankland & David, 2002). The structure of phase-II of 2-chlorophenol was solved using the simulated annealing procedure in the program TOPAS (Bruker-Nonius, 2004). The structure was refined by full-matrix least-squares against F^2 (CRYSTALS). Free refinement of the positional parameters of the non-H atoms yielded carbon-carbon bond lengths varying from 1.34-1.40 Å. The phenyl ring was therefore constrained to be a rigid hexagon. H-atoms were placed on C-atoms in calculated positions and allowed to ride on their parent atoms. The hydroxyl hydrogen atom, which is involved in H-bonding, was located in a difference map; its position was initially refined subject to distance and angular restraints, but later fixed. Only the oxygen and fluorine atoms were modelled with anisotropic displacement parameters, these being subject to rigid body and rigid bond restraints. The final R-factor calculated on F for data with $I/\sigma(I) > 2.0$ was 6.79%.

The structure of 4-fluorophenol-II was solved by direct methods (SIR-92). The molecule occupies an inversion centre with the oxygen and fluorine disordered. The structure was refined by similar procedure to those described above. All non-H atoms were modelled with anisotropic displacement parameters that were subject to displacement parameter restraints. The carbon-carbon bonds lengths are slightly shorter than is expected, possibly because of librational motion of the ring. The displacement parameter for C3 is slightly

elongated along the bond, which supports this hypothesis. The final R-factor calculated on F for data with $I/\sigma(I) > 2.0$ was 10.60%. Final data collection and refinement statistics are collected in Table 5.1. A table of hydrogen-bonding parameters for 2-chlorophenol and 4-fluorophenol is shown in Table 5.2.

Compound	2-Chlorophenol-I	2-Chlorophenol-II	4-Fluorophenol-I	4-Fluorophenol-II
T/P	100K/0GPa	R.T/0.12GPa	150K/0GPa	R.T/0.28GPa
Formula	C ₆ H ₆ ClO	C ₆ H ₆ ClO	C ₆ H ₆ FO	C ₆ H ₆ FO
Weight	128.56	128.56	112.10	112.10
Radiation	Mo-K α	Mo-K α	Mo-K α	Mo-K α
Crystal system	Trigonal	Monoclinic	Trigonal	Monoclinic
Space Group	<i>P</i> 3 ₂	<i>P</i> 2 ₁ / <i>n</i>	<i>R</i> $\bar{3}$	<i>P</i> 2 ₁ / <i>c</i>
<i>a</i> /Å	16.0721(8)	6.4638(12)	22.620(2)	6.2807(7)
<i>b</i> /Å	16.0721(8)	4.9086(4)	22.620(2)	5.7241(9)
<i>c</i> /Å	5.8959(6)	18.131(3)	5.5690(11)	7.7982(12)
α /°	90	90	90	90
β /°	90	98.111(13)	90	106.060(11)
γ /°	120	90	120	90
Volume/Å ³	1318.94(16)	569.49(15)	2467.8(6)	269.41(7)
No. reflections for cell	8931	539	1550	268
2 θ _{max} (°)	57.87	52.79	57.86	46.43
<i>Z</i>	9	4	18	2
<i>D</i> _c (Mg/m ³)	1.457	1.499	1.358	1.382
μ (mm ⁻¹)	0.534	0.550	0.114	0.166
Reflections collected	11871	3522	5190	764
Unique [<i>R</i> _{int}]	3897[0.026]	400[0.087]	1349[0.019]	197[0.032]
No. <i>I</i> > 2 σ	3738	249	955	132
<i>T</i> _{min} / <i>T</i> _{max}	0.44/0.76	0.58/0.91	0.97/0.98	0.62/0.97
Parameters	227	31	76	29
<i>R</i> ₁ [<i>F</i> > 4 σ (<i>F</i>)]	0.0274	0.0679	0.0469	0.1060
w <i>R</i> ₂ (<i>F</i> ² , all data)	0.0704	0.1484	0.0903	0.3259
<i>S</i>	0.9947	1.0517	1.1435	1.3200
$\Delta\rho$ _{max} / eÅ ⁻³)	0.27	0.34	0.48	0.39
$\Delta\rho$ _{min} / eÅ ⁻³	-0.24	-0.30	-0.40	-0.17

Table 5.1: Crystallographic data for 2-chlorophenol and 4-fluorophenol at both ambient and high-pressure.

Compound	Donor	Acceptor	H-bond distances (Å)	
			Low temperature	High-pressure
2-Chlorophenol-I	O71	O71 ⁱ	2.754(2)	-
	O72	O72 ⁱⁱ	2.748(1)	-
	O73	O73 ⁱⁱⁱ	2.762(2)	-
	H42	C181 ^{iv}	2.89	-
	H52	C181 ^v	2.94	-
	H43	C182 ⁱⁱ	2.88	-
	H53	C182 ^{vi}	2.81	-
2-Chlorophenol-II	O7	O7 ^{vii}	-	2.809(11)
	H3	C18 ^{viii}	-	2.98
4-Fluorophenol-I	O7	O7 ^{ix}	2.650(1)	-
	H2	F8 ^x	2.57	-
	H5	F8 ^{xi}	2.65	-
4-Fluorophenol-II	O7	O7 ^{xii}	-	3.017(4)

Symmetry Operators:

i	-y, x-y, z-1/3	vii	3/2-x, y-1/2, 1/2-z
ii	1-y, x-y, z-1/3	viii	2-x, -y, -z
iii	-y, x-y-1, z-1/3	ix	1+y, 1-x+y, 2-z
iv	-x+y, -x, 1/3+z	x	4/3-y, x-y-1/3, 2/3+z
v	-x+y, -x, z-2/3	xi	5/3-x, 1/3-y, 1/3-z
vi	1-y, x-y, 2/3+z	xii	-x-1, y-1/2, -z-1/2

Table 5.2: Table of Hydrogen bonding parameters. The H-bonding distances are from donor to acceptor due to the imprecise determination of hydrogen atom positions. Low temperature datasets were taken at 100 K and 150 K for 2-chlorophenol and 4-fluorophenol, respectively. The high-pressure datasets were collected at room temperature.

5.2.6 Inter-conversion of 4-fluorophenol-I and II.

The high melting-point of 4-fluorophenol (321 K) in principle means that crystals formed at high-pressure may be recoverable at ambient pressure without the sample melting. In the event an attempt to release the pressure on the sample of 4-fluorophenol transformed the crystal into a polycrystalline mass, suggesting that the solid underwent a destructive phase transition, presumably to the ambient pressure phase.

A single crystal of 4-fluorophenol (prepared as described above) was loaded into the Merrill-Bassett cell with paraffin as a hydrostatic medium. Pressure (1.7 GPa) was applied, and data collected as described above. The sample indexed on phase-I of 4-fluorophenol though the diffraction data were very weak; the structure of phase-I refined to $R1 = 8.9\%$ based on 146 data out of 346 with $I > 2\sigma(I)$. The appearance of the crystal changed overnight from being transparent to having regions where the crystal had become opaque, suggesting that the sample was becoming polycrystalline. The Raman spectrum of the polycrystalline material showed a band with a shoulder at 847 cm^{-1} (Figure 5.1). The Raman spectrum of phase-I contains a prominent doublet in this region, whereas that of phase-II consists of one strong peak with a smaller peak to high frequency. On this basis it is possible that the polycrystalline material is 4-fluorophenol-II, though this is a rather tentative conclusion.

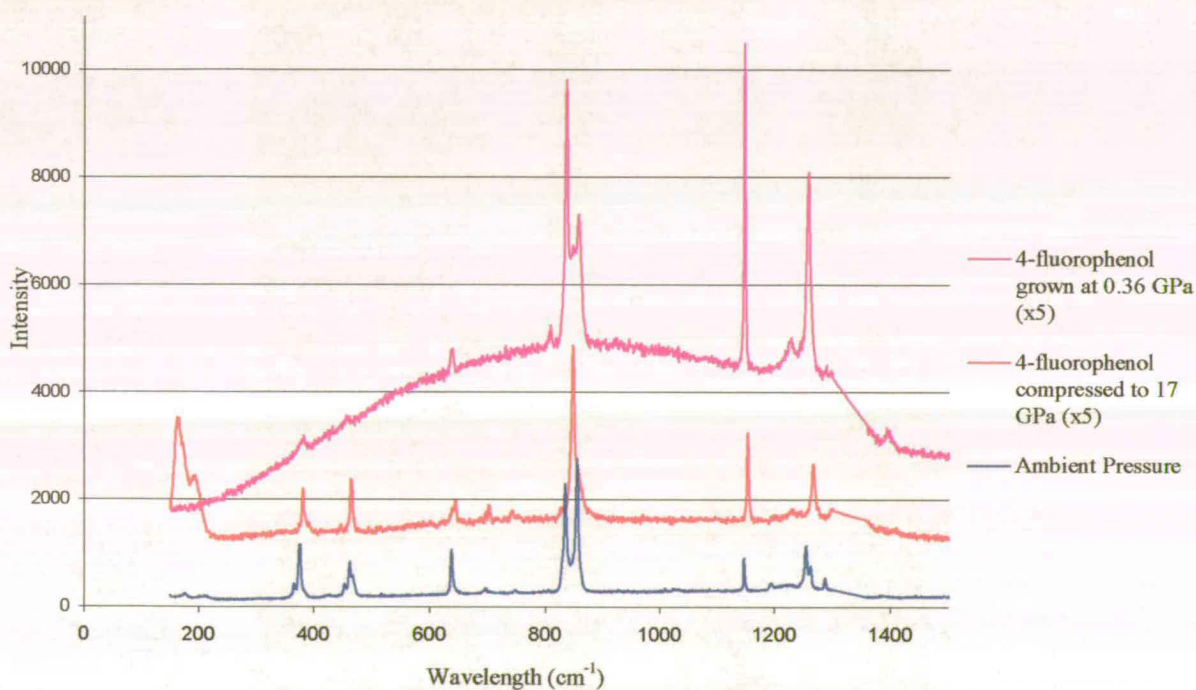


Figure 5.1: Raman spectra of 4-fluorophenol under various conditions; ambient pressure (blue line); 4-fluorophenol (phase-I) compressed to 1.7 GPa (red line); 4-fluorophenol (phase-II) grown from the melt at 0.36 GPa (pink line).

Intriguingly, on release of pressure, the crystal became transparent and was identified as a single crystal of 4-fluorophenol-I (by single crystal diffraction methods). The behaviour described above was reproducible for the same sample. Increasing the pressure on the single crystal resulted in growth of polycrystalline regions; release of pressure returned the crystal to its original condition.

5.2.7 Software and other general crystallographic procedures

The structures were visualised using SHELXTL (Sheldrick, 2001) or MERCURY (Bruno *et al.*, 2002); the figures were produced using CAMERON (Watkin *et al.*, 1993). Other analysis utilised the p.c. version of PLATON (Spek, 2002; Farrugia, 1999). Searches of the Cambridge Structural Database (CSD) were carried out with the program CONQUEST, utilising version 5.25 of the database (Allen, 2002; Allen & Motherwell, 2002). Crystallographic information files for all structures reported here are available on the CD at the back of this Thesis.

5.2.8 Computational Details

Note: The work described in this section was carried out by Dr Graeme Day of the Pfizer Institute, University of Cambridge. The section is included here for the sake of completeness.

The crystal structure prediction part of this study was performed separately from the experimental crystallisations. In keeping the prediction "blind" from the experimental results, the only information about the observed crystals known in advance of the computational work was that two forms were isolated for each molecule, all crystallising with three or fewer molecules in the asymmetric unit. As the choice of space groups is crucial for the success of crystal structure prediction, it was also revealed that at least one form crystallises in a trigonal space group. Searches were performed for low energy crystal structures of 2-chlorophenol and 4-fluorophenol using the simulated annealing search method (Karfunkel & Gdanitz, 1992; Karfunkel *et al.*, 1994; Verwer & Leusen, 1998) implemented in the Cerius2 modelling package. Planar, rigid molecular structures were used throughout the modelling. Two planar conformations of the 2-chlorophenol molecule are possible, so the CSD was searched for structures with neighbouring hydroxyl and chloro- substituents on aromatic rings. In almost all cases where hydrogen positions are reported, the hydroxyl hydrogen points away from the chlorine atom; we therefore assumed the chlorophenol conformation with hydroxyl pointing away from the chlorine atom. Molecular structures were taken from density functional theory optimisations, using the VWN-BP functional (Vosko *et al.*, 1980; Becke, 1988; Perdew & Wang, 1992) and the DNP numerical basis set (Delley, 1990) within the program DMol3.

The initial searches for low energy crystal structures were performed using the *exp-6* model potential parameters for C, H, and O fitted to hydrocarbons (Williams, 1999) and oxohydrocarbons (Williams, 2001), and parameters for chlorine and fluorine fitted to

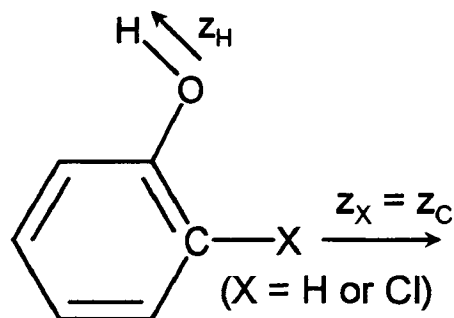
perchlorohydrocarbons (Hsu & Williams, 1980) and perfluorohydrocarbons (Williams & Houpt, 1986). For this model, all C-H and O-H bonds were foreshortened by 0.1 Å, moving the interaction site for hydrogen atoms away from the nucleus, towards the true maximum in charge density. For both molecules, the electrostatics were modelled by atomic charges fitted to the quantum chemically calculated (DFT) electrostatic potential. This *exp-6* + atomic charge model is limited by the assumption that the interaction between atoms is independent of orientation. This isotropic atom approximation can seriously limit the accuracy of crystal structure modelling, especially for the electrostatic interactions in hydrogen bonding crystals and the close contacts with halogen atoms. Hence, for final lattice energy minimisations, we replaced the atomic point charges with an atomic multipole model, calculated from a DFT wavefunction using the B3P91 functional and 6-31G(*d,p*) basis set. This calculation was performed within the program CADPAC (Amos *et al.*, 1995) and multipoles, up to hexadecapole (i.e. charge, dipole, quadrupole, octupole, and hexadecapole) were derived using a distributed multipole analysis (Stone, 1981; Stone & Alderton, 1985).

In the final energy minimisations of the predicted 4-fluorophenol structures, we kept the spherical atom *exp-6* model used in the initial search. However, including anisotropy in the repulsive wall around chlorine atoms appears to be crucially important for modelling crystals of chlorinated molecules (Munowitz *et al.*, 1977; Day & Price, 2003). We therefore used a more elaborate model for the repulsion and dispersion interactions in the final energy minimisations of 2-chlorophenol crystal structures. Recent advances in models for intermolecular interactions involving chlorine atoms have led to successful crystal structure predictions for other chlorinated aromatic molecules (Day & Price, 2003; Tremayne *et al.*, 2004), so we adapted a non-empirical model potential originally derived for chlorobenzenes (Day & Price, 2003). The model has the *exp-6* form for repulsion and dispersion interactions, allowing for anisotropy in the repulsive wall through an orientation-dependent term in the exponential:

$$U = \sum_{i \in M, k \in N} \left[A^{ik} \exp(-\alpha^{ik} [R_{ik} - \rho(\Omega_{ik})]) - \frac{C_6^{ik}}{R_{ik}^6} + U_{elec}(DMA, \Omega_{ik}, R_{ik}^{-n}, n \leq 5) \right] \quad (1)$$

$$\rho^{ik}(\Omega) = \rho_1^i(\hat{\mathbf{z}}_i \cdot \hat{\mathbf{R}}_{ik}) + \rho_1^k(-\hat{\mathbf{z}}_k \cdot \hat{\mathbf{R}}_{ik}) + \rho_2^i \left(3[\hat{\mathbf{z}}_i \cdot \hat{\mathbf{R}}_{ik}]^2 - 1 \right) / 2 + \rho_2^k \left(3[\hat{\mathbf{z}}_k \cdot \hat{\mathbf{R}}_{ik}]^2 - 1 \right) / 2 \quad (2)$$

Here, R_{ik} is the distance between atoms i and k , of type ι and κ , in molecules M and N ; \mathbf{R}^{\wedge}_{ik} is the corresponding unit vector and \mathbf{z}^{\wedge}_k is the unit vector along the atomic z -axis. The atomic axes for this model are shown in Scheme 5.2.



Scheme 5.2: Atomic axes used in the anisotropic repulsion model.

For carbon, chlorine and the hydrogen atoms bonded to carbon, parameters were taken directly from Day & Price (2003) and parameters for oxygen and the hydroxyl hydrogen were empirically fitted to reproduce the known crystal structures and sublimation enthalpies of a set of similar molecules: resorcinol, 3,4-dichlorophenol, 3,5-dichlorophenol and tetrachlorohydroquinone. No anisotropy was used for the repulsion on oxygen atoms, while the ρ_l coefficients from H_C hydrogen atoms were transferred to the hydroxyl hydrogen. This anisotropic term accounts for the shift of electron density away from the nucleus on hydrogen atoms and has a similar effect to the X-H bond foreshortening that was used with the isotropic *exp-6* model. The final parameters are given in Table 5.3.

Atom types		A^{ik}	B^{ik}	C_6^{ik}	ρ_1^i	ρ_1^k	ρ_2^i	ρ_2^k
i	k	kJ mol^{-1}	\AA^{-1}	$\text{\AA}^6 \text{kJ mol}^{-1}$	\AA	\AA	\AA	\AA
Cl	Cl	569746	3.3427	8366.9	+0.0156	+0.0156	-0.0939	-0.0939
C _{Cl}	C _{Cl}	28957	3.2131	2146.4	-0.2054	-0.2054	-0.3109	-0.3109
C _{H/O}	C _{H/O}	107333	3.1936	2146.4	-0.0026	-0.0026	+0.0419	+0.0419
O	O	94728	3.4600	1221.8	0.0	0.0	0.0	0.0
H _C	H _C	2220	3.2575	200.0	-0.0449	-0.0449	+0.0036	+0.0036
H _O	H _O	673	3.6900	15.1	-0.0449	-0.0449	0.0	0.0
Cl	C _{Cl}	277307	3.5474	4234.3	+0.0156	-0.2054	-0.0939	-0.3109
Cl	C _{H/O}	219400	3.2465	4234.3	+0.0156	-0.0026	-0.0939	+0.0419
Cl	O	232316	3.4014	3176.5	+0.0156	0.0	-0.0939	0.0
Cl	H _C	30829	3.2597	1293.1	+0.0156	-0.0449	-0.0939	+0.0036
Cl	H _O	19575	3.5163	355.6	+0.0156	-0.0449	-0.0939	0.0
C _{Cl}	C _H	61374	3.2443	2146.4	-0.2054	-0.0026	-0.3109	+0.0419
C _{Cl}	O	52378	3.3365	1608.9	-0.2054	0.0	-0.3109	0.0
C _{H/O}	O	100838	3.3268	1608.9	-0.0026	0.0	+0.0419	0.0
C _{Cl}	H _C	11254	3.3709	653.7	-0.2054	-0.0449	-0.3109	+0.0036
C _{Cl}	H _O	4413	3.4515	180.1	-0.2054	-0.0449	-0.3109	0.0
C _{H/O}	H _C	16950	3.2654	653.7	-0.0026	-0.0449	+0.0419	+0.0036
C _{H/O}	H _O	8497	3.4418	180.1	-0.0026	-0.0449	+0.0419	0.0
H _C	H _O	1222	3.4738	55.0	-0.0449	-0.0449	+0.0036	0.0

Table 5.3. Final parameters of the 2-chlorophenol model potential. C_{Cl} is a carbon bonded to chlorine, C_{H/O} is a carbon bonded to hydrogen or oxygen. H_C is a hydrogen bonded to carbon, H_O is a hydroxyl hydrogen. Atomic z-axes are defined along the bonds pointing out from the aromatic ring (Scheme 5.2).

In most crystal structure prediction studies, it is common to search only the most common space groups; approximately 95% of homomolecular organic crystal structures are found in fewer than 10 space groups. In this work, we knew in advance that one of the polymorphs of 2-chlorophenol crystallises in a trigonal space group. Therefore, in addition to the most common space groups for organic molecular crystals, the most common trigonal

space groups were also searched (Table 5.4). Furthermore, we did not limit our search to having one molecule in the asymmetric unit; monoalcohols sometimes crystallise with $Z' > 1$ to optimise their hydrogen bonding, so we searched for crystals with one, two and three molecules in the asymmetric unit. The computing time was only available to repeat the simulated annealing search 4 times for each of these space group / Z' combinations. Four repeats usually results in a complete search in $Z' = 1$ (Day *et al.*, 2004b), but we risk missing some low energy structures with $Z' = 2$ and 3.

	Most common space groups searched	Trigonal space groups searched
$Z' = 1$	$P2_1/c$, $P\bar{1}$, $P2_12_12_1$, $P2_1$, $C2/c$, $Pbca$, $Pnma$, $Pna2_1$, $Pbcn$	$P\bar{3}$, $P3_121$ ($P3_221$), $R\bar{3}$, $P3$, $P3_1$ ($P3_2$), $R3$, $R3c$
$Z' = 2$	$P2_1/c$, $P\bar{1}$, $P2_12_12_1$, $P2_1$, $C2/c$, $P1$	$P\bar{3}$, $P3_121$ ($P3_221$), $R\bar{3}$, $P3$, $P3_1$ ($P3_2$), $R3$, $R3c$
$Z' = 3$	$P2_1/c$, $P\bar{1}$, $P2_12_12_1$, $P2_1$, $C2/c$, $P1$	$P\bar{3}$, $P3_121$ ($P3_221$), $R\bar{3}$, $P3$, $P3_1$ ($P3_2$), $R3$, $R3c$

Table 5.4. Space groups searched during crystal structure prediction calculations.

All structures within 15 kJ mol^{-1} of the global minimum from the search with the simple model potential were then re-minimised using the more elaborate anisotropic model within the program DMAREL (Willock *et al.*, 1995; Price *et al.*, 2001). Ewald summation was used for charge-charge, charge-dipole and dipole-dipole interactions, while all higher order electrostatic terms (up to R^{-5}) and the *exp-6* interactions were summed to a 15 \AA cutoff between molecular centres of mass. All structures were energy minimised using symmetry constraints, then tested for stability by calculating ($k = 0$) phonon frequencies and the elastic stiffness matrix. Any structures with instabilities were pushed away from saddle points and re-minimised with all symmetry constraints removed. The final energy minimised structures were clustered using the COMPACK program (Chisholm & Motherwell, 2004) to remove repeats of identical structures.

5.3 Results

The intra-molecular structures of 2-chlorophenol and 4-fluorophenol as derived at low-temperature are illustrated in Scheme 5.1, which also shows the atomic numbering

scheme used. Pressures of a few tenths of a GPa are unlikely to affect intramolecular geometry significantly, and intramolecular distances and angles in the refinements of the high-pressure structures were restrained to be equal to those observed at low-temperature. This is often necessary in high-pressure work to control the effects of low data completeness, and it means that comparison of intramolecular geometry at high and ambient pressures is not possible. It is the effect of pressure on intermolecular geometry and crystal packing which we address in this Chapter.

5.3.1 2-Chlorophenol at 100 K.

Phase-I of 2-chlorophenol crystallises at low-temperature in the trigonal space group $P3_2$ with three molecules in the asymmetric unit; in the accompanying tables these molecules are numbered C11-C181, C12-C182, C13-C183, and are referred to as molecules 1, 2 and 3 below. The bond distances and angles are normal, and do not differ between the components of the asymmetric unit. The molecules interact via ..OH..OH.. H-bonds to form helices disposed about crystallographic 3_2 screw-axes, conforming to a $C(2)$ graph set (Bernstein *et al.*, 1995)(Figure 5.2). Each helix is composed of crystallographically equivalent molecules. All the hydrogen bonds are of similar strength: the distances $O7x...O7x'$ measure 2.754(2), 2.748(1) and 2.762(2) Å for $x = 1, 2$ and 3 respectively.

H...Cl contacts are formed between the helices composed of molecules 1 and 2 and 2 and 3; there are no contacts between molecules 1 and 3. In each case the chlorine of one helix interacts with two hydrogen atoms from the other helix. The contact distances (Å) are: Cl(81)...H(42) 2.89 and Cl(81)...H(52) 2.94; Cl(82)...H(43) 2.88 and Cl(82)...H(53) 2.81 Å. The sum of the van der Waals radii of H and Cl is 2.95 Å, though this has been criticised as a criterion for assessing the importance of hydrogen bonds (Steiner, 2002). Figure 5.2 shows the hydrogen bonding and close contacts in the structure, but, for clarity, only the shortest contact between two groups has been labelled.

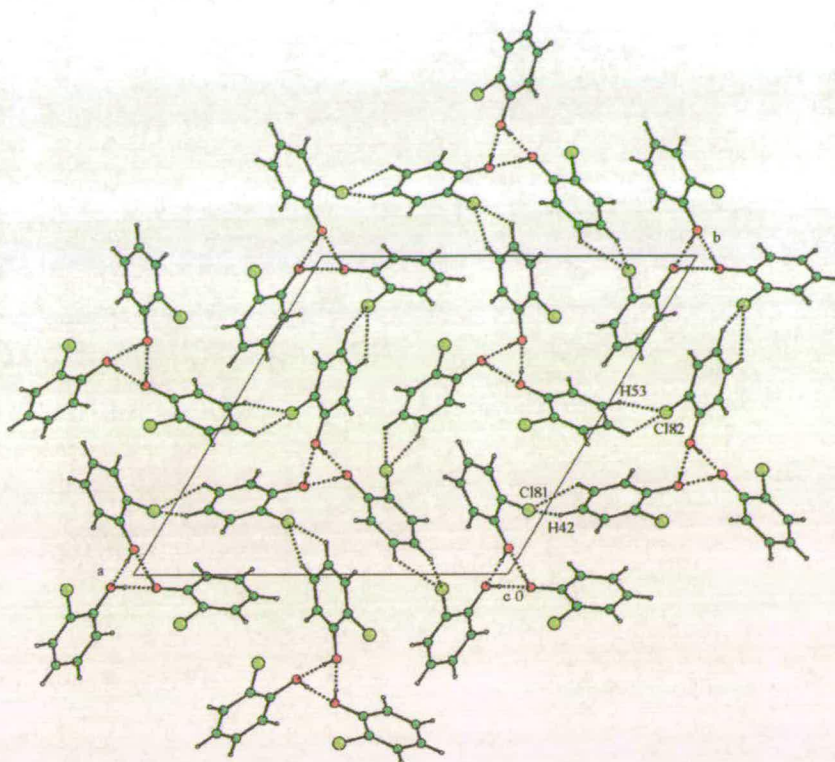


Figure 5.2: Crystal structure of 2-chlorophenol at ambient pressure and 100 K. Helices are formed about 3_2 axes by OH...OH hydrogen bond formation. The helices are linked through close contacts between the chlorine atom of one chain and two hydrogen atoms of the next. Only the shortest H...Cl contacts are labelled for the sake of clarity. Colour scheme: C green, Cl light green, H white, O red; the same scheme is used in Figures 5.3.

5.3.2 2-Chlorophenol at 0.12 GPa

Phase-II of 2-chlorophenol was obtained on crystallisation from the liquid at 0.12 GPa. The structure crystallises in space group $P2_1/n$ with one molecule in the asymmetric unit. As in phase-I, the molecules interact via ..OH..OH.. hydrogen bonds, forming $C(2)$ chains, but by contrast to phase-I, where helices were formed, these chains zig-zag about a 2_1 screw axis (Figure 5.3a). The hydrogen bond connecting the equivalent molecules is actually slightly longer than in phase-I [O7...O7' measures 2.809(11) Å versus 2.748(1) – 2.762(2) Å in phase-I]. The distance between the ring centroids of neighbouring molecules within a chain decreases from 5.90 Å in phase-I to 4.91 Å in phase-II. The elongation of the H-bond in phase-II relative to phase-I may therefore reflect relief of the steric interaction between the phenyl groups in this arrangement.

The H-bonded chains are connected across inversion centres by pairs of weak C3-H3...Cl8 interactions measuring 2.98 Å (the sum of the van der Waals radii of H and Cl is

2.95 Å). Similar 'dimer-like' interactions have been observed by Thalladi *et al.* (1998) in the fluorobenzenes.

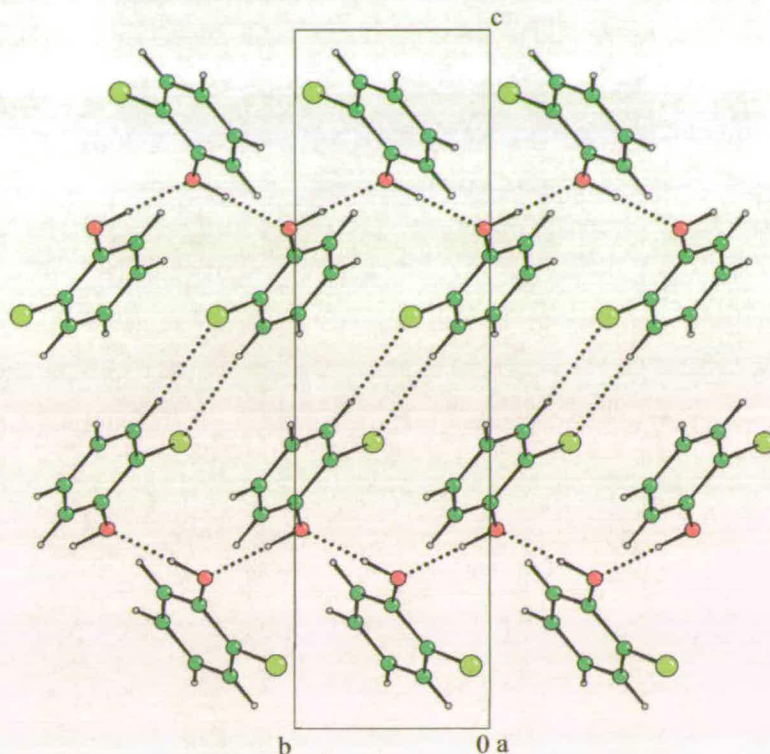


Figure 5.3a: The crystal structure of 2-chlorophenol at 0.12GPa. The application of pressure has changed the behaviour of the chlorophenyl substituent to that of a small group, allowing chains to be formed where molecules are related by a 2_1 -screw axis. Weak H...Cl 'dimer' interactions are shown between the chains.

In the structure, the chains lie along the b -direction at $c = \frac{1}{4}$ and $\frac{3}{4}$ and are aligned parallel to one another in the (1 0 3) planes. When the structure is viewed parallel to this, an A-B-A-B layer structure is observed where regions of chlorine and oxygen atoms are separated by the regions of carbon and hydrogen sites (Figure 5.3b).

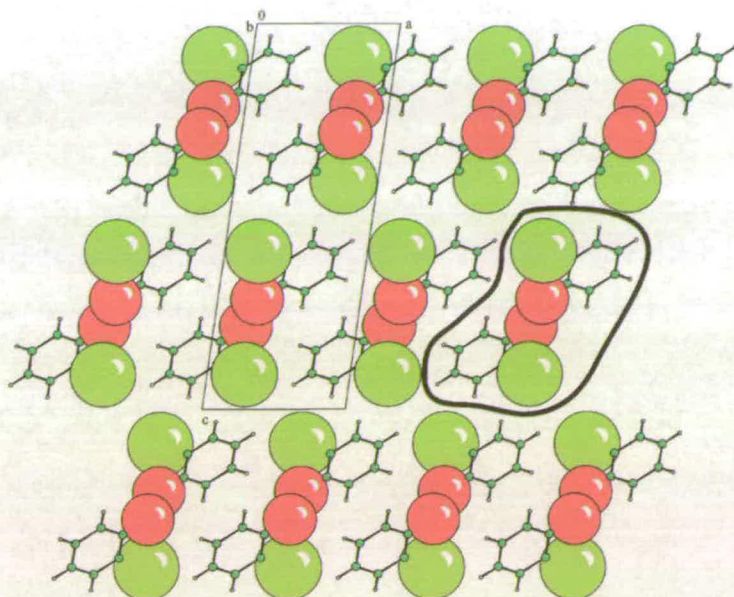


Figure 5.3*b*: The ribbons (circled) lie parallel to one another over the (1 0 3) planes. This diagram shows the separation of regions of ‘organic’ structure by chlorine and oxygen atoms.

5.3.3 4-Fluorophenol at 150 K

4-Fluorophenol is solid at ambient temperatures and pressures and crystallises in space group $R\bar{3}$ with one molecule in the asymmetric unit. Six molecules interact via ..OH..OH.. H-bonds forming an $R_6^6(12)$ ring motif disposed about a $\bar{3}$ special position. The six-membered hydrogen-bonded $R_6^6(12)$ rings are connected together through F...H interactions between H2...F8 (2.57 Å) and H5...F8 (2.65 Å). The fluorine in this structure thus acts as bifurcated acceptor for weak CH...F interactions. The contact to H5 forms a dimer, which is a motif common in fluorinated benzenes (Thalladi *et al.*, 1998) (Figure 5.4).

The OH...OH hydrogen bond at 150 K structure is the shortest to be observed in any of the monohalophenols with an O...O separation of 2.650(1) Å, and we speculated that we might be able to induce a phase transition by applying pressure to a single crystal of phase-I grown *ex situ*. Though no phase transition was observed up to 1.7 GPa, the crystal of 4-fluorophenol developed regions of polycrystallinity over the course of two days, which suggests that the crystal was undergoing a phase transition. When the pressure was released on this sample the polycrystalline regions disappeared to produce single crystal of 4-fluorophenol. This crystal was subsequently identified as phase-I. This process was reproducible in that on application of pressure the crystal became polycrystalline and with the release of pressure it reverted back to the single crystal.

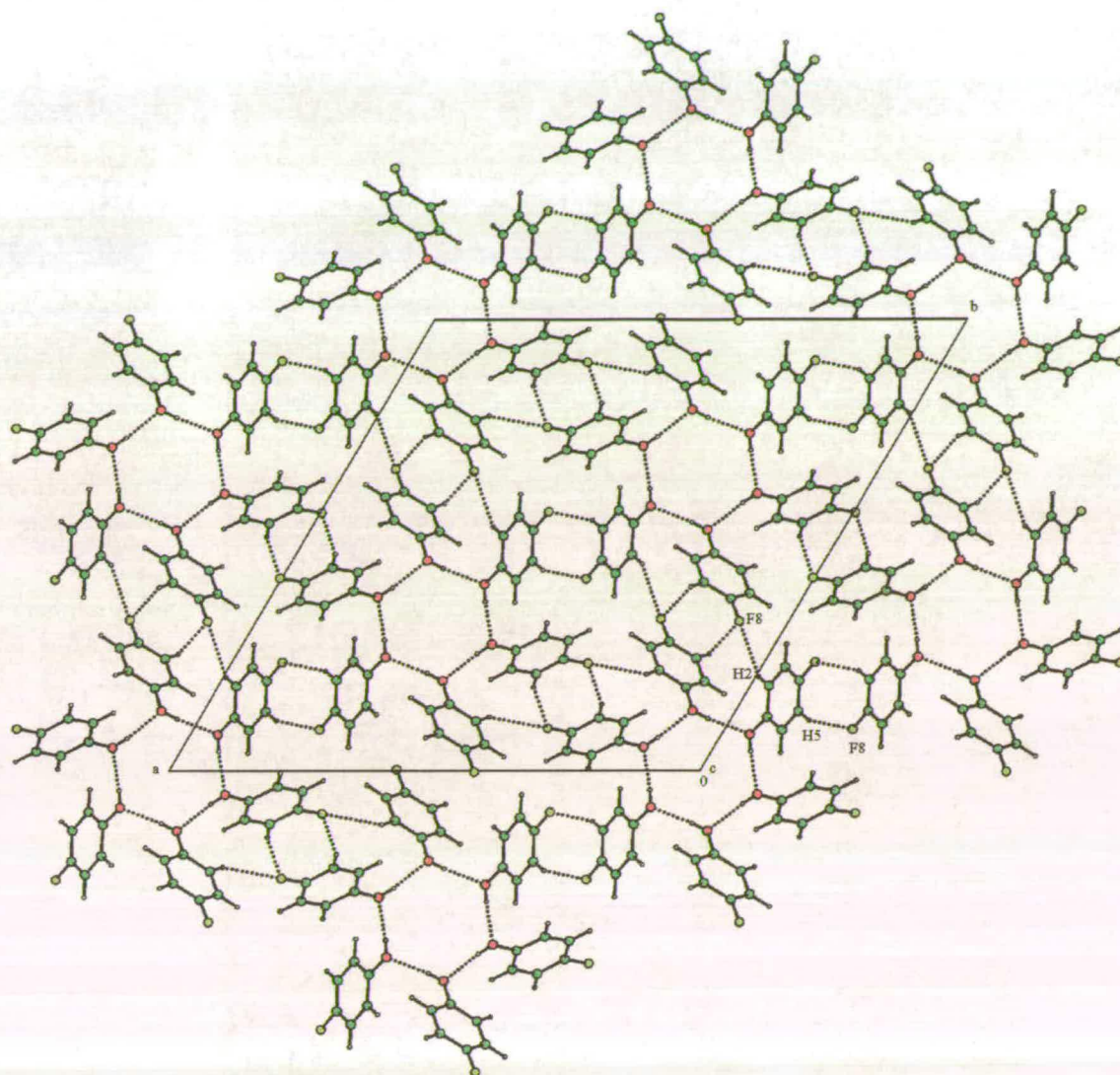


Figure 5.4: Crystal structure of 4-fluorophenol at 150 K viewed down the c -axis. 4-Fluorophenol crystallises around a $\bar{3}$ special position. This type of molecular packing allows close interaction of the hydroxyl groups to form strong hydrogen bonds. The discrete hydrogen bonded motifs are connected through a dimer interaction between H5..F8 (Thalladi *et al.*, 1998). Colour scheme: C green, F light green, H white, O red; the same scheme is used in Figures 5.5.

The unit cell dimensions showed a significant contraction along the a -direction but not along the c -direction. The contraction of the a - and b -axes pushes the H-bonded groups disposed about the $\bar{3}$ site closer together. The c -direction corresponds to a very short axis perpendicular to the H-bonded rings, so any contraction along this direction would severely disrupt the conformation of the six-member hydrogen-bonded rings.

5.3.4 4-Fluorophenol at 0.28 GPa

Growth of a crystal of 4-fluorophenol at 0.28 GPa yields another polymorph. The new polymorph crystallises in space group $P2_1/c$ with half a molecule in the asymmetric unit. The molecule is disordered over an inversion centre.

The molecules are connected into a chain; the contact involved is presumably OH...OH, as OH...F is unlikely to be energetically competitive. The chains interact via F...F contacts to form layers (Figure 5.5). Support for this view comes from the optimised (ordered) structure obtained during the crystal structure prediction study (see below). The hydrogen bonding in this structure appears to be rather long with an O7...O7' distance of 3.017(4) Å. This relatively long distance is likely to be the result of the disorder, which averages OH...O(H) and F...F distances. A search of the CSD for OH...O(H) and C(ar)-F...F-C(ar) contacts show that the mean distance for O...O and F...F contacts are 2.78(9) and 3.1(2) Å, respectively; the average of these values is 2.94 Å.

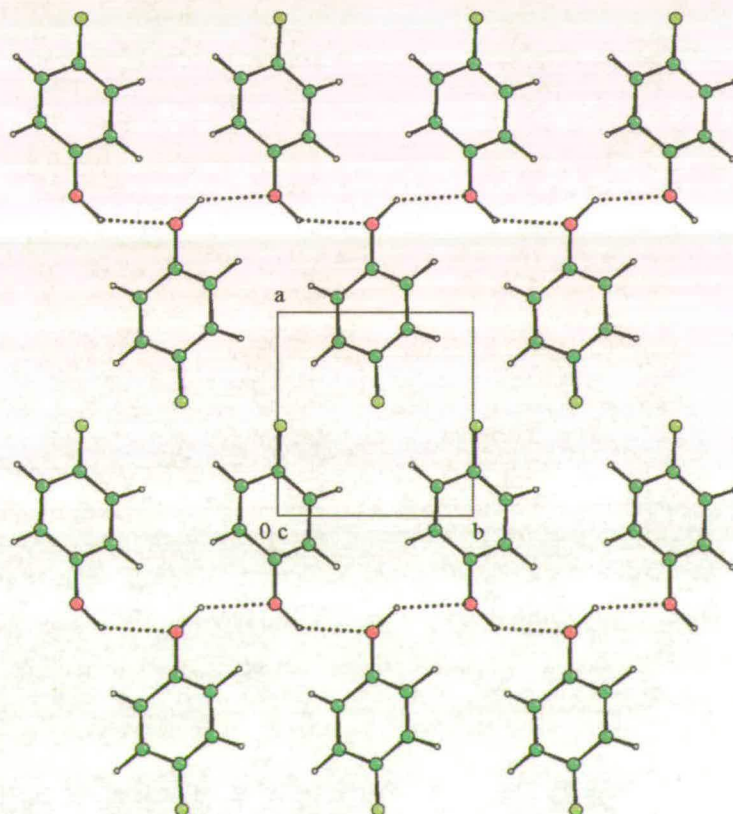


Figure 5.5: Crystal structure of 4-fluorophenol at 0.28 GPa viewed down the c -axis. The 4-fluorophenol molecule sits on an inversion and is disordered about it. The orientation of the molecules has been fixed here for clarity. Pressure alters the behaviour of the fluorophenyl group to act like a small alcohol. The chains lie parallel to each other over the $(\bar{1} 0 2)$.

5.3.5 Crystal Structure Prediction: 2-Chlorophenol

Approximately 60 possible crystal structures of 2-chlorophenol were predicted within 5 kJ mol^{-1} of the global minimum in lattice energy (Figure 5.6).

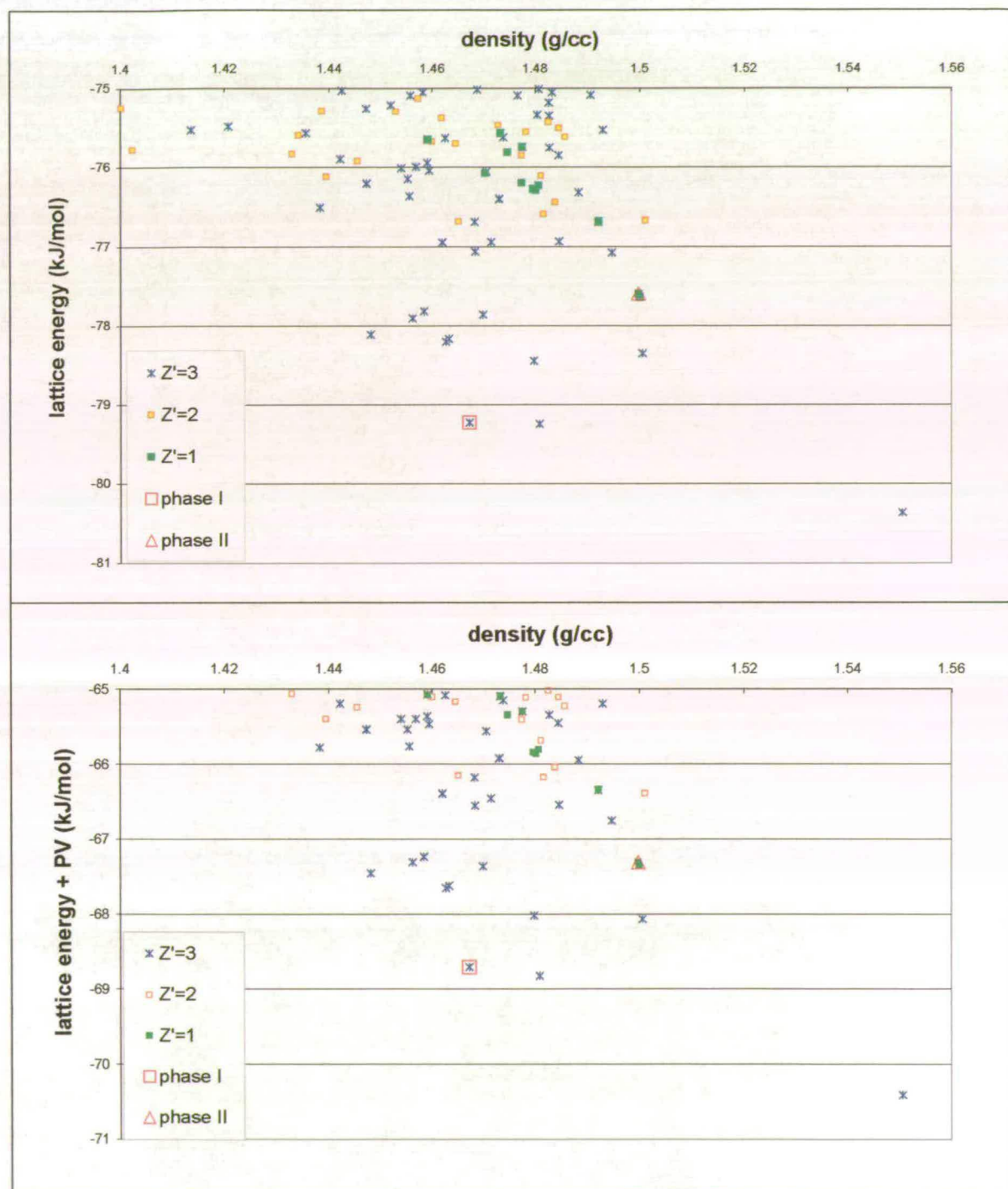


Figure 5.6: Plot of lattice energy against density for the predicted structures of 2-chlorophenol within 5 kJ mol^{-1} of the global minimum (top) and of lattice energy + PV at 0.12 GPa (bottom).

Unit cell parameters, space groups, densities and energies for the 20 lowest in energy are given in Table 5.5. As expected, all of these lowest energy structures contain OH...O hydrogen bonding. About half of these form closed hydrogen-bonding rings (trimers, tetramers or hexamers), while the remainder form OH...O chains. 7 of the 20 lowest energy predicted crystals show the same helical hydrogen bonding as in the observed phase-I structure. However, only two of these (ranks 3 and 6 on lattice energy) form chains around a true 3-fold axis. The remainder make pseudo 3-fold axes in non-trigonal space groups by crystallising with three symmetrically inequivalent molecules, as in the ambient pressure monoclinic polymorph of phenol.

Many of the predicted polymorphs have very long unit cell axes ranging up to 43.4 Å, and this is unusual. The unit cell dimensions of crystal structures of molecules of less than twenty atoms crystallising with three molecules in the asymmetric unit were extracted from the databases CSDsymmetry (Yao *et al.*, 2002) and CSD. The results were plotted as a histogram (Figure 5.7), which showed that unit cell axes with dimensions over 30 Å are rare even with three molecules in the asymmetric unit. This enables 5 of the 12 lowest structures to be ruled-out on the grounds that, though they are not impossible, they are rather unlikely.

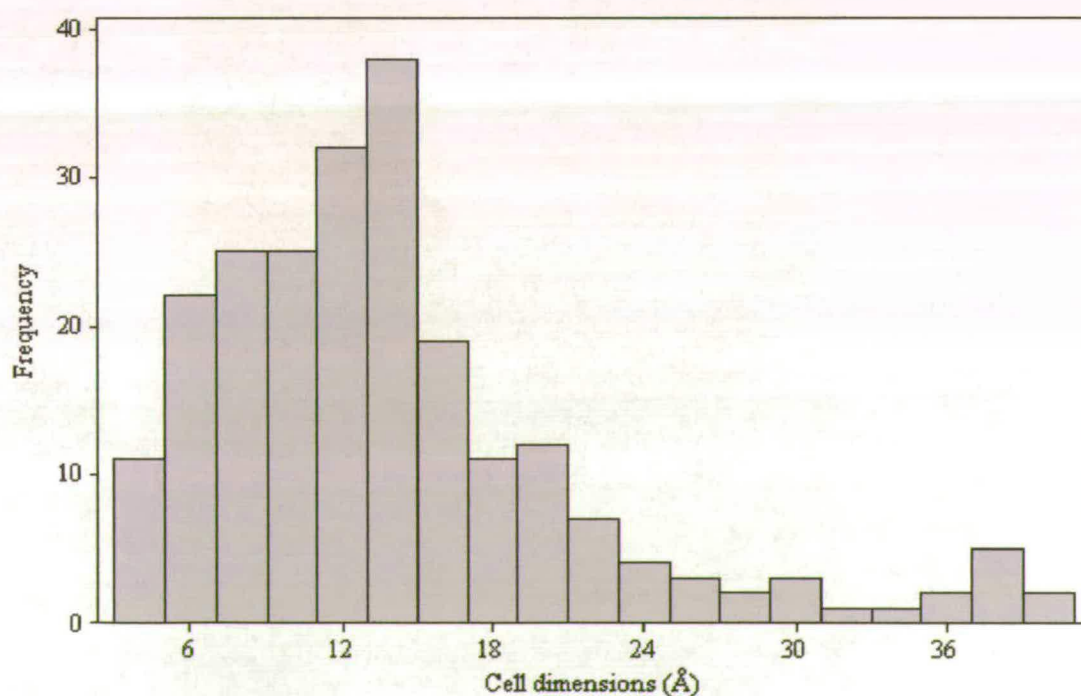


Figure 5.7: Distribution of the cell dimensions for crystal structures of molecules with twenty atoms or less crystallising with three molecules in the asymmetric unit extracted from CSDsymmetry and CSD.

Rank on lattice energy	Space group	Lattice parameters				Density (g cm ⁻³)	Lattice energy (E) (kJ mol ⁻¹)	E + PV, 1.2kbar (kJ mol ⁻¹)	Hydrogen bonding
		a/Å	b/Å	c/Å	Angles/°				
1	<i>P</i> 2 ₁ 2 ₁ 2 ₁ (Z'=3)	7.746	5.391	39.562	90	1.551	-80.36	-70.41	OH...O and OH...Cl chains
2	<i>P</i> 2 ₁ 2 ₁ 2 ₁ (Z'=3)	4.325	13.904	28.767	90	1.481	-79.24	-68.82	OH...O trimers
3 ¹	<i>P</i> 3 ₂ (Z'=3)	18.313	18.313	4.508	90, 90, 120	1.467	-79.22	-68.71	3-fold helical OH...O chains
4	<i>P</i> 2 ₁ 2 ₁ 2 ₁ (Z'=3)	9.452	5.554	32.980	90	1.480	-78.44	-68.02	OH...OH... OH trimers
5	<i>P</i> 2 ₁ 2 ₁ 2 ₁ (Z'=3)	9.001	40.483	4.685	90	1.501	-78.35	-68.07	OH...O 2 ₁ chains
6	<i>P</i> 3 ₂ (Z'=1)	11.141	11.141	4.074	90, 90, 120	1.463	-78.20	-67.65	3-fold helical OH...O chains
7	<i>P</i> 2 ₁ (Z'=3)	4.799	10.296	17.717	90.00	1.463	-78.16	-67.62	pseudo 3-fold helical OH...O chains
8	<i>P</i> 2 ₁ 2 ₁ 2 ₁ (Z'=3)	8.447	43.358	4.830	90	1.448	-78.10	-67.45	OH...O and OH...Cl 2 ₁ chains
9	<i>P</i> 2 ₁ 2 ₁ 2 ₁ (Z'=3)	36.125	4.697	10.367	90	1.456	-77.90	-67.31	pseudo 3-fold helical OH...O chains
10	<i>P</i> 2 ₁ (Z'=3)	4.217	18.745	11.027	β = 91.38	1.470	-77.86	-67.37	pseudo 3-fold helical OH...O chains

Table 5.5: Lowest energy predicted structures of 2-chlorophenol. ¹ Corresponds to the experimentally observed phase-I. ² Corresponds to the experimentally observed phase-II (cont'd overleaf).

Rank on lattice energy	Space group	Lattice Parameters				Density (g cm ⁻³)	Lattice energy (E) (kJ mol ⁻¹)	E + PV, 1.2kbar (kJ mol ⁻¹)	Hydrogen bonding
		a/Å	b/Å	c/Å	Angles/°				
11	<i>P2₁2₁2₁</i> (Z'=3)	4.834	17.895	20.306	90	1.458	-77.81	-68.50	pseudo 3-fold helical OH...O chains
12 ²	<i>P2₁/c</i> (Z'=1)	6.538	4.788	18.666	β = 103.02	1.500	-77.64	-67.62	OH...O 2 ₁ chains
13	<i>P$\bar{1}$</i> (Z'=3)	7.463	10.373	12.297	α = 68.68 β = 79.70 γ = 87.24	1.468	-77.06	-66.67	OH...O hexamers
14	<i>P$\bar{1}$</i> (Z'=3)	9.596	10.008	10.433	α = 114.19 β = 100.72 γ = 96.94	1.462	-76.95	-66.82	OH...O hexamers
15	<i>P$\bar{1}$</i> (Z'=3)	7.332	10.938	12.144	α = 111.88 β = 100.44 γ = 96.70	1.471	-76.94	-66.47	OH...O hexamers
16	<i>P$\bar{1}$</i> (Z'=3)	10.350	10.573	8.844	α = 109.97 β = 95.78 γ = 104.35	1.485	-76.94	-66.39	OH...O hexamers
17	<i>P2₁</i> (Z'=1)	6.883	4.819	8.769	β = 100.33	1.492	-76.69	-66.27	OH...O 2 ₁ chains
18	<i>P2₁2₁2₁</i> (Z'=3)	4.170	32.195	12.997	90	1.468	-76.68	-66.35	pseudo 3-fold helical OH...O chains
19	<i>P2₁/c</i> (Z'=2)	12.747	7.847	14.743	β = 127.77	1.465	-76.68	-66.34	OH...O tetramers
20	<i>P$\bar{1}$</i> (Z'=2)	7.718	7.907	10.282	α = 95.49 β = 94.25 γ = 113.40	1.501	-76.67	-66.17	OH...O tetramers

Table 5.5 (cont'd): Lowest energy predicted structures of 2-chlorophenol. ¹ Corresponds to the experimentally observed phase-I. ² Corresponds to the experimentally observed phase-II.

The remaining structures are viewed with MERCURY in order to exclude any structures that have unusual intermolecular interactions. The structure corresponding to the global minimum in lattice energy lies 1.6 kJ mol⁻¹ lower than any other, but while two of the three independent molecules take part in OH...O hydrogen-bonded chains, the third molecule instead forms OH...Cl chains (Figure 5.8). Such interactions are unlikely to be competitive with OH...OH chains, and the prediction of this structure could be a failing of the partly empirical model potential; the set of crystal structures used to parameterise the hydroxyl parameters did not include OH...Cl contacts, so the calculated energy of such interactions may be overestimated. Other low-energy structures take the form of hydrogen bonded trimers; a search of the CSD revealed that this motif is unusual (only 12 such structures were identified), and so structures 2 and 4 might be ruled-out on these grounds. From the observations above, of the lowest energy structures 3, 6, 7, 10, 11 and 12 seem reasonable.

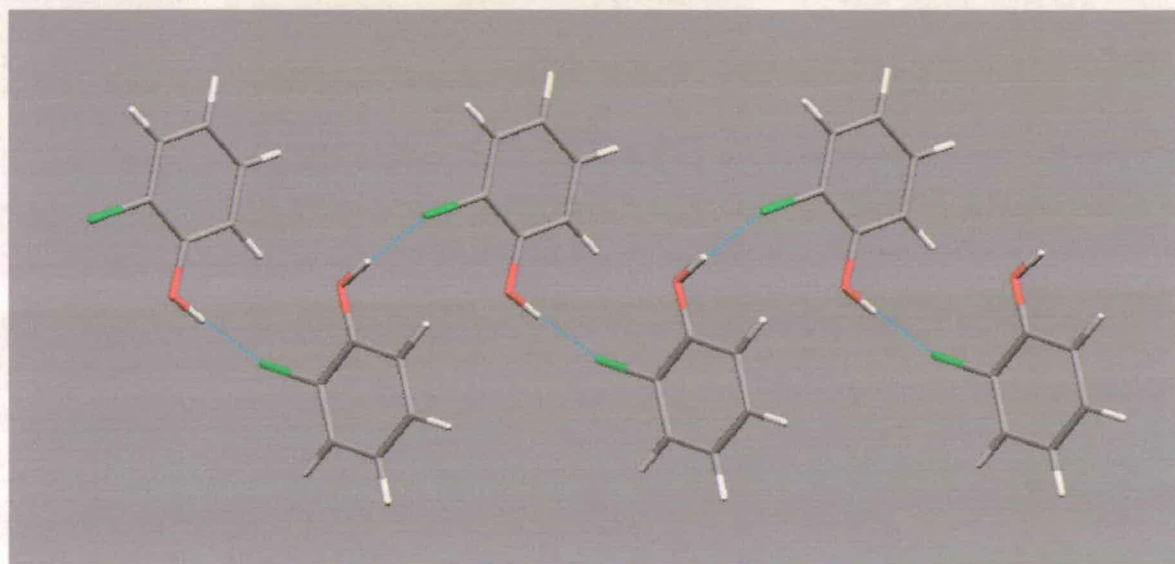


Figure 5.8: OH...Cl chains in the global minimum predicted structure of 2-chlorophenol. These are not expected to be energetically competitive with OH...OH hydrogen bonds and their presence in this structure may reflect the parameterisation of the potential used.

The lowest energy structure remaining after the exclusions (No. 3) is a reasonable reproduction of the observed phase-I structure - the same structure is found by replacing the molecules in the experimental crystal structure by the gas phase optimised molecular structure and minimising the lattice energy. This crystal structure is the third lowest in lattice energy of the predicted structures, just 1.14 kJ mol⁻¹ above the global minimum. The *P2₁/c* phase-II crystal structure was also located as one of the densest structures located in the search -

twelfth in lattice energy, 2.72 kJ mol^{-1} above the global minimum, (Figure 5.6). It has the highest density of structures 3, 6, 7, 10, 11 and 12. The predicted crystal structures were not allowed to relax under pressure (this feature is not yet implemented in the code available to us), but we estimated the effect of the high-pressure by adding the PV contribution to the energy at 0.12 GPa. The PV term favours the higher density structures and improves the ranking of the high-pressure phase-II structure, which has the 8th lowest lattice energy + PV amongst the predicted structures.

The predictions were performed with a rigid planar molecular structure, while the hydroxyl group in the experimentally observed structures is distorted significantly out of the plane of the aromatic ring, presumably to optimise hydrogen bonding interactions in the crystal. To test the effect of this molecular distortion, we energy-minimised the phase-I and II structures with the hydroxyl out-of-plane angle fixed at the experimentally observed values (-8.1° , -13.4° and -19.1° for molecules 1, 2 and 3 in phase-I, and 21.3° in phase-II). The results of these minimisations (Tables 5.6 & 5.7) demonstrate the effect of the assumed molecular structure on the modelling of these structures. For phase-I, the lattice energy minimised structure is improved dramatically with the torsion angles fixed to the experimental values - the RMS error in the lattice parameters, a , b and c are decreased from 17.7% with the planar molecular structure down to 2.2% with the experimentally observed torsion angle. While the crystal structure is very sensitive to the orientation of the hydroxyl groups, the lattice energy is nearly unaffected (Table 5.6). The phase-II lattice energy minimum with the hydroxyl group torsion angle fixed at 21.3° is in slightly worse agreement with the experimentally observed structure than the crystal structure calculated with the planar molecular structure (Table 5.7). However, in this case, the lattice energy is decreased significantly and the density is increased slightly; the molecular distortion appears to have an important stabilising effect on this crystal structure.

	$a = b / \text{\AA}$	$c / \text{\AA}$	Volume / \AA^3	Lattice Energy / kJmol^{-1}
Experimental	16.072	5.896	1318.9	-
Lattice energy minima				
with gas phase (planar) molecular structure	18.313 (+13.9%)	4.508 (-23.5%)	1309.5 (-0.7%)	-79.22
with experimentally observed torsion angles ¹	16.311 (+1.49%)	5.708 (-3.19%)	1315.2 (-0.29%)	-79.14

Table 5.6. Lattice-energy-minimised unit cells of the ambient pressure crystal structure of 2-chlorophenol. ¹ The lattice energy minimised crystal structure with the hydroxyl group out-of-plane torsion angles adjusted to the experimentally observed values (-8.1°, -13.4°, -19.1°).

	$a / \text{\AA}$	$b / \text{\AA}$	$c / \text{\AA}$	$\beta / ^\circ$	Volume / \AA^3	Lattice Energy / kJmol^{-1}
Experimental	6.464	4.909	18.131	98.11	569.57	-
Lattice energy minima						
with gas phase (planar) molecular structure	6.538 (+1.14%)	4.788 (-2.46%)	18.666 (+2.95%)	103.02 (+5.00%)	569.36 (-0.04%)	-77.64
With experimentally observed torsion angle ¹	6.465 (+0.01%)	4.563 (-7.05%)	19.201 (+5.90%)	94.65 (-3.53%)	564.55 (-0.88%)	-82.44

Table 5.7. Lattice-energy-minimised unit cells of the high-pressure crystal structure of 2-chlorophenol. ¹ The lattice energy minimised crystal structure with the hydroxyl group out-of-plane torsion angle adjusted to the experimentally observed value (21.3°).

5.3.6 Crystal Structure Prediction: 4-Fluorophenol

The predictions for 4-fluorophenol produced structures with similar packing motifs as the 2-chlorophenol predictions; about half of the 20 lowest energy structures (Table 5.8) form closed hydrogen-bonded rings, while the rest show OH...O chain motifs (Figure 5.9).

Rank on lattice energy	Space group	Lattice parameters				Density (g cm ⁻³)	Lattice energy (<i>E</i>) (kJ mol ⁻¹)	<i>E</i> + <i>PV</i> , 1.2kbar (kJ mol ⁻¹)	Hydrogen bonding
		<i>a</i> /Å	<i>b</i> /Å	<i>c</i> /Å	Angles/°				
1	<i>P</i> 2 ₁ 2 ₁ 2 ₁ (<i>Z'</i> =2)	5.617	21.687	8.871	90	1.3780	-63.37	-40.59	pseudo 4-fold helical OH...O chains
2	<i>P</i> 2 ₁ / <i>c</i> (<i>Z'</i> =2)	19.744	11.423	4.540	β = 82.92	1.3747	-63.16	-40.33	OH...O tetramers
3	<i>P</i> 1̄ (<i>Z'</i> =2)	4.907	10.137	11.042	α = 85.06 β = 86.30 γ = 82.78	1.3735	-62.91	-40.06	OH...O tetramers
4	<i>P</i> 2 ₁ / <i>c</i> (<i>Z'</i> =2)	8.069	15.243	8.862	β = 90.86	1.3664	-62.83	-39.86	OH...O 2 ₁ chains
5	<i>Pca</i> 2 ₁ (<i>Z'</i> =3)	19.705	4.991	16.456	90	1.3803	-62.52	-39.78	pseudo 3-fold helical OH...O chains
6	<i>P</i> 2 ₁ (<i>Z'</i> =3)	9.489	16.685	5.201	β = 88.42	1.3568	-62.48	-39.35	pseudo 3-fold helical OH...O chains
7	<i>P</i> 2 ₁ 2 ₁ 2 ₁ (<i>Z'</i> =2)	22.896	8.245	5.711	90	1.3813	-62.46	-39.74	pseudo 4-fold helical OH...O chains
8	<i>Pna</i> 2 ₁ (<i>Z'</i> =3)	10.669	8.714	17.986	90	1.3358	-62.44	-38.94	OH...OH... F...OH pseudo 4-fold chains
9	<i>P</i> 2 ₁ / <i>c</i> (<i>Z'</i> =2)	12.499	20.137	4.845	β = 116.12	1.3601	-62.33	-39.25	OH...O tetramers
10	<i>P</i> 2 ₁ (<i>Z'</i> = 1) ²	8.115	5.346	6.438	β = 106.40	1.3893	-62.26	-39.67	OH...O 2 ₁ chains

Table 5.8: Lowest energy predicted structures of 4-fluorophenol. ¹ Corresponds to the experimentally observed phase-I. ² Corresponds to the experimentally observed phase-II (cont'd overleaf).

Rank on lattice energy	Space Group	Lattice parameters				Density (g cm ⁻³)	Lattice energy (E) (kJ mol ⁻¹)	E + PV, 1.2kbar (kJ mol ⁻¹)	Hydrogen bonding
		a/Å	b/Å	c/Å	Angles/°				
11	$P3_2$ (Z'=3)	15.796	15.796	6.101	90,90,120	1.2708	-62.23	-37.53	pseudo 3-fold helical OH...O chains
12	$C2/c$ (Z'=3)	20.417	10.402	16.242	$\beta = 97.83$	1.3074	-62.21	-38.20	OH...O hexamers
13	$P2_1$ (Z'=3)	6.037	9.181	15.854	90.00	1.2710	-62.19	-37.49	pseudo 3-fold helical OH...O chains
14	$P3_1$ (Z' = 1)	9.183	9.183	6.016	90,90,120	1.2713	-62.17	-37.48	3-fold helical OH...O chains
15	$R\bar{3}$ (Z' = 1) ¹	22.264	22.264	5.934	90,90,120	1.3154	-62.12	-38.26	OH...O hexamers
16	$P\bar{1}$ (Z'=2)	7.332	8.127	10.437	$\alpha = 83.32$ $\beta = 73.91$ $\gamma = 67.65$	1.3475	-62.09	-38.80	OH...O tetramers
17	$P2_1$ (Z'=2)	8.767	5.501	11.398	$\beta = 102.69$	1.3885	-62.07	-39.46	OH...O 2 ₁ chains
18	$P\bar{1}$ (Z'=2)	7.436	8.100	9.249	$\alpha = 95.41$ $\beta = 98.99$ $\gamma = 94.70$	1.3660	-61.99	-39.01	OH...O tetramers
19	$P\bar{1}$ (Z'=2)	8.124	7.909	8.773	$\alpha = 99.80$ $\beta = 94.76$ $\gamma = 92.71$	1.3477	-61.95	-38.66	OH...O tetramers
20	$P2_1$ (Z'=2)	7.922	5.502	12.772	$\beta = 105.16$	1.3858	-61.93	-39.28	OH...O 2 ₁ chains

Table 5.8(cont'd): Lowest energy predicted structures of 4-fluorophenol. ¹ Corresponds to the experimentally observed phase-I. ² Corresponds to the experimentally observed phase-II.

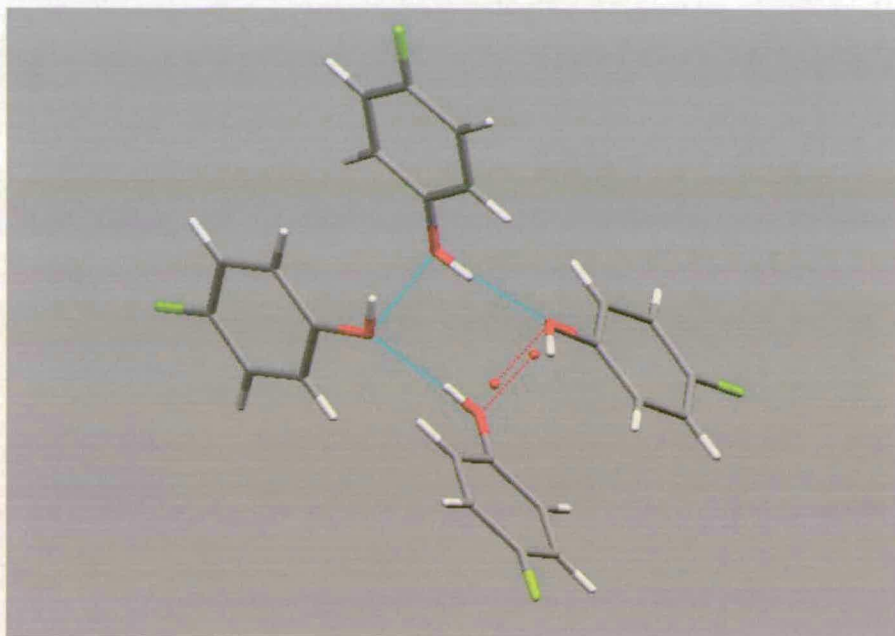


Figure 5.9: Four-fold chains in the global minimum (top) predicted structure of 4-fluorophenol.

The lattice energy was minimised to yield the observed phase-I crystal structure with the molecular structure replaced by the planar model used in the search (Table 5.9); the resulting structure matches exactly to the 15th lowest energy predicted crystal, 1.25 kJ mol⁻¹ above the global minimum. This model also energy minimised with the hydroxyl out-of-plane torsion angle set to the observed value of 9°; the unit cell dimensions are almost unaffected by this change, while the lattice energy is lowered by more than 1 kJ mol⁻¹ (Table 5.9).

	$a = b / \text{Å}$	$c / \text{Å}$	volume / Å ³	lattice energy / kJmol ⁻¹
Experimental	22.620	5.569	2467.7	-
lattice energy minima				
with gas phase (planar) molecular structure	22.263 (-1.58%)	5.935 (+6.56%)	2547.4 (+3.2%)	-62.12
with experimentally observed torsion angle ¹	22.294 (-1.44%)	5.925 (+6.39%)	2550.4 (+3.4%)	-63.42

Table 5.9 - Lattice energy minimised unit cells of the ambient pressure crystal structure of 4-fluorophenol. ¹ The lattice energy minimised crystal structure with the hydroxyl group out-of-plane torsion angle adjusted to the experimentally observed value (9.0°).

The prediction methodology can only generate ordered crystal structures, so the high-pressure polymorph of 4-fluorophenol could not be predicted exactly. However, the 10th lowest energy predicted structure is an ordered version of the observed phase-II - the same lattice energy minimum (Table 5.10) is found by replacing the disordered molecular structure in the observed crystal by the planar molecular model, fixed in one of the two orientations (as in Figure 5.6). As with 2-chlorophenol, this high-pressure crystal is amongst the densest of the predicted structures. As a result, the PV contribution to the energy favours this crystal over most of the other predictions (Table 5.8 & Figure 5.10).

	$a / \text{\AA}$	$b / \text{\AA}$	$c / \text{\AA}$	$\beta / ^\circ$	Volume / \AA^3	Lattice Energy / kJmol^{-1}
Experimental	6.281	5.724	7.798	106.06	267.98	-
lattice energy minimum	6.438 (+2.51%)	5.346 (-6.60%)	8.115 (+4.06%)	106.40 (+0.32%)	267.98 (-0.53%)	-62.26

Table 5.10. Lattice energy minimised unit cell of an ordered model of the high-pressure crystal structure of 4-fluorophenol.

Such sensitivity of the lattice energy to small changes in the molecular structure prevents any better results with the rigid body approximation than achieved here (*i.e.* the observed structure within 1-2 kJ mol^{-1} of the global minimum). This means that selection of likely structures from the list presented in Table 5.8 is more difficult than in 2-chlorophenol, though a few structures (e.g. 8 and 9) can be ruled out by the presence on unreasonable OH...F or O...O intermolecular interactions. We note, though, that almost none of the unobserved predicted polymorphs contain the common H...F motifs described by Thalladi *et al.* (1998), and it may be that there is some room for improvement of methodologies for modelling weak H...halogen interactions.

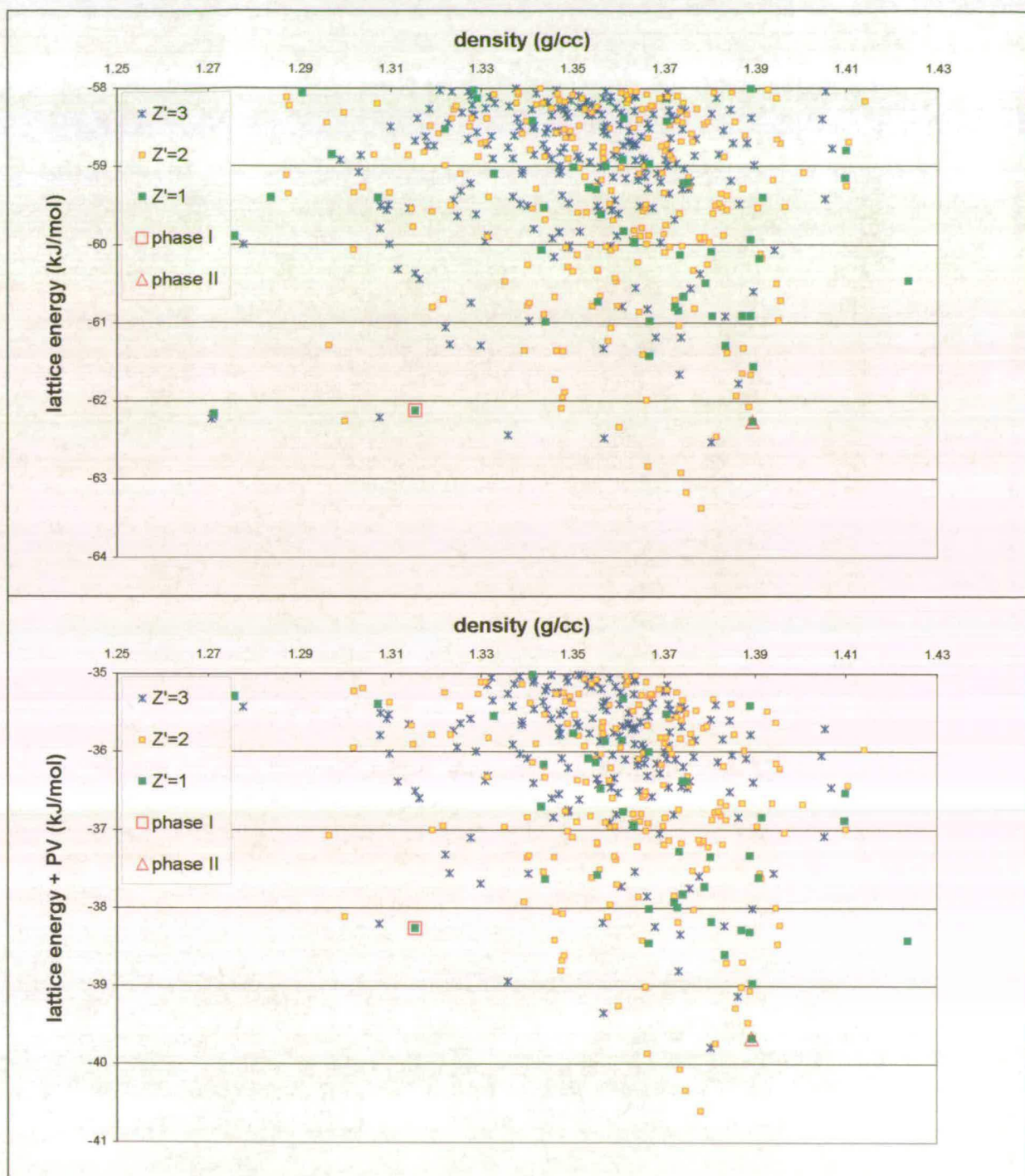


Figure 5.10: Plot of lattice energy against density for the predicted structures of 4-fluorophenol within 5 kJ mol^{-1} of the global minimum (top) and of lattice energy + PV at 0.28 GPa (bottom).

5.4 Discussion

5.4.1 Crystal Packing at low-temperature and high-pressure

Packing in the crystal structure of monoalcohols was investigated first by Brock & Duncan (1994) and subsequently by Taylor & McRae (2000). Both studies showed that the size of the R-group attached to the alcohol functionality is a major factor in the packing behaviour of the molecules. When the R-group is small then the molecules are usually related by a 2_1 screw axis or a glide plane. If the R-group is bulky then the molecules tend to aggregate around 3-, 4- or 6-fold screw, rotation or rotoinversion axes. These operations may be crystallographic - *i.e.* crystallisation occurs in a high-symmetry space group - or non-crystallographic, implying that crystallisation occurs in a low-symmetry space group with $Z' > 1$.

At ambient pressure 2-chlorophenol and 4-fluorophenol behave typically for alcohols with bulky R-groups. Both form structures containing molecules connected by ..OH..OH.. interactions. At ambient pressure, chains are formed in 2-chlorophenol about crystallographic 3_2 screw axes. In 4-fluorophenol the molecules hydrogen bond to form rings about $\bar{3}$ rotoinversion sites. On application of pressure, however, the structures change to ones in which the chains lie along 2_1 screw axes. In effect, pressure has altered the packing behaviour of the halophenyl groups from being characteristic of a large group to more typical of a small group.

In Chapter 6 we show that, rather unusually for simple alcohols, the other monofluoro- and chloro-phenols display quite complicated packing motifs (Oswald *et al.*, 2004). We have only been able in those cases to examine the effects of pressures up to 0.36 GPa (a modest figure by the standards of modern high-pressure crystallography), and it remains to be seen what happens to those systems at higher pressures. The alteration in packing behaviour is observed in phenol itself, however (Allan *et al.*, 2002). Phase-I crystallises at ambient pressure in space group $P2_1$ with three molecules in the asymmetric unit; these H-bond together to form a pseudo three-fold helix (Figure 5.11a). At high-pressure (0.16 GPa) another structure with $Z' = 3$ in $P2_1$ is obtained, the structure consisting of two crystallographically independent chains. The first chain is formed about a 2_1 screw axis, while the second comprises two independent molecules disposed about a pseudo 2_1 screw axis (Figure 5.11b).

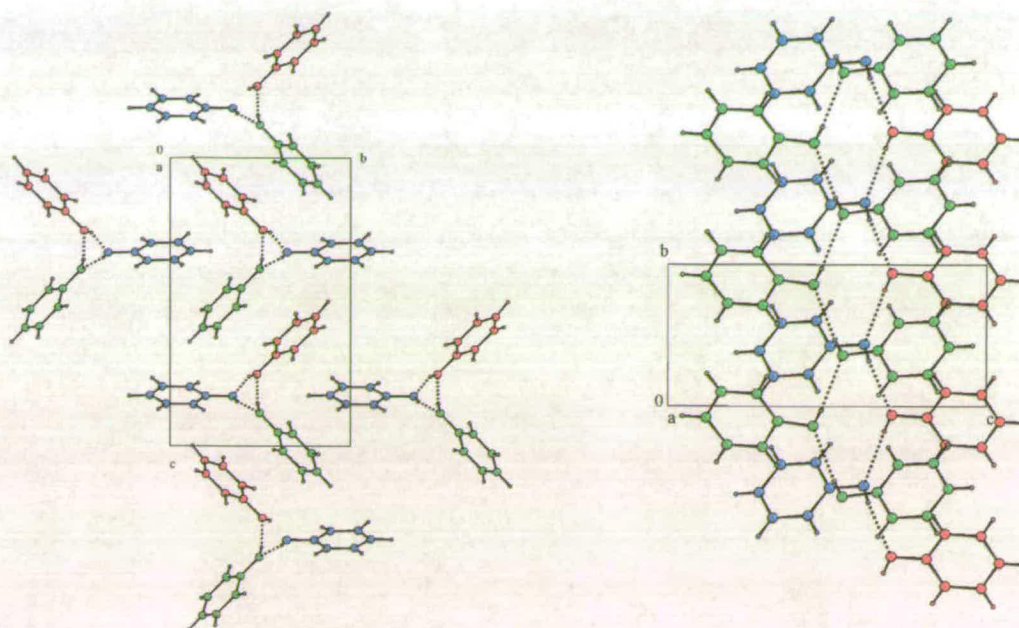


Figure 5.11 Left (a): The crystal structure of phenol at ambient pressure and 123 K. The phenyl ring acts like a bulky substituent. It crystallises with three molecules in the asymmetric unit that emulate a three-fold helix along b in the low-symmetry space group $P2_1$.

Right (b): Phenol at 0.16GPa. The behaviour of the phenyl group resembles that of a small substituent, with symmetry equivalent molecules related by crystallographic or pseudo- 2_1 screw axes. There are three molecules in the asymmetric unit with the blue and red molecules forming a pseudo- 2_1 screw axis and the green molecules forming a chain where the molecules are related by a crystallographic 2_1 screw axis. Colour-coding represents crystallographic equivalence.

Although alcohols tend to crystallise about screw axes, Brock & Duncan recognised that it should, in principle, be possible to generate hydrogen-bonded chains by simple transition in the case of a very small alcohol. They cited no examples of where this has been observed, however. In fact the effect of high-pressure on the crystal structure of methanol can also be interpreted in terms of a shift from small alcohol packing to very small alcohol packing. This is illustrated in Figure 5.12: at ambient pressure and 163 K the crystal structure of methanol contains chains of molecules that are related by a glide plane in an alternating 1-1-1 motif (Figure 5.12a) (Tauer & Lipscomb, 1952). At 7 GPa the high-pressure polymorph exhibits chains forming a 2-1-2-1 motif with three molecules in the asymmetric unit (Figure 5.12b). The pairs of molecules on the same side of the hydrogen-bonded chains in Figure 5.12b are related by a pseudo-translation (Allan *et al.*, 1998), confirming Brock & Duncan's intuitive argument.

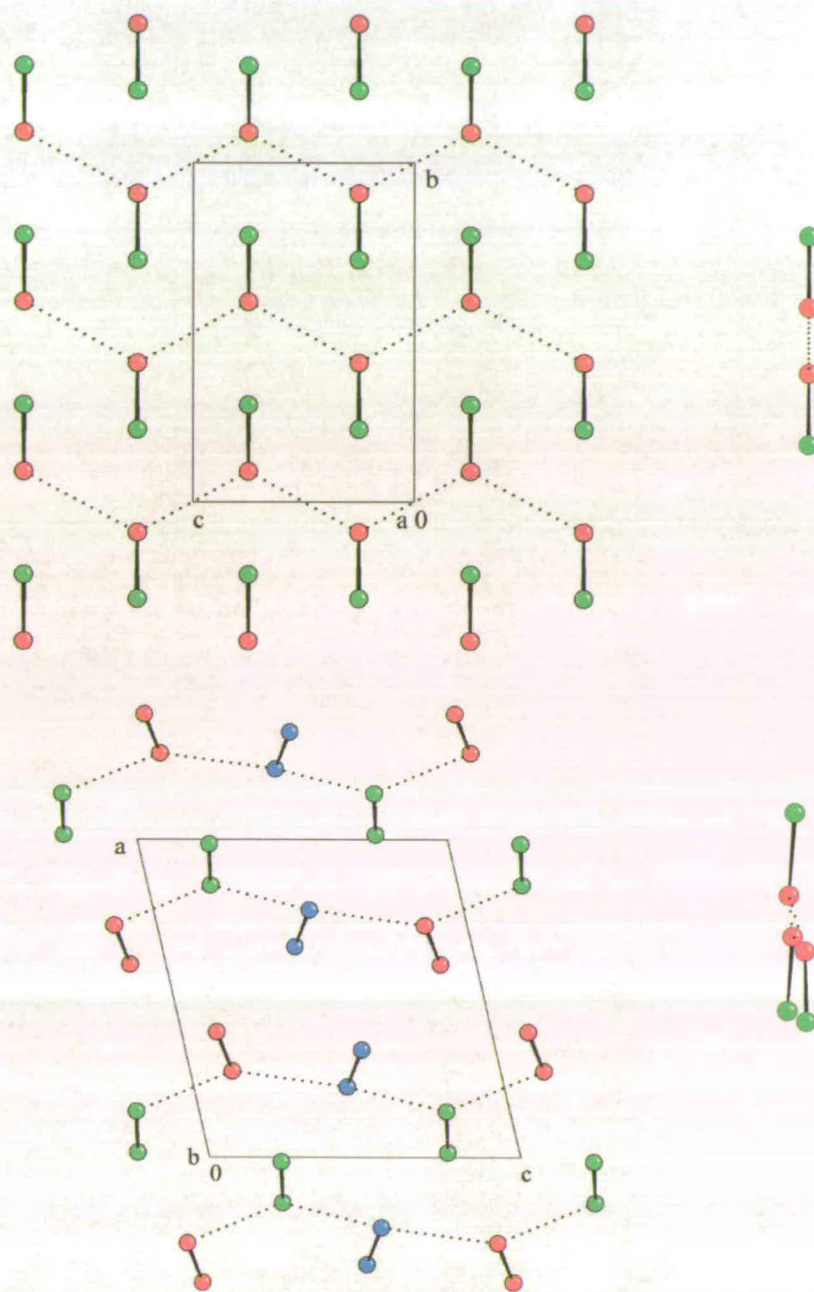


Figure 5.12 top (a): Ambient pressure phase of methanol at 163 K showing packing behaviour typical of a small monoalcohol: symmetry-equivalent molecules are related by a *c*-glide in a 1:1:1 sequence (i.e. one molecule on one side of the chain, one on the other, and so one). Colour scheme: C green and O red.

Bottom (b): At pressure (7 GPa) methanol undergoes a phase transition to three molecules in the asymmetric unit in a 2-1-2-1 sequence. Colour-coding represents crystallographic equivalence.

To the side of the main diagrams, a view down the chains in each of the phases. The pseudo translational symmetry can be seen in the high-pressure phase. The bulky methyl group is preventing the molecules from coming closer together to form perfect translational symmetry

Despite the change in packing behaviour in alcohols with application of high-pressure, the size of the group is important in determining the lengths of intermolecular interactions. In the OH...OH chains of 2-chlorophenol the intermolecular O...O distances are *longer* at 0.12 GPa than at ambient pressure [2.809(11) Å versus 2.748(1) to 2.762(2) Å at 100 K]. The elongation of the hydrogen bond can be seen in 4-fluorophenol where the O7...O7' distance is 2.650(1) Å at 150 K and about 3 Å at 0.28 GPa (it is not possible to be precise because of the O/F disorder in that structure).

This increase in hydrogen bond lengths is also observed in other high-pressure phases of alcohols. The crystal structure of phenol has three different hydrogen bonds in both the ambient and high-pressure phases. All three hydrogen bonds show an increase in length from an average length of 2.671 Å at ambient pressure to 2.964 Å at high-pressure. The high-pressure phase of phenol shows both forms of molecular aggregation in the formation of the two crystallographically unique chains as discussed previously. Interestingly, the H-bond used in the chain formed from symmetry equivalent molecules disposed about a 2_1 axis is longer than the others (disposed about a pseudo 2_1 axis); crystallographically inequivalent molecules that are H-bonded into a chain can deviate from exact symmetry to accommodate the large R-groups whilst minimising the O...O distance.

In methanol at ambient pressure the O...O distance is 2.67 Å. At 7 GPa, O...O distances between molecules on opposite sides of the chain (i.e. those which bear a similar spatial relationship to the molecules in the ambient pressure structure) decrease to 2.43 Å and 2.52 Å, while the H-bond that connects molecules on the same side of the chain elongates to 2.70 Å.

That intermolecular contacts should lengthen under pressure is counter-intuitive, but this occurs in order to accommodate the bulkier R-group in the 'small monoalcohol' packing arrangement. The preference for 'small alcohol packing' at high-pressure is a consequence of the higher densities that appear to be achievable with these motifs. Inspection of space-filling plots of the high and low pressure phases described here shows that the low temperature phases are both characterised by the presence of voids (Figure 5.13). The voids present in the crystal structure of 2-chlorophenol are much less obvious than those in 4-fluorophenol but are formed between the helices formed along the *c*-axis (Figure 5.13*b*). It has recently been shown that the effects of pressure on the crystal structures of amino acids can also be understood by compression of the voids present at ambient pressure (Dawson *et al.*, 2004, Moggach *et al.*, 2004). Similar conclusions have recently been reached by Slebodnick *et al.* (2004). The voids are found to contract under pressure until intermolecular

interactions become so short that the structure becomes unstable; then a phase transition occurs. This effect often leads to destructive phase transitions, but the advantage of studying low melting compounds is denser polymorphs are formed at the time of crystal growth. This has occurred in the two compounds in this study.

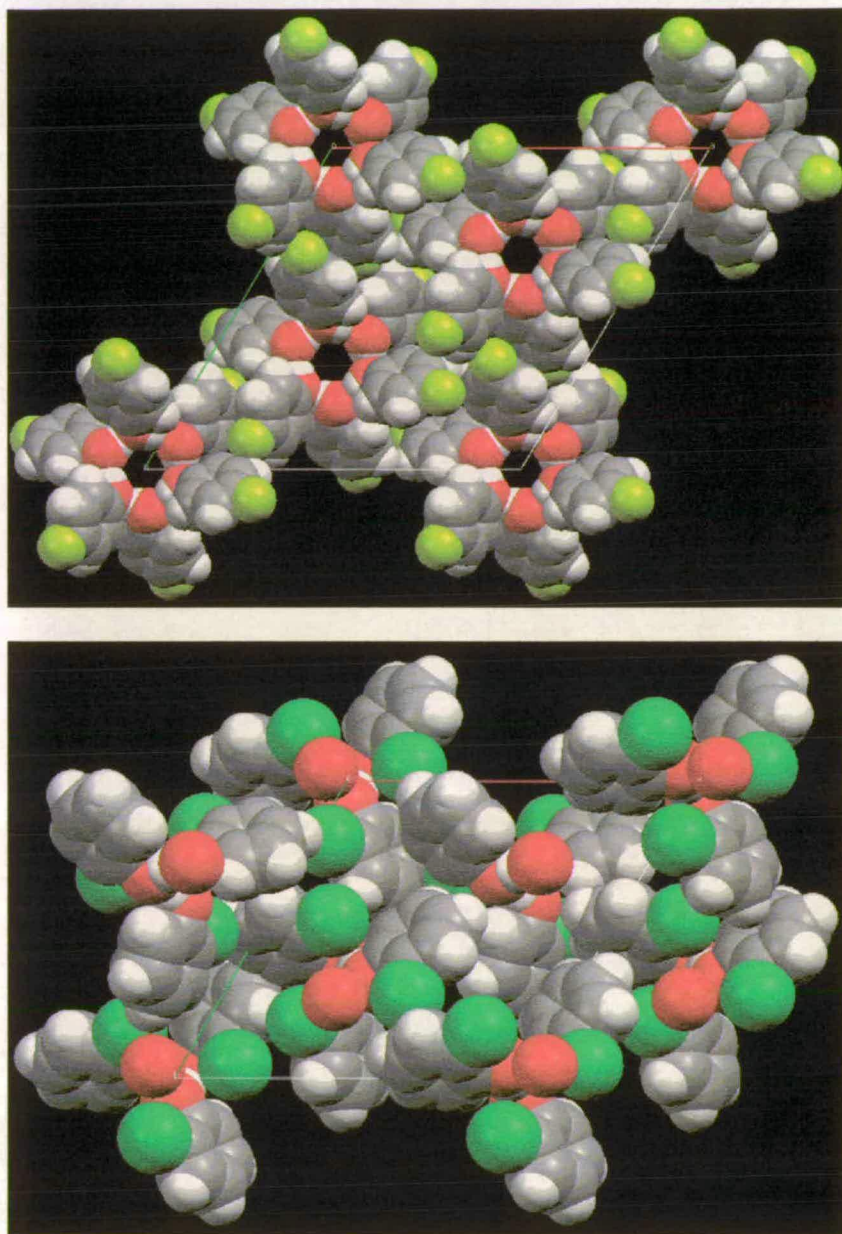


Figure 5.13 top (a): The space filling diagram of 4-fluorophenol. The voids present in the structure are clearly seen running down the c -direction.

Bottom (b): The space filling diagram of 2-chlorophenol. The voids in this structure are present between the symmetry inequivalent helices. High-pressure crystal growth of these two compounds induces molecular rearrangement to a denser structure without voids.

5.4.2 Crystal Structure Predictions

The low and high-pressure polymorphs of both halophenols were predicted amongst the lowest in lattice energy and within a few kJ mol^{-1} of the lowest energy predicted structures. In both cases, the two forms have similar calculated lattice energies and the high-pressure form was predicted as one of the densest possible crystal structures.

Although elaborate models for the intermolecular energy were used, we cannot expect to calculate relative stabilities any better than a few kJ mol^{-1} , given the lack of entropy and explicitly including pressure effects in the energy minimisations. Furthermore, the position of the hydroxyl hydrogen is influenced by the crystal environment, twisting the hydroxyl group up to about 20° out of the plane of the molecule. Thus, the rigid molecule assumption also limits the possible accuracy of the crystal structure prediction.

The results of the crystal structure prediction are especially encouraging because of the success in locating the 2-chlorophenol crystal structure with three symmetrically independent molecules - predicting structures with more than one molecule in the asymmetric unit is one of the major challenges for crystal structure prediction methods (Day *et al.*, 2004a). Many of the methods used to search for possible crystal structures are extensible to multiple molecules and it is mainly a matter of the large increase in computing time required for such searches.

Disordered structures are another challenge for crystal structure prediction. Although current methodologies only predict perfectly ordered crystal structures, such predictions can be useful in interpreting disordered crystals (Tremayne *et al.*, 2004). Here, the packing of some of the lowest energy structures of 4-fluorophenol hinted that disorder is possible in crystals of this molecule. More systematic approaches to predicting disorder in crystals have shown promise (van Eijck, 2002) when there is a suspicion that such behaviour may be important.

5.5 Conclusions

High-pressure is potentially a very valuable tool for tuning the balance between intermolecular interactions such as hydrogen bonding and van der Waals interactions. In this Chapter we have shown that the packing behaviour of 2-chlorophenol and 4-fluorophenol can be transformed from being characteristic of bulky alcohols to that of small alcohols. We have shown that this trend is also followed by phenol and methanol. The transition from bulky to

small behaviour under high-pressure is accompanied by an increase in hydrogen bonding distances; this counter-intuitive effect occurs in order to optimise packing.

Crystal structure predictions almost always generate more hypothetical structures than known polymorphs, and we hypothesised that high-pressure could be a useful method of accessing some of the structures that are not observed under ambient conditions; this view is supported by the results of this study. However, energy-ordering is sensitive to assumed intramolecular conformation; halogen...H interactions also seem to be poorly modelled. We are currently unable to energy-minimise structures under applied pressure, and this was treated in an approximate way. These are evidently serious problems with the approach used here. Nevertheless, the observed low-temperature and high-pressure structures did appear amongst the lowest energy predicted structures, even though one of these had $Z' = 3$. This is a very encouraging result indeed. Furthermore, many proposed structures could be ruled-out on the basis that they seemed unlikely – e.g. because they exhibited unusual intermolecular interactions. Though it is clearly not yet possible to draw a general conclusion on the ability of current methodologies to predict high-pressure crystal structures, our results should encourage the further combined use of extreme conditions and computational approaches to the study of polymorphism and intermolecular interactions in crystals.

5.6 References

- Allan, D. R. & Clark, S. J. (1999). *Phys. Rev. B* **60**, 6328-6334.
- Allan, D. R., Clark, S. J., Brugmans, M. J. P., Ackland, G. J. & Vos, W. L. (1998). *Phys. Rev. B* **58**, R11809-R11812.
- Allan, D. R., Clark, S. J., Dawson, A., McGregor, P. A. & Parsons, S. (2002). *Acta Cryst. B58*, 1018-1024.
- Allan, D. R., Clark, S. J., Ibberson, R. M., Parsons, S., Pulham, C. R. & Sawyer, L. (1999). *Chem. Comm.*, 751-752.
- Allan, D. R., Clark, S. J., Parsons, S. & Ruf, M. (2000). *J. Phys.: Condensed Matter* **12**, L613-L620.
- Allan, D. R., Parsons, S. & Teat, S. J. (2001). *J. Synchrotron Rad.* **8**, 10-17.
- Allen, F. H. (2002). *Acta Cryst. B58*, 380-388.
- Allen, F. H. & Motherwell, W. D. S. (2002). *Acta Cryst. B58*, 407-422.

- Altomare, A., Cascarano, G., Giacovazzo, C. & Guagliardi, A. (1993). *J. Appl. Cryst.* **26**, 343-350.
- Amos, R. D.; with contributions from Alberts, I. L., Andrews, J. S., Colwell, S. M., Handy, N. C., Jayatilaka, D., Knowles, P. J., Kobayashi, R., Koga, N., Laidig, K. E., Maslen, P. E., Murray, C. W., Rice, J. E., Sanz, J., Simandiras, E. D., Stone, A. J. & Su, M.-D. (1995). *CADPAC, 6.0 ed.*, Cambridge.
- Anghel, A. T., Day, G. M. & Price, S. L. (2002). *CrystEngComm.* **4**, 348-355.
- Becke, A. D. (1988). *J. Chem. Phys.* **88**, 2547-2553.
- Bernstein, J., Davis, R.E., Shimoni, L. & Chang, N-L. (1995). *Angew. Chem. Int. Ed. Engl.* **34**, 1555- 1573.
- Betteridge, P. W., Carruthers, J. R., Cooper, R. I., Prout, K. & Watkin, D. J. (2003). *J. Appl. Cryst.* **36**, 1487.
- Beyer, T., Day, G. M. & Price, S. L. (2001). *J. Am. Chem. Soc.* **123**, 5086-5094.
- Blessing, R. H. (1995). *Acta Cryst.* **A51**, 33-38.
- Blessing, R. H. (1997). *J. Appl. Cryst.* **30**, 421-426.
- Boese, R. & Nussbaumer, M. (1994). In *Correlations, Transformations, and Interactions in Organic Crystal Chemistry*, D.W. Jones & A. Katrusiak (Editors). (International Union of Crystallography, Crystallographic Symposia, 7), pages 20-37.
- Brock, C. P. & Duncan, L. L. (1994). *Chem. Mater.* **6**, 1307-1312.
- Bruno, I. J., Cole, J. C., Edgington, P. R., Kessler, M., Macrae, C. F., McCabe, P., Pearson, J. & Taylor, R. (2002). *Acta Cryst.* **B58**, 389-397.
- Bruker-Nonius (2001). SMART version 5.624. Bruker-AXS, Madison, Wisconsin, USA.
- Bruker-Nonius (2003). SAINT version 7. Bruker-AXS, Madison, Wisconsin, USA.
- Bruker-Nonius (2004). TOPAS V3.0: General Profile and Structure Analysis Software for Powder Diffraction Data.
- Chisholm, J., Motherwell, W. D. S. (2004). *Submitted for publication*.
- Cosier, J. & Glazer, A. M. (1986). *J. Appl. Cryst.* **19**, 105-107.
- Dawson, A., Allan, D. R., Parsons, S. & Ruf, M. (2004a). *J. Appl. Cryst.* **37**, 410-416.
- Dawson, A., Allan, D. R., Belmonte, S. A., Clark, S. J., David, W. I. F., McGregor, P. A., Parsons, S, Pulham, C. R. & Sawyer, L. (2004b). *Submitted for publication*.

- Day, G. M. & Price, S. L. (2003). *J. Am. Chem. Soc.* **125**, 16434-16443.
- Day, G. M., Motherwell, W. D. S., Ammon, H., Boerrigter, S. X. M., Della Valle, R. G., Venuti, E., Dzyabchenko, A. V., Dunitz, J. D., van Eijck, B. P., Erk, P., Facelli, J. C., Bazterra, V. E., Ferraro, M. B., Hofmann, D. W. M., Leusen, F. J. J., Liang, C., Pantelides, C. C., Karamertzanis, P. G., Price, S. L., Lewis, T. C., Torrisi, A., Nowell, H., Scheraga, H. A., Arnautova, Y. A., Schmidt, M. U., Schweizer, B. & Verwer, P. (2004a). *In preparation*.
- Day, G. M., Chisholm, J., Shan, N., Motherwell, W. D. S. & Jones, W. (2004b). *Crystal Growth & Design*, *in press*.
- Delley, B. (1990). *J. Chem. Phys.* **92**, 508-517.
- van Eijck, B. P. (2002). *Phys. Chem. Chem. Phys.* **4**, 4789-4794.
- Farrugia, L. J. (1999). *J. Appl. Cryst.*, **32**, 837-838.
- Flack, H. D. (1983). *Acta Cryst.* **A39**, 876-881.
- Hsu, L.-Y. & Williams, D. E. (1980). *Acta Cryst.* **A36**, 277-281.
- Karfunkel, H. R. & Gdanitz, R. J. (1992). *J. Comput. Chem.*, **13**, 1171-1183.
- Karfunkel, H. R., Leusen, F. J. J. & Gdanitz, R. J. (1994). *J. Comput.-Aided Mat. Design*, **1**, 177-185.
- Lommerse, J. P. M., Motherwell, W. D. S., Ammon, H. L., Dunitz, J. D., Gavezzotti, A., Hofmann, D. W. M., Leusen, F. J. J., Mooji, W. T. M., Price, S. L., Schweizer, B., Schmidt, M. U., van Eijck, B. P., Verwer, P. & Williams, D. E. (2000). *Acta Cryst.* **B56**, 697-714.
- Merrill, L. & Bassett, W.A. (1974). *Rev. Sci. Instrum.* **45**, 290-294.
- Moggach, S. A., Allan, D. R., Morrison, C. A., Parsons, S. & Sawyer, L. (2004). *Submitted for publication*.
- Motherwell, W. D. S., Ammon, H. L., Dunitz, J. D., Dzyabchenko, A., Erk, P., Gavezzotti, A., Hofmann, D. W. M., Leusen, F. J. J., Lommerse, J. P. M., Mooji, W. T. M., Price, S. L., Scheraga, H., Schweizer, B., Schmidt, M. U., van Eijck, B. P., Verwer, P. & Williams, D. E. (2002). *Acta Cryst.* **B58**, 647-661.
- Munowitz, M. G., Wheeler, G. L. & Colson, S. D. (1977). *Molecular Physics* **34**, 1727-1737.
- Oswald, I. D. H., Allan, D. R., Motherwell, W. D. S. & Parsons, S. (2004). *Submitted for publication*.
- Parsons, S. ECLIPSE. (2004a) The University of Edinburgh, Edinburgh, U.K.

- Parsons, S. SHADE. (2004b) The University of Edinburgh, Edinburgh, U.K.
- Perdew, J. P. & Wang, Y. (1992). *Phys. Rev. B* **45**, 13244-13249.
- Perrin, P. M. & Michel, P. (1973a). *Acta Cryst.* **B29**, 253-258.
- Perrin, P. M. & Michel, P. (1973b). *Acta Cryst.* **B29**, 258-263.
- Price, S. L., Willock, D. J., Leslie, M. & Day, G. M. (2001). DMAREL version 3.1, University College London, London.
- Shankland, K. & David, W. I. F. (2002). in *Structure Determination from Powder Diffraction Data*, IUCr Monographs on Crystallography, No 13, W. I. F. David, K. Shankland, L. B. McCusker & Ch. Baerlocher (Editors). Oxford University Press, Oxford, UK.
- Sheldrick, G. M. (2001). SHELXTL version 6.01. University of Göttingen, Germany and Bruker-Nonius Inc., Madison, Wisconsin, U.S.A.
- Sheldrick, G. M. (2004). *SADABS Version 2004-1*. Bruker-AXS, Madison, Wisconsin, USA.
- Sleboznick, C., Zhao, J., Angel, R., Hanson, B. E., Song, J., Liu, Z. & Hemley, R. J. (2004). *Inorg. Chem.* **43**, 5245-5252.
- Sparks, R. A. (2000). *GEMINI*. Version 1.01, Bruker-AXS, Madison, Wisconsin, USA.
- Spek, A. L. (2002). *PLATON- A Multipurpose Crystallographic Tool*, Utrecht University, Utrecht, The Netherlands.
- Steiner, T. (2002). *Angew. Chem. Int. Ed.* **41**, 48-76.
- Stone, A. J. (1981). *Chem. Phys. Lett.* **83**, 233-239.
- Stone, A. J. & Alderton, M. (1985). *Mol. Phys.* **56**, 1047-1064.
- Tauer, K. J. & Lipscomb, W. N. (1952). *Acta Cryst.* **5**, 606-612.
- Taylor, R. & Macrae, C. F. (2001). *Acta Cryst.* **B57**, 815-827.
- Thalladi, V. R., Weiss, H.-C., Blaser, D., Boese, R., Nangia, A. & Desiraju, G. R. (1998). *J. Am. Chem. Soc.* **120**, 8702-8710.
- Tremayne, M., Grice, L., Pyatt, J. C., Seaton, C. C., Kariuki, B. M., Tsui, H. H. Y., Price, S. L. & Cherryman, J. C. (2004). *J. Am. Chem. Soc.* **126**, 7071-7081.
- Verwer, P. & Leusen, F. J. J. (1998). *Rev. Comput. Chem.* **12**, 327-365.
- Vosko, S. J., Wilk, L. & Nusair, M. (1980). *Can. J. Phys.* **58**, 1200-1211.

- Watkin, D. J., Pearce, L. & Prout, C. K. (1993). *CAMERON - A Molecular Graphics Package*. Chemical Crystallography Laboratory, University of Oxford, England.
- Williams, D. E. (1999). *J. Mol. Struct.* **486**, 321-347.
- Williams, D. E. (2001). *J. Comp. Chem.* **22**, 1-20.
- Williams, D. E. & Houpt, D. J. (1986). *Acta Cryst.* **B42**, 286-295.
- Willock, D. J., Price, S. L., Leslie, M. & Catlow, C. R. A. (1995). *J. Comp. Chem.* **16**, 628-647.
- Yao, J. W., Cole, J. C., Pidcock, E., Allen, F. H., Howard, J. A. K., Motherwell, W. D. S. (2002). *Acta Cryst.* **B58**, 640-646.

Chapter 6

The Crystal Structures of the Monofluoro- and Monochloro- Phenols at Low Temperature and High-pressure.[§]

[§] Oswald, I. D. H., Allan, D. R., Motherwell, W. D. S. & Parsons, S. (2004). *Submitted for publication*.

6.1 Introduction

Packing in alcohols has been studied by Brock & Duncan (1994) and subsequently by Taylor & Macrae (2001). Both studies showed that the size of the R-group attached to the alcohol functionality is a major factor in the packing behaviour of the molecules. We have recently investigated (Oswald *et al.*, 2004) the effect of high-pressure on the crystal structures of phenols, 2-chlorophenol and 4-fluorophenol, which both exhibit polymorphic behaviour on application of pressure. At ambient pressure 2-chlorophenol and 4-fluorophenol crystallise in high symmetry space groups with the molecules disposed about 3_2 and $\bar{3}$ symmetry operators. Under pressure both systems crystallise in low symmetry space groups with the molecules disposed about a 2_1 screw axes. Figure 6.1 illustrates the change in structure between ambient and high-pressure for 2-chlorophenol. At ambient pressure the molecules adopt a molecular arrangement in which the halophenyl group behaves as a bulky substituent. At high-pressure, both compounds undergo a phase transition to a packing motif characteristic of a small alcohol. This Chapter describes the crystal structure determination of the remaining chloro- and fluorophenols at low temperature and high-pressure to investigate whether the packing behaviour of these phenols can be altered with the application of pressures < 1 GPa.

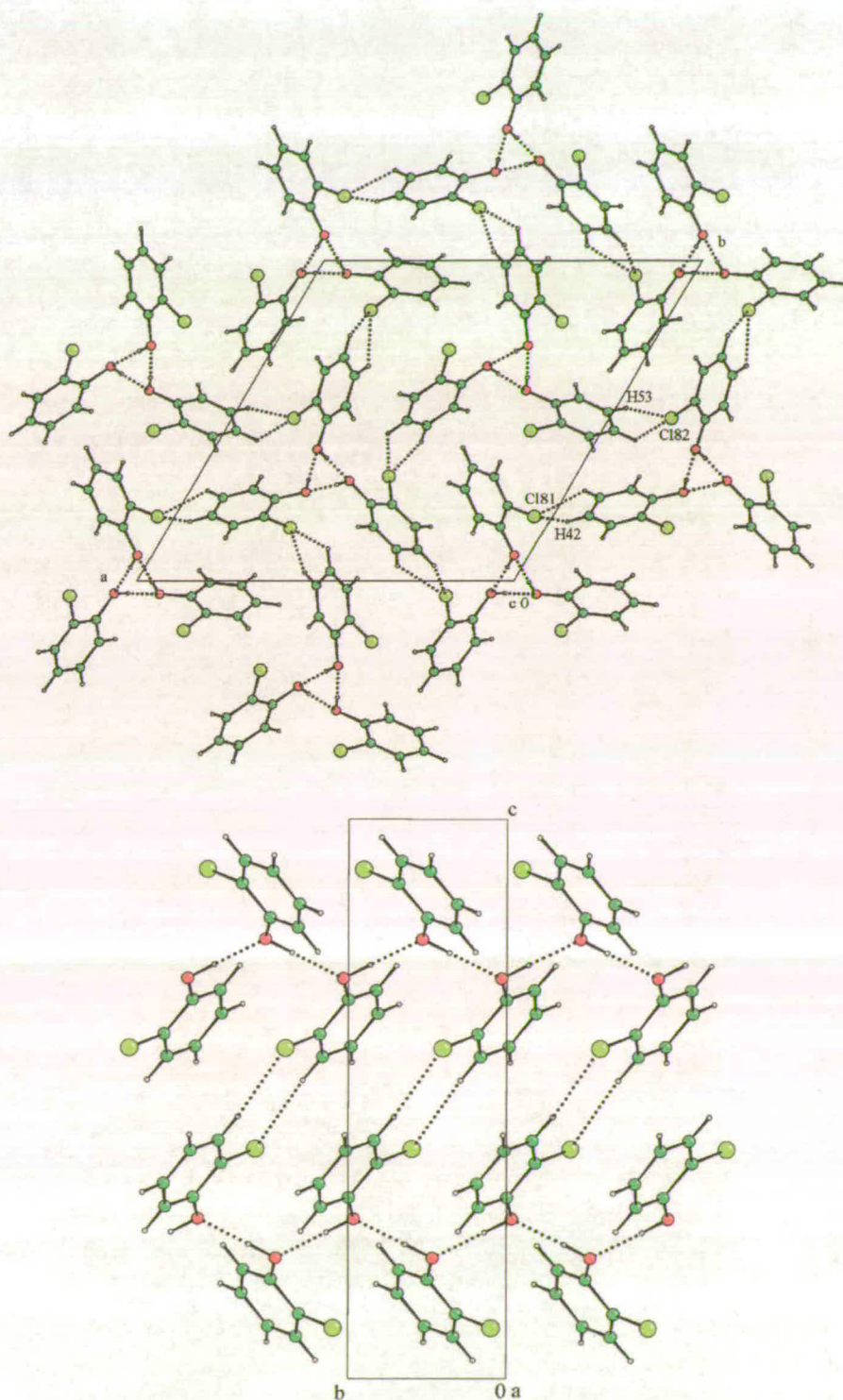


Figure 6.1 top (a): Crystal structure of 2-chlorophenol at ambient pressure and 100 K. Helices are formed about 3_2 axes by OH...OH hydrogen bond formation. The helices are linked through close contacts between the chlorine atom of one chain and two hydrogen atoms of the next. Only the shortest H...Cl contacts are labelled for the sake of clarity.

Bottom (b): The crystal structure of 2-chlorophenol at 0.12GPa. The application of pressure changes the behaviour of the chlorophenyl substituent so that chains are formed where molecules are related by a 2_1 -screw axis. Weak H...Cl 'dimer' interactions are shown between the chains. Colour scheme: C green, Cl light green, H white, O red. This colour scheme is used in Figures 6.3, 6.4 & 6.5.

6.2 *Experimental*

All samples were obtained from Sigma-Aldrich and used as received.

6.2.1 *Low temperature crystal growth*

2-Fluorophenol (*m.pt.* 289 K), 3-fluorophenol (*m.pt.* 287 K) and 3-chlorophenol (*m.pt.* 306 K) were drawn into a capillaries, and polycrystalline masses obtained by freezing at 260 K, 263 K and 283 K, respectively. The samples were then crystallised using the laser-assisted procedure of Boese and Nussbaumer (1994). All capillaries (o.d. 0.32 mm – 0.52 mm) were hand-drawn from Pyrex glass. Phase-I of 4-chlorophenol (*m.pt.* 316 K) was obtained by fusing a sample in a vial and leaving it to recrystallise at room temperature. Small, colourless crystals appeared on the side of the vial. Colourless crystals of phase-II of 4-chlorophenol were obtained by holding a saturated benzene solution at 277 K.

6.2.2 *Crystal structure determination at low temperature*

X-ray diffraction intensities were collected with Mo-K α radiation on a Bruker SMART APEX CCD diffractometer equipped with an Oxford Cryosystems CRYOSTREAM-PLUS variable-temperature device (Cosier & Glazer, 1986) and an OHCD laser-assisted crystallisation device. Absorption corrections were carried out using the multiscan procedure SADABS (Sheldrick, 2004, based on the procedure described by Blessing, 1995). All structures were solved by direct methods (SIR92, Altomare *et al.*, 1993) and refined by full-matrix least squares against F^2 using all data (CRYSTALS, Betteridge *et al.*, 2003). H-atoms were placed on C-atoms in calculated positions and allowed to ride on their parent atoms. Hydrogen atoms involved in H-bonding were located in difference maps and refined with distance restraints. All non-H atoms were modelled with anisotropic displacement parameters.

6.2.3 *High-pressure: General Procedures*

Pressure was applied to the samples using a Merrill-Bassett diamond anvil cell (DAC; Merrill-Bassett, 1974) equipped with 600 μm culets, a tungsten gasket with a 300 μm hole, beryllium backing disks and a chip of ruby for pressure measurement. Pressures were

measured by the ruby-fluorescence method by excitation with a 632.817 nm line from a He-Ne laser using a Jobin-Yvon LabRam 300 Raman spectrometer.

6.2.4 High-pressure crystal growth

The samples were loaded as liquids into the cell. In the case of 4-chlorophenol, both the sample and the cell were heated with a hot-air gun before loading to prevent crystallisation at ambient temperature. In each case, pressure was applied until a polycrystalline mass was produced; the temperature of the cell was increased using a hot-air gun until a single crystallite remained. Slow cooling to ambient temperature yielded a single crystal that filled the entire gasket hole. Crystallisation was monitored visually using a polarising microscope. The crystallisation pressures for each sample were; 3-fluorophenol, 0.12 GPa; 3-chlorophenol, 0.10 GPa; 4-chlorophenol, 0.02 GPa; and 2-fluorophenol, 0.36 GPa.

6.2.5 Crystal structure determinations at high-pressure

Data were collected on a Bruker SMART APEX diffractometer with Mo-K α radiation. Collection and processing procedures followed those described by Dawson *et al.* (2004a).

Shading by the body of the DAC leads to low data completeness for crystals belonging to low-symmetry crystal systems. In all cases, except 2-fluorophenol, datasets were collected with the cell mounted in two different orientations in order to improve completeness. The diffraction patterns were indexed with the program GEMINI (Sparks, 2000). Data integration (to $2\theta = 45^\circ$) was performed using SAINT (Bruker-Nonius, 2003) with dynamic masking to account for the shading from the DAC steel body (ECLIPSE, Parsons, 2004a). The program SHADE (Parsons, 2004b) was also used to take account of absorption effects of the diamonds and beryllium; further systematic errors were treated using SADABS before merging in SORTAV (Blessing, 1997).

The phases obtained for 3-fluorophenol, 3-chlorophenol and 4-chlorophenol corresponded to compressed forms of known ambient-pressure phases. Refinement against the high-pressure data therefore used the ambient-pressure coordinates as a starting model.

The structures were refined by full-matrix least-squares against F^2 (CRYSTALS) using all data. Free refinement of the positional parameters of the non-H atoms yielded carbon-carbon bond lengths varying from 1.34 to 1.40 Å. The phenyl rings were therefore

constrained to be rigid hexagons. H-atoms were placed on C-atoms in calculated positions. The hydroxyl hydrogen atom, which is involved in H-bonding, was geometrically placed except for 4-chlorophenol where the hydroxyl hydrogen was identified from the difference map and refined with distance and angular restraints. All oxygen and halogen atoms were modelled with anisotropic displacement parameters. The refinement of the crystal structure of 3-fluorophenol was subject to distance and angle restraints. 2-Fluorophenol, 3-chlorophenol and 4-chlorophenol were refined so that chemically similar bond distances and angles were subject to similarity restraints.

6.2.6 2-Fluorophenol

Several attempts to grow a single crystal of 2-fluorophenol at high-pressure resulted in the crystal fracturing after cooling to ambient temperature. Though the diffraction patterns obtained from these samples were characterised by broad, split reflections, they could, nevertheless, be indexed on an orthorhombic unit cell with dimensions: $a = 5.8952(17) \text{ \AA}$, $b = 10.9466(19) \text{ \AA}$, $c = 16.459(4) \text{ \AA}$. This is different to the cell obtained at 150 K (see Table 6.1). A solution was obtained using DASH (David *et al.*, 2001, see below), but after refinement the residual stuck in the region of $R_1 = 0.17$. The refined structure, which contains two molecules in the asymmetric unit in space group $P2_12_12_1$, was characterised by high displacement parameters ($0.2 - 0.3 \text{ \AA}^2$) on the F-atoms, while the data, though strong at low angle, had no significant intensity above about $2\theta = 35^\circ$. These observations imply that at 0.36 GPa and room temperature 2-fluorophenol forms a disordered phase. Difference maps failed to provide any clue as to how the structure might be better modelled, probably because of the relatively low completeness or poor reflection peak-shapes. Since we are unable to improve modelling of the data, no further details on this phase are reported here.

A new crystal was grown as above and then maintained at high temperature during data collection with the variable temperature device set at 403 K. This is a nominal temperature, there was presumably a significant temperature gradient across the cell as a whole, though across the sample itself the variation in temperature would have been small. The high temperature dataset indexed on a slightly smaller orthorhombic unit cell with dimensions: $a = 5.7168(7) \text{ \AA}$, $b = 9.9997(19) \text{ \AA}$, $c = 17.868(2) \text{ \AA}$. Both the b - and c -axes show a large change in length compared to the ambient temperature/0.36 GPa cell given

above ($\Delta b = +0.95 \text{ \AA}$; $\Delta c = -1.41 \text{ \AA}$). This cell is also different from that obtained at low temperature (Table 6.1).

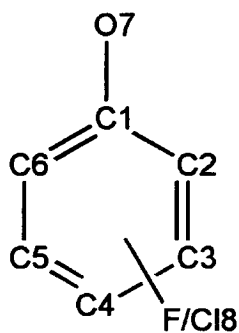
Conventional direct methods applied to the 403 K data set failed to yield a recognisable solution. This is a recurrent problem in high-pressure crystallography, and is the result of low data-completeness, but this can be overcome by using global optimisation methods, originally devised for structure solution from powders. The crystal structure of 2-fluorophenol at high-pressure was therefore solved using the simulated annealing procedure in the program DASH. The refinement of the structure followed the procedures outlined in the preceding section.

6.2.7 Recovery of 4-chlorophenol grown at high-pressure

The high melting-point of 4-chlorophenol allowed the crystals of phase-II formed at high-pressure to be recovered without the sample melting. On release of pressure the sample remained as a single crystal with a slight reduction in size due to melting around the edges. Diffraction data were collected at ambient pressure and 293 K, which showed the crystal to be 4-chlorophenol-I (see Table 6.1).

6.2.8 Software and other general procedures

A consistent numbering scheme was used for all the structures described here, and this is shown in Scheme 6.1. Where there is more than one molecule in the asymmetric unit the labels are augmented with the numbers 1, 2 *etc.* A full listing of crystal, data collection and refinement parameters is given in Table 6.1, a set of H-bonding parameters is given in Table 6.2. The structures were visualised using SHELXTL (Sheldrick, 2001) or MERCURY (Bruno *et al.*, 2002); the figures were produced using CAMERON (Watkin *et al.*, 1993). Other analysis utilised the p.c. version of PLATON (Spek, 2002; Farrugia, 1999). Searches of the Cambridge Structural Database (Allan, 2002; Allen & Motherwell, 2002) were carried out with the program CONQUEST, utilising version 5.25 of the database. Calculations involving projected vectors followed the methods of Sands (1995). Crystallographic information files for all structures reported here are available on the CD at the back of this Thesis.



Scheme 6.1: Conventional structure diagram and numbering scheme for the halophenols under study.

Compound	3-fluorophenol	3-fluorophenol	3-chlorophenol	3-chlorophenol
Code in Table 6.2	3F	3FP	3CL	3CLP
Temperature K	150	293	150	293
Pressure GPa	-	0.12	-	0.1
Formula	C ₆ H ₅ FO	C ₆ H ₅ FO	C ₆ H ₅ ClO	C ₆ H ₅ ClO
Weight	112.10	112.10	128.56	128.56
Radiation	Mo-K α	Mo-K α	Mo-K α	Mo-K α
Crystal system	Monoclinic	Monoclinic	Orthorhombic	Orthorhombic
Space Group	<i>P</i> 2 ₁	<i>P</i> 2 ₁	<i>P</i> 2 ₁ 2 ₁ 2 ₁	<i>P</i> 2 ₁ 2 ₁ 2 ₁
<i>a</i> /Å	5.6510(12)	5.6747(9)	3.9846(5)	4.0949(4)
<i>b</i> /Å	5.0642(10)	5.0760(4)	13.9272(19)	13.875(3)
<i>c</i> /Å	9.3185(19)	9.4753(13)	20.699(3)	20.716(3)
α /°	90	90	90	90
β /°	107.518(4)	107.832(11)	90	90
γ /°	90	90	90	90
Volume/Å ³	254.31(9)	259.82(6)	1148.7(3)	1177.0(3)
No. reflections for cell	711	398	1504	983
2 θ _{max} (°)	57.27	46.40	50.05	46.53
<i>Z</i>	2	2	8	8
<i>D</i> _c (Mg/m ³)	1.464	1.433	1.487	1.451
μ (mm ⁻¹)	0.123	0.120	0.545	0.532
Reflections collected	1603	1310	4548	6533
No. Unique [<i>R</i> _{int}]	672[0.014]	159[0.041]	1977[0.052]	780[0.147]
No. <i>I</i> > 2 σ	608	146	1376	476
<i>T</i> _{min} / <i>T</i> _{max}	0.67/0.96	0.67/0.98	0.22/0.95	0.85/0.91
Parameters	77	32	152	62
<i>R</i> ₁ [<i>F</i> > 4 σ (<i>F</i>)]	0.0373	0.0638	0.0685	0.0978
w <i>R</i> ₂ (<i>F</i> ² , all data)	0.0921	0.1604	0.1425	0.2444
<i>S</i>	1.0473	1.1471	0.9424	0.9863
$\Delta\rho$ _{max} / eÅ ⁻³	0.22	0.17	0.56	0.59
$\Delta\rho$ _{min} / eÅ ⁻³	-0.22	-0.16	-0.58	-0.56

Table 6.1: Crystallographic data for the halophenols at both at ambient pressure and at high-pressure. All ambient pressure data were collected at 150 K and all high-pressure datasets were collected at ambient temperature except for 2-fluorophenol, which was collected at 403 K.

Compound	4-chlorophenol Phase-I	4-chlorophenol Phase-II	4-chlorophenol Phase-II	2-fluorophenol Phase-I	2-fluorophenol Phase-II
Code in Table 6.2	4CL1	4CL2	4CL2P	2F1	2F2P
Temperature K	150	150	293	150	403
Pressure GPa	-	-	0.02	-	0.36
Formula	C ₆ H ₅ ClO	C ₆ H ₅ ClO	C ₆ H ₅ ClO	C ₆ H ₅ FO	C ₆ H ₅ FO
Weight	128.56	128.56	128.56	112.10	112.10
Radiation	Mo-K α	Mo-K α	Mo-K α	Mo-K α	Mo-K α
Crystal system	Monoclinic	Monoclinic	Monoclinic	Monoclinic	Orthorhombic
Space Group	<i>P</i> ₂ / <i>c</i>	<i>P</i> ₂ / <i>c</i>	<i>P</i> ₂ / <i>c</i>	<i>C</i> ₂ / <i>c</i>	<i>P</i> ₂ <i>1</i> ₂ <i>1</i>
<i>a</i> /Å	8.7086(11)	3.9724(5)	4.1096(4)	17.1336(10)	5.7168(7)
<i>b</i> /Å	15.4523(19)	12.7328(17)	12.7665(10)	8.2766(5)	9.9997(19)
<i>c</i> /Å	8.7414(11)	23.155(3)	23.181(3)	11.4975(7)	17.868(2)
α /°	90	90	90	90	90
β /°	93.954(2)	94.126(2)	94.201(14)	100.234(2)	90
γ /°	90	90	90	90	90
Volume/Å ³	1173.5(3)	1168.2(3)	1212.9(2)	1604.50(17)	1021.4(3)
No. reflections for cell	3307	2464	1170	2044	397
2 θ _{max} (°)	57.69	57.81	46.47	57.40	46.50
Z	8	8	8	12	8
D _c (Mg/m ³)	1.455	1.462	1.408	1.392	1.458
μ (mm ⁻¹)	0.534	0.536	0.516	0.117	0.122
Reflections collected	7471	7449	7359	7505	469
No. Unique [<i>R</i> _{int}]	2839[0.024]	2843[0.016]	710[0.063]	1956[0.021]	461[0.099]
No. <i>I</i> > 2 σ	2442	2219	397	1302	261
<i>T</i> _{min} / <i>T</i> _{max}	0.69/0.88	0.49/0.82	0.68/0.91	0.58/1.00	0.96/0.98
Parameters	152	152	61	125	62
<i>R</i> ₁ [<i>F</i> > 4 σ (<i>F</i>)]	0.0387	0.0434	0.0549	0.0562	0.0834
w <i>R</i> ₂ (<i>F</i> ² , all data)	0.1006	0.1102	0.1604	0.1107	0.2506
<i>S</i>	0.7348	0.7469	1.0321	1.0751	0.9365
$\Delta\rho$ _{max} / eÅ ⁻³	0.33	0.44	0.21	0.32	0.27
$\Delta\rho$ _{min} / eÅ ⁻³	-0.31	-0.44	-0.20	-0.40	-0.20

Table 6.1(cont'd): Crystallographic data for the halophenols at both ambient pressure and at high-pressure. All ambient pressure data were collected at 150 K and all high-pressure datasets were collected at ambient temperature except for 2-fluorophenol, which was collected at 403 K.

Compound	Donor	Acceptor	D...A distance (Å)	
			Low Temperature (150 K)	High-pressure
3F	O7	O7 ⁱ	2.819(1)	2.843(8)
	H6	F8 ⁱⁱ	2.61	2.62
3CL	O71	O72 ⁱⁱⁱ	2.734(7)	2.693(4)
	O72	O71	2.700(6)	2.753(4)
4CL1	O71	O72 ^{iv}	2.767(2)	-
	O72	O71	2.779(2)	-
	H62	Cl81 ^v	2.93	-
	H21	Cl82 ^{vi}	2.93	-
4CL2/4CL2P	O71	O72	2.762(2)	2.819(5)
	O72	O71 ^{vii}	2.779(2)	2.749(5)
	H31	Cl82 ^{viii}	2.83	2.85
2F1	O71	O71 ^{ix}	2.774(3)	-
	O71	O72	2.707(2)	-
	O71	F81	2.690(2)	-
	O71	F81 ^{ix}	2.942(2)	-
2F2P	O71	O72 ^x	-	2.860(4)
	O72	O71	-	3.097(3)
	F81	H62 ^x	-	2.56
	F82	H61 ^{xi}	-	2.56
	F82	H52 ^{xii}	-	2.63
	O71	F82	-	2.941(7)

Symmetry Operators:

i	-x, 1/2+y, -z	v	2-x, y-1/2, -1/2-z	ix	1-x, -y, 1-z
ii	1+x, 1+y, z	vi	1+x, y, z	x	1/2+x, 1/2-y, 1-z
iii	x-1/2, -1/2-y, -2-z	vii	2-x, 1-y, 1-z	xi	1+x,y,z
iv	x, 3/2-y, 1/2+z	viii	1-x, 2-y, 1-z	xii	-x, -1/2+y, 3/2-z

Table 6.2: Table of Hydrogen-bonding parameters. The H-bonding distances are from donor to acceptor due to the imprecise determination of hydrogen atom positions. The high-pressure crystal structure of 2-fluorophenol was determined at 403K.

6.3 Results

6.3.1 3-Fluorophenol

3-Fluorophenol crystallises at 263 K in space group $P2_1$ with one molecule in the asymmetric unit. Diffraction data were collected at 150 K. The molecules interact via ..OH..OH.. H-bonds to form chains disposed about the crystallographic 2_1 screw-axes, conforming to a $C(2)$ graph set (Bernstein *et al.*, 1995)(Figure 6.2a). This packing motif is more commonly associated with small alcohols, and was quite unexpected. It appears that stabilisation of this motif occurs through the formation of H6...F8 interactions (2.61 Å) between the chains (Figure 6.2b). Taken on their own these H...F form chains which run along the $\langle 1\ 1\ 0 \rangle$ directions. The hydrogen bond present in this system is slightly longer than those present in the other systems (O7...O7' 2.819(1) Å) described here. In projection onto (0 1 0) each chain is surrounded by six others.

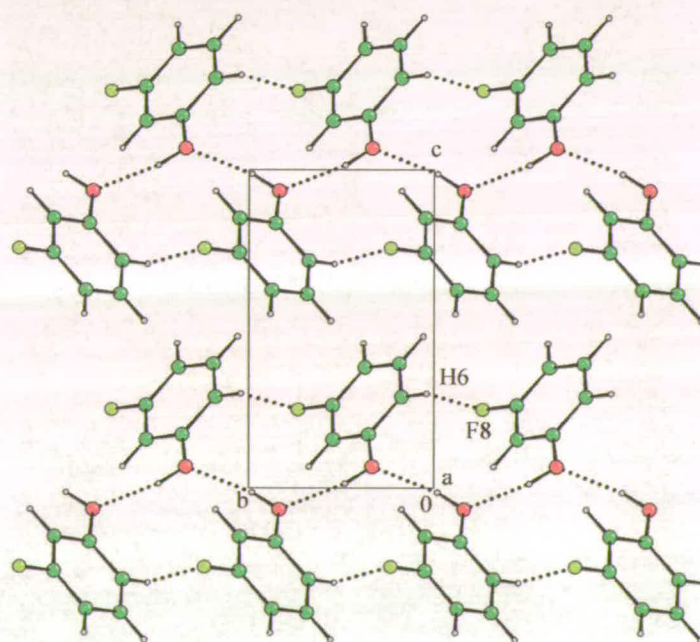


Figure 6.2a: Crystal structure of 3-fluorophenol at 150 K viewed down the a -axis. 3-fluorophenol crystallises with one molecule in the asymmetric unit in space group $P2_1$ thereby forming a chain motif adopted by smaller alcohols. Colour scheme: C green, F light green, H white, O red. This colour scheme is also used in Figures 6.2b, 6.6 & 6.7.

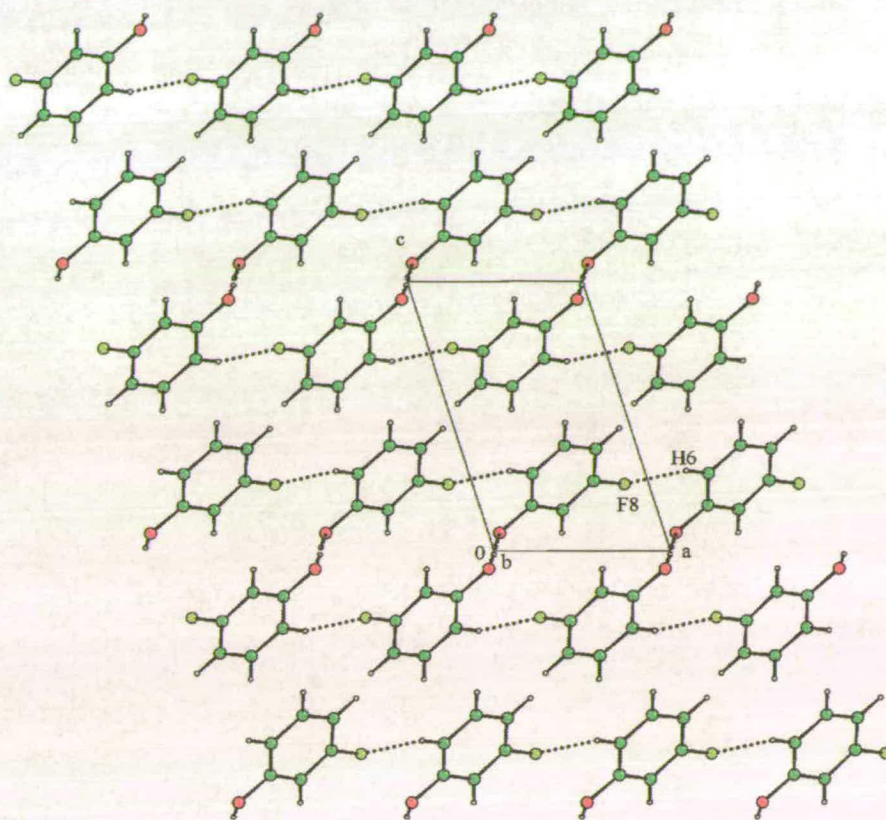


Figure 6.2*b*: Close contacts formed between H6...F8 of different chains (they appear in Figure 6.2*a* to be formed within the chains, but this is an artefact of the projection).

The same phase is obtained on crystallisation at 0.12 GPa. Neither the hydrogen bond nor the stabilising CH...F interaction are significantly different to those in the low temperature structure (O7...O7' 2.843(8) Å; H6...F8 2.62 Å).

6.3.2 3-Chlorophenol

3-Chlorophenol is a liquid under ambient pressure with a melting point of 306 K. At 283 K it crystallises in space group $P2_12_12_1$ with two molecules in the asymmetric unit; diffraction data were collected at 150 K. The molecules interact via ..OH..OH.. H-bonds to form pseudo four-fold helical chains (Figure 6.3*a*). The two crystallographically independent molecules alternate along the chains. The angle between successive C11-O71 and C12-O72 vectors in the chain when projected onto the (1 0 0) plane is 89.75°; in a perfect four-fold helix this value would be 90°. While the departure from projected four-fold symmetry in the ..OH..OH.. interaction is slight, the orientations of the chloro groups do not conform to the

pseudo-symmetry – the angle between Cl-C vectors projected onto (1 0 0) is 17.74°. In addition, the molecules are not regularly spaced along the helix; the separations between the oxygen atoms projected onto [1 0 0] are 0.44 Å or 1.55 Å (Figure 6.3*b*).

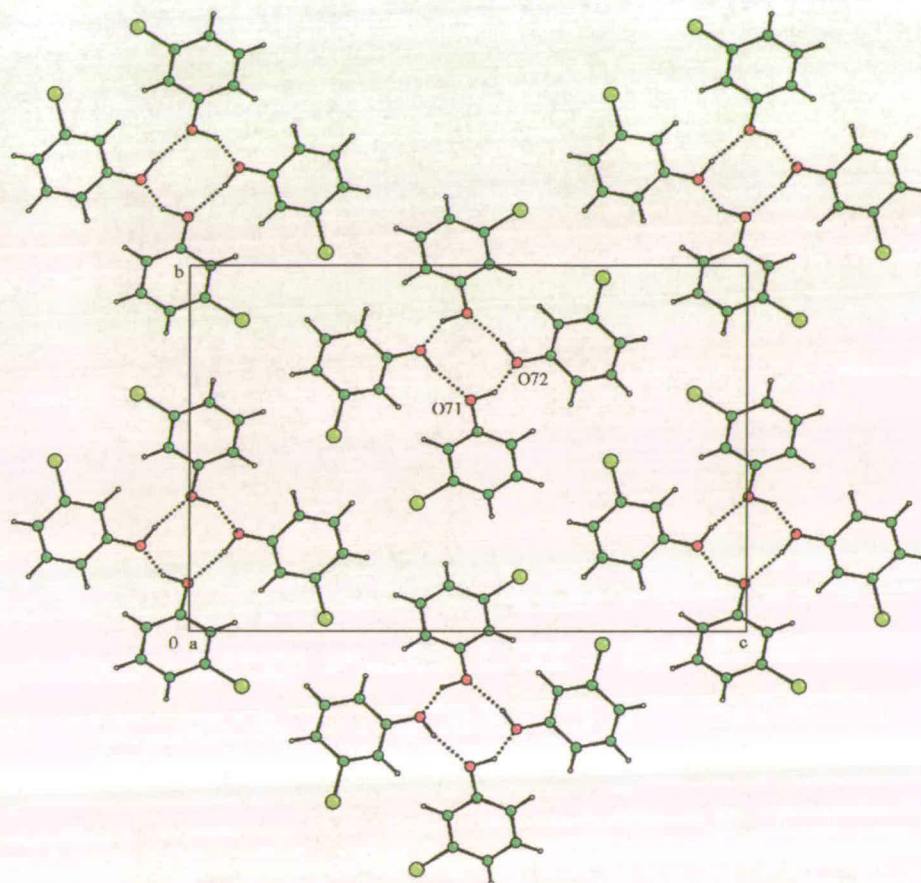


Figure 6.3*a*: Crystal structure of 3-chlorophenol at 150 K. Distorted pseudo four-fold helices are formed through OH...OH hydrogen bonds between the two molecules in the asymmetric unit. The structure at high-pressure (0.1 GPa) is similar to the low temperature structure.

The chains conform to a $C_2^2(4)$ graph set, and are disposed about the 2_1 axes parallel to the a -axis direction (Figure 6.3*a*). The two crystallographically independent hydrogen bonds are moderate in strength O71...O72 ($x-1/2, -1/2-y, -2-z$) 2.734(7) Å and O72...O71 2.700(6) Å (Table 6.2). The chains appear to be close-packed when viewed in projection onto (1 0 0), and, by contrast to the fluoro-derivative, there are no contacts between the chains that fall within the sums of the van der Waals radii.

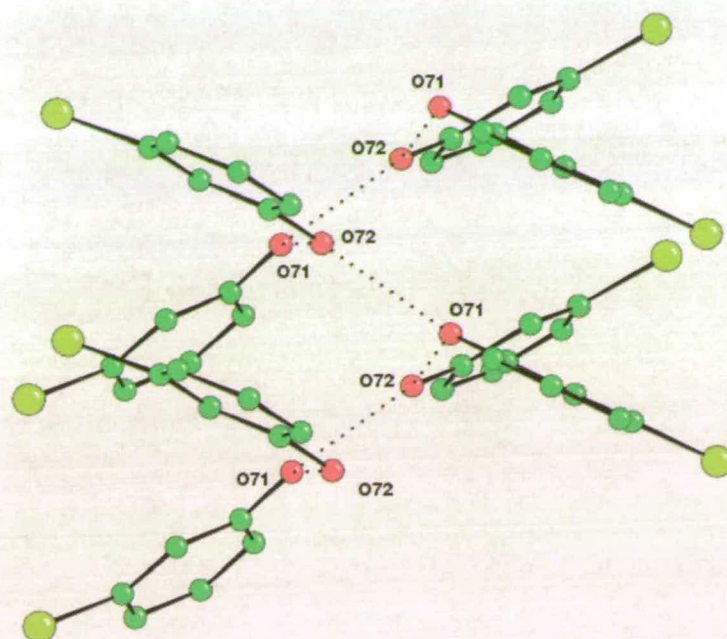


Figure 6.3*b*: Though in projection on [1 0 0] the positions of the C-O bonds resemble those in a four-fold helix, the positions of the molecules along the axis of the helix are irregular.

Crystallisation at 0.1 GPa results in the same structure as at ambient pressure. The interactions between molecules are significantly different to those at ambient pressure (O71...O72 ($x-1/2, -1/2-y, -2-z$) 2.693(4), O72...O71 2.753(4) Å). The interaction between O71...O72 appears to decrease in length at pressure, while O72...O71 increases, though it is not possible to differentiate between the effects of pressure and temperature, since the ambient pressure structure was determined at 150 K, while the high-pressure determination was at room temperature.

6.3.3 4-Chlorophenol phase-I at 150 K

4-Chlorophenol is a solid at room temperature and was characterised by Perrin and Michel (1973*a, b*). It crystallises in two polymorphic forms, and the structures of these have been redetermined at 150 K as part of this study.

Phase-I crystallises from the melt at ambient pressure in space group $P2_1/c$ with two molecules in the asymmetric unit; it is the more stable of the two phases. The two independent molecules alternate along the c -direction, forming ..OH..OH.. hydrogen bonds

resulting in a $C_2^2(4)$ graph set (Figure 6.4a). The hydrogen bonds formed in this structure are of similar strength; O71...O72 ($x, 3/2-y, 1/2+z$) 2.767(2) Å and O72...O71 2.779(2) Å.

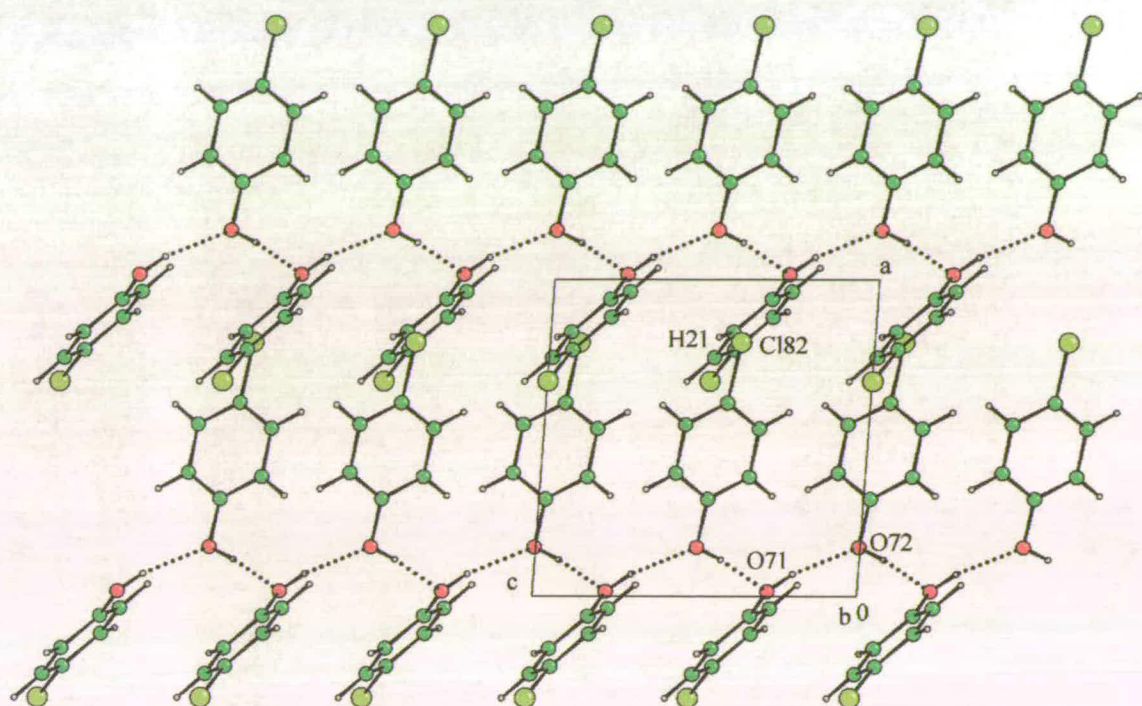


Figure 6.4a: Crystal structure of phase-I of 4-chlorophenol at 150 K viewed along the b -axis showing chains of molecules linked by OH...OH hydrogen bonds.

The graph-set descriptor is the same as that in 3-chlorophenol, but the chain is built by successive application of c -glide operations, rather than a screw-axis. Although the chain is helical, with a repeat at every fourth molecule, the pseudo-four-fold symmetry is even less ideal than in 3-chlorophenol (Figure 6.4b). The angle between O71-C11 and O72-C12 when projected onto (0 0 1) is 133.17° , which compares to 89.75° in 3-chlorophenol. Moreover, the spacing of molecules along the direction of the helix is irregular: projection of the oxygen atoms onto [0 0 1] yields separations of 1.98 and 2.39 Å.

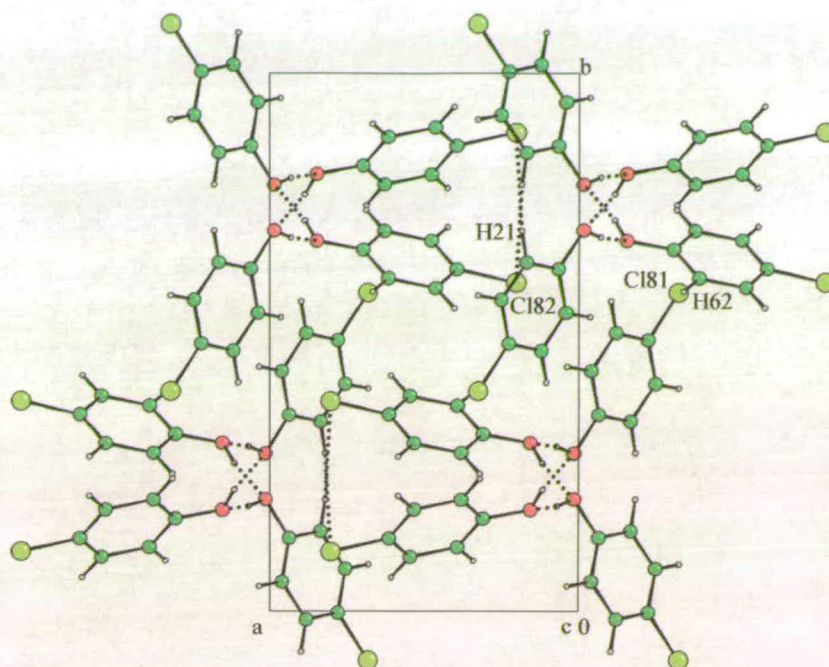


Figure 6.4b: View down $[0\ 0\ 1]$, along the chains. The Cl...H interactions occur between C182...H21 and C181...H62 and lie parallel to the b -axis.

The chains are linked by H21...C182 and H62...C181 interactions, both measuring 2.93 Å (Figure 6.4b). Taken on their own these Cl...H interactions build spiral chains which are disposed about the 2_1 axis parallel to b . Neighbouring chains interact with one another through a π -stacking interaction between molecule 1 and a symmetry equivalent. The distance between the phenyl ring planes is 3.45 Å with the centroids separated by 3.77 Å which equates to a 1.74 Å centroid displacement.

6.3.4 4-Chlorophenol phase-II at 150 K and at 0.02 GPa

The second phase of 4-chlorophenol is obtained by recrystallisation from benzene; it is in the same space group as phase-I, $P2_1/c$, with two molecules in the asymmetric unit. Phase-II is metastable, and transforms spontaneously to phase-I if placed in contact with it (Perrin & Michel, 1973b).

As in phase-I, the molecules interact via ..OH...OH.. H-bonds but the interactions form an $R_4^4(8)$ graph set instead of H-bonded chains (Figure 6.5). These rings stack along the a -direction. The hydrogen bonds are of a similar strength to those in phase-I; O71...O72 2.762(2) Å and O72...O71 (2- x , 1- y , 1- z) 2.779(2) Å. Within the $R_4^4(8)$ rings a secondary CH... π interaction is formed between H21 and the π -system of molecule 2 (comprising atoms

C12-C62). The H21... π -centroid is 3.95 Å, near to the limit for these interactions (4 Å) as defined by Malone *et al.* (1997), and it adopts a 'Type V' motif as defined by the same authors.

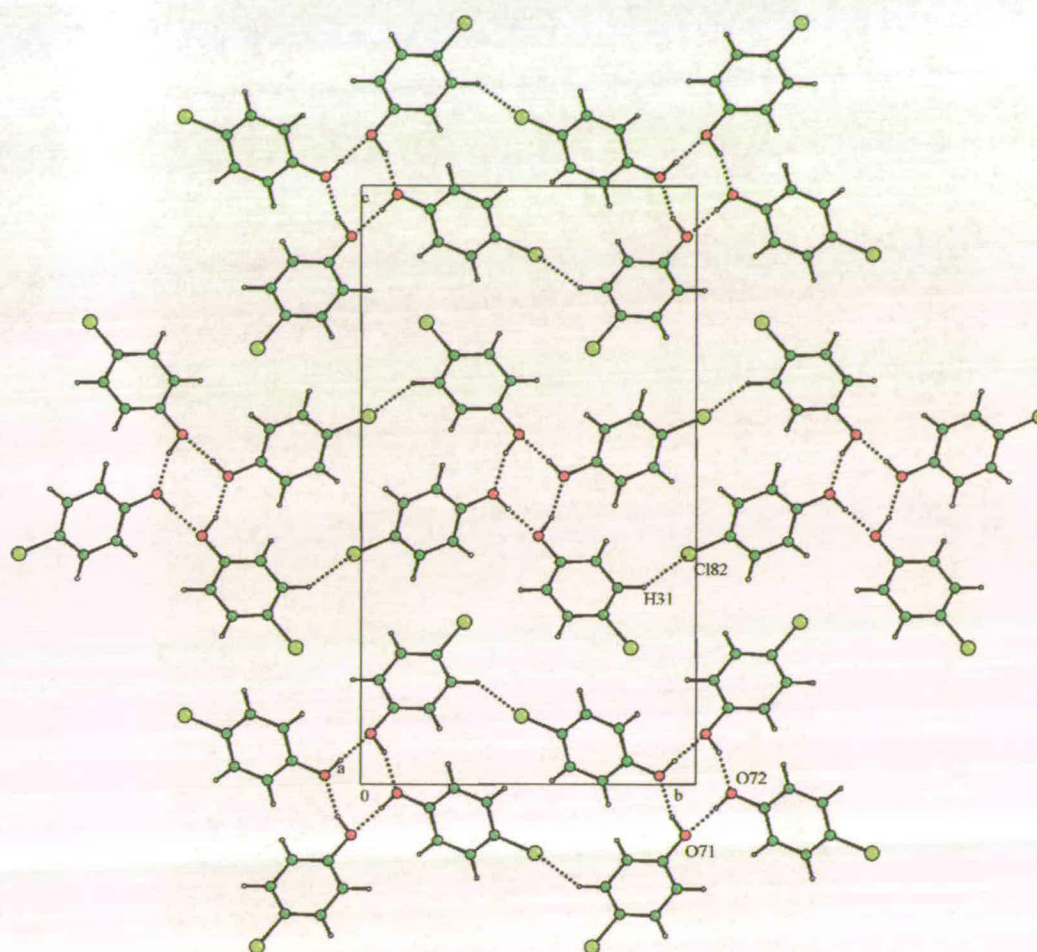


Figure 6.5: Crystal structure of phase-II of 4-chlorophenol at 150 K viewed along the a -axis. The molecules crystallise in a ring motif that forms around an approximate four-fold axis. The discrete H-bonded groups are linked through an interaction between Cl82...H31. The structure at high-pressure is similar to the low temperature structure.

There are close contacts between chlorine and hydrogen atoms (Cl82...H31 2.83 Å *c.f.* sum of vdW 2.95Å) that join the $R_4^4(8)$ groups together into a ribbon. The ribbons lie along the [1 1 0] direction at $c = \frac{1}{2}$ and $[\bar{1} 1 0]$ direction at $c = 0, 1$ etc.

Under ambient conditions crystallisation of 4-chlorophenol from the melt yields phase-I, but when crystallised from the melt under pressure (0.02 GPa), phase-II is formed. This pressure is very slight indeed by the standards of high-pressure crystallography and is barely measurable using the ruby fluorescent technique. The molecular arrangement is the same as the ambient pressure structure, though O71...O72 is significantly longer than at ambient

pressure (2.819(5) Å), while O72...O71 (2-x, 1-y, 1-z) is significantly shorter (2.749(5) Å). A similar effect was observed in 3-chlorophenol.

The crystal of phase-II grown at high-pressure transformed to a single crystal of phase-I when the pressure was released, but this transformation is not reversible *i.e.* applying hydrostatic pressure to a crystal of phase-I does not yield phase-II. It is possible that the II-to-I transformation occurs by conversion of the $R_4^4(8)$ ring motifs, which are stacked by lattice repeats along the *a*-direction in phase-I, into $C_4^4(8)$ chains, developed by a *c*-glide, in phase-II. This would approximately double the length of the lattice repeat in this direction in going from phase-I to II ($a = 3.97$ Å and $c = 8.74$ Å in phases I and II, respectively). In both phases Cl...H interactions build chains which spiral along the 2_1 -axes along the *b*-directions. These similarities presumably promote the preservation of the single crystal through the phase transition.

6.3.5 2-Fluorophenol-I at 150 K

2-Fluorophenol crystallises in space group $C2/c$ with one and a half molecules in the asymmetric unit; this is referenced as phase-I. One molecule (molecule 1, C11 – F81) occupies a general position, and is ordered. A second molecule (molecule 2, C12 – F82) occupies a 2-fold axis with the axis running through atoms O72...C12...C42, and so the hydroxyl hydrogen and the fluorine atoms are disordered.

The molecules interact via ..OH..OH.. H-bonds forming chains; the direction of the H-bonding in these chains must be disordered as a result of the disorder in molecule 2. A pair of molecules of type 1 are connected by a hydrogen bond formed across an inversion centre. These 'dimer' sub-units are then bridged by disordered molecules of type 2 (Figure 6.6a). When projected along *a* the chains have a marked zig-zag structure. When viewed in projection along *c* the chain of molecules somewhat resembles a helix, this is an artefact of the projection: the displacement along *c* of one molecule to another is quite irregular, being 2.18 Å across the inversion centre and 5.75 Å across the two-fold axis, while the angles made between successive OC vectors alternate between 180° and 89.83° (Figure 6.6b). The H-bond lengths are similar to those observed for other compounds in the study: O71...O71 (1-x, -y, 1-z) 2.774(3) Å and O71...O72 2.707(2) Å. There are π -stacking interactions between molecule 1 and a symmetry equivalent molecule in the next chain along the *a*-axis. The

phenyl rings lie parallel to one another 3.62 Å apart with a centroid displacement in the plane of the ring of 1.48 Å.

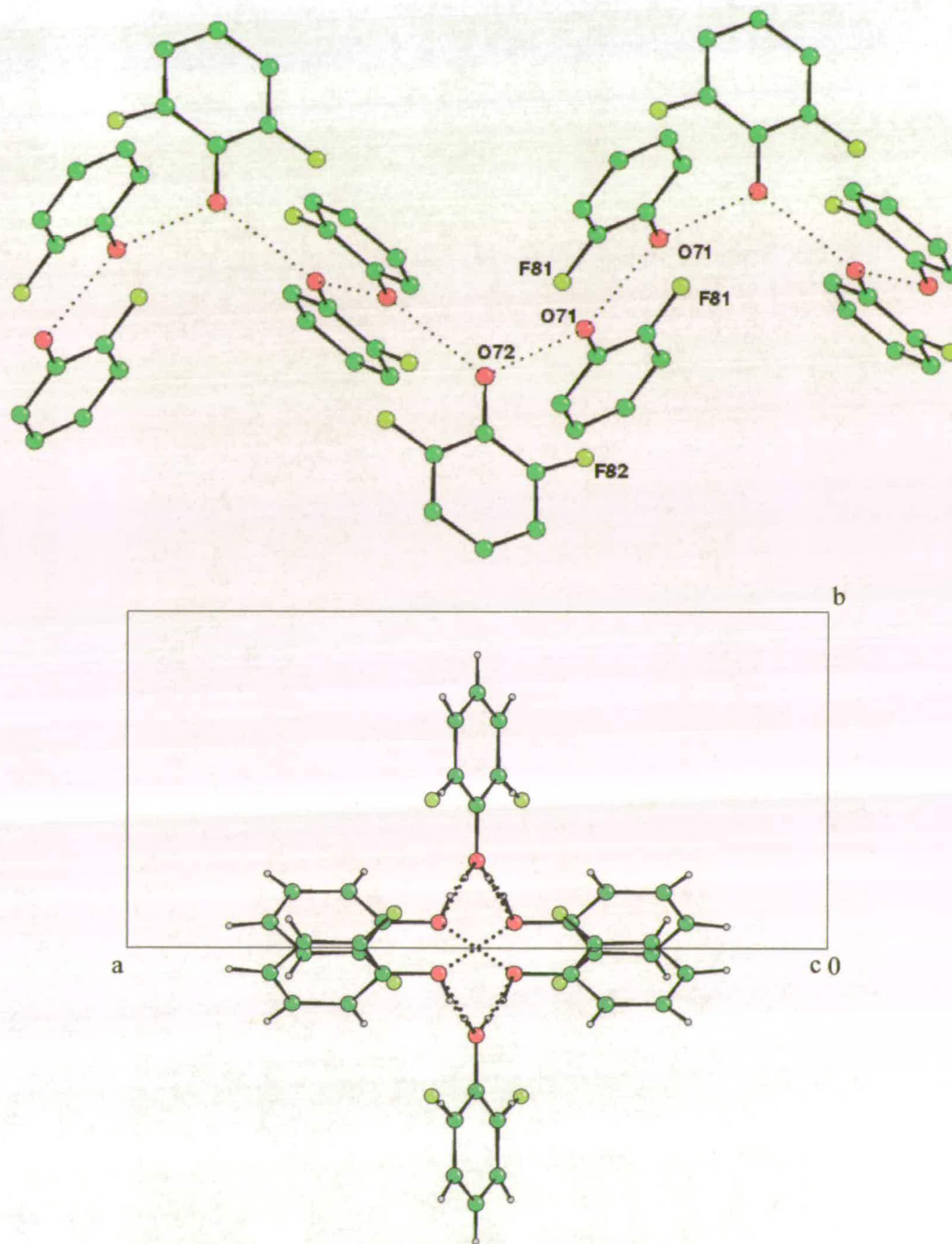


Figure 6.6 top (a): Crystal structure of phase-I of 2-fluorophenol at 150 K showing the disordered H-bonded chain. Molecule 1 forms a dimer with a symmetry equivalent molecule. These dimers are linked through a H-bonding interaction to molecule 2. H-atoms are omitted for clarity. F82 is disordered by the 2-fold axis, which runs through O72-C12.

Bottom (b): View down the H-bonded chain.

6.3.6 2-Fluorophenol-II at 0.36 GPa and 403 K

A crystal of 2-fluorophenol was grown at 0.36 GPa but the crystal fractured a few hours after cooling to ambient temperature. Despite the poor X-ray diffraction data, the diffraction pattern could be indexed on an orthorhombic unit cell ($a = 5.8952 \text{ \AA}$, $b = 10.9466 \text{ \AA}$, $c = 16.459 \text{ \AA}$); this is different to that determined at ambient pressure at 150 K, indicating that a different phase had formed under high-pressure. A tentative structural solution was obtained, but the refinement residuals were unacceptably high, and it is likely that on cooling to room temperature the compound forms a disordered phase.

We found that the crystal obtained at high-pressure was stable if the cell was held above about 363 K, and so a data collection was carried out in which the cell was held at 403 K. This phase of 2-fluorophenol crystallises in space group $P2_12_12_1$ with two molecules in the asymmetric unit. In one molecule the C-F bond refined to an unrealistically short distance, which may indicate high librational disorder of the molecule. This is not unreasonable for a structure at 403 K, though it is difficult to assess from the displacement parameters because of the low data completeness which resulted from shading by the pressure cell.

Oxygen and fluorine have similar X-ray scattering factors, and so assignment of these sites was made on the basis of interatomic contacts. The assumption that oxygen atoms are likely to make at least one hydrogen bond in which the distance between the non-hydrogen atoms is between 2.6 and 3.1 \AA serves to identify O71 as an oxygen atom. The shortest contact (3.37 \AA) made by F81 is to C62 in a neighbouring ring; this distance is similar to those quoted by Thalladi *et al.* (1998) for C...F distances in CH...F hydrogen bonds, which therefore lends support to the assignment.

Atom assignments, O72 and F82, in the second of the two independent molecules were made by refinement of two alternative models with part-weight hydroxyl H-atoms placed in two alternative positions on each oxygen atom. The $R1$ -factors of the model presented here and the alternative were 12.09 % and 12.44%, respectively. The occupancies of alternative H-atom positions refined to 0.85:0.15(13); only the major occupancy H-atoms were retained. The alternative model contains OH...F interactions; organic fluorine is not expected to be competitive with hydroxyl oxygen as a hydrogen bond acceptor.

The ..OH..OH.. chain that is formed (along the a -direction) conforms to a $C_2^2(4)$ graph set. The O71...O72 distances are 2.860(4) and 3.097(3) \AA . In common with other structures

in this series, each chain is surrounded by six others, and there are F82...H52 interactions formed between the chains (2.63 Å, Figure 6.7a). The second of these is the longest observed in this series, and this may reflect the steric effect of F72 ($O71...F72 = 2.941(7)$ Å). This arrangement is stabilised by a secondary F81...H62 and F82...F61 interactions (both 2.56 Å) formed within the chains (Figure 6.7b).

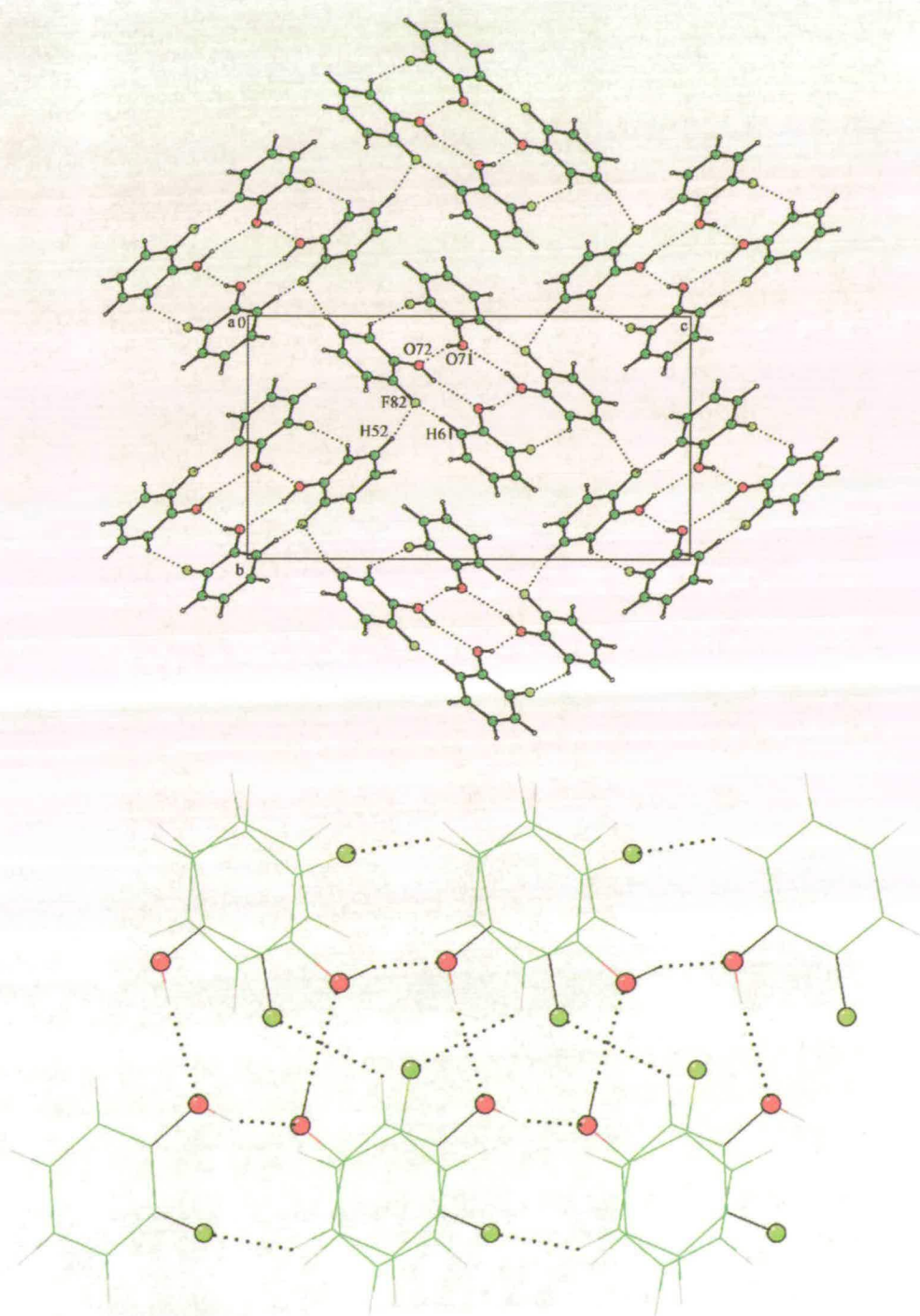


Figure 6.7 top (a): Crystal structure of phase-II of 2-fluorophenol at 0.36 GPa viewed along *a* showing chains of molecules linked by OH...OH hydrogen bonds. The chains are linked by H...F hydrogen bonds between H52 and F82. Bottom (b): The hydrogen bonded chains viewed side-on.

6.4 Discussion

Compounds that are crystallised under ambient conditions and then subjected as single crystals to high-pressure may be reduced to powder during a phase transition. Low-melting compounds are therefore useful for the study of pressure-induced polymorphism because high-pressure phases can be accessed directly by *in situ* crystal growth in a high-pressure cell. A particularly striking example of the simplification in phase behaviour that can be gained by *in situ* crystal growth is that of S₈: the solid region temperature/pressure phase diagram contains no less than twelve different phases when studied by compression of a solid sample, but there are only three when the liquid is allowed to crystallise from the melt (Mezouar, 2001). This series of molecules was chosen for its well-defined hydrogen bonding characteristics and the rigidity of the molecules.

The structures of 2-chlorophenol and 4-fluorophenol have been described in a previous Chapter, and the aim of this Chapter is to complete the survey of the monofluoro- and monochlorophenols. 2-Fluorophenol, 3-fluorophenol and 3-chlorophenol are all liquids under ambient conditions, and crystals for study at low-temperature were grown by the laser-assisted zone-refinement method of Boese and Nussbaumer. They were crystallised at high-pressure using the procedure of Allan *et al.* (1998). 4-Chlorophenol is a solid under ambient conditions, and its two polymorphic forms were crystallised from the melt and from benzene. It was crystallised from a liquid under high-pressure by ensuring that the Merrill-Bassett cell was hot prior to introduction of the sample.

The packing in the crystal structures of monoalcohols has been studied by Brock & Duncan (1994) and Taylor & Macrae (2001). Alcohols with bulky R-groups aggregate around 3-, 4- or 6-fold screw, rotation or rotoinversion axes or crystallise in low-symmetry space groups with $Z' > 1$. Small alcohols tend to pack about 2₁ axes or glide planes. Previous work in our laboratory has shown that phenol, 2-chlorophenol and 4-fluorophenol behave like bulky alcohols under pressure (packing about a pseudo three-fold axis in $P2_1$, a 3₂ axis in $P3_2$ or a $\bar{3}$ site in $R\bar{3}$, respectively). Under high-pressure these compounds behave as small alcohols, and pack about 2₁ axes or glide planes.

3-Chlorophenol behaves typically, and packs with two independent molecules about a 2₁ axis to emulate a four-fold screw axis, though there are significant departures from this ideal arrangement. This structure is obtained both at low-temperature (283 K) and high-pressure (0.1 GPa). The geometric parameters characterising the packing were slightly different.

All or most of the interactions would decrease on further application of pressure, but one disadvantage of the methods used here is that hydrostatic conditions are lost on crystallisation under pressure (the liquid behaves as its own hydrostatic fluid). Increasing the pressure on such samples therefore tends to degrade them.

3-Fluorophenol is unique in this series in crystallising at ambient pressure like a small alcohol, and forming chains disposed about a 2_1 screw axis. The O...O distances in the chain are slightly longer than in the other phenols studied here, and this may reflect steric effects of neighbouring phenyl groups. The structure is stabilised by F...H interactions. The same phase is obtained on crystallisation at 0.12 GPa.

Both 2-fluorophenol and 4-chlorophenol exhibit more interesting phase behaviour with increasing pressure. Neither adopt the packing motif associated with small alcohols at high-pressure; nor do they form very regular helical structures at ambient pressure.

The structure of phase-I 2-fluorophenol at 150 K is depicted in Figure 6.6. The packing is characterised by chains built by ..OH..OH.. hydrogen bonds. Pairs of molecules are linked across inversion centres, and these are bridged by molecules disordered about two-fold axes. The pairs of molecules connected across the inversion centres have a similar spatial relationship to a pair of molecules related by a glide plane or 2_1 axis, as in the structures of small alcohols. The steric effect of the 2-fluorine atom means that this cannot be propagated further though, and the other molecules in the chain are rotated about the chain axis (the *c*-direction) by about 90° . The 2-fluorine atoms point towards the chain axis and there is no scope for the formation of stabilising F...H contacts either within the chains or between them.

A different polymorph (phase-II) was obtained for 2-fluorophenol at 0.36 GPa. The crystal of this phase was stable only above *ca* 363 K, and data were obtained at 403 K. The structure has two molecules in the asymmetric unit, and is also characterised by ..OH..OH.. chain formation. In projection, the chain resembles a four-fold helix, but the repeat along the chain is irregular. The most important difference between this phase and phase-I is the presence of F...H interactions which occur both within the H-bonded chains and between them. Thalladi *et al.* (1998) have shown that that the C-H...F interactions are as important as C-H...O interactions in structure stabilisation. The observation that more of these weak interactions are formed at high-pressure is consistent with results observed in other high-pressure studies, for example on glycine, where high-pressure induces extensive CH...O hydrogen bond formation (Dawson *et al.*, 2004b). A feature exhibited by high-pressure structures of 2-chlorophenol and 4-fluorophenol is the lengthening of ..OH..OH.. hydrogen

bonds in order to accommodate more efficient packing motifs. A similar feature is observed in phase-II of 2-fluorophenol, in which one O...O interaction is 3.097(3) Å.

The two phases of 4-chlorophenol presented here have been described previously, and these structures are redeterminations. Phase-I, which is based on an irregular helical arrangement of molecules linked by OH...OH interactions, crystallises at ambient pressure from the melt. Under a modest pressure of 0.02 GPa, crystallisation from the melt yields phase-II, which is based on cyclic hydrogen-bonded tetramers. In both phases the chlorine atoms link the hydrogen bonded units together through Cl...H interactions. These are somewhat shorter in phase-II than in phase-I. Moreover, the *R*(8) ring has inversion symmetry rather than the $\bar{4}$ symmetry that might be expected for such a motif for a bulky alcohol. Neighbouring phenyl groups approach each other with centroid-centroid distance of 6.22 Å, mediated by a CH...aryl hydrogen bond. The more extensive set of contacts in phase-II, and its more efficient packing of phenyl groups perhaps explains the preference for this phase at high-pressure.

6.5 Conclusions

The behaviour of 3-fluoro-, 3-chloro, 4-chloro- and 2-fluorophenol shows a departure from the behaviour observed in phenol, 2-chlorophenol and 4-fluorophenol. The transition to a small alcohol packing from bulky alcohol packing is not seen in any of these compounds. In general, this study has shown that they crystallise in pseudo helices and ring motifs, though these are markedly distorted from three- or four-fold symmetry often observed in alcohol structures. Only one compound, 2-fluorophenol, shows a phase that is only stable at pressure. Those compounds that do undergo a phase transition, 4-chlorophenol and 2-fluorophenol show a transition to a phase which possesses a greater number of weaker intermolecular contacts in the form of CH... π and CH...F interactions, respectively.

6.6 References

- Allan, D. R., Clark, S. J., Brugmans, M. J. P., Ackland, G. J. & Vos, W. L. (1998). *Phys. Rev. B* **58**, 18, R11809-R11812.
- Allan, D. R., Clark, S. J., Dawson, A., McGregor, P. A. & Parsons, S. (2002). *Acta Cryst. B* **58**, 1018-1024.

- Allen, F. H. (2002). *Acta Cryst.* **B58**, 380-388.
- Allen, F. H., Motherwell, W. D. S. (2002). *Acta Cryst.* **B58**, 407-422.
- Altomare, A., Cascarano, G., Giacovazzo, C. & Guagliardi, A. (1993). *J. Appl. Cryst.* **26**, 343-350.
- Bernstein, J., Davis, R.E., Shimoni, L. & Chang, N-L. (1995). *Angew. Chem. Int. Ed. Engl.* **34**, 1555- 1573.
- Betteridge, P. W., Carruthers, J. R., Cooper, R. I., Prout, K. & Watkin, D. J. (2003). *J. Appl. Cryst.* **36**, 1487.
- Blessing, R. H. (1995). *Acta Cryst.* **A51**, 33-38.
- Blessing, R. H. (1997). *J. Appl. Cryst.* **30**, 421-426.
- Boese, R. & Nussbaumer, M. (1994). In *Correlations, Transformations, and Interactions in Organic Crystal Chemistry*, D.W. Jones & A. Katrusiak (Editors). (International Union of Crystallography, Crystallographic Symposia, 7), pages 20-37.
- Brock, C. P. & Duncan, L. L. (1994). *Chem. Mater.* **6**, 1307-1312.
- Bruker-Nonius (2003). SAINT version 7. Bruker-Nonius Inc., Madison, Wisconsin, USA.
- Bruno, I. J., Cole, J. C., Edgington, P. R., Kessler, M., Macrae, C. F., McCabe, P., Pearson, J. & Taylor, R. (2002). *Acta Cryst.* **B58**, 389-397.
- Cosier, J. & Glazer, A. M. (1986). *J. Appl. Cryst.* **19**, 105-107.
- David, W. I. F., Shankland, K., Cole, J., Maginn, S., Motherwell, W. D. S. & Taylor, R. (2001). *DASH User's Manual*. Cambridge Crystallographic Data Centre, Cambridge, UK.
- Dawson, A., Allan, D. R., Parsons, S. & Ruf, M. (2004a). *J. Appl. Cryst.* **37**, 410-416.
- Dawson, A., Allan, D. R., Belmonte, S. A., Clark, S. J., David, W. I. F., McGregor, P. A., Parsons, S., Pulham, C. R. & Sawyer, L. (2004b). *Submitted for publication*.
- Farrugia, L. J. (1999). *J. Appl. Cryst.* **32**, 837-838.
- Malone, J. F., Murray, C. M., Charlton, M. H., Docherty, R. & Lavery, A. J. (1997). *J. Chem. Soc., Faraday Trans.* **93**, 3429-3436.
- Merrill, L. & Bassett, W. A. (1974). *Rev. Sci. Instrum.* **45**, 290-294.

- Mezouar, M. (2001). *High-pressure Powder Diffraction Using Synchrotron Radiation*. British Crystallographic Association Physical Crystallography Group Meeting, Daresbury Laboratory, Warrington, UK. November 2001.
- Oswald, I. D. H., Allan, D. R., Day G. M, Motherwell, W. D. S. & Parsons, S. (2004). *Manuscript in preparation*.
- Parsons, S. ECLIPSE. (2004a). The University of Edinburgh, Edinburgh, U.K.
- Parsons, S. SHADE. (2004b). The University of Edinburgh, Edinburgh, U.K.
- Perrin, P. M. & Michel, P. (1973a). *Acta Cryst.* **B29**, 253-258.
- Perrin, P. M. & Michel, P. (1973b). *Acta Cryst.* **B29**, 258-263.
- Sands, D. E. (1995). *Vectors and Tensors in Crystallography*. Dover, New York. Chapter 2.
- Sheldrick, G. M. (2001). SHELXTL version 6.01. University of Göttingen, Germany and Bruker-Nonius Inc., Madison, Wisconsin, U.S.A.
- Sheldrick, G. M. (2004). SADABS, Version 2004-1. University of Göttingen, Germany and Bruker-AXS, Madison, Wisconsin, USA.
- Sparks, R. A. (2000). GEMINI. Version 1.01. Bruker-AXS, Madison, Wisconsin, USA.
- Spek, A. L. (2002). *PLATON- A Multipurpose Crystallographic Tool*, Utrecht University, Utrecht, The Netherlands.
- Taylor, R. & Macrae, C. F. (2001). *Acta Cryst.* **B57**, 815-827.
- Thalladi, V. R., Weiss, H.-C., Blaser, D., Boese, R., Nangia, A. & Desiraju, G. R. (1998). *J. Am. Chem. Soc.* **120**, 8702-8710.
- Watkin, D. J., Pearce, L. & Prout, C. K. (1993). *CAMERON - A Molecular Graphics Package*. Chemical Crystallography Laboratory, University of Oxford, England.

Chapter 7

Conclusions

7.1 Conclusions

This thesis has described the determination and analysis of the crystal structures of a series of hydrogen-bonded, organic compounds. The subjects chosen for study were targeted with the aim of forming closely-related structural motifs in the solid state.

Chapters 2 and 3 have shown that it is possible to rationalise the formation of several co-crystals through knowledge-mining the Cambridge Structural Database. The choice of guest molecule was key to the success of these projects. Systematic modification of the guest molecules yields crystal structures that have similar hydrogen bonding motifs. These motifs are only disrupted when steric effects are introduced into the system. Chapter 4 has also shown that knowledge gained from previous experiments in the CSD can help to achieve successful crystallisations; hydrogen bonding in the subject of this Chapter was also shown to be temperature dependent.

Chapter 5 described the alteration of the packing characteristics of 2-chlorophenol and 4-fluorophenol with the application of pressure. 2-Chlorophenol and 4-fluorophenol crystallised in a manner that is associated with bulky alcohols at ambient pressure; around a 3_2 screw axis and a $\bar{3}$ site, respectively. At pressure, the packing is more characteristic of a small alcohol, crystallising around a 2_1 screw axis. Although the arrangement of molecules has changed, the hydrogen bonding chain motif observed in the ambient pressure phase of 2-chlorophenol was still observed at high-pressure. However, the hydrogen-bonded ring motif of 4-fluorophenol is altered to a hydrogen-bonded chain motif on application of pressure.

Most of the remaining chloro- and fluorophenols do not show a change in their packing characteristics. Only 2-fluorophenol crystallises as a new polymorph at pressure; the packing characteristics, however, do not change from those of a bulky alcohol. 3-Fluorophenol shows a different behaviour to the other halophenols as it crystallises in a small packing motif at ambient pressure. This can be attributed to stabilising H...F interactions that occur in the crystal structure. The investigation of these compounds with pressure, however, is limited by the experimental procedure used to grow the crystals. Knowledge gained from Chapter 5 may lead to the conclusion that those compounds that crystallise in an arrangement associated with bulky alcohols may undergo a phase transition at higher pressure to a structure similar to those observed in 2-chlorophenol and 4-fluorophenol.

The experiments performed in this Thesis have given insight as to the hydrogen bonding and packing behaviour of a range of molecules at ambient and high-pressure. Systematic

studies of molecules can provide knowledge that may be utilised in further computational and crystal engineering studies.

Appendix

A paracetamol–morpholine adduct

Iain D. H. Oswald,^{a*} W. D. Sam Motherwell,^b Simon Parsons^a and Colin R. Pulham^a

^aSchool of Chemistry, The University of Edinburgh, King's Buildings, West Mains Road, Edinburgh EH9 3JJ, Scotland, and ^bCambridge Crystallographic Data Centre, 12 Union Road, Cambridge CB2 1EZ, England

Correspondence e-mail: iain.oswald@ed.ac.uk

Key indicators

Single-crystal X-ray study

$T = 150\text{ K}$

Mean $\sigma(\text{C}-\text{C}) = 0.005\text{ \AA}$

Disorder in solvent or counterion

R factor = 0.054

wR factor = 0.178

Data-to-parameter ratio = 13.9

For details of how these key indicators were automatically derived from the article, see <http://journals.iucr.org/e>.

Paracetamol [also known as acetaminophen or *N*-(4-hydroxyphenyl)acetamide] is an important analgesic drug that has recently been cocrystallized with a series of cyclic N- and O-donor compounds. This paper describes the formation of a paracetamol adduct with morpholine, *viz.* paracetamol–morpholine (1/2.5), $\text{C}_8\text{H}_9\text{NO}_2 \cdot 2.5\text{C}_4\text{H}_9\text{NO}$. There are five morpholine molecules and two paracetamol molecules in the unit cell. The paracetamol molecules are held together by hydrogen bonding *via* morpholine molecules, one of which is disordered about an inversion centre.

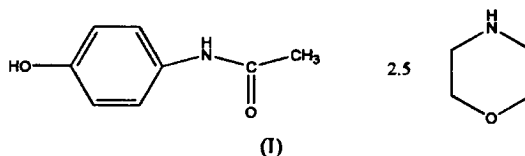
Received 25 September 2002

Accepted 2 October 2002

Online 25 October 2002

Comment

Paracetamol (acetaminophen) in its various polymorphic forms has been studied extensively in recent years. It has been shown (Fachaux *et al.*, 1995) that the different polymorphs (monoclinic and orthorhombic) have different compressive properties. This ability for plastic deformation is of great interest to the pharmaceutical industry. The monoclinic form is the thermodynamically more stable form of paracetamol under normal conditions, but shows no plastic deformation. The orthorhombic polymorph is much harder to prepare and, so far, can only be obtained reproducibly from the melt or by seeding a saturated solution (Nichols & Frampton, 1998). This polymorph possesses plastic deformation and, therefore, mass production of this form would facilitate the manufacture of paracetamol for pharmaceutical purposes. In a recent study, our group has explored the use of cocrystals as a means of producing the orthorhombic polymorph. Paracetamol was found to cocrystallize with a number of different solvents (Oswald *et al.*, 2002). Though the majority of the cocrystals formed were hemisolvates, we also produced a 1:2.5 cocrystal, (I), of paracetamol with morpholine.



There are two and a half morpholine molecules (designated A, B and C; see Fig. 1) present in the asymmetric unit of (I). One of the morpholine molecules (C) is disordered over a crystallographic inversion centre, with the N and O atoms sharing an equivalent site. A composite scattering factor [$0.5f(\text{N}) + 0.5f(\text{O})$] was used for this site. The hydrogen occupancy was fixed at 0.5 in an axial position, which was inferred from a difference map.

The amine function of morpholine is a weak hydrogen-bond acceptor and a moderately strong donor. The ether moiety is a

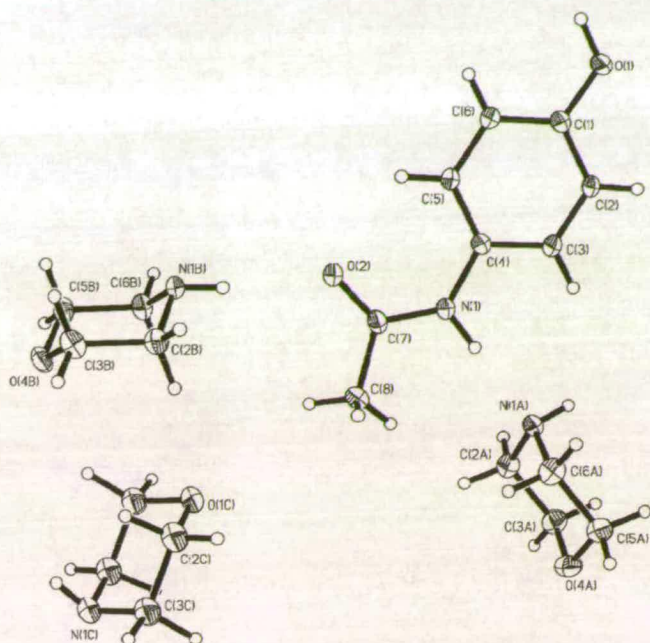


Figure 1

A plot of adduct (I), with ellipsoids at the 30% probability level. Morpholine molecule *C* is disordered about a crystallographic inversion centre, with atoms N1C and O1C refined as 50% occupied with equal *x*, *y*, *z* coordinates and isotropic displacement parameters. All crystallographically independent non-H atoms are labelled.

rather weak acceptor. In paracetamol, the amide and hydroxyl groups are strong donors, and the carbonyl group a strong acceptor; the hydroxyl group is a weak acceptor. The structure of adduct (I) is consistent with this hierarchy of interactions. All direct links between paracetamol molecules are absent in the structure of (I) (Fig. 2). Successive paracetamol molecules, related by lattice repeats along *c*, are linked *via* pairs of crystallographically independent morpholine molecules through C=O...H-N, O...H-N and N...H-N interactions. This scheme establishes a chain of molecules in the series paracetamol-morpholine (*B*)-morpholine (*A*)-paracetamol, which can be described with a $C_3^3(11)$ graph at the ternary level (Bernstein *et al.*, 1995). A second chain is related to this *via* a crystallographic inversion centre, and is linked to the first *via* O-H...N hydrogen bonds to morpholine *B*, to form a ribbon-like structure. This scheme satisfies all the hydrogen-bonding characteristics of the paracetamol molecules, with the exception of the weak OH acceptor functionality, although this arguably interacts with an aromatic CH group (O...H = 2.62 Å). The hydrogen-bonding functionality of the morpholine is also satisfied with the exception of the donor character of the ether moiety in molecule *A*. It is notable that, in order to accommodate this scheme, the morpholine molecules *A* and *B* are in different conformations, with the amino H adopting the expected equatorial position in molecule *B*, but the less favourable axial position in molecule *A*.

Neighbouring ribbons are related to each other by inversion centres, which are occupied by a third crystallographically

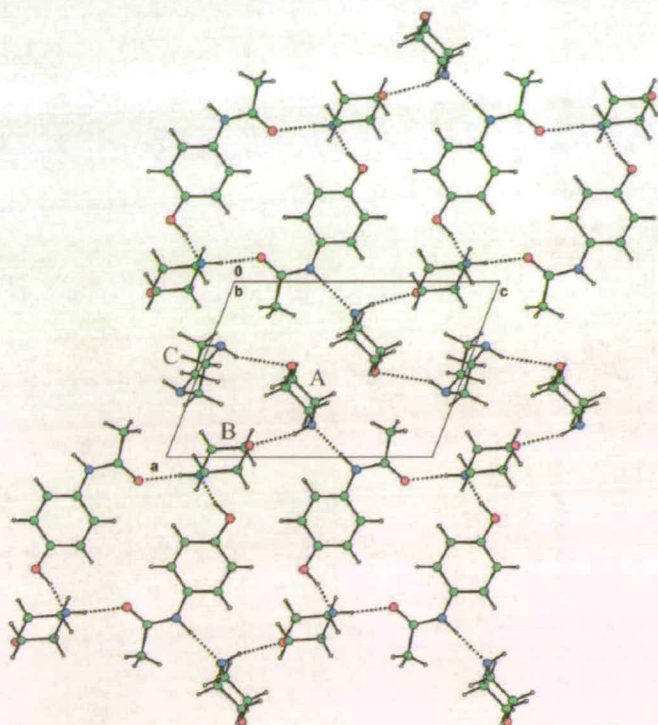


Figure 2

A section of the structure of the title paracetamol-morpholine (1/2.5) adduct. The view is along the *b* axis. O atoms are shown in red, N atoms in blue, C atoms in green and H atoms in grey. Paracetamol molecules within the outlined unit cell are generated from those shown by translation along the (210) direction.

independent molecule of morpholine (*C*). This molecule is disordered about the inversion centre, but forms weak hydrogen bonds [2.59 (5) Å] to one of the ether moieties of the two morpholine *A* molecules related by the inversion centre. Overall then, the structure of (I) consists of layers formed by weakly connected ribbons. The layers are formed parallel to the $(\bar{1}20)$ planes. The distance between the mean paracetamol planes in successive layers alternates between 5.32 and 4.03 Å. The average distance, 4.68 Å, is commensurate with $d(\bar{1}20)$ (4.55 Å). The mean planes of all the morpholine molecules are perpendicular to the plane of the paracetamol molecule. The angles that the mean planes of molecules *A*, *B* and *C* make with the paracetamol plane are 83.73 (10), 79.60 (10) and 75.15 (16)°, respectively. The paracetamol molecules thus form a 'groove' in the layers, which align so that the morpholine molecules lie above and below this 'groove' in successive layers.

The large number of solvent molecules within this structure has resulted in the formation of solvent bridges between the paracetamol molecules, with no paracetamol-paracetamol interactions, as seen in our previous study.

Experimental

Starting materials were obtained from Sigma-Aldrich and were used as received. Paracetamol (0.49 g, 3.24 mmol) was refluxed in 1 ml morpholine (11.42 mmol) and allowed to cool. Pale-yellow crystals were formed on maintaining the solution at 277 K.

Crystal data

$C_8H_9NO_2 \cdot 2.5C_4H_9NO$
 $M_r = 368.97$
 Triclinic, $P\bar{1}$
 $a = 8.710$ (4) Å
 $b = 9.920$ (5) Å
 $c = 12.385$ (5) Å
 $\alpha = 102.35$ (3)°
 $\beta = 108.33$ (2)°
 $\gamma = 96.68$ (3)°
 $V = 972.7$ (7) Å³

$Z = 2$
 $D_x = 1.260$ Mg m⁻³
 Cu $K\alpha$ radiation
 Cell parameters from 48
 reflections
 $\theta = 20$ – 22°
 $\mu = 0.74$ mm⁻¹
 $T = 150$ (2) K
 Plate, colourless
 $0.27 \times 0.23 \times 0.06$ mm

Data collection

Stoe Stadi-4 four-circle
 diffractometer
 ω - θ scans
 Absorption correction: empirical
 via ψ scans [SHELXTL
 (Sheldrick (2001) based on
 method of North *et al.* (1968))]
 $T_{min} = 0.717$, $T_{max} = 0.889$
 3596 measured reflections
 3416 independent reflections

1951 reflections with $I > 2\sigma(I)$
 $R_{int} = 0.028$
 $\theta_{max} = 70.3^\circ$
 $h = -10 \rightarrow 10$
 $k = -12 \rightarrow 11$
 $l = -14 \rightarrow 15$
 3 standard reflections
 frequency: 120 min
 intensity decay: 5%

Refinement

Refinement on F^2
 $R[F^2 > 2\sigma(F^2)] = 0.054$
 $wR(F^2) = 0.178$
 $S = 1.03$
 3416 reflections
 246 parameters
 H-atom parameters constrained

$w = 1/[\sigma^2(F_o^2) + (0.0983P)^2 + 0.3346P]$
 where $P = (F_o^2 + 2F_c^2)/3$
 $(\Delta/\sigma)_{max} < 0.001$
 $\Delta\rho_{max} = 0.35$ e Å⁻³
 $\Delta\rho_{min} = -0.26$ e Å⁻³
 Extinction correction: SHELXL97
 Extinction coefficient: 0.0077 (14)

The diffractometer was equipped with an Oxford Cryosystems low-temperature device operating at 150 K. H atoms were placed in

calculated positions and allowed to ride on their parent atoms, except for those involved in hydrogen bonding, which were located in a difference map; these were treated with a riding model, following several cycles of refinement in which a C–H distance restraint of 0.9 Å was applied.

Data collection: DIF4 (Stoe & Cie, 1990); cell refinement: DIF4; data reduction: REDU4 (Stoe & Cie, 1990); program(s) used to solve structure: SHELXS97 (Sheldrick, 1990); program(s) used to refine structure: SHELXL97 (Sheldrick, 1997); molecular graphics: SHELXTL (Sheldrick, 2001); software used to prepare material for publication: SHELXTL and CAMERON (Watkin *et al.*, 1996).

The authors thank the EPSRC and Cambridge Crystallographic Data Centre for funding.

References

- Bernstein, J., Davis, R. E., Shimoni, L. & Chang, N.-L. (1995). *Angew. Chem. Int. Ed. Engl.* **34**, 1555–1573.
 Fachaux, J.-M., Guyot-Hermann, A.-M., Conflant, P., Drache, M., Veessler, S. & Boisselle, R. (1995). *Powder Technol.* **82**, 123–128.
 Nichols, G. & Frampton, C. S. (1998). *J. Pharm. Sci.* **87**, 684–693.
 North, A. C. T., Phillips, D. C. & Mathews, F. S. (1968). *Acta Cryst.* **A24**, 351–359.
 Oswald, I. D. H., Allan, D. R., McGregor, P. A., Motherwell, W. D. S., Parsons, S. & Pulham, C. R. (2002). *Acta Cryst.* **B58**. In the press.
 Sheldrick, G. M. (1997). SHELXS97 and SHELXL97. University of Göttingen, Germany.
 Sheldrick, G. M. (2001). SHELXTL. Version 6. Bruker AXS Inc., Madison, Wisconsin, USA.
 Stoe & Cie (1990). DIF4 and REDU4. Stoe & Cie, Darmstadt, Germany.
 Watkin, D. J., Prout, C. K. & Pearce, L. J. (1996). CAMERON. Chemical Crystallography Laboratory, Oxford, England.

A 1:1 co-crystal of quinol and pyridine

Iain D. H. Oswald,^{a*} W. D. Sam Motherwell^b and Simon Parsons^a^aSchool of Chemistry, The University of Edinburgh, King's Buildings, West Mains Road, Edinburgh EH9 3JJ, Scotland, and ^bCambridge Crystallographic Data Centre, 12 Union Road, Cambridge CB2 1EZ, England

Correspondence e-mail: iain.oswald@ed.ac.uk

Key indicators

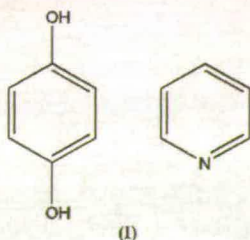
Single-crystal X-ray study
T = 150 K
Mean $\sigma(\text{C}-\text{C}) = 0.002 \text{ \AA}$
R factor = 0.048
wR factor = 0.120
Data-to-parameter ratio = 16.7For details of how these key indicators were automatically derived from the article, see <http://journals.iucr.org/e>.

A co-crystal of quinol and pyridine would be expected to form with 1:2 stoichiometry because quinol has two hydrogen-bond donors and pyridine has one hydrogen-bond acceptor which is more basic than phenolic oxygen. We report the structure of a 1:1 co-crystal, *viz.* quinol-pyridine (1/1), $\text{C}_6\text{H}_6\text{O}_2 \cdot \text{C}_5\text{H}_5\text{N}$, which does not conform to this expectation. Its stability appears to imply that a combination of individually relatively weak $\text{C}-\text{H} \cdots \text{O}$, $\text{C}-\text{H} \cdots \pi$ and $\pi-\pi$ stacking interactions are energetically competitive with $\text{O}-\text{H} \cdots \text{N}$ hydrogen bonds. Quinol molecules lie on inversion centres, while pyridine is in a general position.

Received 24 August 2004
Accepted 30 September 2004
Online 3 October 2004

Comment

Quinol shows a great propensity for forming co-crystals, and it is widely used to stabilize compounds that are susceptible to polymerization. A search of the Cambridge Structural Database (CSD, Version 5.25; Allen & Motherwell, 2002) shows that there are 92 co-crystals of quinol with a range of organic compounds. Of all these structures in the CSD, over half contain hydrogen-bond acceptors, *e.g.* 1,4-dioxane (Barnes *et al.*, 1990). We have recently reported (Oswald *et al.*, 2004) a series of crystal structures of co-crystals of quinol with pyrazine, piperazine, morpholine, pyridine, piperidine and 4,4'-bipyridine (hereafter referred to as guest molecules). These all have closely related packing motifs in which pairs of quinol and guest molecules are connected *via* $\text{N}-\text{H} \cdots \text{O}$ or $\text{C}-\text{H} \cdots \text{O}$ interactions.



Amine N atoms are more strongly basic than phenol O atoms and the shortest, and by implication strongest, hydrogen bonds formed in our previous studies were those from a phenol OH donor to an amine or a pyridine N atom. Pyrazine and piperazine, which both have two acceptor sites per molecule, were found to form 1:1 co-crystals with quinol, which contains two strong donor functions. In the co-crystals of quinol with molecules with N, NH or NMe and O, CH or CH_2 , respectively in the 1 and 4 positions of a six-membered ring, quinol was found to form hydrogen bonds exclusively to the nitrogen moiety, promoting the formation of quinol-guest co-crystals in a 1:2 ratio. This trend is exemplified by pyridine,

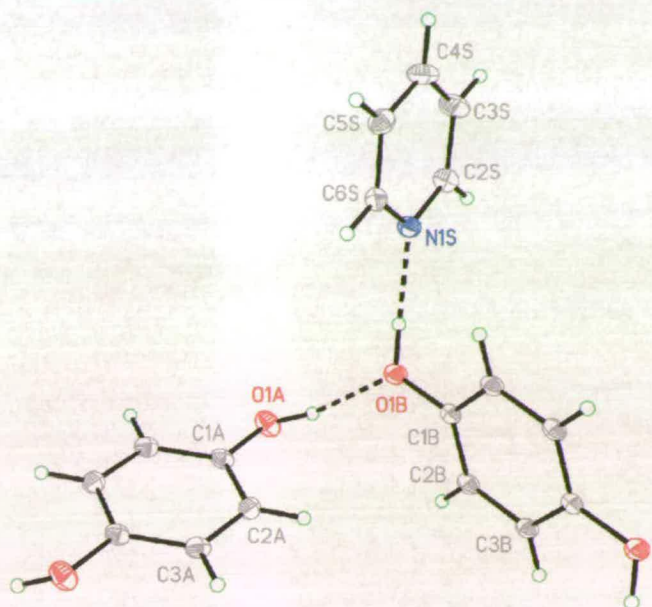


Figure 1
Displacement ellipsoid plot of (I), showing the two crystallographically independent quinol molecules (labelled A and B) and the pyridine molecule (labelled S). Ellipsoids are drawn at the 30% probability level.

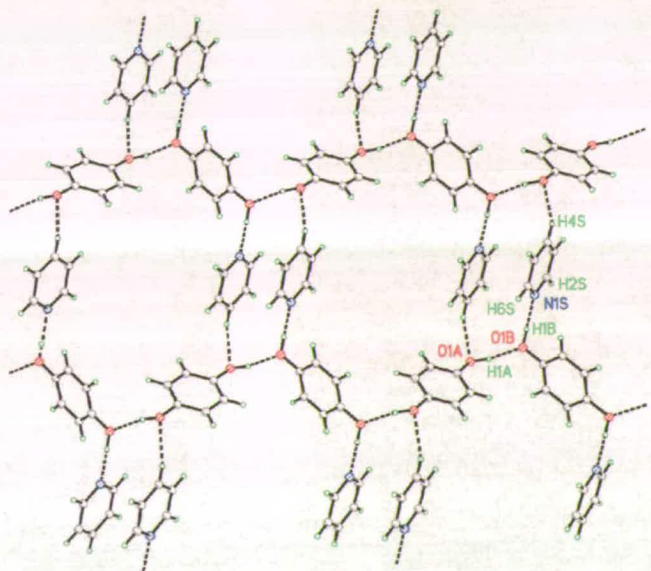


Figure 2
Strong O—H...O hydrogen bonds connect quinol molecules into chains. Pyridine molecules are connected on either side of the chains by O—H...N hydrogen bonds. π - π Stacking and C—H...O interactions involving the pyridine molecules also link the chains into a layer. The O—H...O and O—H...N hydrogen bonds are shown as heavy dashed lines and the weaker C—H...O interactions as open dashes. This view is along the $(\bar{1}12)$ reciprocal lattice direction.

which forms a co-crystal containing quinol and pyridine in 1:2 ratio.

In this paper, we report the crystal structure of a 1:1 co-crystal of quinol and pyridine, (I), which is an exception to the general stoichiometry rules described above. It was obtained

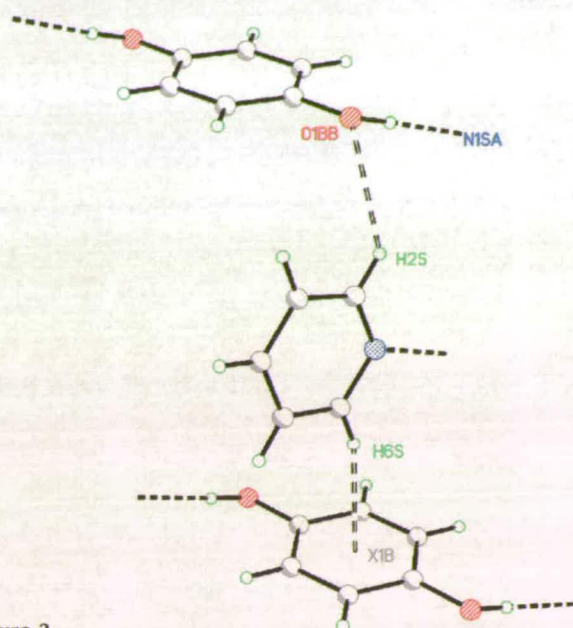


Figure 3
The layers (see Fig. 2) are connected through C—H... π and C—H...O interactions to the layers above and below. X1B is the centroid of the benzene ring (see Table 1). This view is along [010].

by refluxing and then cooling a solution of quinol dissolved in a minimum quantity of pyridine.

Co-crystal (I) crystallizes in space group $P\bar{1}$ and the asymmetric unit consists of one molecule of pyridine in a general position and two half-molecules of quinol (labelled A and B) residing on crystallographic inversion centres (Fig. 1). Primary bond distances and angles are normal and are listed in the deposited CIF.

The shortest and strongest intermolecular interactions in the structure are O—H...O and O—H...N hydrogen bonds (Fig. 2 and Table 1). Quinol molecules A and B alternate along a chain built by O—H...O hydrogen bonds, in which molecule A provides the OH-donor functions, while molecule B acts as the acceptor. The chains run along the [110] direction and form a $C_2^2(14)$ graph set (Bernstein *et al.*, 1995). Molecule B donates to pairs of pyridine molecules, which lie on either side of the chain. Successive pyridine molecules are related by the $\bar{1}$ operations centred in the middle of the quinol rings. Co-crystal (I) is the only co-crystal in our study that we have observed in which quinol molecules are directly hydrogen bonded to one another.

The only conventional hydrogen-bonding function 'unsatisfied' by the N—H...O and O—H...O hydrogen bonding described above is the phenol O atom of molecule A. There is a close contact between this phenol group and a pyridine attached to an adjacent chain ($C4S-H4S...O1A = 2.57 \text{ \AA}$ and 127°).

Inter-chain connections are also formed by π - π stacking between pairs of pyridine molecules. The distance between the atoms in one ring and the mean plane of the other varies in the range 3.532 – 3.538 (2) \AA ; the planes are exactly parallel by symmetry. The symmetry code relating the rings in this

interaction is $(2 - x, 1 - y, -z)$.

The C4S—H4S···O1A and π – π stacking interactions connect the chains into a layer parallel to $(\bar{1}12)$. The layers are stacked, with quinol molecules above and below the rather 'open' region between the pairs of π -stacked pyridine rings in Fig. 2. The layers are connected in this region by C6S—H6S··· π and C2S—H2S···O1B interactions, where the π acceptor is the aromatic ring from a quinol (molecule B, see Fig. 3). The distance between H6S and the centroid of the benzene ring (*X1B*) in this interaction is 2.53 Å, with an angle of 162° subtended at the H atom. The weak C2S—H2S···O1B interaction measures 2.69 Å, with an angle at H2S of 136°.

C—H···O hydrogen bonding is now widely accepted (Desiraju & Steiner, 1999), and weak hydrogen bonding can be exploited in supramolecular chemistry and crystal structure design. For example, C—H···O bonds may play a very important role in protein folding (Derewenda *et al.*, 1995). The CH groups in pyridine rings are often observed to act as donor groups in CH···acceptor interactions. Related interactions also occur in heterocyclic compounds related to pyridine, for example, in quinol–pyrazine (Oswald *et al.*, 2004). Such interactions are strong enough that they can be used in crystal engineering, as demonstrated, for example, by Bond (2003) in a series of co-crystals of pyrazine with carboxylic acids. π – π Stacking has also been observed to be competitive with conventional hydrogen bonding in, for example, the 1:2 co-crystal of quinol with 4,4'-bipyridine (Oswald *et al.*, 2004).

That a co-crystal with 1:1 stoichiometry should be obtained from a mixture of quinol and pyridine must imply that the combination of C—H···O, π – π stacking and C—H··· π interactions is competitive with O—H···N hydrogen bonding, even for a relatively basic centre such as pyridine.

Experimental

Starting materials were obtained from Sigma–Aldrich and were used as received. Quinol (0.49 g, 4.45 mmol) was refluxed in a minimum volume of pyridine to dissolve the solid. The solution was allowed to cool to room temperature to produce colourless blocks.

Crystal data

$C_6H_6O_2 \cdot C_5H_5N$	$Z = 2$
$M_r = 189.21$	$D_x = 1.310 \text{ Mg m}^{-3}$
Triclinic, $P\bar{1}$	Mo $K\alpha$ radiation
$a = 5.7451 (5) \text{ \AA}$	Cell parameters from 2033 reflections
$b = 9.1570 (9) \text{ \AA}$	$\theta = 2-29^\circ$
$c = 9.6247 (9) \text{ \AA}$	$\mu = 0.09 \text{ mm}^{-1}$
$\alpha = 89.002 (2)^\circ$	$T = 150 (2) \text{ K}$
$\beta = 76.222 (2)^\circ$	Block, colourless
$\gamma = 77.478 (2)^\circ$	$0.33 \times 0.18 \times 0.18 \text{ mm}$
$V = 479.76 (8) \text{ \AA}^3$	

Data collection

Bruker SMART APEX CCD area-detector diffractometer with Cryostream cooler (Cosier & Glazer, 1986)	4349 measured reflections
ω scans	2248 independent reflections
Absorption correction: multi-scan (SADABS; Sheldrick, 2004)	1853 reflections with $I > 2\sigma(I)$
$T_{\min} = 0.841, T_{\max} = 0.980$	$R_{\text{int}} = 0.018$
	$\theta_{\text{max}} = 28.7^\circ$
	$h = -7 \rightarrow 7$
	$k = -12 \rightarrow 12$
	$l = -12 \rightarrow 13$

Refinement

Refinement on F^2
 $R[F^2 > 2\sigma(F^2)] = 0.048$
 $wR(F^2) = 0.120$
 $S = 1.04$
 2248 reflections
 135 parameters
 H atoms treated by a mixture of independent and constrained refinement

$$w = 1/[\sigma^2(F_o^2) + (0.049P)^2 + 0.1585P]$$

where $P = (F_o^2 + 2F_c^2)/3$
 $(\Delta/\sigma)_{\text{max}} = 0.001$
 $\Delta\rho_{\text{max}} = 0.28 \text{ e \AA}^{-3}$
 $\Delta\rho_{\text{min}} = -0.21 \text{ e \AA}^{-3}$

Table 1

Hydrogen-bonding geometry (Å, °).

$D-H\cdots A$	$D-H$	$H\cdots A$	$D\cdots A$	$D-H\cdots A$
O1A—H1A···O1B ⁱ	0.94 (3)	1.81 (3)	2.7392 (16)	168 (2)
O1B—H1B···N1S ⁱⁱ	0.93 (2)	1.79 (2)	2.7178 (17)	178 (2)
C2S—H2S···O1B	0.95	2.69	3.436 (2)	136
C4S—H4S···O1A	0.95	2.57	3.225 (2)	127
C6S—H6S··· <i>X1B</i> ⁱⁱⁱ	0.95	2.53	3.45	162

Symmetry codes: (i) $1 + x, y, z$; (ii) $1 - x, 1 - y, -z$; (iii) $1 + x, y, z - 1$. *X1B* is the centroid of the benzene ring.

H atoms were placed on C atoms in calculated positions (C—O = 0.95 Å) and allowed to ride on their parent atoms [$U_{\text{iso}}(\text{H}) = 1.2U_{\text{eq}}(\text{C})$]. Hydroxyl H atoms were located in difference maps and refined freely.

Data collection: SMART (Bruker–Nonius, 2001); cell refinement: SAINT (Bruker–Nonius, 2003); data reduction: SAINT; program(s) used to solve structure: SHELXTL (Sheldrick, 2001); program(s) used to refine structure: SHELXTL; molecular graphics: SHELXTL; software used to prepare material for publication: SHELXTL, PLATON [Spek (2004) as incorporated in WinGX (Farrugia, 1999)] and enCIFer (Version 1.1; Allen *et al.*, 2004).

The authors thank the EPSRC, The University of Edinburgh and The Cambridge Crystallographic Data Centre for funding.

References

- Allen, F. H., Johnson, O., Shields, G. P., Smith, B. R. & Towler, M. (2004). *J. Appl. Cryst.* **37**, 335–338.
- Allen, F. H. & Motherwell, W. D. S. (2002). *Acta Cryst.* **B58**, 407–422.
- Barnes, J. C., Paton, J. D. & Blyth, C. S. (1990). *Acta Cryst.* **C46**, 1183–1184.
- Bernstein, J., Davis, R. E., Shimoni, L. & Chang, N.-L. (1995). *Angew. Chem. Int. Ed. Engl.* **34**, 1555–1573.
- Bond, A. D. (2003). *Chem. Commun.* pp. 250–251.
- Bruker–Nonius (2001). SMART. Version 5.624. Bruker–Nonius Inc., Madison, Wisconsin, USA.
- Bruker–Nonius (2003). SAINT. Version 7. Bruker–Nonius Inc., Madison, Wisconsin, USA.
- Cosier, J. & Glazer, A. M. (1986). *J. Appl. Cryst.* **19**, 105–107.
- Derewenda, Z. S., Lee, L. & Derewenda, U. (1995). *J. Mol. Biol.* **252**, 248–262.
- Desiraju, G. R. & Steiner, T. (1999). *The Weak Hydrogen Bond*. IUCr Monographs on Crystallography, No. 9. Oxford University Press.
- Farrugia, L. J. (1999). *J. Appl. Cryst.* **32**, 837–838.
- Oswald, I. D. H., Motherwell, W. D. S. & Parsons, S. (2004). Submitted. [Which J.]
- Sheldrick, G. M. (2001). SHELXTL. Version 6.01. Bruker–Nonius Inc., Madison, Wisconsin, USA.
- Sheldrick, G. M. (2004). SADABS. University of Göttingen, Germany.
- Spek, A. L. (2004). PLATON. Utrecht University, The Netherlands.

Acta Cryst. (2004). C60, 000–000

A 1:2 co-crystal of isonicotinamide and propionic acid

IAIN D. H. OSWALD,^a W. D. SAM MOTHERWELL^b AND SIMON PARSONS^a

^a*School of Chemistry, The University of Edinburgh, King's Buildings, West Mains Road, Edinburgh, Scotland, EH9 3JJ, and* ^b*Cambridge Crystallographic Data Centre, 12 Union Road, Cambridge, England, CB2 1EZ. E-mail: s.parsons@ed.ac.uk*

Abstract

Isonicotinamide has been shown to form many 1:1 co-crystals with monofunctional carboxylic acids, but with propionic acid it forms a co-crystal containing two acid molecules per formula unit. The crystal structure consists of 'supermolecules' consisting of one isonicotinamide and two acids hydrogen bonded to the pyridine and amide functions. Further NH...O hydrogen bonds connect these supermolecules into chains.

Comment

Isonicotinamide has been shown to crystallize with carboxylic acids in a 1:1 stoichiometry to form a robust building block or 'supermolecule' consisting of two amide and two acid molecules, I (Aakeröy *et al.*, 2002). When a saturated solution of isonicotinamide in warm propionic acid was allowed to cool, colourless crystalline laths were obtained. Single crystal X-ray diffraction revealed these to be a co-crystal consisting of isonicotinamide and propionic acid in 1:2 ratio (II). Similar preparative routes with formic and acetic acids both yielded 1:1 co-crystals (Oswald *et al.*, 2004). Attempts to prepare a 1:1 co-crystal with propionic acid failed. For example, a 1:1 mixture of propionic acid and isonicotinamide in ethanol yielded only crystals of II; even in the presence of excess isonicotinamide the only crystals obtained were isonicotinamide itself and II.

The crystal structure of II consists of supermolecules comprising two acid and one isonicotinamide molecule. One acid forms an R²₂(8) motif with the amide moiety (Bernstein *et al.*, 1995). Another acid molecule forms a hydrogen bond to the pyridine nitrogen, supported by a weaker CH...O hydrogen bond (Fig. 1, Table 1). There are two supermolecules in the asymmetric unit, and, in the terminology of Aakeröy *et al.* (2002) both are in the *trans-trans* conformation.

The independent supermolecules H-bond together using the second amide donor and the carbonyl group from the propionic acid molecules located at the pyridine end of the supermolecules. This builds-up a chain in which successive supermolecules are aligned perpendicular to one another (Fig. 2a; H-bond dimensions are listed in Table 1). These motifs comprise all the conventional NH...O and OH...O hydrogen bonds in the crystal (see Table 1); additional CH...O interactions (C5A—H5A...O2U and C5B—H5B...O2V) are also formed within the

chains (Desiraju & Steiner, 1999).

Supermolecules in neighbouring chains are interleaved (Fig 2*b*). There are no direct hydrogen bonding interactions between interleaved supermolecules, though the pair of molecules shown in outline in Fig. 2*b* interact *via* a CH...O interaction; (C2A—H2A...O3T; other such interactions involve C2B—H2B...O3S).

The array of interleaving chains builds-up a layer which is parallel to (0 1 0) (Fig. 2*c*). The layers are connected *via* CH...O hydrogen bonds involving pairs of C4T—H4T1...O2T and C4V—H4V1...O2S interactions disposed about inversion centres (for clarity these are not shown in Fig. 2*c*).

Experimental

All materials were obtained from Aldrich and used as received. Isonicotinamide (0.50 g, 4.10 mmol) was dissolved in an excess of propionic acid (2.40 g, 32.43 mmol) and warmed until all the solid dissolved. The solution was cooled to room temperature producing colourless laths.

Crystal data

$C_6H_6N_2O \cdot 2(C_3H_6O_2)$

$M_r = 270.28$

Triclinic

$P\bar{1}$

$a = 10.038 (3) \text{ \AA}$

$b = 11.559 (4) \text{ \AA}$

$c = 12.740 (4) \text{ \AA}$

$\alpha = 103.203 (6)^\circ$

$\beta = 90.140 (6)^\circ$

$\gamma = 102.247 (6)^\circ$

$V = 1404.5 (8) \text{ \AA}^3$

$Z = 4$

$D_x = 1.278 \text{ Mg m}^{-3}$

D_m not measured

Mo $K\alpha$ radiation

$\lambda = 0.71073 \text{ \AA}$

Cell parameters from 1107 reflections

$\theta = 2.58\text{--}22.20^\circ$

$\mu = 0.100 \text{ mm}^{-1}$

$T = 150 (2) \text{ K}$

Lath

Colourless

$0.75 \times 0.20 \times 0.08 \text{ mm}$

Data collection

CCD area detector diffractometer

3362 reflections with

Phi and ω scans>2 $\sigma(I)$

Absorption correction:

 $R_{\text{int}} = 0.0441$

multi-scan SADABS (Sheldrick, 2004)

 $\theta_{\text{max}} = 28.92^\circ$ **Please give reference** $h = -13 \rightarrow 13$ $T_{\text{min}} = 0.783, T_{\text{max}} = 1.000$ $k = -15 \rightarrow 15$

12519 measured reflections

 $l = -17 \rightarrow 17$

6498 independent reflections

intensity decay: none

RefinementRefinement on F^2 $w = 1/[\sigma^2(F_o^2) + (0.0681P)^2 + 0.3798P]$ $R[F^2 > 2\sigma(F^2)] = 0.0876$ where $P = (F_o^2 + 2F_c^2)/3$ $wR(F^2) = 0.1975$ $(\Delta/\sigma)_{\text{max}} = 0.000$ $S = 1.044$ $\Delta\rho_{\text{max}} = 0.362 \text{ e } \text{\AA}^{-3}$

6498 reflections

 $\Delta\rho_{\text{min}} = -0.209 \text{ e } \text{\AA}^{-3}$

379 parameters

Extinction correction: none

riding or All H-atom parameters refined

Scattering factors from *International Tables for Crystallography* (Vol. C)Table 1. *Hydrogen-bonding geometry* ($\text{\AA}, ^\circ$)

$D-H \cdots A$	$D-H$	$H \cdots A$	$D \cdots A$	$D-H \cdots A$
O3S—H3S \cdots O8A	0.79 (4)	1.86 (4)	2.639 (4)	170 (4)
O3T—H3T \cdots O8B	0.76 (5)	1.89 (5)	2.639 (4)	169 (5)
O3U—H3U \cdots N1B ⁱ	0.87 (4)	1.78 (4)	2.649 (4)	177 (5)
O3V—H3V \cdots N1A ⁱⁱ	0.87 (5)	1.79 (5)	2.657 (4)	174 (5)
N9A—H91A \cdots O2S	0.96 (5)	1.92 (4)	2.868 (4)	170 (5)
N9B—H91B \cdots O2T	0.93 (4)	1.96 (4)	2.880 (4)	168 (3)
N9A—H92A \cdots O2U ⁱⁱⁱ	0.92 (3)	2.02 (3)	2.901 (4)	161 (3)
N9B—H92B \cdots O2V	0.93 (3)	2.01 (3)	2.900 (4)	160 (3)
C2A—H2A \cdots O3T ^{iv}	0.95	2.50	3.267 (5)	138
C2B—H2B \cdots O3S ^v	0.95	2.51	3.281 (5)	138
C5A—H5A \cdots O2U ⁱⁱⁱ	0.95	2.40	3.328 (4)	167
C5B—H5B \cdots O2V	0.95	2.39	3.322 (4)	168
C6A—H6A \cdots O2V ^{vi}	0.95	2.73	3.348 (4)	123
C6B—H6B \cdots O2U ⁱ	0.95	2.72	3.333 (4)	123
C4T—H4T1 \cdots O2T ^{vii}	0.99	2.58	3.513 (5)	157
C4V—H4V1 \cdots O2S ^{viii}	0.99	2.57	3.551 (4)	170

Symmetry codes: (i) $1-x, 2-y, -z$; (ii) $1+x, 1+y, z-1$; (iii) $1-x, 1-y, 1-z$; (iv) $x-1, y-1, z$; (v) $x, 1+y, z$; (vi) $x-1, y-1, 1+z$; (vii) $2-x, 1-y, -z$; (viii) $x, y, z-1$.

X-ray diffraction intensities were collected on a Bruker SMART APEX CCD diffractometer equipped with an Oxford Cryosystems low-temperature device (Cosier & Glazer, 1986). H-atoms were placed on C-atoms in calculated positions [with $U_{\text{iso}}(\text{H}) = 1.2U_{\text{eq}}(\text{C})$] and allowed to ride on their parent atoms. Amide and hydroxyl H-atoms were located in difference maps and refined freely, the former subject to the restraint $r(\text{N—H}) = 0.95(3)$. All non-H atoms were modelled with anisotropic displacement parameters.

Data collection: SMART (Bruker–Nonius, 2001). Cell refinement: SMART. Data reduction: SAINT (Bruker–Nonius, 2003). Program(s) used to solve structure: *SHELXTL* (Sheldrick, 2001). Program(s) used to refine structure: *SHELXTL*. Molecular graphics: *SHELXTL MERCURY* (Taylor & Macrae, 2001). Software used to prepare material for publication: *SHELXTL EnCIFer* (CCDC, 2004) *PLATON* (Spek, 2004) and incorporated into WinGX (Farrugia, 1999).

We thank the EPSRC, The University of Edinburgh and The Cambridge Crystallographic Data Centre for funding.

References

- Aakeröy, C. B., Beatty, A. M. & Helfrich, B. A. (2002). *J. Am. Chem. Soc.* **124**, 14425–14432.
- Bernstein, J., Davis, R. E., Shimoni, L. & Chang, N—L. (1995). *Angew. Chem. Int. Ed. Engl.* **34**, 1555–1573.
- Bruker-Nonius (2001). SMART, version 5.624. Area-Detector Software Package, Madison, Wisconsin, USA.
- Bruker-Nonius (2003). SAINT, Version 7. Area-Detector Integration Software, Madison, Wisconsin, USA.
- CCDC (2002). EnCIFer. Program for editing cifs, version 1.1. Cambridge Crystallographic Data Centre, 12 Union Road, Cambridge, England.
- Cosier, J. & Glazer, A. M. (1986). *J. Appl. Cryst.* **19**, 105–107.
- Desiraju, G. R. & Steiner, T. (1999). *The Weak Hydrogen Bond*. IUCr Monographs on Crystallography No. 9. Oxford University Press, Oxford, UK.
- Farrugia, L. J. (1999). *J. Appl. Cryst.* **32**, 837–838.
- Oswald, I. D. H., Motherwell, W. D. S. & Parsons, S. (2004). Submitted for publication.
- Sheldrick, G. M. (2001). *SHELXTL* version 6.01. University of Göttingen, Germany and Bruker-Nonius Inc., Madison, Wisconsin, USA.
- Sheldrick, G. M. (2004). *SADABS*. University of Göttingen, Germany.
- Spek, A. L. (2004). *PLATON*, Utrecht University, Utrecht, The Netherlands.
- Taylor, R. & Macrae, C. F. (2001). *Acta Cryst.* **B57**, 815–827.

Fig. 1: ‘Supermolecules’ are formed in the crystal structure of II, which consisting of one isonicotinamide and two acids hydrogen-bonded to the pyridine and amide functions. There are two crystallographically independent supermolecules these are shown in (a) and (b) with atomic numbering. Probability ellipsoids enclose 30% probability surfaces. Conventional hydrogen bonds are shown in heavy dashes, and the H···O distances span 1.78 (4) to 1.96 (4) Å (see Table 1). The CH...O hydrogen bonds (shown as open dashes) quite weak for this type of interaction (2.73 and 2.72 Å).

Fig. 2: Packing in the crystal structure of II. (a) Hydrogen bonds link spermolecules into chains. This view is approximately along (0 1 0). (b) Successive chains are interleaved. Supermolecules from two neighbouring chains are shown in outline. Molecules A, S and V are vertical, molecules B, T and U are horizontal. This forms layers which are parallel to the (0 1 0) planes (c).

Supplementary data

The tables of data shown below are not normally printed in *Acta Cryst. Section C* but the data will be available electronically *via* the online contents pages at

<http://journals.iucr.org/c/journalhomepage.html>

Table S1. Fractional atomic coordinates and equivalent isotropic displacement parameters (\AA^2)

$$U_{\text{eq}} = (1/3)\Sigma_i\Sigma_j U^{ij} a^i a^j a_i \cdot a_j.$$

	<i>x</i>	<i>y</i>	<i>z</i>	<i>U</i> _{eq}
N1A	0.0374 (3)	-0.1364 (2)	0.5184 (2)	0.0340 (6)
C2A	0.0899 (3)	-0.1354 (3)	0.4224 (3)	0.0399 (9)
H2A	0.0424	-0.1899	0.3598	0.048
C3A	0.2125 (3)	-0.0566 (3)	0.4114 (3)	0.0367 (8)
H3A	0.2482	-0.0576	0.3423	0.044
C4A	0.2807 (3)	0.0225 (3)	0.5023 (2)	0.0307 (7)
C5A	0.2266 (3)	0.0211 (3)	0.6018 (3)	0.0358 (8)
H5A	0.2724	0.0739	0.6659	0.043
C6A	0.1023 (3)	-0.0605 (3)	0.6056 (3)	0.0372 (8)
H6A	0.0635	-0.0610	0.6734	0.045
C7A	0.4134 (3)	0.1076 (3)	0.4875 (3)	0.0300 (7)
O8A	0.4515 (2)	0.1028 (2)	0.39475 (18)	0.0422 (6)
N9A	0.4801 (3)	0.1821 (3)	0.5743 (2)	0.0400 (7)
H91A	0.559 (4)	0.239 (4)	0.561 (4)	0.13 (2)
H92A	0.448 (4)	0.177 (4)	0.641 (2)	0.075 (14)
N1B	0.6050 (2)	1.1345 (2)	-0.0179 (2)	0.0347 (7)
C2B	0.6559 (3)	1.1321 (3)	0.0769 (3)	0.0363 (8)
H2B	0.6352	1.1865	0.1396	0.044
C3B	0.7394 (3)	1.0525 (3)	0.0886 (3)	0.0372 (8)
H3B	0.7738	1.0521	0.1580	0.045
C4B	0.7705 (3)	0.9749 (3)	-0.0022 (2)	0.0318 (8)
C5B	0.7187 (3)	0.9781 (3)	-0.1016 (3)	0.0343 (8)
H5B	0.7395	0.9262	-0.1658	0.041
C6B	0.6340 (3)	1.0601 (3)	-0.1058 (3)	0.0358 (8)
H6B	0.5967	1.0620	-0.1738	0.043
C7B	0.8617 (3)	0.8898 (3)	0.0125 (3)	0.0315 (8)
O8B	0.9029 (2)	0.8942 (2)	0.10510 (18)	0.0435 (6)
N9B	0.8926 (3)	0.8168 (3)	-0.0743 (2)	0.0402 (7)
H91B	0.943 (4)	0.761 (3)	-0.064 (3)	0.079 (14)
H92B	0.855 (3)	0.817 (3)	-0.141 (2)	0.059 (11)
C1S	0.7475 (3)	0.3193 (3)	0.4192 (3)	0.0380 (8)
O2S	0.7115 (3)	0.3378 (2)	0.5096 (2)	0.0546 (7)
O3S	0.6802 (3)	0.2306 (2)	0.34051 (19)	0.0442 (7)
H3S	0.618 (4)	0.189 (3)	0.361 (3)	0.052 (13)
C4S	0.8744 (4)	0.3943 (3)	0.3861 (3)	0.0473 (9)
H4S1	0.8645	0.4799	0.4013	0.057
H4S2	0.9519	0.3916	0.4329	0.057
C5S	0.9112 (4)	0.3599 (4)	0.2720 (3)	0.0597 (11)
H5S1	0.9249	0.2763	0.2558	0.090
H5S2	0.9955	0.4155	0.2611	0.090
H5S3	0.8374	0.3652	0.2241	0.090
C1T	1.0981 (3)	0.6806 (3)	0.0803 (3)	0.0374 (8)
O2T	1.0571 (2)	0.6652 (2)	-0.0116 (2)	0.0521 (7)
O3T	1.0671 (3)	0.7648 (3)	0.1601 (2)	0.0468 (7)
H3T	1.029 (5)	0.809 (4)	0.145 (4)	0.10 (2)
C4T	1.1877 (4)	0.6048 (3)	0.1135 (3)	0.0468 (9)
H4T1	1.1369	0.5189	0.0955	0.056
H4T2	1.2686	0.6099	0.0691	0.056
C5T	1.2363 (4)	0.6365 (4)	0.2284 (3)	0.0621 (12)
H5T1	1.2872	0.7214	0.2480	0.093
H5T2	1.2960	0.5829	0.2395	0.093

H5T3	1.1579	0.6263	0.2736	0.093
C1U	0.5951 (3)	0.7137 (3)	0.1200 (3)	0.0331 (8)
O2U	0.5695 (2)	0.7875 (2)	0.19782 (18)	0.0417 (6)
O3U	0.5494 (3)	0.7069 (2)	0.02220 (19)	0.0440 (6)
H3U	0.496 (4)	0.757 (4)	0.021 (3)	0.086 (16)
C4U	0.6782 (3)	0.6226 (3)	0.1251 (3)	0.0442 (9)
H4U1	0.7507	0.6291	0.0730	0.053
H4U2	0.6191	0.5400	0.1026	0.053
C5U	0.7439 (4)	0.6374 (4)	0.2361 (3)	0.0574 (11)
H5U1	0.8006	0.7198	0.2602	0.086
H5U2	0.8010	0.5777	0.2326	0.086
H5U3	0.6727	0.6243	0.2873	0.086
C1V	0.7618 (3)	0.7141 (3)	-0.3789 (3)	0.0319 (8)
O2V	0.8246 (2)	0.7852 (2)	-0.30190 (18)	0.0417 (6)
O3V	0.8021 (3)	0.7075 (2)	-0.47843 (18)	0.0410 (6)
H3V	0.876 (5)	0.763 (4)	-0.479 (4)	0.11 (2)
C4V	0.6318 (3)	0.6233 (3)	-0.3745 (3)	0.0419 (9)
H4V1	0.6485	0.5401	-0.3985	0.050
H4V2	0.5621	0.6322	-0.4254	0.050
C5V	0.5763 (4)	0.6378 (4)	-0.2626 (3)	0.0572 (11)
H5V1	0.6443	0.6283	-0.2118	0.086
H5V2	0.4925	0.5756	-0.2645	0.086
H5V3	0.5561	0.7189	-0.2393	0.086

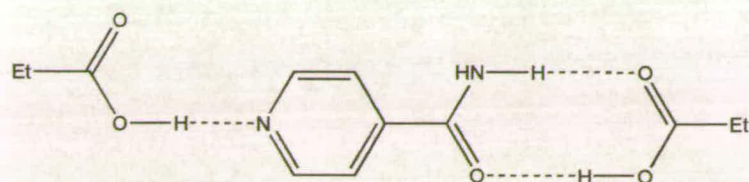
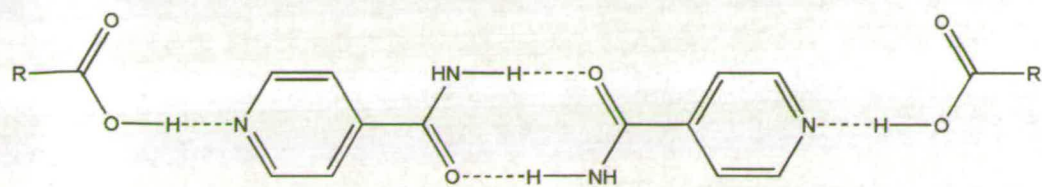
Table S2. Anisotropic displacement parameters (\AA^2)

	U_{11}	U_{22}	U_{33}	U_{12}	U_{13}	U_{23}
N1A	0.0336 (15)	0.0404 (17)	0.0301 (16)	0.0147 (13)	0.0006 (12)	0.0068 (13)
C2A	0.044 (2)	0.048 (2)	0.0270 (19)	0.0148 (18)	0.0026 (15)	0.0027 (16)
C3A	0.039 (2)	0.043 (2)	0.0292 (19)	0.0145 (16)	0.0062 (15)	0.0059 (16)
C4A	0.0311 (18)	0.0397 (19)	0.0268 (18)	0.0192 (15)	0.0031 (14)	0.0082 (15)
C5A	0.040 (2)	0.041 (2)	0.0266 (18)	0.0118 (16)	-0.0037 (14)	0.0062 (15)
C6A	0.038 (2)	0.051 (2)	0.0258 (18)	0.0168 (17)	0.0034 (15)	0.0081 (16)
C7A	0.0331 (18)	0.0347 (19)	0.0273 (18)	0.0168 (15)	0.0033 (14)	0.0086 (15)
O8A	0.0419 (14)	0.0506 (15)	0.0308 (14)	0.0072 (11)	0.0074 (11)	0.0053 (11)
N9A	0.0385 (18)	0.053 (2)	0.0293 (17)	0.0112 (15)	0.0020 (14)	0.0098 (15)
N1B	0.0327 (15)	0.0389 (17)	0.0283 (16)	-0.0003 (12)	0.0036 (12)	0.0066 (13)
C2B	0.0356 (19)	0.042 (2)	0.0260 (18)	0.0049 (16)	0.0013 (14)	0.0008 (15)
C3B	0.0333 (19)	0.045 (2)	0.0300 (19)	0.0028 (16)	-0.0016 (14)	0.0074 (16)
C4B	0.0247 (17)	0.0384 (19)	0.0256 (18)	-0.0044 (14)	0.0012 (13)	0.0041 (15)
C5B	0.0316 (18)	0.041 (2)	0.0261 (18)	0.0027 (15)	0.0051 (14)	0.0039 (15)
C6B	0.0305 (18)	0.047 (2)	0.0277 (19)	0.0027 (16)	0.0031 (14)	0.0097 (16)
C7B	0.0240 (17)	0.040 (2)	0.0267 (18)	0.0002 (14)	0.0046 (14)	0.0058 (15)
O8B	0.0443 (14)	0.0561 (16)	0.0298 (14)	0.0148 (12)	-0.0054 (11)	0.0060 (12)
N9B	0.0369 (17)	0.057 (2)	0.0296 (17)	0.0164 (15)	0.0024 (13)	0.0105 (15)
C1S	0.037 (2)	0.036 (2)	0.041 (2)	0.0110 (16)	-0.0024 (17)	0.0075 (17)
O2S	0.0603 (17)	0.0601 (18)	0.0367 (16)	0.0011 (13)	0.0122 (13)	0.0086 (13)
O3S	0.0406 (15)	0.0520 (17)	0.0380 (16)	0.0037 (13)	0.0121 (12)	0.0123 (14)
C4S	0.048 (2)	0.046 (2)	0.048 (2)	0.0055 (18)	0.0052 (18)	0.0144 (19)
C5S	0.051 (2)	0.051 (3)	0.068 (3)	-0.001 (2)	0.015 (2)	0.007 (2)
C1T	0.0295 (18)	0.038 (2)	0.044 (2)	0.0010 (15)	0.0086 (16)	0.0140 (18)
O2T	0.0605 (17)	0.0616 (17)	0.0381 (16)	0.0204 (13)	-0.0049 (13)	0.0128 (13)
O3T	0.0473 (16)	0.0573 (18)	0.0402 (16)	0.0202 (14)	-0.0039 (12)	0.0122 (14)
C4T	0.041 (2)	0.053 (2)	0.048 (2)	0.0085 (18)	-0.0012 (17)	0.0167 (19)
C5T	0.071 (3)	0.062 (3)	0.055 (3)	0.027 (2)	-0.011 (2)	0.005 (2)
C1U	0.0280 (17)	0.038 (2)	0.032 (2)	0.0005 (15)	0.0009 (14)	0.0135 (16)
O2U	0.0442 (14)	0.0499 (15)	0.0316 (14)	0.0156 (12)	0.0041 (11)	0.0058 (12)
O3U	0.0492 (15)	0.0549 (17)	0.0311 (14)	0.0223 (14)	0.0019 (11)	0.0066 (12)
C4U	0.043 (2)	0.044 (2)	0.050 (2)	0.0134 (17)	0.0062 (17)	0.0182 (18)
C5U	0.055 (3)	0.055 (3)	0.069 (3)	0.018 (2)	-0.008 (2)	0.023 (2)
C1V	0.0361 (19)	0.038 (2)	0.0297 (19)	0.0199 (16)	0.0084 (15)	0.0135 (16)
O2V	0.0384 (13)	0.0551 (16)	0.0276 (14)	0.0075 (12)	0.0012 (11)	0.0042 (12)
O3V	0.0427 (15)	0.0500 (16)	0.0279 (13)	0.0070 (13)	0.0062 (11)	0.0070 (11)
C4V	0.041 (2)	0.039 (2)	0.048 (2)	0.0101 (17)	0.0103 (16)	0.0142 (17)
C5V	0.051 (2)	0.059 (3)	0.064 (3)	0.010 (2)	0.023 (2)	0.022 (2)

Table S3. Geometric parameters (\AA , $^\circ$)

N1A—C6A	1.318 (4)	C4S—H4S1	0.9900
N1A—C2A	1.333 (4)	C4S—H4S2	0.9900
C2A—C3A	1.396 (5)	C5S—H5S1	0.9800
C2A—H2A	0.9500	C5S—H5S2	0.9800
C3A—C4A	1.375 (4)	C5S—H5S3	0.9800
C3A—H3A	0.9500	C1T—O2T	1.201 (4)
C4A—C5A	1.383 (4)	C1T—O3T	1.325 (4)
C4A—C7A	1.519 (4)	C1T—C4T	1.502 (5)
C5A—C6A	1.404 (4)	O3T—H3T	0.75 (5)
C5A—H5A	0.9500	C4T—C5T	1.479 (5)
C6A—H6A	0.9500	C4T—H4T1	0.9900
C7A—O8A	1.235 (4)	C4T—H4T2	0.9900
C7A—N9A	1.315 (4)	C5T—H5T1	0.9800
N9A—H91A	0.96 (3)	C5T—H5T2	0.9800
N9A—H92A	0.91 (2)	C5T—H5T3	0.9800
N1B—C2B	1.318 (4)	C1U—O2U	1.218 (4)
N1B—C6B	1.321 (4)	C1U—O3U	1.307 (4)
C2B—C3B	1.401 (4)	C1U—C4U	1.488 (5)
C2B—H2B	0.9500	O3U—H3U	0.87 (4)
C3B—C4B	1.375 (4)	C4U—C5U	1.517 (5)
C3B—H3B	0.9500	C4U—H4U1	0.9900
C4B—C5B	1.378 (4)	C4U—H4U2	0.9900
C4B—C7B	1.518 (4)	C5U—H5U1	0.9800
C5B—C6B	1.411 (4)	C5U—H5U2	0.9800
C5B—H5B	0.9500	C5U—H5U3	0.9800
C6B—H6B	0.9500	C1V—O2V	1.201 (4)
C7B—O8B	1.236 (4)	C1V—O3V	1.323 (4)
C7B—N9B	1.310 (4)	C1V—C4V	1.502 (4)
N9B—H91B	0.93 (2)	O3V—H3V	0.87 (5)
N9B—H92B	0.93 (2)	C4V—C5V	1.518 (5)
C1S—O2S	1.194 (4)	C4V—H4V1	0.9900
C1S—O3S	1.321 (4)	C4V—H4V2	0.9900
C1S—C4S	1.501 (5)	C5V—H5V1	0.9800
O3S—H3S	0.79 (4)	C5V—H5V2	0.9800
C4S—C5S	1.485 (5)	C5V—H5V3	0.9800

C6A—N1A—C2A	119.4 (3)	C4S—C5S—H5S1	109.5
N1A—C2A—C3A	121.9 (3)	C4S—C5S—H5S2	109.5
N1A—C2A—H2A	119.1	H5S1—C5S—H5S2	109.5
C3A—C2A—H2A	119.1	C4S—C5S—H5S3	109.5
C4A—C3A—C2A	118.9 (3)	H5S1—C5S—H5S3	109.5
C4A—C3A—H3A	120.5	H5S2—C5S—H5S3	109.5
C2A—C3A—H3A	120.5	O2T—C1T—O3T	122.7 (3)
C3A—C4A—C5A	119.2 (3)	O2T—C1T—C4T	122.4 (3)
C3A—C4A—C7A	117.6 (3)	O3T—C1T—C4T	114.9 (3)
C5A—C4A—C7A	123.2 (3)	C1T—O3T—H3T	117 (4)
C4A—C5A—C6A	118.2 (3)	C5T—C4T—C1T	117.1 (3)
C4A—C5A—H5A	120.9	C5T—C4T—H4T1	108.0
C6A—C5A—H5A	120.9	C1T—C4T—H4T1	108.0
N1A—C6A—C5A	122.4 (3)	C5T—C4T—H4T2	108.0
N1A—C6A—H6A	118.8	C1T—C4T—H4T2	108.0
C5A—C6A—H6A	118.8	H4T1—C4T—H4T2	107.3
O8A—C7A—N9A	124.2 (3)	C4T—C5T—H5T1	109.5
O8A—C7A—C4A	118.0 (3)	C4T—C5T—H5T2	109.5
N9A—C7A—C4A	117.8 (3)	H5T1—C5T—H5T2	109.5
C7A—N9A—H91A	115 (3)	C4T—C5T—H5T3	109.5
C7A—N9A—H92A	119 (3)	H5T1—C5T—H5T3	109.5
H91A—N9A—H92A	126 (4)	H5T2—C5T—H5T3	109.5
C2B—N1B—C6B	119.4 (3)	O2U—C1U—O3U	122.0 (3)
N1B—C2B—C3B	122.4 (3)	O2U—C1U—C4U	124.7 (3)
N1B—C2B—H2B	118.8	O3U—C1U—C4U	113.2 (3)
C3B—C2B—H2B	118.8	C1U—O3U—H3U	112 (3)
C4B—C3B—C2B	118.7 (3)	C1U—C4U—C5U	113.9 (3)
C4B—C3B—H3B	120.6	C1U—C4U—H4U1	108.8
C2B—C3B—H3B	120.6	C5U—C4U—H4U1	108.8
C3B—C4B—C5B	118.9 (3)	C1U—C4U—H4U2	108.8
C3B—C4B—C7B	117.8 (3)	C5U—C4U—H4U2	108.8
C5B—C4B—C7B	123.3 (3)	H4U1—C4U—H4U2	107.7
C4B—C5B—C6B	118.6 (3)	C4U—C5U—H5U1	109.5
C4B—C5B—H5B	120.7	C4U—C5U—H5U2	109.5
C6B—C5B—H5B	120.7	H5U1—C5U—H5U2	109.5
N1B—C6B—C5B	121.9 (3)	C4U—C5U—H5U3	109.5
N1B—C6B—H6B	119.0	H5U1—C5U—H5U3	109.5
C5B—C6B—H6B	119.0	H5U2—C5U—H5U3	109.5
O8B—C7B—N9B	124.1 (3)	O2V—C1V—O3V	122.6 (3)
O8B—C7B—C4B	118.2 (3)	O2V—C1V—C4V	125.0 (3)
N9B—C7B—C4B	117.7 (3)	O3V—C1V—C4V	112.5 (3)
C7B—N9B—H91B	117 (3)	C1V—O3V—H3V	110 (3)
C7B—N9B—H92B	119 (2)	C1V—C4V—C5V	113.2 (3)
H91B—N9B—H92B	123 (3)	C1V—C4V—H4V1	108.9
O2S—C1S—O3S	122.9 (3)	C5V—C4V—H4V1	108.9
O2S—C1S—C4S	122.5 (3)	C1V—C4V—H4V2	108.9
O3S—C1S—C4S	114.5 (3)	C5V—C4V—H4V2	108.9
C1S—O3S—H3S	112 (3)	H4V1—C4V—H4V2	107.7
C5S—C4S—C1S	117.6 (3)	C4V—C5V—H5V1	109.5
C5S—C4S—H4S1	107.9	C4V—C5V—H5V2	109.5
C1S—C4S—H4S1	107.9	H5V1—C5V—H5V2	109.5
C5S—C4S—H4S2	107.9	C4V—C5V—H5V3	109.5
C1S—C4S—H4S2	107.9	H5V1—C5V—H5V3	109.5
H4S1—C4S—H4S2	107.2	H5V2—C5V—H5V3	109.5



Scheme 1: Conventional structure diagram of robust building block or 'supermolecule' consisting of two amide and two acid molecules, I, formed in a number of co-crystals of *isonicotinamide* and carboxylic acids (Aakeröy *et al.*, 2002). Many attempts to crystallise I from *isonicotinamide* and propionic acid yielded 'supermolecule' II.

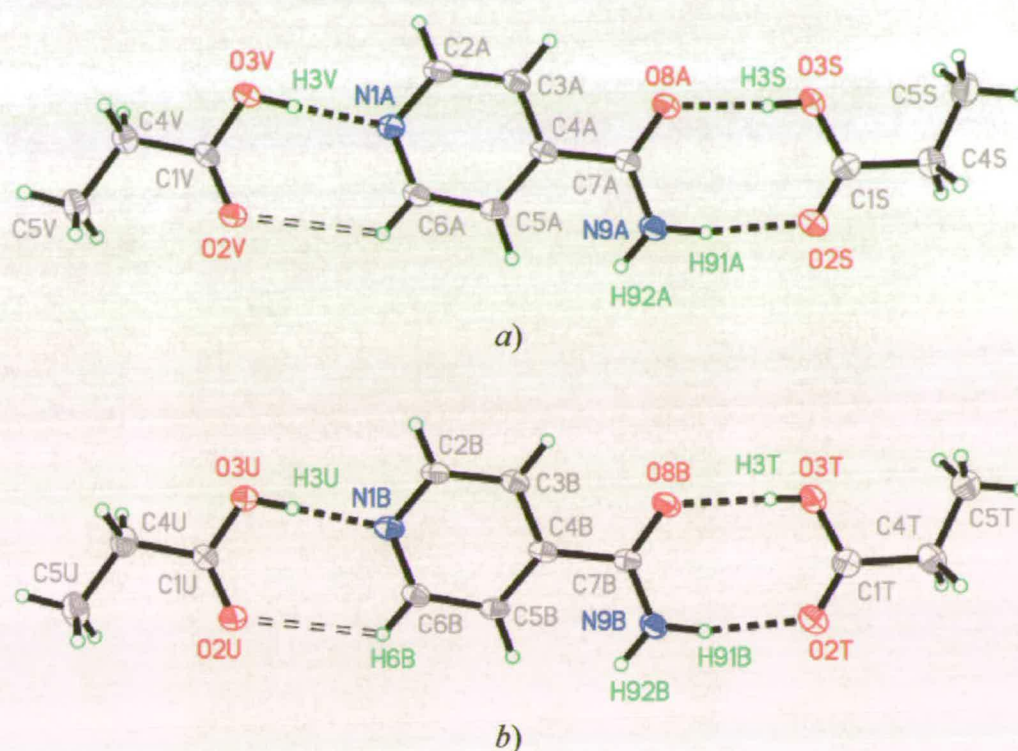
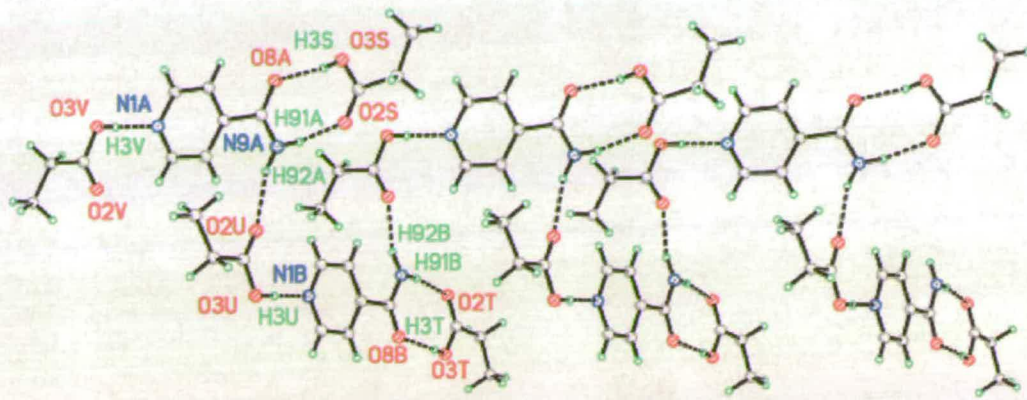
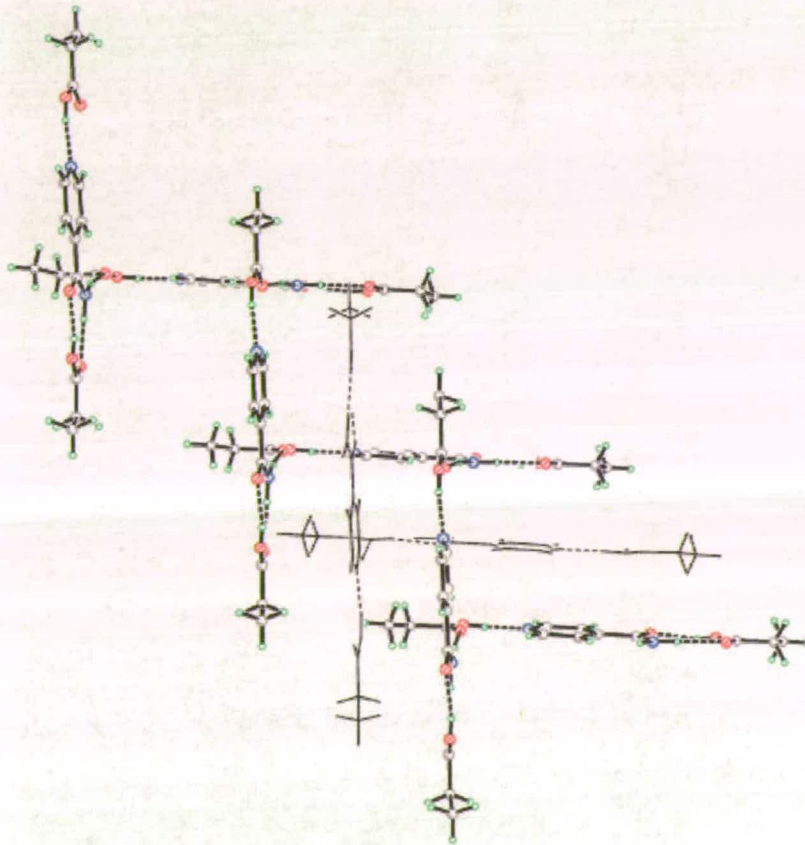


Figure 1: 'Supermolecules' are formed in the crystal structure of II, which consisting of one isonicotinamide and two acids hydrogen-bonded to the pyridine and amide functions. There are two crystallographically independent supermolecules these are shown in (a) and (b) with atomic numbering. Probability ellipsoids enclose 30% probability surfaces. Conventional hydrogen bonds are shown in heavy dashes, and the H...O distances span 1.78(4) to 1.96(4) Å (see table 1). The CH...O hydrogen bonds (shown as open dashes) quite weak for this type of interaction (2.73 and 2.72 Å).



a)



b)

Figure 2: Packing in the crystal structure of II. (a) Hydrogen bonds link supermolecules into chains. This view is approximately along (0 1 0). (b) Successive chains are interleaved. Supermolecules from two neighbouring chains are shown in outline. Molecules A, S and V are vertical, molecules B, T and U are horizontal.

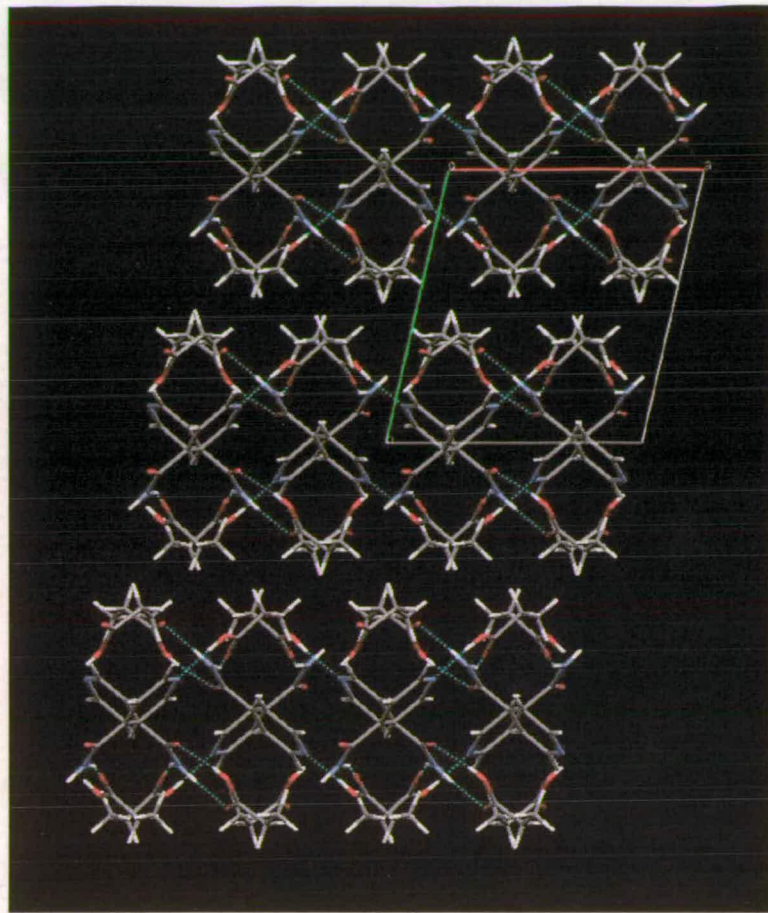


Figure 2c: The interleaved chains form layers, which are parallel to the (0 1 0) planes.

Acta Cryst. (2004). C60, 000–000

A 1:2 co-crystal of isonicotinic acid and formic acid

IAIN D. H. OSWALD,^a W. D. SAM MOTHERWELL^b AND SIMON PARSONS^a

^a*School of Chemistry, The University of Edinburgh, King's Buildings, West Mains Road, Edinburgh, Scotland, EH9 3JJ, and* ^b*Cambridge Crystallographic Data Centre, 12 Union Road, Cambridge, England, CB2 1EZ. E-mail: s.parsons@ed.ac.uk*

Abstract

Isonicotinamide has been shown to form many co-crystals with various guest molecules ranging from carboxylic acids to alcohols and amides. The carboxylic acid derivative, isonicotinic acid, forms very few co-crystals. We report the crystal structure of a co-crystal of isonicotinic acid and formic acid, formed with 1:2 stoichiometry. The structure is composed of chains of isonicotinic acid molecules interacting through a hydrogen bond between the acid and the pyridine moieties. Formic acid hydrogen bonds to the carbonyl group of isonicotinic acid with the second formic acid molecule hydrogen bonding to the carbonyl moiety of the first.

Comment

Isonicotinamide has been shown to crystallize with various molecules including carboxylic acids, alcohols and amides. Aakerøy *et al.* (2003) have associated polymorphism with an ability to form co-crystals, because it implies some flexibility in the types and geometries of interactions that a molecule can form. The existence of two polymorphic forms of isonicotinamide may therefore explain its propensity towards co-crystal formation.

Isonicotinic acid is related to isonicotinamide by substitution of the amide group by a carboxylic acid group. However, the physicochemical properties of isonicotinic acid are quite different: it is, for example, less soluble in common solvents, only one polymorph is known (Takusagawa & Shimada, 1976), and the only structurally authenticated co-crystal is with 3,5-dinitrosalicylic acid (AJECAT, Smith *et al.*, 2003). We now report the crystal structure of another co-crystal, isonicotinic acid: 2formic acid (I).

Crystallisation of isonicotinic acid with formic, acetic, propionic acids, formamide, acetamide and propionamide by conventional co-crystallisation methods failed to yield any new co-crystals, only isonicotinic acid itself. However, laser-assisted zone-refinement (Boese & Nussbaumer, 1994) of a frozen mixture of isonicotinic acid and formic acid at 250 K yielded a crystal of I.

I crystallises in space group $P\bar{1}$ with one molecule of isonicotinic acid and two molecules of formic acid in the asymmetric unit (Fig. 1). Hydrogen sites were clearly visible in difference maps, and the isonicotinic acid is in its zwitterionic tautomer in I; this contrasts with the crystal

structure isonicotinic acid itself, where the proton resides on the acid group. The formic acid molecules are present in the *anti* conformation.

The crystal structure of isonicotinic acid consists of chains of molecules interacting *via* OH...N hydrogen bonds in a head-to-tail fashion. The chains have a C(7) graph-set descriptor (Bernstein *et al.*, 1995). Weaker CH...O interactions are formed between the carbonyl group and a CH group adjacent to the N atom of the pyridine moiety. Further CH...O interactions link the chains into layers. (Fig. 2)

Likewise, in I, the isonicotinic acid molecules form C(7) chains through NH...O interactions. The chains run along the $[\bar{1} 0 1]$ direction (Fig. 3). In isonicotinic acid the C—N...O—C torsion angle formed between successive molecules in the C(7) chains is 178.4°; the corresponding value in I is 74.9 (4)°. The rotation about the OH...N H-bond breaks the supporting C—H...O interaction that is observed in isonicotinic acid. In addition, rather than being linear, as they are in isonicotinic acid, the chains display a shallow undulation. These features occur in order to accommodate two formic acid molecules, which link alternate members of the C(7) chain through discrete OH...O(carboxylate), OH...O(carboxylic acid) and CH...O(carboxylic acid) hydrogen bonds. The last of these involves the C2—H2 group adjacent to the nitrogen of the pyridinium ring.

In both isonicotinic acid and I the chains are surrounded by six other chains in a close-packed arrangement (Fig. 4a and b) with CH...O interactions formed between the chains. The network of CH...O interactions produces two-dimensional sheets in isonicotinic acid, but a more three-dimensional array in I. When viewed along the $[\bar{1} 0 1]$ direction the structure of I partitions so that formic acid molecules occupy regions at $b = 0, \frac{1}{2}, 1, \text{etc.}$, whilst the isonicotinic acid molecules occupy regions at $b = 1/4, 3/4 \text{ etc.}$. Overall the carbonyl moieties of both formic acid molecules are acceptors in two further CH...O interactions which link different chains into a three-dimensional array. This scheme means that one O atom (O22) does not accept any conventional hydrogen bonds, and instead takes part only in CH...O hydrogen bonds (H2...O22 2.51 Å; H11...O22 2.39 Å) (Fig. 5).

Experimental

Isonicotinic acid (0.50 g, 4.10 mmol) was dissolved in an excess of formic acid (1.50 g, 32.61 mmol) and drawn into a glass capillary (*o.d.* 0.32 mm). A polycrystalline sample was obtained on freezing the sample at 250 K and a crystal grown using the laser-assisted zone-refinement procedure of Boese and Nussbaumer (1994).

Crystal data

C₆H₅NO₂·2(CH₂O₂)

$M_r = 215.16$

Monoclinic

Cc

$a = 3.7154 (14) \text{ \AA}$

$b = 17.504 (7) \text{ \AA}$

$c = 14.444 (5) \text{ \AA}$

$\beta = 91.084 (7)^\circ$

$V = 939.2 (6) \text{ \AA}^3$

$Z = 4$

$D_x = 1.522 \text{ Mg m}^{-3}$

D_m not measured

Mo $K\alpha$ radiation

$\lambda = 0.71073 \text{ \AA}$

Cell parameters from 2233 reflections

$\theta = 3.45\text{--}28.31^\circ$

$\mu = 0.133 \text{ mm}^{-1}$

$T = 150 (2) \text{ K}$

Cylinder

Colourless

$1.00 \times 0.32 \times 0.32 \text{ mm}$

Data collection

CCD area detector diffractometer

Phi and ω scans

Absorption correction:

multi-scan SADABS (Sheldrick, 2004)

Please give reference

$T_{\min} = 0.737, T_{\max} = 1.000$

3981 measured reflections

2088 independent reflections

1939 reflections with

$>2\sigma(I)$

$R_{\text{int}} = 0.0370$

$\theta_{\text{max}} = 28.63^\circ$

$h = -4 \rightarrow 4$

$k = -23 \rightarrow 23$

$l = -18 \rightarrow 18$

intensity decay: none

Refinement

Refinement on F^2

$R[F^2 > 2\sigma(F^2)] = 0.0613$

$wR(F^2) = 0.1366$

$S = 1.213$

2088 reflections

149 parameters

riding/All H-atom parameters refined

$w = 1/[\sigma^2(F_o^2) + (0.0392P)^2 + 1.0260P]$

where $P = (F_o^2 + 2F_c^2)/3$

$(\Delta/\sigma)_{\text{max}} = 0.005$

$\Delta\rho_{\text{max}} = 0.283 \text{ e \AA}^{-3}$

$\Delta\rho_{\text{min}} = -0.264 \text{ e \AA}^{-3}$

Extinction correction: none

Scattering factors from *International Tables*

for *Crystallography* (Vol. C)

Absolute structure: Flack H D (1983), *Acta*

Cryst. A39, 876-881

Flack parameter = 1.4 (19)

Table 1. *Hydrogen-bonding geometry* (\AA , $^\circ$)

$D-H\cdots A$	$D-H$	$H\cdots A$	$D\cdots A$	$D-H\cdots A$
N1—H1 \cdots O41 ⁱ	0.79 (4)	1.84 (4)	2.606 (4)	162 (5)
O31—H31 \cdots O42	0.83 (5)	1.71 (5)	2.498 (4)	160 (5)
O32—H32 \cdots O21	0.84 (4)	1.80 (4)	2.618 (4)	163 (4)
C2—H2 \cdots O22 ⁱⁱ	0.95	2.51	3.430 (4)	163
C3—H3 \cdots O21 ⁱⁱⁱ	0.95	2.48	3.268 (4)	140
C6—H6 \cdots O32 ^{iv}	0.95	2.44	3.150 (5)	131
C11—H11 \cdots O22 ^v	0.95	2.39	3.342 (5)	178
C12—H12 \cdots O42 ^{vi}	0.95	2.57	3.450 (5)	154

Symmetry codes: (i) $\frac{1}{2} + x, \frac{1}{2} - y, \frac{1}{2} + z$; (ii) $1 + x, y, 1 + z$; (iii) $x, 1 - y, \frac{1}{2} + z$; (iv) $\frac{3}{2} + x, \frac{1}{2} - y, \frac{1}{2} + z$; (v) $1 + x, 1 - y, \frac{1}{2} + z$; (vi) $x, 1 - y, z - \frac{1}{2}$.

X-ray diffraction intensities were collected on a Bruker SMART APEX CCD diffractometer equipped with an Oxford Cryosystems low-temperature device (Cosier & Glazer, 1986). H-atoms were placed on C-atoms in calculated positions [with $U_{\text{iso}}(\text{H}) = 1.2U_{\text{eq}}(\text{C})$] and allowed to ride on their parent atoms. Hydroxyl H-atoms were located in difference maps and refined freely subject to the restraint $r(\text{O—H}) = 0.85$ (3). All non-H atoms were modelled with anisotropic displacement parameters.

Data collection: SMART (Bruker–Nonius, 2001). Cell refinement: SMART. Data reduction: SAINT (Bruker–Nonius, 2003). Program(s) used to solve structure: *SHELXTL* (Sheldrick, 2001). Program(s) used to refine structure: *SHELXTL*. Molecular graphics: *SHELXTL* MERCURY (Taylor & Macrae, 2001). Software used to prepare material for publication: *SHELXTL* EnCIFer (CCDC, 2004) *PLATON* (Spek, 2004) as incorporated into WinGX (Farrugia, 1999).

We thank the EPSRC, The University of Edinburgh and The Cambridge Crystallographic Data Centre for funding.

References

- Aakeröy, C. B., Beatty, A. M., Helfrich, B. A. & Nieuwenhuyzen, M. (2003). *Cryst. Growth & Des.*, **3**(2), 159–165.
- Bernstein, J., Davis, R. E., Shimon, L. & Chang, N–L. (1995). *Angew. Chem. Int. Ed. Engl.* **34**, 1555–1573.
- Boese, R. & Nussbaumer, M. (1994). In *Correlations, Transformations, and Interactions in Organic Crystal Chemistry*, D. W. Jones & A. Katrusiak (Editors). (International Union of Crystallography, Crystallographic Symposia, 7), pages 20–37.
- Bruker-Nonius (2001). SMART, version 5.624. Area-Detector Software Package, Madison, Wisconsin, USA.
- Bruker-Nonius (2003). SAINT, Version 7. Area-Detector Integration Software, Madison, Wisconsin, USA.
- CCDC (2002). EnCIFer. Program for editing cifs, version 1.1. Cambridge Crystallographic Data Centre, 12 Union Road, Cambridge, England.
- Cosier, J. & Glazer, A. M. (1986). *J. Appl. Cryst.* **19**, 105–107.
- Farrugia, L. J. (1999). *J. Appl. Cryst.* **32**, 837–838.
- Sheldrick, G. M. (2001). *SHELXTL* version 6.01. University of Göttingen, Germany and Bruker-Nonius Inc., Madison, Wisconsin, USA.
- Sheldrick, G. M. (2004). SADABS. University of Göttingen, Germany.
- Smith, G., Wermuth, U. D., Healy, P. C. & White, J. M. (2003). *Aust. J. Chem.* **56**, 707–713.
- Spek, A. L. (2004). *PLATON*, Utrecht University, Utrecht, The Netherlands.
- Takusagawa, F. & Shimada, A. (1976). *Acta Cryst.* **B32**, 1925–1927.
- Taylor, R. & Macrae, C. F. (2001). *Acta Cryst.* **B57**, 815–827.

Fig. 1: The asymmetric unit of isonicotinic acid:2formic acid with numbering scheme. Colours scheme: Carbon green; nitrogen, blue; oxygen, red. The same colour scheme applies for all figures.

Fig. 2: The crystal structure of isonicotinic acid (Takusagawa & Shimada, 1976). The structure is composed of 1-D chains where the molecules are H-bonded through an OH...N interaction [1.51 (4) Å]. These interactions are stabilised by a secondary CH...O interaction [2.66 (3) Å]. Neighbouring chains are linked by more CH...O interactions [2.46 (3) Å].

Fig. 3: Intermolecular hydrogen bonding in I. The isonicotinic acid molecules are linked directly via O...HN hydrogen bonds forming a C(7) graph set. Pairs of formic acid molecules link alternate members of the C(7) chains. Geometric parameters are listed in Table 1 and in the caption to Fig. 5.

Fig. 4: a) Structure of isonicotinic acid viewed along the *b*-axis. b) Structure of I viewed along $[\bar{1} 0 1]$. In both crystal structures the chains (see Figs. 2 and 3) pack in a similar way, with chain

surrounded by six others.

Fig. 5: Neighbouring chains interact through a number of weaker interactions between the isonicotinic acid and formic acid molecules (H3···O21 2.48 Å; H2···O22 2.51 Å; H11···O22 2.39 Å). O22 does not accept any hydrogen bonds from NH or OH groups, and forms two CH...O interactions instead.

Supplementary data

The tables of data shown below are not normally printed in *Acta Cryst. Section C* but the data will be available electronically *via* the online contents pages at

<http://journals.iucr.org/c/journalhomepage.html>

Table S1. Fractional atomic coordinates and equivalent isotropic displacement parameters (Å²)

$$U_{\text{eq}} = (1/3)\Sigma_i\Sigma_j U^{ij} a^i a^j a_i \cdot a_j.$$

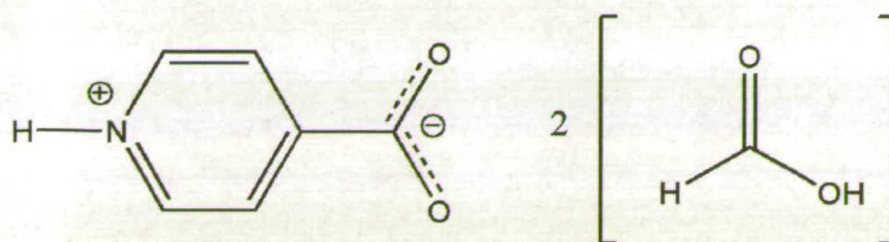
	<i>x</i>	<i>y</i>	<i>z</i>	<i>U</i> _{eq}
N1	0.3460 (8)	0.25689 (17)	1.1057 (2)	0.0196 (6)
H1	0.383 (13)	0.243 (3)	1.157 (3)	0.036 (14)
C2	0.1903 (10)	0.3250 (2)	1.0928 (2)	0.0220 (7)
H2	0.1548	0.3582	1.1438	0.026
C3	0.0816 (9)	0.3467 (2)	1.0049 (2)	0.0200 (7)
H3	-0.0324	0.3946	0.9949	0.024
C4	0.1402 (9)	0.29774 (19)	0.9313 (2)	0.0171 (6)
C5	0.3089 (8)	0.22727 (18)	0.9474 (2)	0.0171 (7)
H5	0.3524	0.1931	0.8978	0.020
C6	0.4103 (9)	0.20854 (19)	1.0369 (2)	0.0195 (7)
H6	0.5260	0.1612	1.0494	0.023
C41	0.0120 (9)	0.31800 (19)	0.8336 (2)	0.0182 (7)
O41	0.0976 (7)	0.27247 (15)	0.77155 (18)	0.0275 (6)
O42	-0.1719 (7)	0.37744 (15)	0.82566 (17)	0.0254 (6)
C11	-0.3244 (10)	0.4787 (2)	0.6494 (2)	0.0224 (7)
H11	-0.1661	0.5043	0.6916	0.027
O21	-0.4085 (7)	0.51108 (15)	0.57728 (18)	0.0289 (6)
O31	-0.4391 (8)	0.41189 (15)	0.67127 (18)	0.0251 (6)
H31	-0.351 (17)	0.390 (3)	0.717 (3)	0.08 (2)
C12	-0.6431 (11)	0.4561 (2)	0.3643 (3)	0.0258 (8)
H12	-0.4500	0.4914	0.3602	0.031
O22	-0.7645 (9)	0.42862 (18)	0.2942 (2)	0.0373 (7)
O32	-0.7662 (9)	0.43925 (18)	0.4459 (2)	0.0363 (7)
H32	-0.663 (11)	0.470 (2)	0.482 (3)	0.026 (11)

Table S2. Anisotropic displacement parameters (Å²)

	<i>U</i> ₁₁	<i>U</i> ₂₂	<i>U</i> ₃₃	<i>U</i> ₁₂	<i>U</i> ₁₃	<i>U</i> ₂₃
N1	0.0253 (15)	0.0246 (15)	0.0088 (13)	-0.0034 (12)	-0.0010 (11)	0.0044 (11)
C2	0.0262 (19)	0.0265 (18)	0.0132 (16)	0.0001 (14)	0.0015 (14)	-0.0038 (13)
C3	0.0206 (19)	0.0215 (16)	0.0179 (16)	-0.0021 (14)	-0.0019 (13)	0.0008 (14)
C4	0.0177 (16)	0.0216 (16)	0.0119 (15)	-0.0037 (13)	-0.0016 (12)	0.0028 (12)
C5	0.0221 (18)	0.0177 (15)	0.0114 (15)	-0.0019 (13)	0.0010 (13)	-0.0021 (13)
C6	0.0230 (18)	0.0182 (16)	0.0175 (17)	0.0011 (13)	0.0004 (13)	0.0077 (13)
C41	0.0220 (17)	0.0186 (15)	0.0136 (15)	-0.0053 (13)	-0.0065 (13)	0.0026 (13)
O41	0.0391 (16)	0.0303 (14)	0.0128 (12)	0.0044 (12)	-0.0063 (11)	-0.0010 (10)
O42	0.0384 (15)	0.0242 (13)	0.0135 (11)	0.0075 (11)	-0.0041 (10)	0.0060 (10)
C11	0.0233 (18)	0.0245 (18)	0.0194 (16)	0.0026 (14)	0.0007 (13)	0.0001 (13)
O21	0.0403 (17)	0.0253 (12)	0.0208 (13)	-0.0016 (12)	-0.0046 (11)	0.0072 (11)
O31	0.0390 (15)	0.0210 (12)	0.0152 (12)	0.0017 (11)	-0.0055 (10)	0.0074 (10)
C12	0.028 (2)	0.0271 (18)	0.0225 (18)	0.0011 (15)	0.0021 (15)	0.0034 (15)
O22	0.0452 (18)	0.0416 (16)	0.0246 (15)	0.0030 (15)	-0.0091 (13)	-0.0070 (13)
O32	0.0461 (18)	0.0382 (16)	0.0244 (14)	-0.0199 (14)	-0.0009 (12)	-0.0006 (12)

Table S3. Geometric parameters (\AA , $^\circ$)

N1—C6	1.330 (5)	C6—H6	0.9500
N1—C2	1.336 (5)	C41—O41	1.245 (4)
N1—H1	0.79 (5)	C41—O42	1.249 (4)
C2—C3	1.378 (5)	C11—O21	1.221 (4)
C2—H2	0.9500	C11—O31	1.287 (4)
C3—C4	1.386 (4)	C11—H11	0.9500
C3—H3	0.9500	O31—H31	0.83 (3)
C4—C5	1.401 (4)	C12—O22	1.201 (5)
C4—C41	1.524 (4)	C12—O32	1.306 (5)
C5—C6	1.379 (4)	C12—H12	0.9500
C5—H5	0.9500	O32—H32	0.83 (3)
C6—N1—C2	123.1 (3)	N1—C6—C5	119.9 (3)
C6—N1—H1	118 (4)	N1—C6—H6	120.0
C2—N1—H1	118 (4)	C5—C6—H6	120.0
N1—C2—C3	119.5 (3)	O41—C41—O42	127.9 (3)
N1—C2—H2	120.2	O41—C41—C4	116.0 (3)
C3—C2—H2	120.2	O42—C41—C4	116.1 (3)
C2—C3—C4	119.3 (3)	O21—C11—O31	123.4 (3)
C2—C3—H3	120.4	O21—C11—H11	118.3
C4—C3—H3	120.4	O31—C11—H11	118.3
C3—C4—C5	119.6 (3)	C11—O31—H31	119 (5)
C3—C4—C41	121.1 (3)	O22—C12—O32	122.6 (4)
C5—C4—C41	119.3 (3)	O22—C12—H12	118.7
C6—C5—C4	118.6 (3)	O32—C12—H12	118.7
C6—C5—H5	120.7	C12—O32—H32	105 (3)
C4—C5—H5	120.7		



Scheme 1: Conventional structure diagram for *isonicotinic acid:2formic acid* (I).

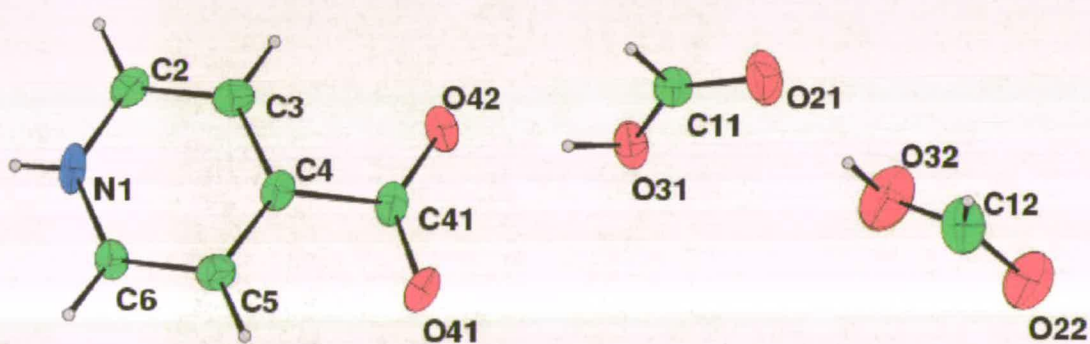


Figure 1: The asymmetric unit of *isonicotinic acid:2formic acid* with numbering scheme. Colours scheme: Carbon green; nitrogen, blue; oxygen, red. The same colour scheme applies for all figures.

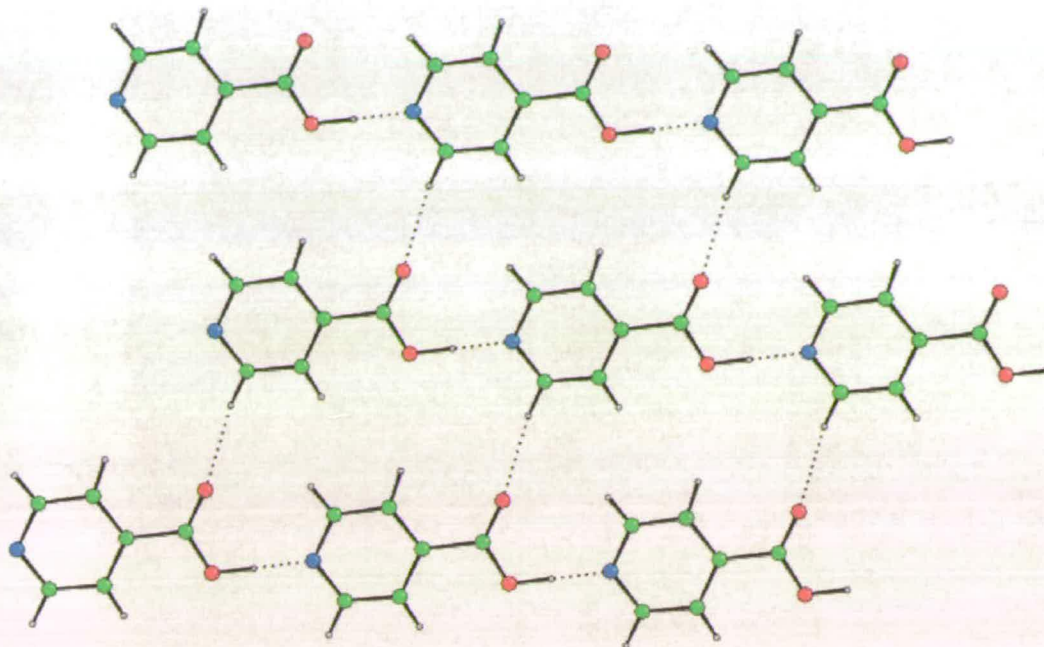


Figure 2: The crystal structure of isonicotinic acid (Takusagawa & Shimada, 1976). The structure is composed of 1-D chains where the molecules are H-bonded through an OH...N interaction [1.51(4) Å]. These interactions are stabilised by a secondary CH...O interaction [2.66(3) Å]. Neighbouring chains are linked by more CH...O interactions [2.46(3) Å].

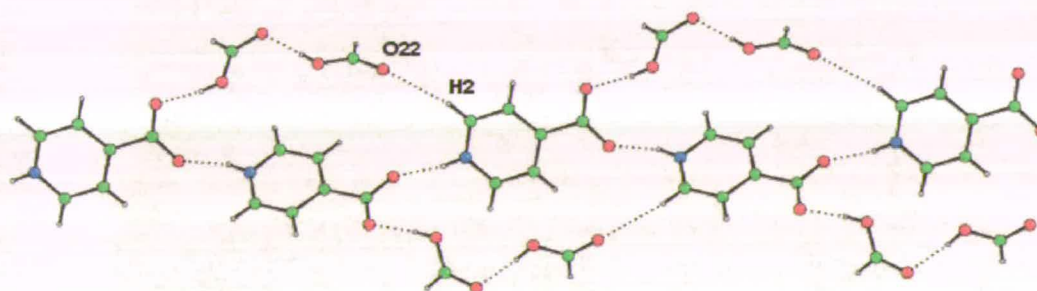


Figure 3: Intermolecular hydrogen bonding in I. The isonicotinic acid molecules are linked directly via O...HN hydrogen bonds forming a $C(7)$ graph set. Pairs of formic acid molecules link alternate members of the $C(7)$ chains. Geometric parameters are listed in Table 1 and in the caption to Figure 5.

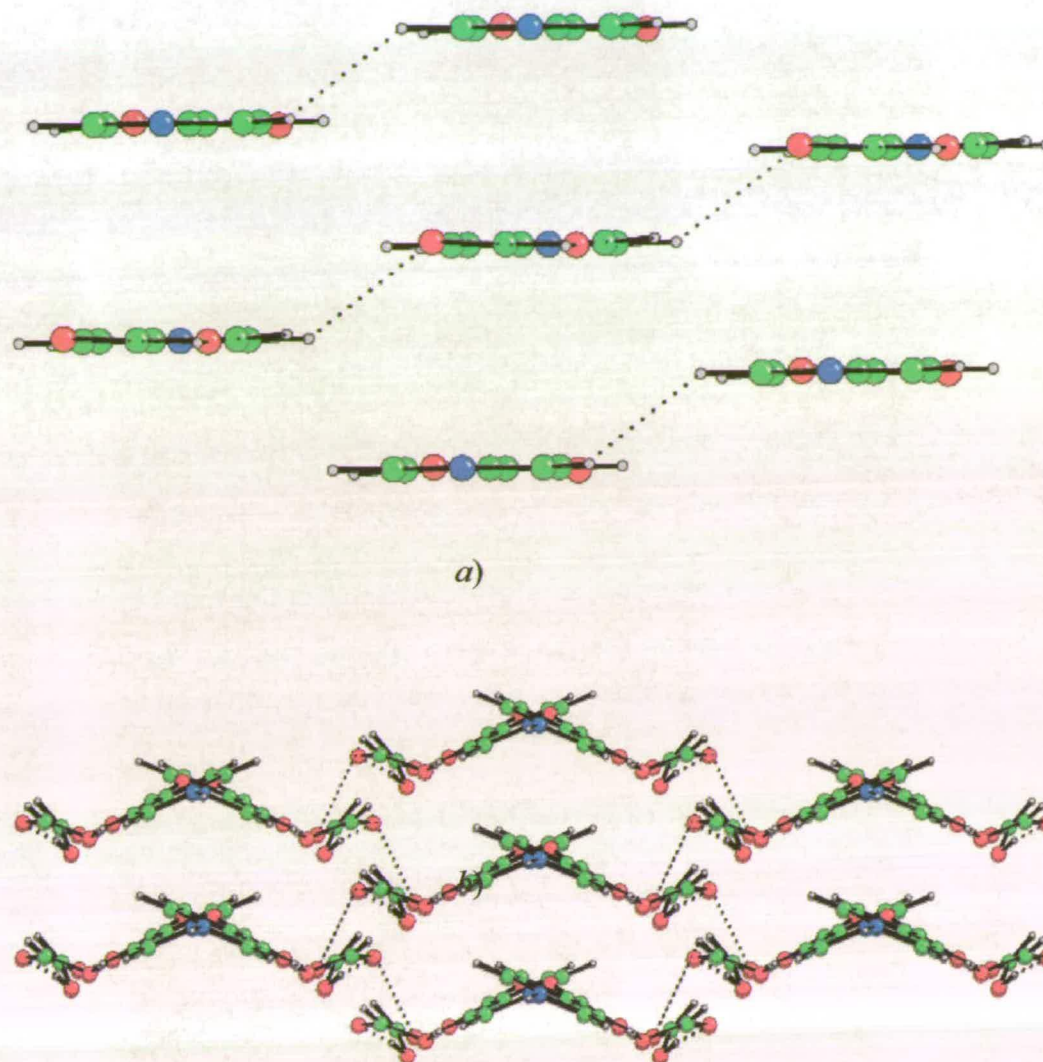


Figure 4: *a*) Structure of isonicotinic acid viewed along the b -axis. *b*) Structure of I viewed along $[1\ 0\ 1]$. In both crystal structures the chains (see Figures 2 and 3) pack in a similar way, with chain surrounded by six others.

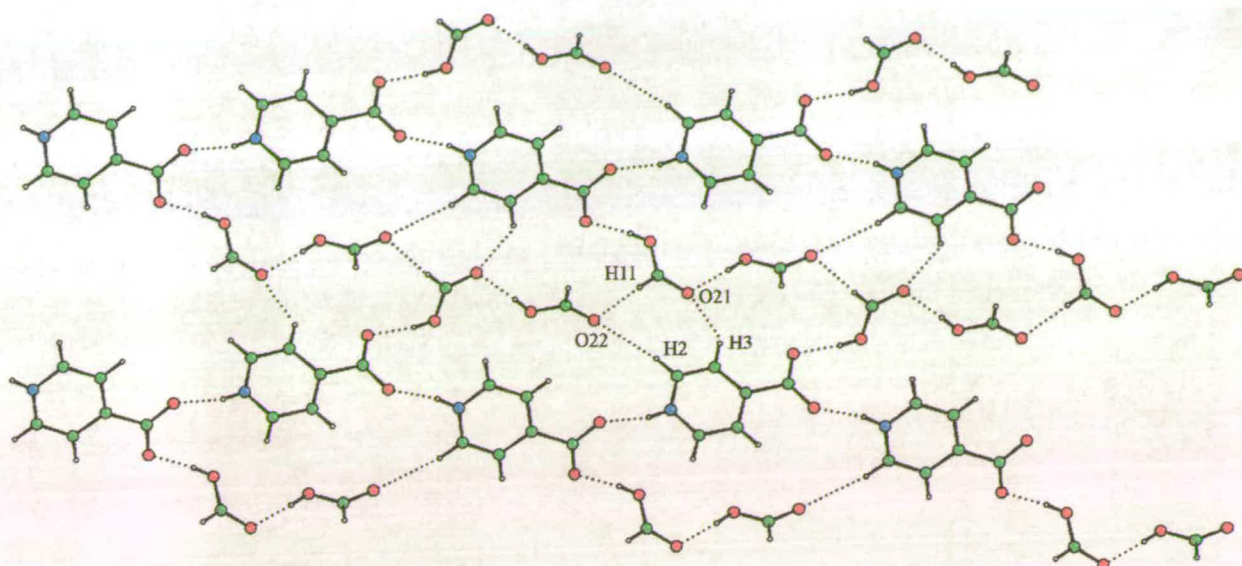


Figure 5: Neighbouring chains interact through a number of weaker interactions between the isonicotinic acid and formic acid molecules (H3...O21 2.48 Å; H2...O22 2.51 Å; H11...O22 2.39 Å). O22 does not accept any hydrogen bonds from NH or OH groups, and forms two CH...O interactions instead.

The formation of paracetamol (acetaminophen) adducts with hydrogen-bond acceptors

Iain D. H. Oswald,^a David R. Allan,^b Pamela A. McGregor,^b W. D. Samuel Motherwell,^c Simon Parsons^{a*} and Colin R. Pulham^a

^aSchool of Chemistry, The University of Edinburgh, King's Buildings, West Mains Road, Edinburgh EH9 3JJ, UK, ^bSchool of Physics and Astronomy, The University of Edinburgh, King's Buildings, West Mains Road, Edinburgh EH9 3JZ, UK, and ^cCambridge Crystallographic Data Centre, 12 Union Road, Cambridge CB2 1EZ, UK

Correspondence e-mail: s.parsons@ed.ac.uk

Received 29 July 2002
Accepted 4 September 2002

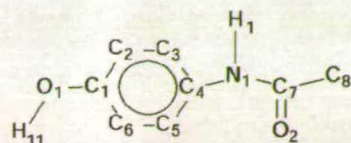
The crystal structures of five hemiadducts of paracetamol with 1,4-dioxane, *N*-methylmorpholine, morpholine, *N,N*-dimethylpiperazine and piperazine and a related 1:1 adduct of paracetamol with 4,4'-bipyridine are described. All structures are characterized by the formation of chains of paracetamol molecules, which are linked *via* either OH...O=C interactions [*C*(9) chains in graph-set notation] or NH...O=C interactions [*C*(4) chains], depending on the presence or absence of substituent groups on the guest molecule. In all cases except for the morpholine and bipyridine adducts these chains are connected by hydrogen-bond interactions with the guest molecules, which reside on crystallographic inversion centres. In the bipyridine adduct this linkage also involves a π -stacking interaction; in the morpholine adduct it is formed between the OH groups of two opposed paracetamol molecules. Most adducts (that with 4,4'-bipyridine is an exception) decompose on heating to give monoclinic paracetamol. This is the first systematic study of a series of co-crystals containing paracetamol.

1. Introduction

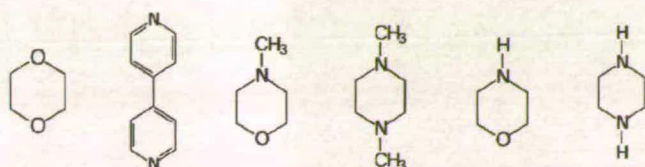
There have been a number of detailed studies on the polymorphic behaviour of paracetamol (acetaminophen, *p*-hydroxylacetanilide or Tylenol). Form I, which is monoclinic, was first characterized by Haisa *et al.* (1976), and has since been shown to be the thermodynamically more stable form. Form II is orthorhombic and was also described by Haisa *et al.* in 1974 (Haisa *et al.*, 1974). The orthorhombic form can be grown using a single orthorhombic crystal as a seed from a super-saturated aqueous solution of paracetamol. This method, however, can result in the crystals changing to the monoclinic form if left in contact with the solution for any length of time (Nichols & Frampton, 1998). The same authors showed that the only method that gives the orthorhombic polymorph reproducibly is growth from the melt. They also showed that this form is stable if dried and stored in a stoppered vial and that neither grinding nor compression induces a transition to the monoclinic form. In a very careful study, Boldyreva *et al.* (2000) have shown that application of hydrostatic pressures up to 4.2 GPa does not induce a transition from the monoclinic to the orthorhombic form. The behaviour of the orthorhombic form is of interest for its ability to undergo plastic deformation when compressed, thereby facilitating the production of tablets of paracetamol.

With the exception of our own recent report of paracetamol trihydrate (McGregor *et al.*, 2002), little structural work appears to have been carried out on solvates or other co-crystals of paracetamol, although a thermochemical study showed the existence of a hemisolvate of paracetamol with

1,4-dioxane (Fachaux *et al.*, 1995). In this report, we describe the preparation and characterization of six new adducts of paracetamol with 1,4-dioxane, 4,4'-bipyridine, *N*-methylmorpholine, *N,N*-dimethylpiperazine, morpholine and piperazine (these are referred to as *guest molecules* below; see Schemes). All these molecules, except for morpholine, can be considered to be at least pseudo-centrosymmetric with respect to their hydrogen-bonding properties.



Paracetamol, with atomic numbering scheme.



Guest molecules used to form adducts with paracetamol. Left to right: dioxane, bipyridine, *N*-methylmorpholine, *N,N*-dimethylpiperazine, morpholine and piperazine.

2. Experimental

2.1. Synthesis

All starting materials were obtained from Sigma-Aldrich except for 1,4-dioxane (May & Baker) and were used as received.

Paracetamol:0.5 1,4-dioxane. A saturated solution of paracetamol (1.51 g, 10 mmol) in 1,4-dioxane (2 cm³, 23 mmol) was refluxed and allowed to cool. Colourless crystals were formed overnight at 293 K according to the published procedure (Fachaux *et al.*, 1995).

Paracetamol:4,4'-bipyridine. Paracetamol (0.51 g, 3.40 mmol) was refluxed with an equimolar amount of 4,4'-bipyridine (0.52 g, 3.33 mmol) in ethanol (1 cm³). Pale-yellow needle-like crystals were formed on standing overnight at room temperature.

Paracetamol:0.5 *N*-methylmorpholine. Paracetamol (0.43 g, 2.85 mmol) and *N*-methylmorpholine (1 cm³, 9.11 mmol) were refluxed and allowed to cool. The flask was maintained at 277 K, leading to the formation of colourless rod-shaped crystals.

Paracetamol:0.5 *N,N*-dimethylpiperazine. Paracetamol (0.55 g, 3.64 mmol) and *N,N*-dimethylpiperazine (3 cm³, 22.2 mmol) were refluxed together and allowed to cool. A large excess of dimethylpiperazine was required to dissolve the paracetamol completely. The flask was maintained at 277 K leading to the formation of colourless rod-shaped crystals.

Paracetamol:0.5 piperazine. Paracetamol (0.62 g, 4.1 mmol) was refluxed together with piperazine (0.35 g, 4.1 mmol) in ethanol (1 cm³). Colourless crystals formed on cooling to 293 K.

Paracetamol:0.5 morpholine. Paracetamol (0.57 g, 3.8 mmol) was refluxed with morpholine (0.37 g, 4.3 mmol). Colourless crystals formed directly from the reaction mixture after a week at 277 K.

Ethanol was required in the reactions of paracetamol with piperazine and 4,4'-bipyridine because these compounds are both solids at room temperature.

2.2. Differential scanning calorimetry (DSC)

DSC traces were recorded using a Perkin Elmer Pyris DSC 1. Samples were contained in open aluminium pans and purged with helium during the temperature scans to facilitate the removal of any volatile products of thermal decomposition. Samples were heated from 298 K to 453 K at a rate of 10 K min⁻¹.

2.3. Crystallography

X-ray diffraction intensities were collected on either a Stoe Stadi-4 diffractometer with Cu K α radiation or a Bruker SMART APEX CCD diffractometer with Mo K α radiation. Both instruments were equipped with Oxford Cryosystems low-temperature devices. An absorption correction for the four-circle data was applied using ψ scans [*SHELXTL* (Sheldrick, 1997*a*), based on the procedure described by North *et al.* (1968)]; the multiscan procedure *SADABS* [(Sheldrick, 1997*b*), based on the procedure described by Blessing (1995)] was applied to the CCD data sets. All structures were in space group *P*₂₁/*c*, except the morpholine adduct, which formed in *P*₂₁2₁2₁. All structures were solved by direct methods and refined by full-matrix least squares against *F*² using all data (*SHELXTL*). H atoms were placed in calculated positions and allowed to ride on their parent atoms; methyl groups were treated with the Sheldrick (1997) rotating rigid group model. H atoms involved in hydrogen bonding were located in difference maps and refined freely. All non-H atoms were modelled with anisotropic displacement parameters.

One of the two crystallographically independent dioxane molecules in the 1,4-dioxane adduct was disordered over two orientations about a crystallographic inversion centre. The occupancies of the two components were fixed at 0.75 and 0.25 after competitive refinement. Similarity restraints were applied to the geometries and displacement parameters of the two components. The program *ROTAX* (Cooper *et al.*, 2002) suggested that the crystal may have been twinned by a twofold rotation about the [100] direct lattice direction. Incorporation of this into the model reduced *R*₁ slightly from 7.02% to 6.86%, with a twin scale factor of 2.6 (3)%. This is barely significant, and the twinning is omitted in the model presented here.

In the *N*-methylmorpholine adduct, the *N*-methylmorpholine is disordered over a crystallographic inversion centre with

Table 1
Experimental details.

All data were collected at 150 K.

	1,4-Dioxane adduct	Dimethylpiperazine adduct	N-methylmorpholine adduct
Crystal data			
Chemical formula	2[C ₈ H ₉ O ₂ N][C ₄ H ₈ O ₂]	2[C ₈ H ₉ NO ₂][C ₆ H ₁₄ N ₂]	2[C ₈ H ₉ NO ₂][C ₅ H ₁₁ NO]
Chemical formula weight	390.43	416.52	403.47
Cell setting, space group	Monoclinic, <i>P</i> ₂ ₁ / <i>c</i>	Monoclinic, <i>P</i> ₂ ₁ / <i>c</i>	Monoclinic, <i>P</i> ₂ ₁ / <i>c</i>
<i>a</i> , <i>b</i> , <i>c</i> (Å)	12.421 (5), 12.056 (4), 13.396 (3)	10.6970 (9), 11.0240 (9), 9.4896 (8)	10.5749 (8), 11.0221 (8), 9.3894 (7)
β (°)	91.51 (3)	100.684 (2)	101.145 (2)
<i>V</i> (Å ³)	2005.4 (11)	1099.65 (16)	1073.77 (14)
<i>Z</i>	4	2	2
<i>D_s</i> (Mg m ⁻³)	1.293	1.258	1.248
<i>D_m</i> (Mg m ⁻³)	Not measured	Not measured	Not measured
Radiation type	Cu <i>K</i> α	Mo <i>K</i> α	Mo <i>K</i> α
No. of reflections for cell parameters	80	3488	2729
θ range (°)	20–22	2.5–29	2.5–27.5
μ (mm ⁻¹)	0.795	0.088	0.090
Temperature (K)	220 (2)	150 (2)	150 (2)
Crystal form, colour	Lath, colourless	Plate, colourless	Rod, colourless
Crystal size (mm)	0.78 × 0.19 × 0.16	0.56 × 0.18 × 0.08	0.34 × 0.09 × 0.07
Data collection			
Diffractometer	Stoe Stadi-4	Bruker SMART APEX CCD	Bruker SMART APEX CCD
Data collection method	ω - θ scans	φ and ω scans	φ and ω scans
Absorption correction	Empirical	Multiscan	Multiscan
<i>T_{min}</i>	0.602	0.833	0.792
<i>T_{max}</i>	0.826	1	0.962
No. of measured, independent and observed reflections	4865, 3499, 2508	7034, 2724, 2512	6517, 2444, 1890
Criterion for observed reflections	<i>I</i> > 2 σ (<i>I</i>)	<i>I</i> > 2 σ (<i>I</i>)	<i>I</i> > 2 σ (<i>I</i>)
<i>R_{int}</i>	0.0532	0.0164	0.0221
θ_{max} (°)	69.79	29.08	27.49
Range of <i>h</i> , <i>k</i> , <i>l</i>	–15 → <i>h</i> → 15 0 → <i>k</i> → 14 0 → <i>l</i> → 15	–8 → <i>h</i> → 14 –15 → <i>k</i> → 14 –12 → <i>l</i> → 12	–13 → <i>h</i> → 13 –14 → <i>k</i> → 14 –11 → <i>l</i> → 12
No. and frequency of standard reflections	3 every 60 min	Not measured	Not measured
Intensity decay (%)	10.9	0	0
Refinement			
Refinement on	<i>F</i> ²	<i>F</i> ²	<i>F</i> ²
$R[F^2 > 2\sigma(F^2)]$, $wR(F^2)$, <i>S</i>	0.0702, 0.2243, 1.078	0.0525, 0.1339, 1.059	0.0408, 0.1082, 0.973
No. of reflections and parameters used in refinement	3499, 285	2724, 146	2444, 147
H-atom treatment	Riding	Riding/All H-atom parameters refined	Riding/All H-atom parameters refined
Weighting scheme	$w = 1/[\sigma^2(F_o^2) + (0.125P)^2 + 1.1494P]$ where $P = (F_o^2 + 2F_c^2)/3$	$w = 1/[\sigma^2(F_o^2) + (0.069P)^2 + 0.4625P]$ where $P = (F_o^2 + 2F_c^2)/3$	$w = 1/[\sigma^2(F_o^2) + (0.0658P)^2]$ where $P = (F_o^2 + 2F_c^2)/3$
$(\Delta/\sigma)_{max}$	0.002	0.009	0.000
$\Delta\rho_{max}$, $\Delta\rho_{min}$ (e Å ⁻³)	0.503, –0.260	0.401, –0.193	0.216, –0.220
Extinction method	SHELXL	None	SHELXL
Extinction coefficient	0.0019 (6)	0	0.008 (3)
	Piperazine adduct	4,4'-Bipyridine adduct	Morpholine adduct
Crystal data			
Chemical formula	2[C ₈ H ₉ NO ₂][C ₄ H ₁₀ N ₂]	[C ₈ H ₉ NO ₂][C ₁₀ H ₈ N ₂]	2[C ₈ H ₉ NO ₂][C ₄ H ₉ O]
Chemical formula weight	388.46	307.35	389.45
Cell setting, space group	Monoclinic, <i>P</i> ₂ ₁ / <i>c</i>	Monoclinic, <i>P</i> ₂ ₁ / <i>c</i>	Orthorhombic, <i>P</i> ₂ ₁ 2 ₁ 2 ₁
<i>a</i> , <i>b</i> , <i>c</i> (Å)	15.893 (5), 5.1664 (17), 12.993 (4)	11.2906 (10), 24.103 (2), 11.5526 (10)	7.2791 (9), 14.6277 (18), 18.303 (2)

the N and O atoms sharing an equivalent site. A composite scattering factor [0.5*f*(N) + 0.5*f*(O)] was used for this site; the occupancy of the methyl group was fixed at 0.5.

A consistent numbering scheme was used for the paracetamol molecules in all structures and this is shown in the schemes above. Where there is more than one paracetamol molecule in the asymmetric unit the labels in the schemes are augmented with the letters *A* and *B*. Labels for atoms forming part of the guest molecules carry the letters *S*, *T* etc. A full listing of crystal, data collection and refinement parameters is given in Table 1; a set of hydrogen-bonding parameters is given in Table 2.¹ The figures were produced using CAMERON (Watkin *et al.*, 1993). Other analyses utilized the PC version of the program PLATON (Spek, 2002; Farrugia, 1999).

3. Results

3.1. Paracetamol

Crystal structures of the monoclinic and orthorhombic polymorphs of paracetamol have been reported several times, but here we have used the structures reported by Nichols & Frampton (1998) [Cambridge Structural Database (CSD; Allen *et al.*, 1983) reference codes HXACAN07 and HXACAN08]. Our motive for discussing them here is to highlight certain features of their graph sets that enable structural relationships to be drawn between them and the adducts that form the subject of the rest of this paper.

Packing in both polymorphs is dominated by the formation of NH...OH and OH...O=C hydrogen bonds (Fig. 1) giving rise to layered two-dimensional networks. Both polymorphs of paracetamol have identical graph sets (Bernstein *et al.*, 1995), in which the

¹Supplementary data for this paper are available from the IUCr electronic archives (Reference: AN0622). Services for accessing these data are described at the back of the journal.

Table 1 (continued)

	Piperazine adduct	4,4'-Bipyridine adduct	Morpholine adduct
β ($^\circ$)	113.633 (5)	96.1484 (16)	90
V (\AA^3)	977.4 (6)	3125.8 (5)	1948.9 (4)
Z	2	8	4
D_x (Mg m^{-3})	1.320	1.306	1.327
D_m (Mg m^{-3})	Not measured	Not measured	Not measured
Radiation type	Mo $K\alpha$	Mo $K\alpha$	Mo $K\alpha$
No. of reflections for cell parameters	1227	5375	3801
θ range ($^\circ$)	2.5–29	2–28.5	2.5–24.5
μ (mm^{-1})	0.093	0.087	0.096
Temperature (K)	150 (2)	150 (2)	150 (2)
Crystal form, colour	Plate, colourless	Block, colourless	Block, colourless
Crystal size (mm)	0.77 \times 0.28 \times 0.11	0.46 \times 0.28 \times 0.18	0.54 \times 0.52 \times 0.28
Data collection			
Diffractionmeter	Bruker Smart Apex CCD	Bruker SMART APEX CCD	Bruker SMART APEX CCD
Data collection method	ω and φ scans	ω and φ scans	φ and ω scans
Absorption correction	Multiscan	Multiscan	Multiscan
T_{\min}	0.690	0.830	0.868
T_{\max}	1	1	1
No. of measured, independent and observed reflections	5628, 2309, 1778	20270, 7766, 6044	12312, 4733, 4265
Criterion for observed reflections	$I > 2\sigma(I)$	$I > 2\sigma(I)$	$I > 2\sigma(I)$
R_{int}	0.0458	0.0220	0.0308
θ_{\max} ($^\circ$)	28.55	29.18	28.97
Range of h, k, l	–17 \rightarrow h \rightarrow 21 –6 \rightarrow k \rightarrow 6 –17 \rightarrow l \rightarrow 16	–14 \rightarrow h \rightarrow 14 –19 \rightarrow k \rightarrow 31 –15 \rightarrow l \rightarrow 15	–9 \rightarrow h \rightarrow 7 –19 \rightarrow k \rightarrow 18 –24 \rightarrow l \rightarrow 22
No. and frequency of standard reflections	Not measured	Not measured	Not measured
Intensity decay (%)	0	0	0
Refinement			
Refinement on	F^2	F^2	F^2
$R[F^2 > 2\sigma(F^2)]$, $wR(F^2)$, S	0.0779, 0.1652, 1.179	0.0471, 0.128, 1.038	0.0462, 0.1028, 1.066
No. of reflections and parameters used in refinement	2309, 140	7766, 433	4733, 276
H-atom treatment	Riding/All H-atom parameters refined	Riding/All H-atom parameters refined	Riding/All H-atom parameters refined
Weighting scheme	$w = 1/[\sigma^2(F_o^2) + (0.052P)^2 + 0.5663P]$ where $P = (F_o^2 + 2F_c^2)/3$	$w = 1/[\sigma^2(F_o^2) + (0.0676P)^2 + 0.5669P]$ where $P = (F_o^2 + 2F_c^2)/3$	$w = 1/[\sigma^2(F_o^2) + (0.049P)^2 + 0.2716P]$ where $P = (F_o^2 + 2F_c^2)/3$
$(\Delta/\sigma)_{\max}$	0.002	0.001	0.001
$\Delta\rho_{\max}$, $\Delta\rho_{\min}$ ($e \text{\AA}^{-3}$)	0.336, –0.447	0.357, –0.246	0.256, –0.270
Extinction method	None	None	SHELXL
Extinction coefficient	0	0	0.0031 (7)

Computer programs used: Stoe *DIF4* (Stoe & Cie, 1990a), Stoe *REDU4* (Stoe & Cie, 1990b), Bruker *SMART* (Bruker, 2001), Bruker *SAINTE* (Bruker, 2002), *SHELXTL* (Sheldrick, 1997a).

OH...O=C and NH...OH hydrogen bonds, respectively, form C(9) and C(7) motifs at the unitary level.² In both polymorphs, these are disposed about crystallographic glide planes. In the monoclinic form, the hydrogen-bonded layers are arranged parallel to the (010) planes, which means that the layers are polar: in Fig. 1(a) all the molecules have the methyl group on the left. This polarity is reversed in neighbouring layers by crystallographic inversion centres. In the ortho-

² Note that where no sub- and superscripts appear in the graph-set descriptor, one donor and one acceptor are implied.

rhombic form, glide planes run perpendicular to the layers, so that the layers are non-polar: in Fig. 1(b) the methyl groups lie on the left- and right-hand sides of the molecules in alternate C(9) chains.

The angles between mean planes of the amide and phenyl groups in orthorhombic and monoclinic paracetamol are 17.7° and 20.5°, respectively. Analogous angles observed in this work are given in the figure captions and range from 3.03° to 41.72°. π – π bonding between the phenyl ring and the amide group favours a dihedral angle of zero, and some correlation between this angle and the N–C(phenyl) bond length might have been expected, though none is evident at the precision of these structure determinations. This angle is evidently a rather easily deformed structural parameter, and is presumably at the mercy of crystal-packing forces. As we show in the following sections, hydrogen bonding is the dominant feature in these structures, and the torsion observed is presumably a consequence of the optimization of these interactions.

3.2. The paracetamol:1,4-dioxane adduct

The asymmetric unit in the crystal structure of the dioxane adduct of paracetamol consists of two paracetamol molecules and two half molecules of dioxane. The latter both reside on crystallographic inversion centres. One of the dioxane molecules (labelled *T/U* in the tables and supplemental data) is disordered, although both compo-

nents participate in hydrogen bonding. The occupancy ratio is 0.75:0.25 and in the discussion that follows we have ignored the minor component (*U*). There is some evidence from electron-density difference maps that the other dioxane molecule (labelled *S*) is disordered as well, although, if present, the distinction between the components is at the limit of the resolution of our data set. An ordered model for this part of the structure is therefore presented here. The structure is depicted in Fig. 2. Primary bond lengths and angles are normal and have been deposited; hydrogen-bonding parameters are listed in Table 2.

The C(9) chains formed by hydrogen bonding between OH...O=C moieties of neighbouring molecules described above with regard to the crystal structures of paracetamol are also observed in the structure of the 1,4-dioxane adduct. In order to accommodate the dioxane molecules these chains are sinusoidal, with the two crystallographically independent paracetamol molecules alternating along the chain. The NH groups point towards the O atoms of dioxane molecules forming NH...O hydrogen bonds. Since both dioxane molecules reside on inversion centres, the space-group symmetry builds up two-dimensional sheets in which chains of paracetamol are linked by dioxane bridges (Fig. 2). In graph-set notation, the bridges can be described as $D_2^2(6)$. The two-dimensional sheets are parallel to the (210) lattice planes, and the rather open structure depicted in Fig. 2 is 'filled in' by symmetry-equivalent sheets parallel to (210).

Table 2
Hydrogen-bonding parameters.

Standard uncertainties are omitted in the case of the dioxane adduct because the H-atom positions were calculated and not refined. N—H and O—H distances were normalized to 1.009 Å and 0.983 Å, respectively, to aid comparison with Cambridge Structural Database search results (Fig. 7).

Adduct	Donor	Acceptor	Observed distance (Å)	Normalized distance (Å)	Typical normalized distance (Å)
1,4-Dioxane	N1A—H1A	O1S	2.03	1.90	1.96
	O1A—H11A	O2B	1.82	1.67	1.78
	O1B—H11B	O2A ⁱ	1.86	1.71	1.78
	N1B—H1B	O1U	1.92	1.77	1.96
	N1B—H1B	O1T	2.13	2.00	1.96
4,4'-Bipyridine	O1A—H11A	O2B	1.755 (19)	1.68	1.78
	N1A—H1A	N10S	2.047 (18)	1.92	1.96
	O1B—H11B	O2A ⁱⁱ	1.81 (2)	1.71	1.78
	N1B—H1B	N1T ⁱⁱⁱ	2.100 (18)	2.01	1.96
<i>N,N</i> -dimethylpiperazine	N1—H1	O2 ^{iv}	1.98 (2)	1.84	1.92
	O1—H11	N1S ^v	1.81 (2)	1.82	1.82
<i>N</i> -methylmorpholine	O1—H11	O1S/N1S ^{vi}	1.88 (2)	1.81	1.81/1.82
	N1—H1	O2 ^{vii}	1.925 (16)	1.80	1.92
Piperazine	O1—H11	N1S	1.79 (3)	1.74	1.82
	N1—H1	O2 ^{viii}	2.14 (3)	2.06	1.92
	N1S—H1S	O1 ^{ix}	2.30 (3)	2.21	2.03
Morpholine	O1A—H11A	O1B ^x	1.97 (2)	1.76	1.87
	N1A—H1A	O2B ^x	2.033 (18)	1.87	1.92
	O1B—H11B	N4S ^{xi}	1.79 (3)	1.69	1.82
	N1B—H1B	O2A ^{xii}	2.061 (19)	1.86	1.92

(i) $x, y, z + 1$; (ii) $x - 1, y, z - 1$; (iii) $-x, y - \frac{1}{2}, -z + \frac{1}{2}$; (iv) $x, -y + \frac{1}{2}, z - \frac{1}{2}$; (v) $-x + 1, -y, -z$; (vi) $-x + 1, -y + 2, -z$; (vii) $x, -y + \frac{1}{2}, z - \frac{1}{2}$; (viii) $x, y + 1, z$; (ix) $x + \frac{1}{2}, -y + \frac{1}{2}, -z$; (x) $x + \frac{1}{2}, -y + \frac{1}{2}, -z$; (xi) $-x + 1, y + \frac{1}{2}, -z + \frac{1}{2}$; (xii) $-x + 1, y - \frac{1}{2}, -z + \frac{1}{2}$.

3.3. The paracetamol:4,4'-bipyridine adduct

The O atoms in 1,4-dioxane formally have two lone pairs of electrons, each of which could potentially act as a hydrogen-bond acceptor. In practice, however, motifs in which ethers act as double hydrogen-bond acceptors occur rarely, and so for practical crystal-packing purposes it can be considered to be a centrosymmetric molecule containing two hydrogen-bond acceptors. 4,4'-Bipyridine is similar, although a torsion about the central C—C bond breaks the inversion symmetry. Recrystallization of paracetamol from a solution of 4,4'-bipyridine in ethanol yields a 1:1 co-crystal rather than the hemisolvate obtained with dioxane, a possible effect of the greater basicity of bipyridine.

The crystal structure of paracetamol:bipyridine contains two independent molecules each of paracetamol and bipyridine. Primary bond lengths and angles are normal and have been deposited; hydrogen-bonding parameters are listed in Table 2. As in the dioxane adduct, the paracetamol molecules form C(9) chains through OH...O=C hydrogen bonds (Fig. 3). The two crystallographically independent paracetamol molecules alternate along the chain. The disposition of the molecules within the chains is rather similar to that in orthorhombic paracetamol, except that alternate molecules are rotated through 180° about the chain axis in order to accommodate the bipyridine molecules.

The NH bonds of paracetamol act as hydrogen-bond donors to the aromatic N atoms of the bipyridine molecules, forming a discrete (D) graph set. However, since this crystal is a 1:1 adduct there are insufficient hydrogen-bond donors for the

number of acceptors present, and only one of the two N atoms in each bipyridine acts as an acceptor. The result is that there are no hydrogen-bonded pathways connecting the C(9) paracetamol chains. The structure thus consists of a paracetamol backbone with attached bipyridine molecules. These motifs are interconnected by π -stacking between the bipyridine molecules, building up sheets that run parallel to the (101) planes.

3.4. The paracetamol adducts with *N*-methylmorpholine and *N,N*-dimethylpiperazine

N,N-dimethylpiperazine and *N*-methylmorpholine are closely related to 1,4-dioxane by the substitution of one or both O atoms by N—Me; paracetamol forms 2:1 adducts with both compounds, as it does with dioxane. The *N,N*-dimethylpiperazine adduct consists of one crystallographically independent paracetamol molecule with the *N,N*-dimethylpiperazine residing on a crystallographic inversion centre. The *N*-methylmorpholine adduct is isostructural with this, with the guest molecule disordered about the inversion centre. Primary bond lengths and angles are unremarkable and have been deposited; hydrogen-bonding parameters are listed in Table 2.

The crystal structures are similar to those of the dioxane and bipyridine adducts in that the packing can be described with reference to chains of paracetamol molecules. However, rather than C(9) motifs formed through OH...O=C H bonds, the paracetamol molecules define a C(4) graph set through NH...O=C bonds (Fig. 4). The NH moiety of the para-

cetamol now fulfils the role of the OH groups in the dioxane structure, and *N,N*-dimethylpiperazine and *N*-methylmorpholine are similar to dioxane with regard to their hydrogen-

bonding properties. Therefore, although the nature of the paracetamol chain differs from that of the dioxane adduct, the roles of the *N*-methylmorpholine and dimethylpiperazine molecules are similar, and both act to link paracetamol chains via the $D_2^2(6)$ graph set. Overall, this structure consists of a two-dimensional network, although the sheets formed have a corrugated or zigzag appearance in cross section. Alternate regions of the network are approximately parallel to the (310) and $(\bar{3}\bar{1}0)$ planes. Just as in the dioxane adduct, the open structure of Fig. 4 is filled in by symmetry-equivalent networks.

3.5. The paracetamol:morpholine adduct

Morpholine is related to *N*-methylmorpholine by the substitution of the methyl group for hydrogen, and it is unique in this series because the hydrogen-bonding characteristics of the two hetero-centres are not the same: the NH group is a donor and acceptor, the ether O atom potentially a double, but more usually a single, acceptor. The asymmetric unit of the morpholine hemiadduct consists of two crystallographically independent paracetamol molecules (labelled *A* and *B*) and one molecule of morpholine (labelled *S* in the tables). Primary bond lengths and angles are normal and have been deposited; hydrogen-bonding parameters are listed in Table 2.

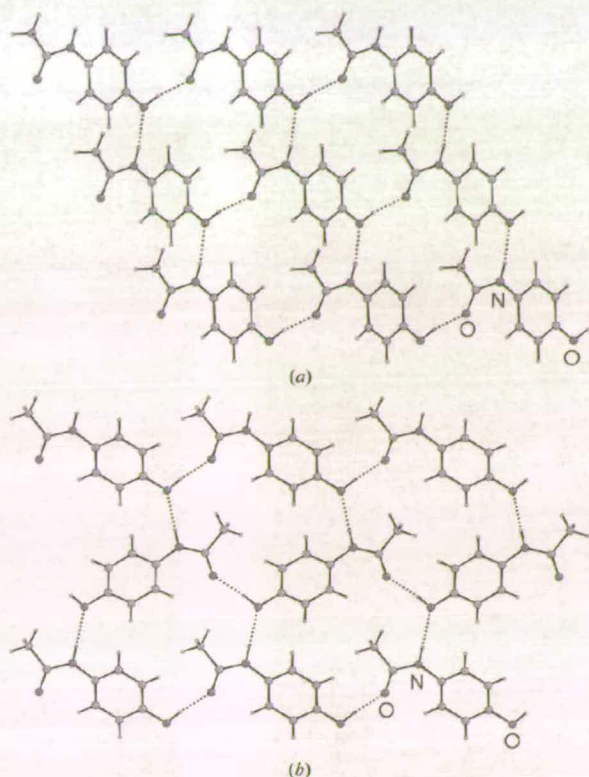


Figure 1
(a) Monoclinic paracetamol (Form I) viewed along the *b* axis; the *c* axis runs diagonally from top left to bottom right, so that the *C*(9) chains are established by the *n*-glide. (b) Orthorhombic paracetamol (Form II) viewed along the *c* axis; the *a* axis runs horizontally, the *b* axis runs from top to bottom. The *C*(9) chains referred to in the text run from left to right and the *C*(7) chains run approximately vertically. [Colour versions of this and the other figures are available in the online edition of this journal.]

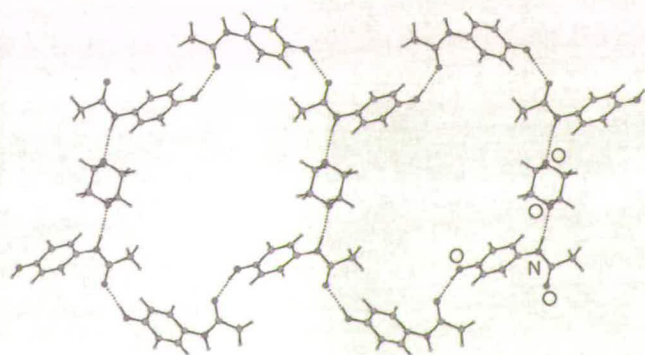


Figure 2
Paracetamol:1,4-dioxane adduct viewed perpendicular to (210); the *c* axis runs horizontally. The *C*(9) chains referred to in the text run from left to right and are linked together by dioxane molecules. The dihedral angles between the amide and phenyl mean planes in the two independent paracetamol molecules are 41.72 (15)° and 39.37 (14)° for molecules *A* and *B*, respectively.

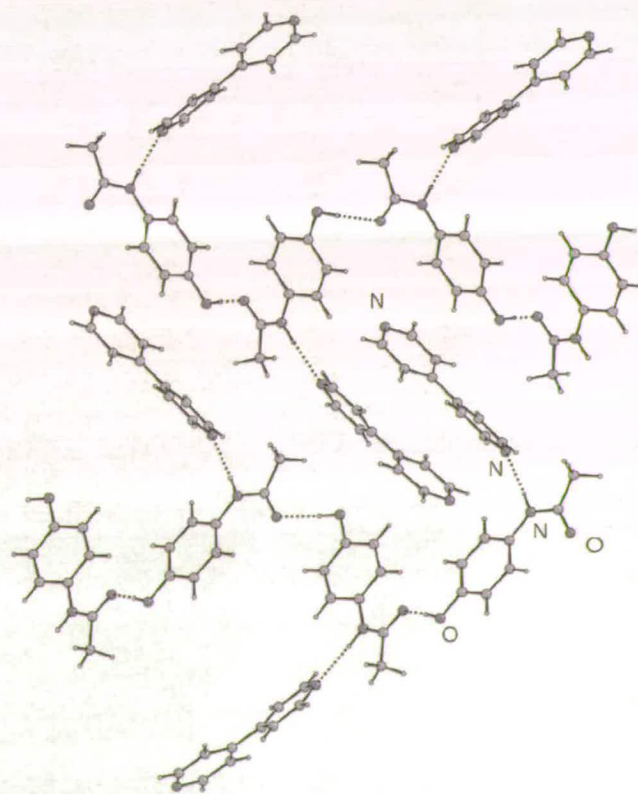


Figure 3
Paracetamol:4,4-bipyridine viewed perpendicular to (101); the *b* axis runs from top to bottom. The *C*(9) chains referred to in the text run from left to right and are linked together by a pair of π -stacked bipyridine molecules. The dihedral angles between the amide and phenyl mean planes in the two independent paracetamol molecules are 14.68 (8)° and 13.27 (9)° for molecules *A* and *B*, respectively.

The crystallographically independent paracetamol molecules alternate in the pattern ...*ABABAB*... along a chain formed by ...*HNCO*...*NHCO*... linkages between neighbouring amide groups. Because these molecules are crystallographically independent, these hydrogen bonds formally constitute discrete graphs at the unitary level, although it is clear from Fig. 5 that they are closely related to the *C*(4) graphs observed in the crystal structures of the *N*-methylmorpholine and *N,N*-dimethylpiperazine adducts described above. For consistency we continue to use this designation, although it is not formally correct [the binary graph $C_2^2(8)$ takes proper account of symmetry].

The chains are formed by 2_1 operations parallel to *c*, leading to a pairwise alternation of the centres of the paracetamol molecules above and below the chain. This pattern is reminiscent of the structures of the *N*-methylmorpholine and *N,N*-dimethylpiperazine adducts, except that in these cases the alternation applies to single molecules. The potential for this arrangement to lead to some steric hindrance between the phenyl groups of neighbouring molecules is avoided by adjacent molecules veering slightly away from each other and an increase in the torsional angle between the phenyl group and

amide group from 3.04 (3)° in molecule *B* to 36.03 (6)° in molecule *A*.

Lattice translation along the *b* direction generates further *C*(4) chains, and these are linked together by discrete [*D*] hydrogen bonds in which an OH group from an 'A' molecule in one chain acts as a donor to an OH group of a 'B' molecule in a neighbouring chain. This is the only structure in the series in which pairs of paracetamol molecules interact *via* their hydroxyl moieties.

The two sets of hydrogen bonds described above – the *C*(4) chains and the *D* links between chains – form a grid-like network parallel to the (100) planes. The morpholine molecules fit into the cavities of the grid. As in the *N*-methylmorpholine adduct, the amine N atom acts as an acceptor to the OH group of one of the paracetamol molecules (*B*), but this is the only hydrogen-bonding interaction formed by the morpholine. The NH group of the morpholine is in an axial position to accommodate this interaction.

This scheme satisfies all the hydrogen-bonding potential of the two paracetamol molecules, with the exception of the hydroxyl acceptor of molecule *A*. The weakest acceptor in the system (the ether function of the morpholine) does not

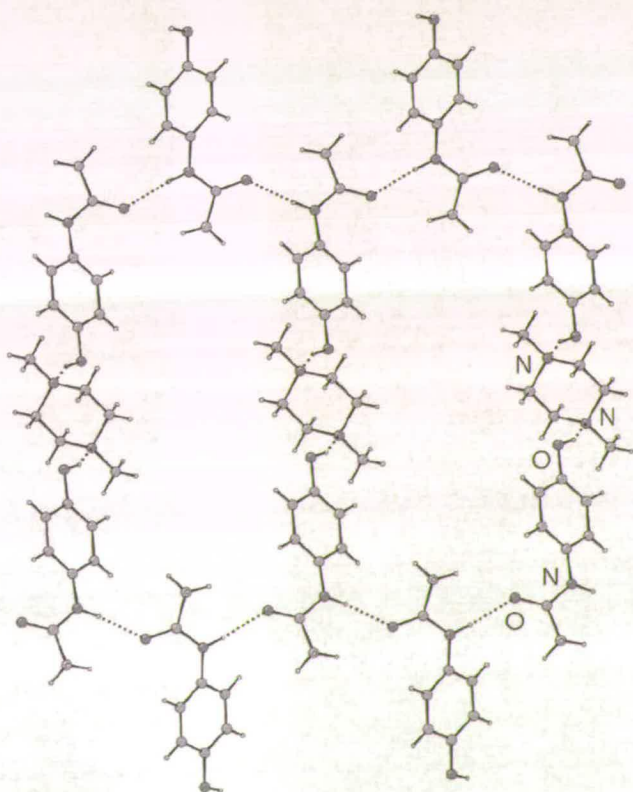


Figure 4

Paracetamol:*N,N*-dimethylpiperazine adduct (isostructural to the *N*-methylmorpholine adduct) viewed along the *a* axis; the *c* axis runs from left to right and the *b* axis from top to bottom. The *C*(4) chains referred to in the text run from left to right and are linked together by *N,N*-dimethylpiperazine molecules. The dihedral angles between the amide and phenyl mean planes in the paracetamol molecules are 33.75 (7)° and 34.11 (6)° in the *N,N*-dimethylpiperazine and *N*-methylmorpholine adducts, respectively.

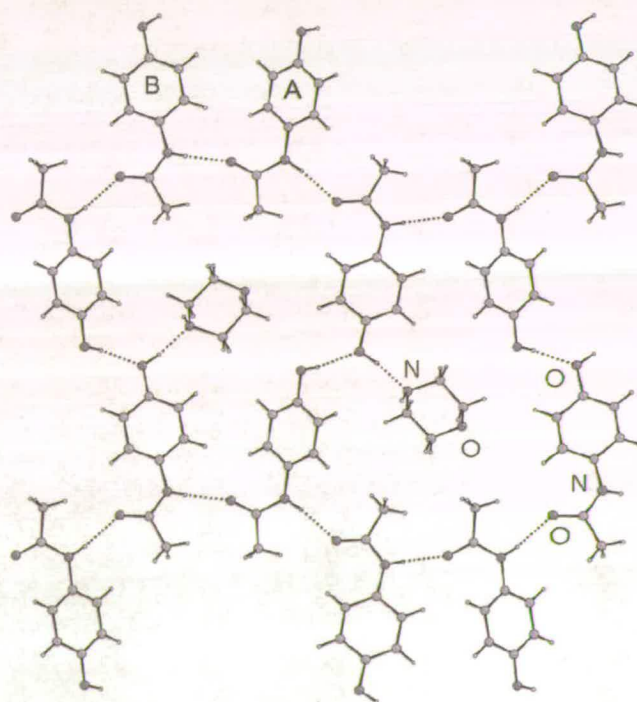


Figure 5

Paracetamol:morpholine adduct viewed along the *a* axis. The *c* direction runs from left to right, the *b* direction up and down. The labels *A* and *B* refer to the crystallographically independent paracetamol molecules referred to in the text. The *C*(4) chains referred to in the text run from left to right and are linked together by hydrogen bonds between opposed OH groups. This forms a grid-like array with the morpholine molecules residing in the grid cavities. The dihedral angles between the amide and phenyl mean planes in the two independent paracetamol molecules are 36.03 (6)° and 3.04 (3)° for molecules *A* and *B*, respectively.

participate in hydrogen bonding at all. A rather surprising feature of this structure, given the excess of acceptors present, is that the NH donor functionality of the morpholine amine moiety is also unsatisfied. However, this is consistent with the relatively long NH...OH hydrogen bonds observed in the piperazine adduct (which is described in the next section) and the generally poor hydrogen-bond-donor ability of secondary amines (see below).

3.6. The paracetamol:piperazine adduct

Piperazine is related to *N,N*-dimethylpiperazine by substitution of the two methyl groups by hydrogen. The asymmetric unit of the piperazine adduct, in common with the *N,N*-dimethylpiperazine adduct, consists of one paracetamol molecule and a molecule of piperazine on a crystallographic inversion centre. Primary bond lengths and angles are normal and have been deposited; hydrogen-bonding parameters are listed in Table 2. There are *C*(4) chains, consisting of NH...O=C hydrogen bonds, linked via $D_2^2(6)$ motifs consisting of OH...N bonds (Fig. 6). Piperazine is a weak hydrogen-bond donor as well as an acceptor, and the extra NH-donor moiety is satisfied by rotating alternate paracetamol molecules about the *C*(4) chain axis, leading to *D*-type NH...OH hydrogen bonds. This rotation produces ribbons that run parallel to the *b* axis rather than the infinite two-dimensional networks.

3.7. Differential scanning calorimetry

Decomposition of a co-crystal of paracetamol is a potential strategy for the production of the orthorhombic polymorph. In

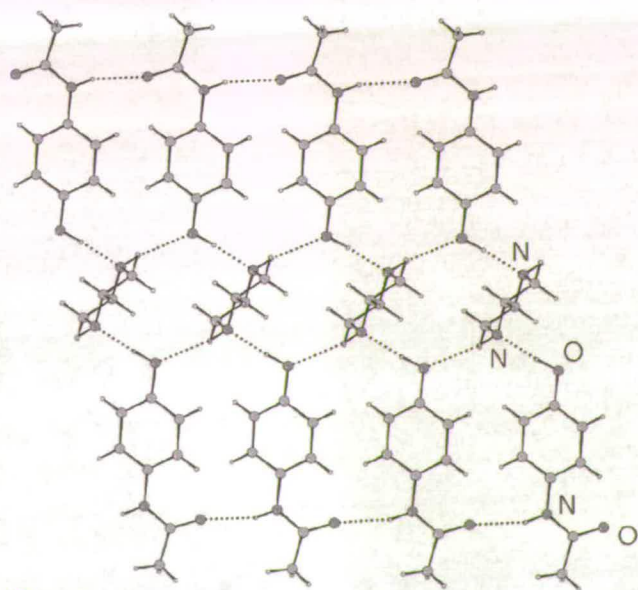


Figure 6
Paracetamol:piperazine adduct viewed perpendicular to (302); the *b* axis runs from left to right. The *C*(4) chains referred to in the text run from left to right and are linked together by piperazine molecules. The latter also act as weak hydrogen-bond donors. The dihedral angles between the amide and phenyl mean planes in the paracetamol molecule is 33.21 (14)°.

all cases except for the 4,4'-bipyridine adduct, DSC traces exhibited thermal events attributable to loss of the guest molecule followed by a strong endotherm, corresponding to melting, at 438–444 K. The melting point of monoclinic paracetamol is 442 K (Nichols & Frampton, 1998). The same authors showed that DSC traces for orthorhombic paracetamol show either melting at 430 K or a phase transition to the monoclinic form at the same temperature, depending on the method of preparation. The DSC traces observed in this study can therefore be interpreted in terms of decomposition leading to formation of the monoclinic polymorph.

Thermal decomposition temperatures follow the trend that might be predicted on the basis of the boiling points of 1,4-dioxane (374 K), *N*-methylmorpholine (388 K), morpholine (401 K), *N,N*-dimethylpiperazine (404 K) and piperazine (419 K). Two exotherms were observed for the dioxane solvate at 299 K and 338 K, in agreement with the previous study (Fachaux *et al.*, 1995). This is plausibly interpreted as sequential loss of the two crystallographically independent dioxane molecules. Dioxane is readily lost at room temperature from a crystalline sample of this adduct, and the DSC trace of a sample that had been allowed to stand for 10 min showed only one exotherm with an onset temperature of 330 K. Decomposition of the morpholine, *N*-methylmorpholine and *N,N*-dimethylpiperazine adducts occur as broad exotherms with onsets at approximately 327, 335 and 373 K, respectively. The DSC trace of the piperazine adduct showed one endotherm at 413 K.

4,4'-Bipyridine sublimates at 578 K under ambient pressure, and it is the least volatile compound to have been studied in this work. The DSC trace of the co-crystal exhibits a weak endotherm at 399 K followed by a strong endotherm at 402 K; no thermal event attributable to the melting of pure paracetamol was observed. The strong endotherm occurs at a similar temperature to the decomposition events observed for the other adducts, and it is likely to correspond to a melting process forming paracetamol solvated by liquid bipyridine (m.p. 374–377 K). Unlike the other solvents studied here, bipyridine is not lost to leave pure paracetamol, because its boiling point is well beyond the temperature of adduct decomposition. It is likely that the small peak corresponds to a phase transition.

4. Discussion and conclusions

This paper has described the formation of five new paracetamol hemiadducts with 1,4-dioxane, *N,N*-dimethylpiperazine, *N*-methylmorpholine, morpholine and piperazine and a 1:1 adduct with 4,4'-bipyridine. This is the first such systematic study of paracetamol co-crystals to have been undertaken. As is to be expected, the crystal structures of all adducts are dominated by hydrogen-bond formation, and comparisons between them were much facilitated by the use of graph-set analysis in the form described in the illuminating review by Bernstein *et al.* (1995).

Although ether oxygen can potentially act as a double acceptor, it rarely does so, and so with the exception of

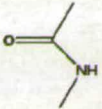
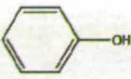
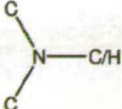


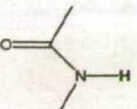
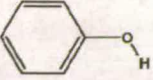
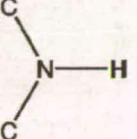
		Acceptor (O or N in each case)				
Donor (NH or OH)						
	Sample size Max NH...A /Å Min NH...A /Å Mean NH...A /Å	1250 (2.2) * 1.73 1.92	14 2.14 1.79 2.01	11 2.17 1.80 1.96	31 2.19 1.83 2.03	40 2.19 1.81 1.96
	Sample size Max OH...A /Å Min OH...A /Å Mean OH...A /Å	49 2.19 1.60 1.78	256 2.20 1.67 1.87	49 2.19 1.66 1.82	53 2.20 1.62 1.90	76 2.18 1.53 1.81
	Sample size Max NH...A /Å Min NH...A /Å Mean NH...A /Å	5 2.17 2.08 2.13	1 (HOLZOD) - - 2.03	12 2.20 2.00 2.14	4 2.18 2.11 2.13	Not applicable

Figure 7

Summary of the results of searches of the CSD (Version 5.23, April 2002) for typical distances (in Å) in hydrogen-bonded systems containing identical functional groups to the paracetamol adducts studied. The distances to H atoms were normalized to typical neutron distances (C—H 1.803, N—H 1.009 and O—H 0.983 Å). Only 'organic' structures where the *R* factor is less than 0.05 with no errors or disorder were included, and ionic or polymeric structures were excluded. The C atoms attached to the amine moieties were specified to be *sp*³ hybridized. The donor-H-to-acceptor distance was specified to be 1.50–2.20 Å. The asterisk denotes the limit of search.

morpholine all the guest molecules studied are at least pseudo-centrosymmetric with respect to their hydrogen-bonding properties. The dioxane, *N*-methylmorpholine, *N,N*-dimethylpiperazine and piperazine adducts all consist of hydrogen-bonded chains of paracetamol molecules linked together by the guest molecules, which all reside on crystallographic inversion centres. In the bipyridine adduct the chains are linked *via* a pair of π -stacked pyridine rings, though the structure as a whole is still centrosymmetric. The morpholine adduct does not conform to this pattern, although chains of paracetamol are still present. The arrangements of paracetamol chains described in this paper tend to lend themselves to the formation of centrosymmetric crystal structures, and this seems to favour adduct formation in the centrosymmetric guest molecules. It is perhaps significant that we have been unable to prepare an adduct with 1,3,5-trioxane, a molecule closely related to dioxane but which lacks inversion symmetry.

The donor groups that appear in this series are amidic NH, phenol OH and secondary amine NH; the acceptors are amidic O, phenolic O, secondary or tertiary amine N, ether O, and pyridine N. The results of searches of the CSD for typical hydrogen-bond geometries involving these functionalities are shown in Fig. 7; searching criteria are given in the legend to that figure. The pattern of adduct formation observed in this study is quite consistent with the data in Fig. 7 if the reasonable assumption is made that the hydrogen-bond strength is related to the average donor-hydrogen—acceptor distance.

The donor group O—H or N—H to acceptor distances observed in this study were normalized to typical neutron values (O—H 0.983 Å and N—H 1.009 Å) to aid ready comparison with typical H-to-acceptor distances derived from our CSD search, and this comparison is made in Table 2. Our hydrogen-bond distances agree tolerably well with typical values; they are often on the short side, as might be expected with low-temperature data.

The strongest hydrogen bonds in Fig. 7 are formed between phenolic OH (as donor) and amide O (as acceptor). These are observed in the *C*(9) chains formed in structures of both polymorphs of paracetamol. In pure paracetamol, hydrogen bonds are formed between the remaining NH donor and OH acceptor to form *C*(7) chains, but on adduct formation with 1,4-dioxane and 4,4'-bipyridine it is these, weaker, interactions that break to accommodate the guest molecules, preserving the strongly bound *C*(9) chains and forming hydrogen bonds between the amide NH of paracetamol and either the ether O or the pyridyl N atoms of the guest molecule. These observations are consistent with the results obtained in the variable-pressure study of monoclinic paracetamol by Boldyreva *et al.* (2000), where the NH...O contacts were found to be more compressible than the OH...O contacts.

Neither dioxane nor bipyridine has any group attached to the donor O or N atoms. All of the other molecules studied carry either hydrogen or methyl groups in these positions, and reference to Fig. 2 or Fig. 3 shows that a structure based on the *C*(9) paracetamol chains would suffer some steric crowding

between these groups and either the phenyl or the methyl group attached to the amide moiety. In order to avoid steric overcrowding in the morpholine, piperazine, *N,N*-dimethylpiperazine and *N*-methylmorpholine adducts, the paracetamol utilizes its NH group as a donor. Fig. 7 shows that the most effective acceptor for this group is amide CO and this explains the formation of *C*(4) paracetamol chains in all four of these structures.

In the structures of *N*-methylmorpholine and *N,N*-dimethylpiperazine, hydrogen bonds are formed between the OH group of paracetamol and the N or O of the guest molecule. In morpholine and piperazine, both the OH group of paracetamol and the NH group(s) of the guest could act as either donors or acceptors. Fig. 7 shows that secondary aliphatic amines are particularly poor hydrogen-bond donors, and so the hydroxyl group acts as the donor in both cases. In fact, so poor a donor is secondary amine NH that it is left unsatisfied in the morpholine adduct, even in the presence of excess acceptor functions. The weakness of these NH...N hydrogen bonds relative to OH...O or NH...O systems may be a consequence of the size of N relative to O, a feature recently emphasized by Brown (2002). However, in piperazine the NH groups do act as weak donors, and this induces a change in conformation of these *C*(4) chains relative to the *N,N*-dimethylpiperazine adduct that condenses the sheets into ribbons.

In the case of morpholine, the *C*(4) chains are linked by the OH group of a paracetamol molecule in one chain acting as a hydrogen-bond donor to a similar group in a neighbouring chain. On the basis of the structures of the other adducts, the role might have been expected to be fulfilled by the ether moiety of the morpholine. Fig. 7 shows that these interactions are of rather similar strength, and this might explain the apparently anomalous behaviour observed in this adduct.

In the 1,4-dioxane adduct, alternate *C*(9) paracetamol chains have reversed polarity. In the adducts based on *C*(4) chains, the resemblance to orthorhombic paracetamol is less obvious, although inspection of Fig. 1(b) shows that removal of alternate molecules along the *C*(7) graph followed by a small displacement would yield NH...O=C *C*(4) chains. Viewed in this light, desolvation might have been predicted to yield the orthorhombic polymorph of paracetamol, although in practice it was shown by DSC that in all cases except for paracetamol:bipyridine (for which we did not observe desol-

vation at all) the thermodynamically more stable monoclinic polymorph was formed.

We thank Mrs A. Dawson and Dr A. Parkin for assistance with data collection, and the EPSRC, the Cambridge Crystallographic Data Centre and the University of Edinburgh for funding.

References

- Allen, F. H., Kennard, O. & Taylor, R. (1983). *Acc. Chem. Res.* **16**, 146–153.
- Bernstein, J., Davis, R. E., Shimoni, L. & Chang, N.-L. (1995). *Angew. Chem. Int. Ed. Engl.* **34**, 1555–1573.
- Blessing, R. H. (1995). *Acta Cryst.* **A51**, 33–38.
- Boldyreva, E. V., Shakhshneider, T. P., Vasilchenko, M. A., Ahsbahs, H. & Uchtmann, H. (2000). *Acta Cryst.* **B56**, 299–309.
- Brown, I. D. (2002). *The Chemical Bond in Inorganic Chemistry*, ch. 7. IUCr Monographs on Crystallography. Oxford University Press.
- Bruker (2001). *SMART*. Bruker-AXS, Madison, Wisconsin, USA.
- Bruker (2002). *SAINTE*. Bruker-AXS, Madison, Wisconsin, USA.
- Cooper, R. I., Gould, R. O., Parsons, S. & Watkin, D. J. (2002). *J. Appl. Cryst.* **35**, 168–174.
- Fachaux, J.-M., Guyot-Hermann, A.-M., Guyot, J.-C., Conflant, P., Drache, M., Veessler, S. & Boistelle, R. (1995). *Powder Technol.* **82**, 123–128.
- Farrugia, L. J. (1999). *J. Appl. Cryst.* **32**, 837–838.
- Haisa, M., Kashino, S., Kawai, R. & Maeda, H. (1976). *Acta Cryst.* **B32**, 1283–1285.
- Haisa, M., Kashino, S. & Maeda, H. (1974). *Acta Cryst.* **B30**, 2510–2512.
- McGregor, P. A., Allan, D. R., Parsons, S. & Pulham, C. R. (2002). *J. Pharm. Sci.* **91**, 1308–1311.
- Nichols, G. & Frampton, C. S. (1998). *J. Pharm. Sci.* **87**, 684–693.
- North, A. C. T., Phillips, D. C. & Mathews, F. S. (1968). *Acta Cryst.* **A24**, 351–359.
- Sheldrick, G. M. (1997a). *SHELXTL*. Bruker-AXS, Madison, Wisconsin, USA.
- Sheldrick, G. M. (1997b). *SADABS*. Bruker-AXS, Madison, Wisconsin, USA.
- Spek, A. L. (2002). *PLATON. A Multipurpose Crystallographic Tool*. Utrecht University, The Netherlands.
- Stoe & Cie (1990a). *DIF4. Diffractometer Control Program*. Stoe & Cie, Darmstadt, Germany.
- Stoe & Cie (1990b). *REDU4. Data Reduction Program*. Stoe & Cie, Darmstadt, Germany.
- Watkin, D. J., Pearce, L. & Prout, C. K. (1993). *CAMERON – A Molecular Graphics Package*. Chemical Crystallography Laboratory, University of Oxford, UK.